A FRAMEWORK FOR STOCHASTIC FINITE ELEMENT ANALYSIS OF REINFORCED CONCRETE BEAMS AFFECTED BY REINFORCEMENT CORROSION

Darek Baingo

Thesis submitted to
the Faculty of Graduate and Postdoctoral Studies
in partial fulfillment of the requirements
for the **PhD** degree in Civil Engineering

Department of Civil Engineering
Faculty of Engineering
University of Ottawa

Abstract

Corrosion of reinforcing bars is the major cause of deterioration of reinforced concrete (RC) structures in North America, Europe, the Middle East, and many coastal regions around the world. This deterioration leads to a loss of serviceability and functionality and ultimately affects the structural safety. The objective of this research is to formulate and implement a general stochastic finite element analysis (SFEA) framework for the time-dependent reliability analysis of RC beams with corroding flexural reinforcement. The framework is based on the integration of nonlinear finite element and reliability analyses through an iterative response surface methodology (RSM). Corrosion-induced damage is modelled through the combined effects of gradual loss of the cross-sectional area of the steel reinforcement and the reduction bond between steel and concrete for increasing levels of corrosion. Uncertainties in corrosion rate, material properties, and imposed actions are modelled as random variables. Effective implementation of the framework is achieved by the coupling of commercial finite element and reliability software. Application of the software is demonstrated through a case study of a simply-supported RC girder with tension reinforcement subjected to the effects of uniform (general) corrosion, in which two limit states are considered: (i) a deflection serviceability limit state and (ii) flexural strength ultimate limit state.

The results of the case study show that general corrosion leads to a very significant decrease in the reliability of the RC beam both in terms of flexural strength and maximum deflections. The loss of strength and serviceability was shown to be predominantly caused by the loss of bond strength, whereas the gradual reduction of the cross-sectional area of tension reinforcement was found to be insignificant. The load-deflection response is also significantly affected by the deterioration of bond strength (flexural strength and stiffness). The probability of failure at the end of service life, due to the effects of uniform corrosion-induced degradation, is observed to be approximately an order of magnitude higher than in

the absence of corrosion. Furthermore, the results suggest that flexural resistance of corroded RC beams is controlled by the anchorage (bond) of the bars and not by the yielding of fully bonded tensile reinforcement at failure. This is significant since the end regions can be severely corroded due to chloride, moisture, and oxygen access at connections and expansion joints. The research strongly suggests that bond damage must be considered in the assessment of the time-dependent reliability of RC beams subjected to general corrosion.

Acknowledgements

First and foremost I would like to express my sincere gratitude to my mentor and supervisor, Professor Beatriz Martín-Pérez. Her kind and thoughtful guidance throughout this very challenging work have been very inspiring. It has been a great honour and a pleasure for me to be her student. My sincere thanks also go to Professor Jim Beaudoin, my co-supervisor, for his keen interest and support throughout the research.

I would also like to thank the members of the thesis defence committee, Professors Murat Saatcioglu and Dan Palermo from the University of Ottawa, Professor Ted Sherwood of Carleton University, and Professor Michael Bartlett from the University of Western Ontario, for their insights, advice, and valuable comments about this research in general.

The work on practical aspects of reliability analysis and response surface methodologies has greatly benefited from many discussions with Dr. Akpan and Dr. Koko at Martec Ltd in Halifax, NS. I thank them for allowing me full access to their excellent reliability analysis program – COMPASS. I extend my thanks to Professor Frank Vecchio at the University of Toronto for providing me with access to VecTor2, a non-linear FEA software for reinforced concrete structures.

Tremendous gratitude is due to Dr. Anthony Ashley, Director General of Defence R&D Canada - Centre for Security Studies (DRDC-CSS), for his interest in my research, and most significantly, for his support during the final months of work on my dissertation. My appreciation for his gracious generosity in allowing me dedicated time to complete this dissertation cannot be overstated. I am also indebted to Dr. Paul Chouinard, my supervisor at DRDC-CSS, for his support and patience while I was completing this work.

I would like to acknowledge the Natural Sciences and Engineering Research Council of Canada (NSERC), the Ontario Graduate Scholarship in Science and Technology program

(OGSST) and the University of Ottawa Academic Excellence scholarship for their financial support over a four year period. It would not have been feasible for me to undertake my doctoral studies without these scholarships and this support is gratefully acknowledged.

Finally, and most importantly, I thank my wife Anita for her love, patience, encouragement, and understanding over all these years, especially during the most difficult moments in our lives. I dedicate this work to our sons, Kacper and Sebastian, who were born during the course of this research. Nothing has been more difficult than the countless times I turned down their loving requests for play. I look forward to spending much more time with them.

Table of Contents

List of Tables

List of Figures

Notation

The following symbols are used in this thesis:

a = polynomial coefficients;

A = atomic weight in g/mol;

A_b = cross-sectional area of an individual reinforcing bar;

A_s = total area of longitudinal reinforcement on the tension side of the member;

b = width of a member / width of the compression face of a member;

$\boldsymbol{B}$ = the strain matrix;

c = percentage of corrosion at time t;

$\boldsymbol{C}$ = uncorrelated random vector;

COV = coefficient of variation (σ/μ);

d = distance from extreme compression fibre to centroid of tension reinforcement;

d_b = reinforcing steel diameter (mm);

d_{bo} = initial diameter of reinforcing steel (mm);

Δd = increase in reinforcing bar diameter due to growth of corrosion products;

$\boldsymbol{D}$ = the elasticity matrix;

E_c = elastic modulus of concrete (MPa);

E_s = elastic modulus of non-prestressed reinforcing steel (MPa);

E_{sh} = strain hardening modulus of non-prestressed reinforcing steel (MPa);

f'_c = specified cylinder compressive strength of concrete (MPa);

f_r = rupture modulus of concrete (MPa);

f_R = probability density function for the capacity random variable R;

f_s = calculated stress in reinforcing steel at specified load;

f_{su} = maximum stress in reinforcing steel at failure;

f_S = probability density function for the demand random variable S;

f_y = specified yield strength of non-prestressed steel reinforcement (MPa);

F = Faraday's constant (96487 C/mol of electrons or Coulombs);

$\boldsymbol{F}$ = vector of nodal loads in a finite element formulation;

F_R = cumulative probability density function for the capacity random variable R;

F_S = cumulative probability density function for the demand random variable S;

$g(\,)$ = a performance function;

$\hat{g}(\,)$ = surrogate/approximate performance function;

h = overall thickness or height of member;

i_{corr} = rate of corrosion in reinforcing steel ($\mu A/cm^2$);

I = moment of inertia of section about centroidal axis;

I_{corr} = corrosion current in amperes;

$\boldsymbol{k}^e$ = element stiffness matrix;

$\boldsymbol{K}$ = global stiffness matrix in a linear-elastic finite element formulation;

l_n = clear span;

M_f = moment due to factored loads;

M_r = factored moment resistance;

M_u = unfactored moment resistance/capacity;

n = number of longitudinal bars in RC section;

p_f = probability of failure;

$\boldsymbol{R}$ = random variable related to the structure capacity (resistance);

s = bond slip;

s_p = pullout bond slip;

s_s = splitting bond slip;

$\boldsymbol{S}$ = random variable related to the structure demand (loads);

SF = nominal safety factor;

t = time (units as noted);

$\boldsymbol{U}$ = vector of nodal displacements in a finite element formulation;

v = mean outcrossing rate;

v_c = factored shear resistance provided by the concrete;

v_f = factored shear stress resistance;

v_r = factored shear stress resistance;

v_s = factored shear stress resistance provided by shear reinforcement;

V_c = shear resistance attributed to the concrete factored by ϕ_c;

V_f = factored shear force;

$V_{r,max}$ = maximum possible factored shear resistance;

$\hat{\boldsymbol{V}}_{XX}$ = covariance matrix of vector $\boldsymbol{X}$;

w = uniformly distributed load;

$\boldsymbol{x}^*$ = coordinates of the most probable point MPP/failure point;

X = basic random variable;

$\boldsymbol{X}$ = vector of basic random variables;

$\boldsymbol{Y}$ = vector of basic random variables in normal space (after Rosenblatt transformation);

Z = ionic valence number or ion charge;

α = importance factors;

β = reliability index;

β_{HL} = Hasofer-Lind reliability index;

β_{T} = target reliability index, as per design or code/standard objectives;

$\gamma_p(t)$ = time-dependent progressive reliability;

δ = Kronecker delta;

ε_{co} = concrete strain at peak compressive stress;

ε_{cu} = maximum strain in the extreme compression fibre at ultimate load;

ε_r = concrete rupture strain;

ε_s = strain in steel reinforcement;

ε_{sh} = strain in steel reinforcement at initiation of hardening;

ε_{su} = ultimate strain in steel reinforcement at failure;

ρ = ratio of non-prestressed tension reinforcement (A_s/bd);

= auto-correlation coefficient function of a random field;

λ = continuous conditional probability function / hazard rate;

μ = mean value of a random variable;

ρ_s = density of steel;

ρ_v = ratio of shear friction reinforcement;

σ = standard deviation of a random variable;

$\boldsymbol{\tau}$ = bond stress;

τ_p = pullout bond stress;

τ_s = splitting bond stress;

ϕ = resistance factor applied to a specified material property or the resistance of a member, connection, or structure, which for the limit state under consideration takes into account the variability of dimensions and material properties, quality of work, type of failure, and uncertainty in the prediction of resistance;

ϕ_c = resistance factor for concrete;

ϕ_s = resistance factor for steel;

Φ = standard normal distribution function;

$\boldsymbol{\Phi}$ = orthogonalization matrix;

$\boldsymbol{\Lambda}$ = eigenvalue matrix containing the variances of the uncorrelated random vector $\boldsymbol{C}$;

χ = random field;

$\hat{\chi}$ = discretized random field defined by means of a finite set of random variables $\boldsymbol{X}$;

ν = Poisson's ratio;

Ψ = a multidimensional Hermite polynomial;

Ω = an open set describing the system domain or geometry;

Chapter 1. Introduction

1.1 Background

Corrosion of reinforcing bars is the major cause of deterioration of reinforced concrete (RC) structures in North America, Europe, the Middle East, and many coastal regions around the world (Hansson et al., 2007; Rostam, 2003). Damage is manifested in the form of cracking, delamination, and spalling of the concrete cover due to the disproportionately large volume of the iron oxide corrosion products accumulating around the reinforcement. Over time this problem can reduce the strength capacity of affected structures due to the loss of bonding action between the steel and the concrete and a decrease in the tensile capacity of the reinforcing bars due to loss of cross-sectional area. This deterioration leads to a loss of serviceability and functionality and ultimately affects the structural safety. The economic losses and damage caused by the corrosion of steel in concrete makes it arguably the largest single infrastructure problem facing industrialized countries (Broomfield, 2007). It is estimated that billions of dollars are spent annually on the maintenance and repairs of corroding RC structures in North America alone (ASCE 2009). Given the limited resources of infrastructure authorities and owners, a need clearly exists for the optimal allocation of resources for design, construction, inspection, and maintenance. This can be achieved if the amount of deterioration that a structure may suffer during its service life can be accurately estimated, and if this information is utilized in a lifecycle design approach.

Current standards for the design of reinforced concrete structures are mainly concerned with structural performance, without an explicit attempt to evaluate the effect of deterioration mechanisms, such as reinforcement corrosion, over long periods of time. Although a durability limit state is mentioned in the latest edition of the CAN/CSA A23.3-04 concrete design standard (2004), as referenced to CSA A23.1(2004) and CAN/CSA-S413 (2007), it is

merely a prescriptive specification on concrete mix design and minimum concrete cover thickness in RC members. In effect, the treatment of load carrying capacity and durability has been separated, not only in the codes but also in the profession of structural engineering (Vrouwenvelder and Schiessl 1999). Furthermore, current codes, which have been explicitly developed for new designs, are not applicable to the assessment of existing structures because of significant differences between the designs and assessment situations (Allen 1991).

A more rational structural design process can be achieved if degradation mechanisms are explicitly included in the design phase. Since current structural design practice is primarily based on the limit states philosophy, wherein the performance of a structure is checked against various limiting conditions at appropriate load levels, it follows that the same framework can be applied to durability design in order to integrate it with the former. This approach would also satisfy the current need to quantify performance and service life of concrete structures affected by reinforcement corrosion, so that optimum design or rehabilitation strategies are adopted in order to minimize costs over the lifetime of the structure.

1.2 Objectives and Scope

The objective of the proposed research program is to develop a general computational framework which allows computation of time-dependent reliability of reinforced concrete beams affected by corrosion-induced deterioration. The resulting framework will be based on the theory and implementation of Stochastic Finite Element Analysis (SFEA), which replaces the deterministic safety check with a probabilistic assessment of the safety of the affected structure at the different levels of corrosion-induced damage. The SFEA formulation will treat the uncertainty associated with predicting the response of a structure given uncertainties in geometry, material properties, and imposed actions, in order to describe the limit states of deflection and flexural failure. This research encompasses the following general tasks:

1. Literature review of corrosion-induced damage models and SFEA methodologies and modelling.

2. Development of a corrosion-induced damage model, combining the effects of reductions of reinforcement section and bond.
3. Compilation of published field data to define probability density functions for corrosion rate and time distributions to each limit state.
4. Development and implementation of a computational SFEA framework.
5. Demonstration of the framework to the time-dependent reliability analysis of an RC beam affected by corrosion-induced deterioration of the steel reinforcement.

1.3 Research Significance

It is expected that the computational SFEA framework will facilitate more realistic performance prediction of RC beams affected by corrosion over time. Combined with acceptable limiting performance criteria for RC beams (limit states), the SFEA framework may be used as a basis for development of rational criteria for serviceability and strength requirements for RC beams subjected to the effects of corrosion-induced deterioration. The coupling of finite element based deterioration models with statistical modelling of the uncertainties in the loads, material, and geometrical properties together with time-dependent analysis, provides important information about expected performance and relative risk. Such predictions can lead to practical recommendations for future experimental, computational and analytical research programs, as well as development of decision support tools for optimizing design, maintenance, and rehabilitation strategies, all issues of critical importance to those concerned with the effective management of affected structures. The probability concept provides a unified framework for quantitative analysis of uncertainty and assessment of risk as well as the formulation of trade-off studies for the design of resilient RC infrastructure. Furthermore, although most reliability-based codes in current practice only apply to the design of structural members, not structural systems, in the near future, one can expect further acceleration in the development of analytical methods used to model the behaviour of structural systems. It is expected that this focus on the system behaviour will lead to additional applications of reliability theory at the systems level, and a SFEA Framework can be extended to system level analyses.

1.4 Outline of the Thesis

Chapter 2 presents a current review of the literature related to the corrosion of reinforcement in concrete structures. The chapter begins with a brief overview of the causes, processes, and variables governing the corrosion of reinforcing steel in concrete. Fundamentals of corrosion-induced damage mechanisms in concrete are presented, followed by a discussion of the effects of damage propagation on the strength, deformability, and failure mode of reinforced concrete flexural elements. The rate of corrosion, considered the principal parameter determining the progression of corrosion-induced damage, is reviewed in detail. Probabilistic models of corrosion-induced damage in RC as well as a review of probabilistic methods for durability design are also summarized. The chapter closes with a discussion of gaps in the current state-of-the-art.

Chapter 3 provides a detailed overview of the proposed Stochastic Finite Element Analysis Framework. The concepts and philosophy of SFEA are introduced and the various methodologies, as well as practical implementation strategies are explained and evaluated. The ideas and reasoning behind the development of the SFEA framework are thoroughly explained and the principal components of the framework are presented in the form of a process diagram. A practical case study of a RC girder subjected to corrosion of the tension reinforcement is then introduced. The case study is intended to demonstrate practical application of time-dependent stochastic finite element analysis, the functionality of each component of the framework, and generate preliminary results of the effects of deterioration of bond strength in the reliability of RC beams over time.

Development, implementation, and validation of the finite element analysis component, including the formulation of a corrosion damage model, are presented in Chapter 4. Following a brief review of structural reliability concepts, random variables, and limit state functions, Chapter 5 also explains the methodology derived for the calculation of time-dependent reliabilities. Evaluation and discussion of the results of time-dependent reliability analyses of the RC girder introduced, is also presented in this chapter. An in-depth explanation of Response Surface Methodology (RSM) and the algorithm used in the proposed framework is presented in Chapter 6. The chapter also demonstrates the

experimental design and generation of the response surfaces used in the SFEA analysis of the case study RC girder.

The final results of the case study using the SFEA framework are analysed and discussed in Chapter 7, while Chapter 8 closes the thesis with a summary of the research results, conclusions, and recommendations for future work. Finally, several Appendices provide additional details and example calculations showing the application of the various theories and techniques used in the development of the proposed SFEA framework.

Chapter 2. Literature Review

2.1 Introduction

Reinforced concrete is a versatile, economical and successful construction material. It can be moulded to a variety of shapes and finishes, and it is usually durable and strong, performing well throughout its service life. However, sometimes it does not perform adequately as a result of poor design, poor construction quality, inadequate materials selection, very aggressive environments, or a combination of all these factors. According to the American Society of Civil Engineering (ASCE 2009), the United States would have to spend $2.2 trillion over the next five years to remedy current infrastructure deficiencies. More than 26% of the bridges in the U.S. are either structurally deficient or functionally obsolete, which would require an annual investment of $17 billion to substantially improve current bridge conditions (ASCE 2009). The same report states that "only a fraction of that amount is spent annually on the maintenance of bridges".

It is now universally recognized that corrosion of steel reinforcement is the most serious cause of costly and premature deterioration in reinforced concrete structures (Hansson et al., 2007; Rostam, 2003). Because corrosion is a slow process and it is usually easy to detect the signs of damage before catastrophic failure, the consequences of corrosion have in the past been mostly economic. However, with the rapid increase in the volume of ageing concrete infrastructure requiring maintenance or replacement, cases of serious failures identified to be the result of corrosion damage have been on the rise. The consequences of corrosion can range from progressive weakening of a reinforced concrete member and the structure over time to catastrophic failures resulting in injury and death, such as the collapse of the Berlin Congress Hall (Borgard 1990). In the United States, failures attributed to the use of de-icing salts led to serious injuries and deaths when large pieces of concrete fell from a bridge and two multi-storey parking structures collapsed in Minnesota (Broomfield 2007).

The economic loss and damage caused by the corrosion of steel in concrete makes it arguably the largest single infrastructure problem facing industrialized countries (Broomfield 2007). Bridges, public utilities, chemical plants and buildings are ageing. Some can be replaced, while others would cause great cost and disruption to the functioning of infrastructure systems if taken out of commission. With major political arguments about how many more bridges, power plants and other structures we can build, it becomes crucial that the existing structures perform effectively and safely throughout their design lives.

2.2 Corrosion of Reinforcing Steel in Concrete

In general, concrete provides reinforcing steel with a non-aggressive environment. During cement hydration the aqueous phase rapidly acquires a high pH (~13) that is buffered to resist downward changes in pH values by the sparingly soluble hydration products of cement (Glass and Buenfeld 2000). The steel reinforcement in contact with this alkaline solution is normally passive. The thermodynamically most stable corrosion products are insoluble oxides, and a passive oxide film covers the surface, presenting a barrier to further metal dissolution. For corrosion to occur, a process of depassivation is essential. Two processes can break down the passive environment in concrete: carbonation and chloride attack. Carbonation is the process by which carbon dioxide (CO_2) in the atmosphere reacts with water in the concrete pores to form carbonic acid, which then neutralizes the alkalis in the pores. This can then lead to the corrosion of the reinforcing steel. In contrast, the introduction of chlorides, such as sodium chloride (NaCl) found in sea and de-icing salt or calcium chloride (CaCl) still found in concrete admixtures in the Middle East, can result in chloride attack and depassivation of the steel reinforcement.

Carbonation is more common in older structures, particularly older RC buildings and reconstituted stone elements containing reinforcement that often have low cement content and are very porous. Conversely, it is relatively rare in modern highway bridges and other civil engineering structures where water-cement ratios are low, cement contents are high, and proper compaction, curing, and cover are provided to prevent the carbonation front from advancing into the concrete to the depth of the steel within the lifetime of the structure

(Broomfield 2007). In RC structures in coastal regions, exposed to sea water, or RC structures in colder climates where the seasonal use of de-icing salts is standard practice, the chlorides usually penetrate to the reinforcement and cause corrosion long before carbonation becomes a problem (Page 2007).

Once the reinforcing steel is depassivated, corrosion proceeds in electrochemical cells formed on the surface of the metal and an electrolyte or solution surrounding the metal. As illustrated in Figure 2-1, each cell consists of a pair of electrodes on the surface of the metal (the anode and its counterpoint, the cathode), a return circuit, and the electrolyte. In reinforced concrete, the anode and the cathode are located on the reinforcing steel bars, which also serve as the return circuits, while the surrounding concrete acts as the electrolyte. Concrete exposed to wet-dry cycles has sufficient conductivity to serve as the electrolyte. At the anodic location on the metal, the iron undergoes oxidation, which is accompanied by production of electrons and subsequent iron dissolution (Ahmad 2003). In other words, the anode is the location on a reinforcing bar where corrosion is taking place, metal is being consumed, and iron atoms lose electrons becoming iron ions (Fe^{+2}). The donated electrons move through a return circuit, which is a path in the metal itself to reach a cathodic spot on the metal, where these electrons are consumed through reactions involving substances found in the electrolyte. At the cathode, oxygen, in the presence of water, accepts these electrons to form hydroxyl ions (OH^-). Both the anodic and cathodic reactions are essential for the corrosion process to occur, and they must take place concurrently.

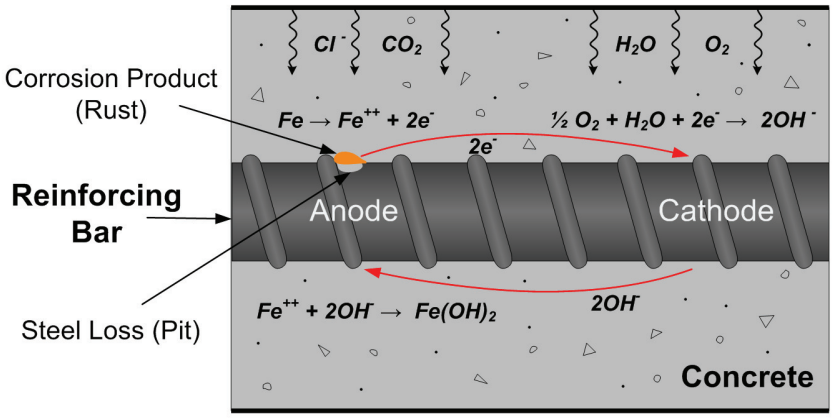

Figure 2-1: Schematic illustration of the corrosion of reinforcement steel in concrete as an electrochemical process (adapted from Ahmad, 2003).

If the iron were to dissolve in the pore water (ferrous ion Fe^{2+} is soluble), there would be no cracking and spalling of the concrete. However, unhydrated ferric oxide Fe_2O_3 has a volume of about twice that of the steel it replaces when fully dense. When it becomes hydrated, it dilates even more, which implies that the volume increase at the steel-concrete interface is even larger. The various corrosion products resulting from the corrosion of steel reinforcing bars occupy a volume that varies from two to six times that of the original steel (Liu and Weyers 1998), as illustrated by Figure 2-2.

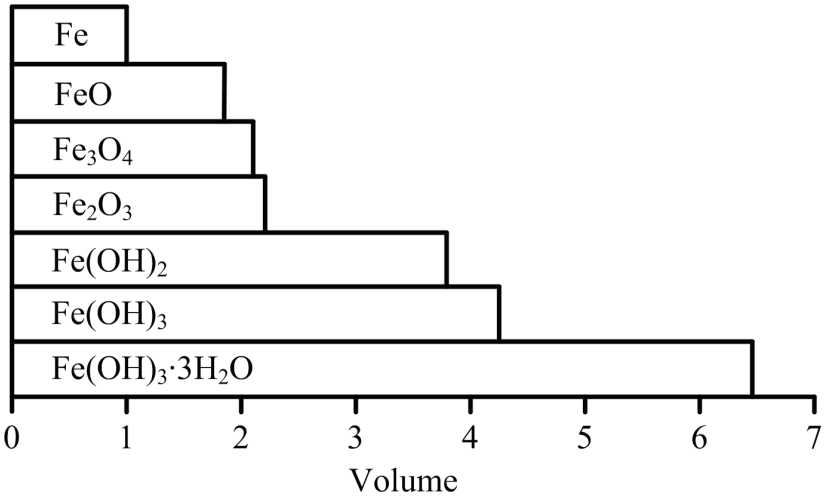

Figure 2-2: Relative volumes of iron and its corrosion products (adapted from Liu and Weyers 1998a).

Expansion of the corrosion products results in very high pressure stresses in the concrete surrounding the corroding steel, causing cracking, delamination, and spalling of the concrete cover (see Figure 2-3), which in turn further accelerates the corrosion process by providing an easy pathway for the water and chlorides to reach the steel. If left unattended, this process can ultimately lead to the loss of serviceability, strength, and safety of the affected structure.

The initiation of corrosion in an RC beam is likely to occur at the stirrup reinforcement surface, which has the minimum concrete cover. Then the overall corrosion mechanism of the tensile steel becomes more complex with portions of longitudinal bars acting as anodes and others as cathodes. If the anode and cathode are well separated (by several hundred millimetres) and the anode is starved of oxygen, for instance by being underwater, the iron as Fe^{2+} will stay in solution (Broomfield 2007). As a result there will be no expansive forces to

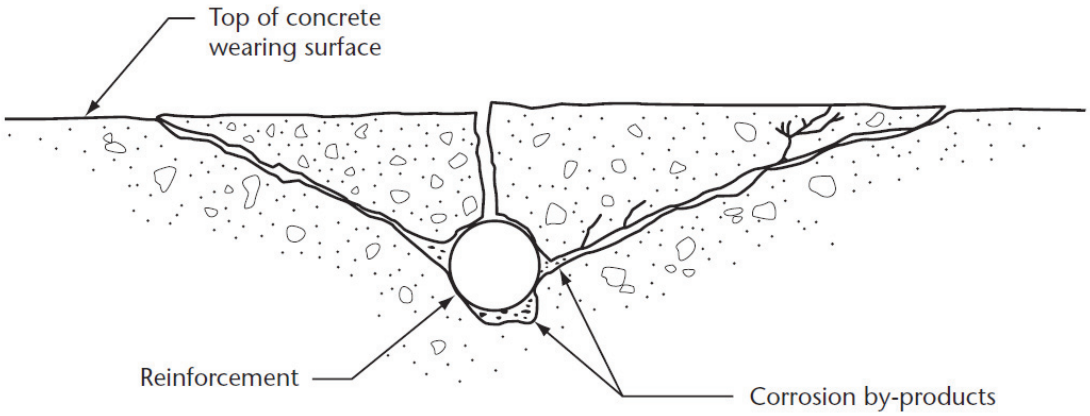

Figure 2-3: Corrosion-induced cracking and spalling of the concrete cover (reproduced from CAC 1995).

crack the concrete, thus the corrosion remains undetected. This type of corrosion, known as "black" rust due to the colour of the affected bar when first exposed to air after breakout, is often found under damaged waterproof membranes and in underwater and other water saturated conditions (Broomfield 2007). It is potentially dangerous as there is no indication of corrosion by cracking and spalling of the concrete and the reinforcing steel may be severely weakened before corrosion is detected. The rebar may be rapidly hollowed out or even completely penetrated and severed. Although occasional rust staining on the concrete surface may be indicative of this type of attack, the presence of water under a membrane excludes oxygen, making it unlikely that the iron solution will reach the concrete surface where it will precipitate out to form rust stains.

2.2.1. Generalized Corrosion

In the case of generalized corrosion the removal of the surface layer of steel is uniformly distributed over the surface area of the reinforcement bar. The changes in the surface conditions due to generalized corrosion are characterized initially by changes in the roughness of the surface, and then by the development of a less firmly adhering interstitial layer of corrosion products between concrete and steel (Capozucca 1995; Batis and Rakanta 2005). Visible signs of generalized corrosion, such as water staining, rust staining and concrete cracking, are normally apparent from routine inspection long before significant

structural weakening occurs. Generalized corrosion is typical of carbonation of the concrete cover.

2.2.2. Localized Corrosion

Chloride contamination of concrete in the field normally results in localized or pitting corrosion of reinforcement in the early stages. Localised corrosion occurs at discrete sites along the steel, often causing deep pits, the consequence of which leads to very rapid and significant loss of steel cross section (Batis and Rakanta 2005). Pitting corrosion can penetrate completely through the cross section of a reinforcing bar in a relatively short period of time. The corrosion products are the lower hydrated forms of iron oxide and are black in colour. These products are less expansive than the higher forms of iron oxides, or the orange-brown rust, commonly seen in the case of general corrosion. As a result, little disruption of the concrete is caused, and localised corrosion is far more difficult to detect than general corrosion. Localized corrosion usually occurs on the top reinforcement of bridge decks and substructures near leaking joints. At a more advanced stage of deterioration, which leads to serviceability failure, this type of corrosion can become widespread due to the formation of multiple pitting sites. The resulting deterioration resembles the effects of uniform corrosion, causing extensive cracking, staining, and spalling of the cover concrete.

According to Broomfield (2007), particular problems arise when the corrosion product is the black rust in unbonded post-tensioned structures, where corrosion is difficult to detect as the tendons are enclosed in ducts. Moreover, tendon failure can be catastrophic as tendons are loaded to more than 50% of their ultimate tensile strength, and modest section loss leads to failure under load. Although it is intended that in theory the tendon ducts be filled with an alkaline grout, which protects against water ingress and corrosion, in practice poor or incomplete grouting can allow the tendons to come into contact with water, leading to corrosion and fracture (Beard, Lowe et al. 2003). The problem is aggravated by the presence of salts from road treatments, which tend to further accelerate the corrosion process. The tendons are critical to the strength of the structure, and failure can result in the transfer of load to other tendons, leading to a chain reaction of failures that will eventually cause the

structure to collapse. Such catastrophic failure have occurred in the United States and the Europe, for example the collapse of a bridge at Ynys-y-Gwas in the United Kingdom (Woodward and Williams 1988).

2.3 Rate of Corrosion

Once the reinforcing steel has been depassivated, the corrosion rate is the determining parameter of the progress of corrosion-induced damage (Andrade and Alonso 1996). The corrosion rate can be described as the loss of metal per unit of surface area per unit of time. A model for the time-dependent loss of steel cross-sectional area as a function of corrosion rate can be derived using the relations for mass loss of reinforcing steel based on Faraday's Law, which is given by:

$$\Delta m_s = \frac{I_{\text{corr}} t A}{ZF} \tag{2.1}$$

where Δm_s is the mass loss in grams (g), I_{corr} is the corrosion current in amperes (A), t is the time in seconds (s), A is the atomic weight of iron (55.847g/mol), Z is the valence number or ion charge of Fe (2), and F is Faraday's constant (96487 Coulombs). Since the mass loss of iron may also be expressed as:

$$\Delta m_s = A_\phi y \rho_s \tag{2.2}$$

where A_ϕ is the surface area of bar (mm^2), ρ_s is the density of steel (0.00785 g/mm^3), and y is the amount of bar material depth loss due to corrosion (mm), as illustrated in Figure 2-4, by equating expressions (2.1) and (2.2), and solving for y results in:

$$y = \frac{I_{\text{corr}} t A}{\rho_s A_\phi ZF} \tag{2.3}$$

Since the corrosion current density, or rate of corrosion, i_{corr} ($\mu A/mm^2$) is the corrosion current I_{corr} (μA) per surface area of the bar ($i_{\text{corr}} = I_{\text{corr}} / A_\phi$), the above equation can be further simplified by expressing y in terms of the corrosion rate:

$$y = \frac{i_{\text{corr}} t A}{\rho_s ZF} \tag{2.4}$$

To facilitate calculation of the rate of bar depth loss as a function of time, Eq. (2.4) may also be expressed as:

$$\frac{dy}{dt} = \frac{i_{\text{corr}} A}{\rho_s Z F} \tag{2.5}$$

which, after substituting the known constants and assuming a constant annual rate of corrosion, evaluates to:

$$\frac{dy}{dt} = 0.0116 \cdot i_{\text{corr}} \tag{2.6}$$

The reduction in bar diameter as a function of time assuming uniform corrosion is therefore $\Delta d_b(t) = d_{bo} - 2y$. Hence the bar diameter at time t is simply:

$$d_b(t) = d_{bo} - 0.0232 \cdot i_{\text{corr}} \cdot t \tag{2.7}$$

where d_{bo} is the initial bar diameter in mm and t is the time elapsed since corrosion initiation in years.

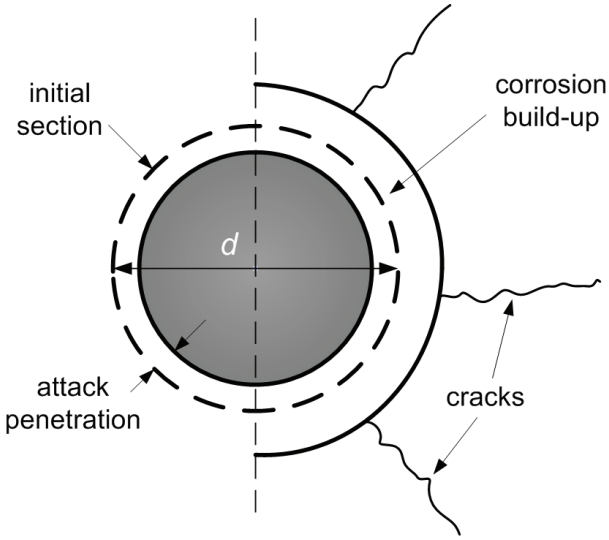

Figure 2-4: Consequences of bar corrosion (adapted from Martín-Pérez 1999).

Corrosion rates may be expressed as a current density (current per unit surface area), a rate of weight loss, or a rate of section loss. For steel, a corrosion current of 1 mA/m^2 approximates a weight loss of 10 g/m^2/yr, which in turn approximates to a section loss of 1 μm/yr. Reinforcing steel corrosion rates of 1 mA/m^2 or less are considered to be negligible and are

not likely to result in disruption of the concrete cover. Higher corrosion rates are considered to be significant and if oxygen has relatively easy access to the steel (the pore system is not saturated with water) general corrosion rates may exceed 100 mA/m^2. Local corrosion rates of up to 1000 mA/m^2 are possible (Glass and Buenfeld 2000).

The main factors that govern the rate of corrosion include the rate of oxygen diffusion to the reinforcing steel (Tuutti 1982), resistivity of the concrete pore solution (López and González 1993; Andrade and Alonso 1996), and temperature in the concrete (Tuutti 1982). Modelling the period during which reinforcing steel corrosion proceeds (propagation stage) is dependent on several random variables with large scatter and time- and space-variability. These include the rate of corrosion, type of corrosion products formed, and the geometry of corrosion build-up. Figure 2-5 illustrates the influence of corrosion time on the rate of corrosion, while the spatial and time variability of temperature inside an RC structure is shown in Figure 2-6.

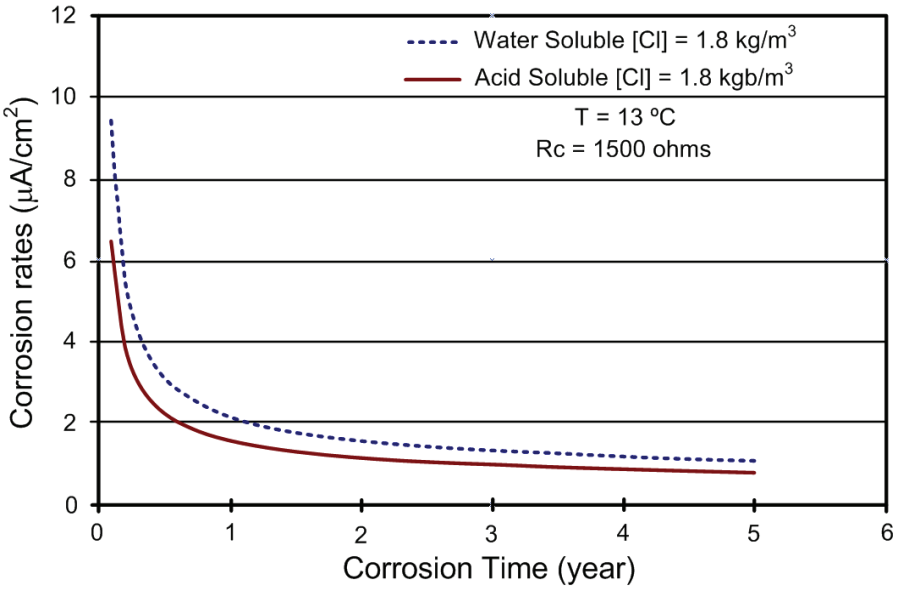

Figure 2-5: Effects of corrosion time on corrosion rate (adapted from Liu and Weyers 1998a).

In submerged marine environments, chloride contamination occurs relatively easily. However, access to oxygen is severely restricted by its low concentration in solution and its slow transport rate through waterlogged concrete. The corrosion rate will then depend on the rate at which oxygen can reach the steel. In above-ground structures, the presence of a passive film often restricts the overall rate, the corrosion rate effectively being under anodic

control. To increase the corrosion rate, further passive film breakdown must occur. One of the factors affecting the corrosion rate is therefore the level of chloride contamination. The chloride content will also affect the corrosion rate in dry or carbonated concrete via its effect on the resistivity of the environment. Chloride contamination may restrict the drying process. Other factors such as temperature and relative humidity will also affect the corrosion rate (Glass and Buenfeld 2000).

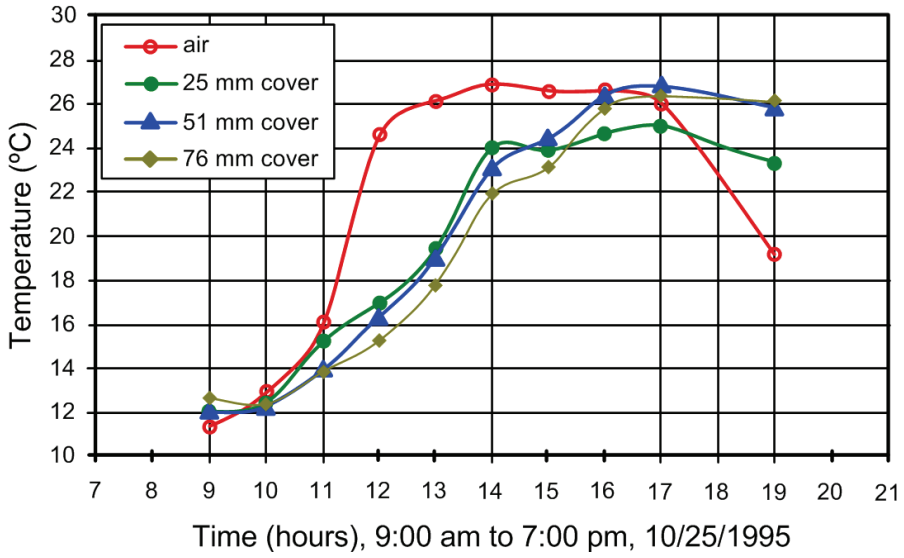

Figure 2-6: Changes of temperatures at different cover depths during daytime (adapted from Liu and Weyers 1998a).

If a certain amount of steel and concrete deterioration is considered to be part of the design service life of new structures or of the residual life of existing structures, then the corrosion rate that governs the propagation period should be included in service or residual life estimations. According to Liu and Wyers (1998) the time-to-cracking, from corrosion initiation to cracking of the cover concrete, is one of the critical time periods for modelling the time to repair, rehabilitate, and replace reinforced concrete structures in corrosive environments.

Vu and Stewart (2000) developed a structural deterioration reliability model to calculate probabilities of structural failure of RC slab bridges. Their model is an extension of a previous model proposed by Stewart and Rosowsky (1998b), in which the corrosion rate of steel reinforcement is governed by the availability of water and oxygen at the steel surface.

When relative humidity is high, the oxygen availability at the cathode is the controlling factor affecting corrosion rate. Because for many locations in Australia, U.S., Europe and Asia the average relative humidity is over 70%, the model assumes that the corrosion rate is limited by the availability of oxygen at the steel surface. As such, the oxygen availability depends on concrete quality (*w/c* ratio), cover, and environmental conditions (temperature and relative humidity). The oxygen diffusion rate is calculated from Fick's first law of diffusion with the oxygen diffusion coefficient obtained from Tuutti (1982). Based on these calculations, for a typical environmental condition (ambient relative humidity of 75% and temperature of 20ºC), the authors proposed an empirical equation for the influence of water-cement ratio *w/c* and cover on corrosion rate, given by:

$$i_{\text{corr}}(1) = \frac{37.8(1 - w/c)^{-1.64}}{\text{cover}} \tag{2.8}$$

where $i_{\text{corr}}(1)$ is the corrosion rate at the start of the corrosion propagation with units of μA/cm^2, and the cover is given in cm. The water-cement ratio is estimated from Bolomey's formula (1927), namely:

$$w/c = \frac{27}{f'_{\text{cyl}} + 13.5} \tag{2.9}$$

where f'_{cyl} is the concrete compressive strength of a standard test cylinder in MPa. Furthermore, unlike in earlier reliability models, the corrosion rate is not assumed to remain constant during the propagation period. This is based on the idea that the formation of rust products on the steel surface will reduce the diffusion of the iron ions away from the steel surface, which suggests that the corrosion rate will reduce with time (rapidly during the first few years after initiation, but then more slowly as it approaches a nearly uniform level). Using the data reported by Liu and Weyers (1998), Vu and Stewart (2000) developed an empirical relationship between the corrosion rate i_{corr} and the time elapsed since corrosion initiation t_P:

$$i_{\text{corr}}(t_{\text{P}}) = i_{\text{corr}}(1) \cdot 0.85 t_{\text{P}}^{-0.29} \tag{2.10}$$

where $i_{\text{corr}}(1)$ is given by Eq. (2.8), t_P is given in years, and $i_{\text{corr}}(t_{\text{p}})$ in units of μA/cm^2.

2.4 Corrosion-induced Damage in RC Flexural Members

Structural reinforced concrete has considerable reserves of strength, and thus safety is normally not an issue until the effects of deterioration, such as cracking, spalling, and excessive deformations, are clearly visible. In general concrete damage has to be well advanced before a reinforced concrete structure is at risk. Probably the most obvious effect of rebar corrosion is the loss of reinforcement volume. Certainly, the strength, serviceability, and ultimately, the safety of RC structures are diminished when significant loss of the reinforcing steel cross-sectional area has taken place. However, the fundamental problem with corrosion-induced deterioration of RC structures is not caused so much by loss of mechanical strength in the reinforcing steel but rather by the products of corrosion along the bar surface exerting stresses in the concrete matrix (Cabrera 1996). These stresses in turn lead to various other deterioration mechanisms including: (1) the loss of bond along the steel/concrete interface, (2) reduction of the flexural capacity (strength, stiffness, and ductility) of the member, (3) loss of serviceability, and (4) modification of the failure mechanism (for example from ductile to brittle behaviour). Figure 2-4 (page 13) shows a simplified schematic of the reduction of steel area together with expansion of corrosion products, which generate mechanical pressure resulting in longitudinal cracking of the surrounding concrete.

Current understanding of the damage mechanisms caused by corrosion of reinforcing steel originates primarily from two types of research efforts: (i) experimental investigations of RC beams and slabs subjected to electrically accelerated corrosion of the reinforcement, and (ii) detailed inspections of in-service RC structures, mainly bridges and parking structures located in aggressive environments. More recently, but to a much lesser extent, data is being collected from the very few RC structures instrumented for corrosion monitoring and data collection, such as the Confederation Bridge between New Brunswick and Prince Edward Island, Canada (Andersen 2006). This does not imply that active corrosion has been observed on the Confederation Bridge, but simply that current densities in the reinforcement are being monitored.

The results of a representative selection of such investigations are analysed in the following sections. It is very important to mention that the results of many experimental research studies on corroding RC beams are, for obvious practical reasons, conducted under accelerated corrosion regimes, while deformations are generally obtained under short-term loading conditions, leading to significant differences with behaviour observed in in-service structures or elements tested under sustained loading.

2.4.1. Influence of Corrosion on Reinforcement Bond Strength

According to results of experimental studies on pullout specimens (Al-Sulaimani, Kaleemullah et al. 1990; Cabrera 1996; Cairns and Millard 1999; Chung, Kim et al. 2008), following the initiation of corrosion and before cracking, there is a slight increase in the bond strength up to approximately 1% corrosion (percentage loss of reinforcement weight). This increase in bond strength is attributed to an increase in the friction force at the concrete/steel interface due to the accumulation of corrosion products (Cairns, 2000). This is in agreement with results obtained from RC beam tests damaged by accelerated corrosion, where bond strength increases up to a degree of corrosion of 0.4% due to the increase of radial pressure caused by the expansive corrosive products (Mangat and Elgarf 1999b). Beyond this degree of corrosion, bond strength decreases quite linearly as the percentage of corrosion increases, while the slip between steel and concrete increases significantly. Figure 2-7 illustrates the relationship between bond strength and percentage of corrosion based on published experimental data from pullout tests, for various bar diameters. Even though these tests were carried out to only 8% to 13% of corrosion, depending on bar diameter, the authors concluded that bond strength at higher corrosion levels was insignificant. However, results of tests at corrosion levels higher than 13% by Almusallam et al. (1996) indicate that residual bond strengths of approximately 10% to 15% of the original bond strengths remained up to about 80% of corrosion. Based on these observations, Val et al. (1998) proposed a model in which bond strength decreases linearly from a corrosion level of $c_1 = 0.4\%$ to $c_2 = 12\%$, after which the bond strength remains at 10%-15% of the original value (see Figure 2-8).

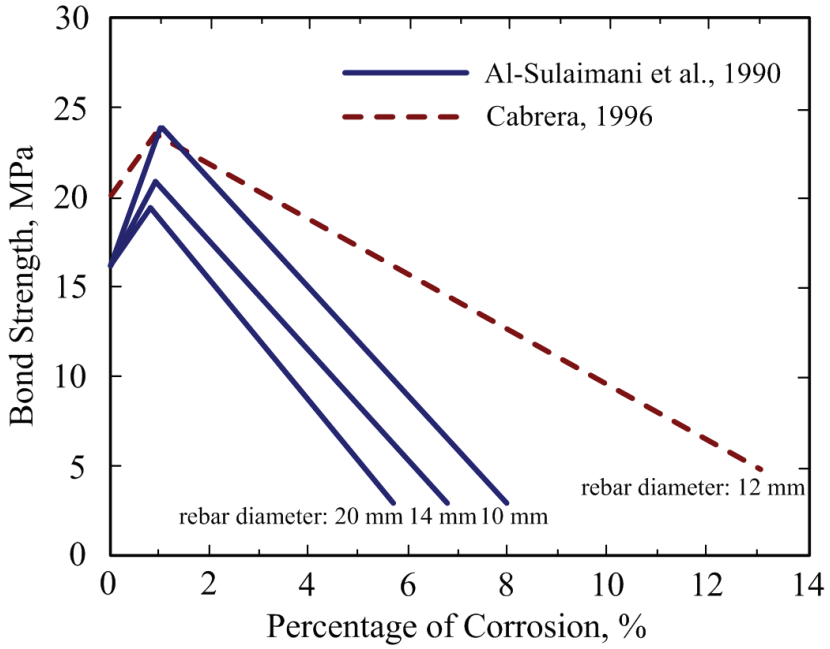

Figure 2-7: Test results for bond stress versus percentage of corrosion

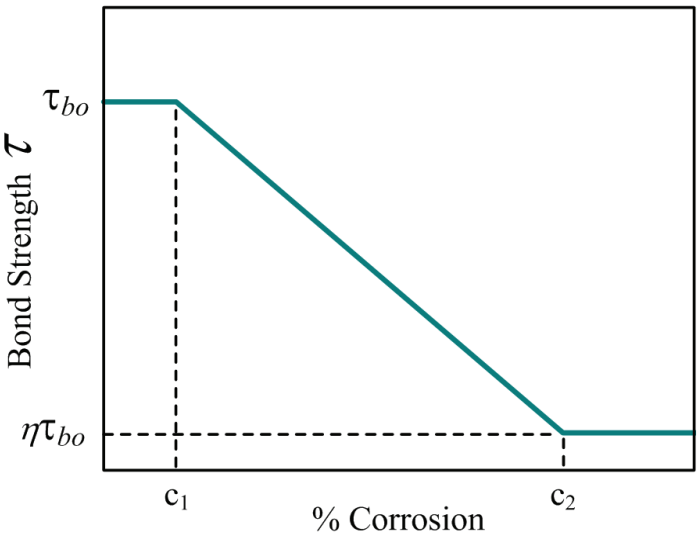

Figure 2-8: Assumed relationship for bond strength versus % corrosion (adapted from Val et al. 1998)

Overall, research shows that the reduction of bond strength is due to several concurrent deterioration processes, including: the loss of confinement provided by splitting of the surrounding concrete, the formation of a weak layer of corrosion products at the reinforcement interface, and a reduction of the effective area of the ribs that result in the weakening of the mechanical interlock between the rebar and concrete (Almusallam, Al-

Gahtani et al. 1996; Amleh and Mirza 2008; Berto, Simioni et al. 2008; Al-Hammoud, Soudki et al. 2010). The loss of bond strength due to corrosion influences beam behaviour differently depending on whether or not the loss happens at midspan or at end anchorages. When the bond loss occurs at midspan, loads are transferred to supports through a compressive tied arch, causing concrete crushing failure at smaller deflections than those of uncorroded beams (Rodriguez, Ortega et al. 1997). Cousin and Martín-Pérez (2010) reported the results of experimental research on the effects of corrosion on pre-tensioned pre-stressed beams subjected to sustained four-point loading. The authors reported that up to 60% of the loading capacity was lost at higher degrees of corrosion, whereas at lower corrosion rates the loading capacity was decreased up to 60% if the corrosion affected the anchorage length. Conversely, no significant decrease of the loading capacity was observed when the anchorage zone was not affected by corrosion (i.e., corrosion occurs in the midspan region). Therefore, corrosion-induced failure of bond at anchorages can be of significant consequences at negative moment regions in continuous beams, in particular at locations of lap splices.

Loss of bond strength also leads to a decrease in the effective development lengths in anchorage zones (Tastani and Pantazopoulou 2007). Further, it has been shown that transverse reinforcement is effective in reducing the effects of corrosion on bond strength, whereas the absence of transverse reinforcement or other confinement measures has a very substantial impact on deterioration of bond (Mangat and Elgarf 1999b; Fang, Lundgren et al. 2004). The observations of bond strength described above are based mainly on experimental tests of RC beams subjected to accelerated generalized corrosion. Castel et al. (2000) carried out experiments to study the behaviour of RC beams subjected to non-uniform corrosion, distributed randomly in intensity and space along the reinforcement. The test specimens consisted of four l6-year-old RC beams: two beams subjected to corrosion and two control beams. The corroded beams failed in flexure due to post yield rupture of the tension reinforcement at mid-span, at a 20% corrosion loss of steel. Since the flexural capacity of the corroded beams was observed to be 20% lower than that of the control specimens, the authors concluded that the loss of bond strength had no influence on the ultimate behaviour of reinforced concrete beams. However, the beams tested by Castel et al. (2000) were

subjected to short-term loads and not sustained loading, which was shown by Yoon et al. (2000) to have very significant impact on strength degradation and deflections of corroding RC beams. Together with the fact that these beams developed localized/pitting type of corrosion (not generalized), it is hardly surprising that loss of bond strength was not observed.

2.4.2. Influence of Corrosion on Flexural Capacity

The loss of flexural capacity of beams or girders is likely to be insignificant when localized pockets of pitting corrosion occur on the stirrup and longitudinal reinforcement bars. Large reductions in flexural capacity (strength and rigidity), rendering a beam inadequate for service loads, are likely to occur only when localized pitting has extended to many sites resulting in extensive and relatively uniform levels of corrosion. Such corrosion would cover a sufficiently large surface area of reinforcement to cause considerable cracking, staining, and spalling of the concrete cover zone. Once substantial amounts of deterioration have occurred, the mechanisms by which a beam resists load are modified. Complete breakdown of the bond between steel and concrete would result in a beam being incapable of behaving as a conventional RC beam. Instead, such a member could carry the load by acting as a tied arch, provided there was adequate mechanical anchorage at the bar ends.

Most research indicates that reduction of flexural capacity is clearly related to the degree of corrosion. Experimental studies by Almusallam et al. (1996) and Mangat and Elgarf (1999a) provide a representative example of flexural strength degradation as a function of corrosion, as illustrated in Figure 2-9. Load deflection curves for one-way slabs tested at various degrees of corrosion in Figure 2-10 further underline the empirical observations related to loss of capacity. As observed in studies on bond strength, Figure 2-9 shows a slight increase in the ultimate flexural strength of the slab up to approximately 1% corrosion loss, followed by a non-linear decay in strength with increasing degree of corrosion. Similarly, the load-deflection curves in Figure 2-10 illustrate not only the loss of load carrying capacity at various degrees of corrosion, but also the dramatic reduction in deflection limits and severe loss of ductility. This phenomenon has been observed by other researchers as well (Al-Hammoud, Soudki et al. 2010).

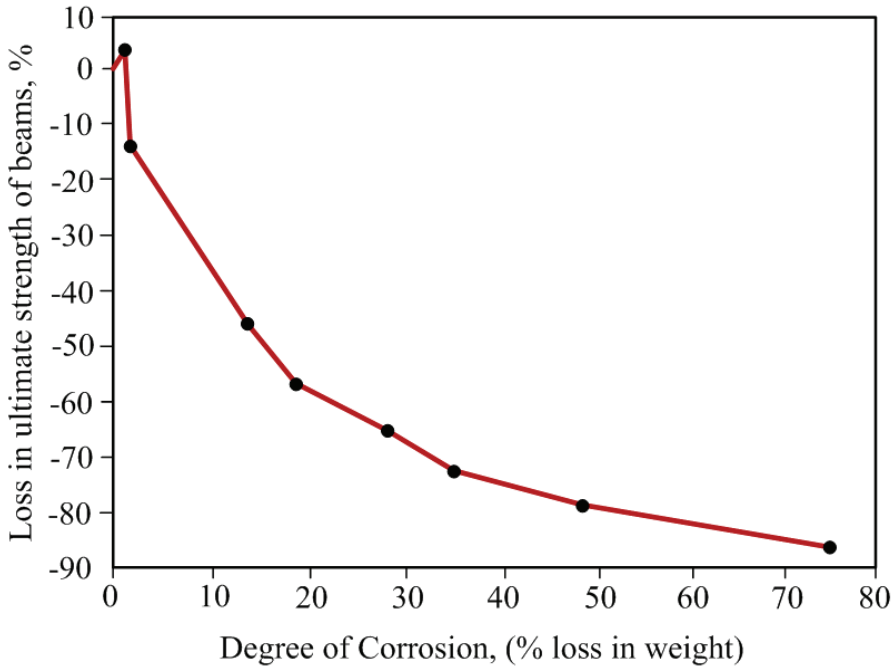

Figure 2-9: Loss of ultimate strength in RC slabs with varying degrees of corrosion (adapted from Almusallam et al. 1996).

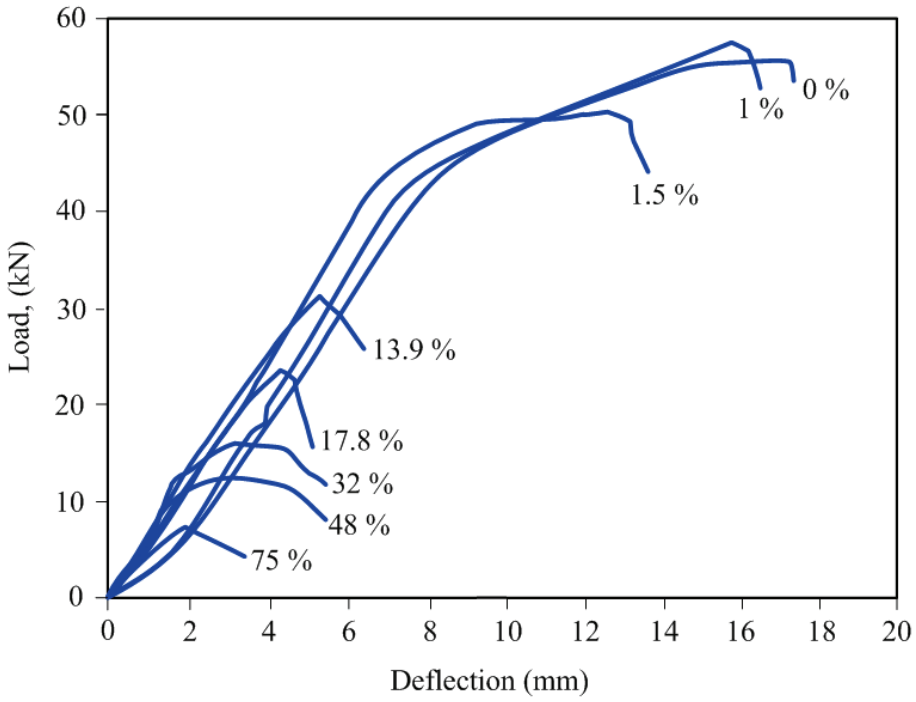

Figure 2-10: Load-deflection curves for RC slabs with varying degrees of corrosion (adapted from Almusallam et al. 1996).

These graphs show corrosion-induced degradation of RC flexural elements due to a combination of causes and not only to the reduction of reinforcement cross-section/weight. The loss of ultimate capacity is due to several mechanisms including: loss of bar section, loss of bond strength, and possible loss of bar ductility (Palsson and Mirza 2002; Cairns, Plizzari et al. 2005). Calculations of flexural capacities based only on reduced areas of reinforcement showed little agreement with the flexural strengths observed in experimental results. For instance, for a 10% loss of steel section the calculations indicated a flexural strength of 80% of uncorroded beam capacity, while the corresponding experimentally observed remaining moment capacity was less than 30%, strongly suggesting that bond strength reduction is the primary mechanism responsible for the reduction in flexural capacity (Mangat and Elgarf 1999a). The authors also investigated the effect of different constant corrosion rates. The results show that rebar subjected to high rates of corrosion in beams with the reinforcement already at a high degree of corrosion lead to a significant decrease in flexural capacity. Conversely, rebar subjected to various corrosion rates (low to high) at low degrees of corrosion had insignificant effect on the flexural strength of the beams investigated.

Similarly, the load-deflection curves in Figure 2-10 were obtained from experimental tests of RC slabs subjected to accelerated corrosion regimen in the absence of sustained loading, which is drastically different from actual in-situ service conditions. This is not conservative since the corrosion and associated degradation processes would be enhanced under sustained loading leading to earlier than predicted loss of strength, stiffness, and ductility. Furthermore, the above curves imply that the initial stiffness of the members at increased levels of corrosion (from 1.5% to 75%) is significantly higher than for members with low degrees of corrosion (0% and 1%). However, results of experimental studies of RC beams subjected to corrosion attack under sustained loading not only show large increases in deflections, but more importantly, no increases in the stiffness during the corrosion process (Malumbela et al., 2009).

In corrosion-induced loss of flexural capacity in RC-beams, the variables of highest impact are: the degree and rate of corrosion, the size (diameter) of bar, and the yield strength and ductility of the steel. The strength of concrete does not have much direct influence on

strength loss; however, high strength/quality concretes perform better due to the denser mix slowing diffusion of chlorides. Bar diameter has a more complex influence on flexural performance of RC beams. Obviously, large diameter bars lose far less (%) sectional-area/mass of steel for a given rate of corrosion in proportion to smaller diameter bars. Conversely, as mentioned in the previous section, larger bars produce more corrosion products resulting in the transfer of higher radial stresses into the concrete matrix than smaller diameter bars. This in turn leads to a more rapid breakdown in bond strength, which in turn accelerates the reduction of flexural capacity of the beam. More research is required to investigate which effect governs the strength degradation of RC beams at various bar diameters, allowing the optimal selection of bar diameters in design to minimize the effects of corrosion.

2.4.3. Influence of Corrosion on Serviceability

In the context of corrosion, both cracking and deflections should be considered together because they are coupled. The loss of bond strength and beam rigidity lead to increasing deflections, which in turn cause cracks to open and grow, providing greater access for chlorides, carbon dioxide, oxygen, and water to enter the RC structure, further fuelling and perhaps increasing the processes of corrosion. This was confirmed by Yoon et al. (2000) in tests of beams under sustained loading conditions. The authors argued that the effect of the service load level and the extent of cracking should be included in service life predictions of structures in corrosive environments. The corrosion causes the formation of longitudinal cracks along the plane of the bar and corner cracking around the end bars. The extension of the cracks to the outer face of the member can result in delamination and loss of cover concrete, with the added risk of large pieces of concrete falling away from the structure. The corners of members generally crack first due to the fact that the oxygen, water, chlorides and carbon dioxide have multiple pathways to the steel from the orthogonal faces.

Experimental and analytical research on RC beams conducted by Cabrera (1996) focused on the relationship between corrosion rate and loss of structural serviceability, particularly cracking and deflections. The experimental component consisted of tests on small-scale simply-supported RC beams exposed to accelerated corrosion and short-term four-point

loading. Tension steel was not anchored at beam ends. It was concluded that: (i) there is an inverse relationship between the depth of cover to reinforcement and the degree of corrosion; crack intensity increases with increasing depth of cover and this can be related numerically to the degree of corrosion expressed as weight loss per unit area; and, (ii) corrosion caused significant increases in the mid-span deflection of the beams tested. At a corrosion level of 9%, the deflections observed in the corroded beams were 50% greater than deflections of the non-corroded beams. Some of the beams failed due to excessive slip of the reinforcement at the free ends of the beam (anchorage zone).

However, like many other experimental tests, the beams tested by Cabrera (1996) were not subjected to sustained loading, leading some researchers to argue that applied loads play a central role in the opening and growth of cracks, which significantly affects the supply of oxygen and moisture required for corrosion. Moreover, Ballim and Reid (2003) argued that not only do the stresses induced by corrosion affect the serviceability of the structure but also the duration of the applied loads. The analytical results were also challenged, because analytical equations predict lower deflections than those observed in the lab and in the field, by not accounting for the coupled action of sustained loads and corrosion processes.

The main variables influencing the cracking in corroding RC beams include: rate of corrosion, bar diameter, spacing between bars, and the proximity of bars to the member faces/corners, simpler put, the clear cover. Deflections are further a function of the bond strength, steel ductility, and sectional rigidity, which are directly influenced by the cracking parameters.

2.4.4. Influence of Corrosion on Failure Mode

The mechanical pressure due to the volume expansion of corrosion products along the bar surface leads to longitudinal cracking. The opening and growth of longitudinal cracks and the consequential loss of bond can affect the failure mode of RC flexural members resulting in brittle failure (Al-Sulaimani, Kaleemullah et al. 1990). As observed by Almusallam (1996), the reduced ductility of the beam with increasing degree of corrosion (Figure 2-10) results in a sudden failure mode similar to the brittle failure of over-reinforced beams. It is believed

that this brittle splitting failure occurs when the longitudinal cracks extend vertically into the concrete compression zone. Although Castel et al. (2000) observed cracks in the compression zone in one of their tested beams, this seemed to have no effect on the flexural strength of that specimen and brittle failure did not occur. Furthermore, it was reported that as the applied load was being increased, the crack widths gradually decreased. However, as proposed by Yoon et al. (2000), the propagation of vertical cracks into the compression zone is controlled by the microcracking resulting from the sustained loading.

The failure mode is also very strongly influenced by the corrosion process, whether it is generalized or localized corrosion. While general corrosion usually leads to the loss of bond, local corrosion is associated with the loss of cross sectional area and ductility of reinforcement. As a result, the failure modes corresponding to each corrosion mechanism can be stated as follows: generalized corrosion results in bond failure, whereas localized (pitting) corrosion leads to premature yielding (loss of serviceability) and ultimately failure due to rupture of tension reinforcement. These observations are supported by research done by Castel et al. (2000), who observed that the local loss of steel section under long-term localized corrosion regime was much greater than the uniform loss of sectional area in accelerated generalized corrosion, resulting in the mode of failure being yielding rather than bond failure. Hence, the assumption that the effects of damage are similar at the advanced stages of corrosion regardless of whether damage is randomly distributed or uniform is not necessarily accurate. As suggested by Cairns and Millard (1999), generalized and localized corrosions should be assessed separately.

2.5 Probabilistic Methods in Durability Design

A framework to account for the durability and performance of concrete structures throughout their service life has recently been developed by a European Brite-Euram project termed – DuraCrete (DuraCrete 2000; Rostam 2003). This framework allows for the treatment of deterioration mechanisms to be modelled on a probabilistic level and introduces them in the general design of structures, implying that design for safety and for durability can be performed using similar procedures. Similar provisions for durability design are

recommended in CSA S408-11 (2011). In theory, this would allow infrastructure owners to make decisions regarding acceptable long-term performance and the consequences regarding future maintenance and total life-cycle costs.

The DuraCrete methodology was developed by taking into account:

- The geometry of the structure
- The materials used for construction
- The environment in which the structure is located
- The quality of the execution of concrete works
- The main deterioration mechanisms, but especially highlighting reinforcement corrosion
- The planned inspection of the structure

This new durability design methodology is based on the reliability theory as traditionally used in structural design. The purpose of a reliability analysis is to determine the probability of a given event; here the event is that one marking the end of the service life. This formal, or design, end of service life may not necessarily be the real end of the useful life of the structure (Rostam 2003). In the past, steel depassivation has often been used as the end of the design life for the design of a new structure subjected to a corrosive environment (Broomfield 2007), and it has been treated as a serviceability limit state. Figure 2-11 shows in principle the life performance of a reinforced concrete structure with respect to reinforcement corrosion and related events. The following events can be used to identify the service life limit states (Rostam 2003; CSA S408-11 2011):

1. Depassivation of reinforcement
2. Cracking of concrete cover
3. Spalling of concrete cover (or delamination)
4. Collapse

In general, points 1 and 2 in Figure 2-11 represent events related to the serviceability of the structure, point 3 is related to both serviceability and ultimate limit states, and point 4 represents an ultimate limit state (Rostam 2003).

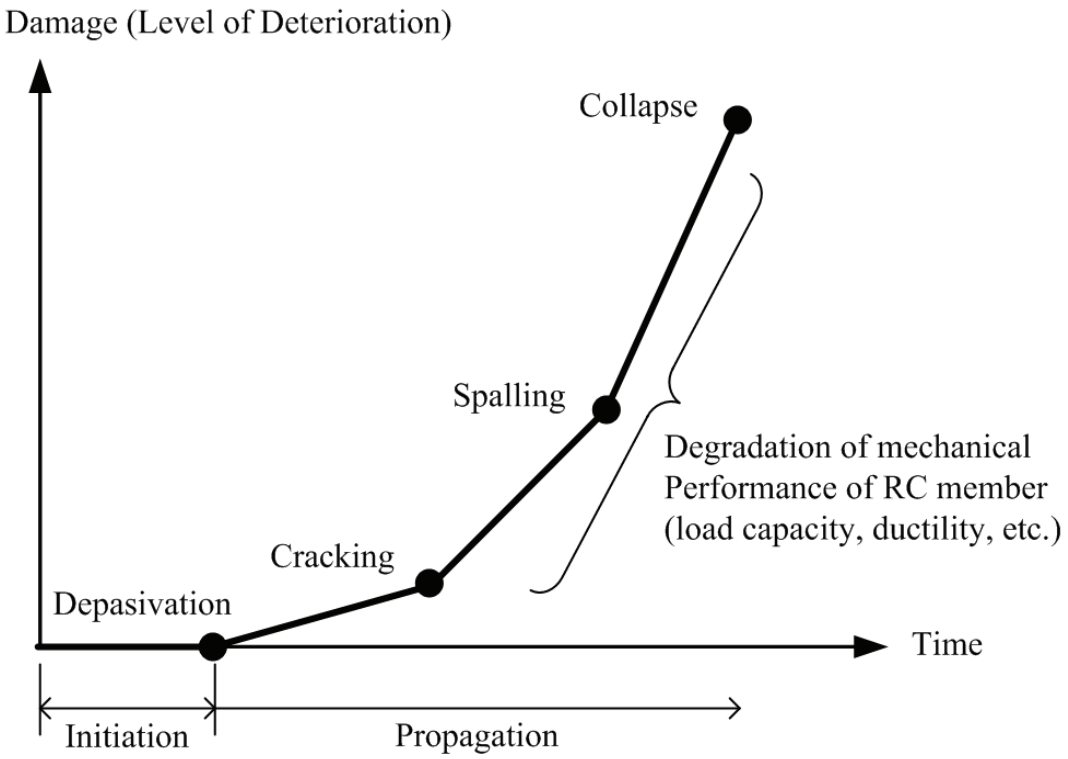

Figure 2-11: Deterioration stages of an RC structure with respect to reinforcement corrosion (adapted from Rostam 2003)

Reaching the considered limit state is described in terms of a limit state function $g(\boldsymbol{X},t)$, where $\boldsymbol{X}$ denotes the vector of basic variables and t is time. Having identified the failure event or limit state relevant for a design, the second step in the durability design process is to analyse the environmental actions and to identify the relevant degradation mechanisms. The limit state function can thus be rewritten as $g(\boldsymbol{X},t) = R(\boldsymbol{X},t) - S(\boldsymbol{X},t)$, where $R(\boldsymbol{X},t)$ and $S(\boldsymbol{X},t)$ denote a time-variant resistance (resistance against ingress of aggressive substances and resistance against deterioration) and a load variable (aggressiveness of the environment), respectively. A schematic representation of this problem is shown in Figure 2-12 (Rostam 2003; CSA S408-11 2011). The problem can be solved using reliability methods such as FORM / SORM, which are briefly explained in Appendix A.

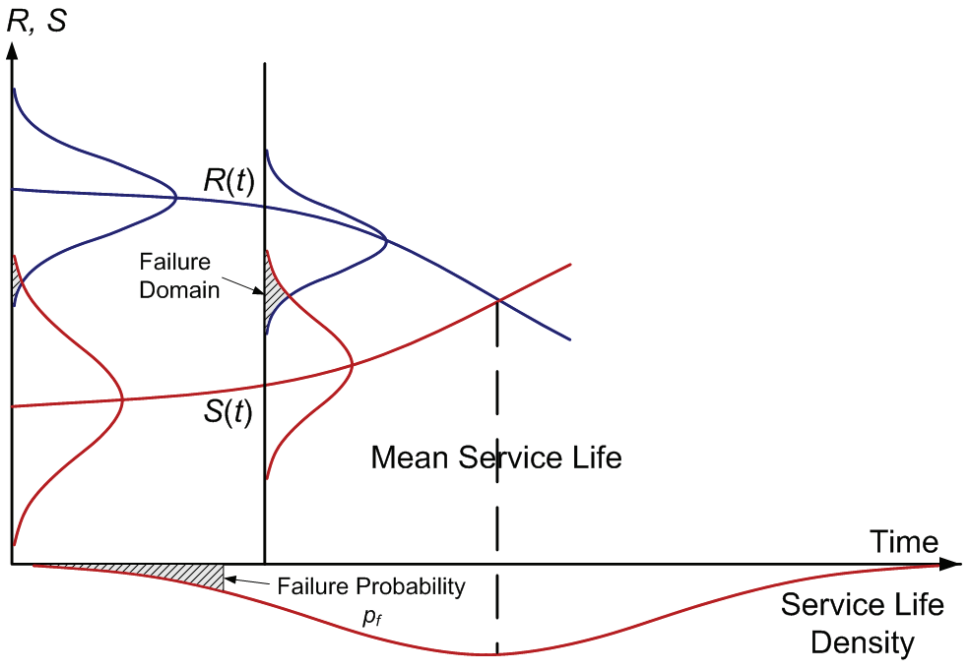

Figure 2-12: Probability of corrosion initiation and target service life.

2.6 Probabilistic Models of Corrosion-Induced Damage in RC

Although frameworks for durability design against reinforcement corrosion have been developed, the application of these probabilistic methods to the modelling of corrosion-induced damage in RC has been very limited. Most of the available models were developed to determine when corrosion is initiated (steel depassivation), while ignoring the corrosion propagation stage when damage actually occurs. Often it had been assumed that failure occurs when corrosion is initiated. This section summarizes the most recent and relevant probabilistic models of corrosion-induced damage in RC structures found in the literature.

Enright and Frangopol (1998) proposed a probabilistic model of the resistance degradation in RC bridge beams subjected to reinforcement corrosion. The model considers both the initiation and propagation stages of corrosion. An equation to calculate the corrosion initiation time is derived from Fick's law of diffusion, based on the assumptions that corrosion is initiated by the diffusion of chloride ions and that the concentration of chloride ions near the surface of the reinforcement is constant. For corrosion propagation, the authors

assumed that loss of strength of an RC beam is due primarily to the reduction of cross-sectional area of the steel reinforcement (i.e., bond loss was not considered). The time-variant area of steel reinforcement for an RC element with equal diameter bars and with the same corrosion initiation times was given by:

$$A(t)=\begin{cases}\dfrac{n\pi}{4}D_i^2 & \text{for } t \le T_1 \\ \dfrac{n\pi}{4}D(t)^2 & \text{for } T_t < t < T_1 + D_i/(0.0232\cdot i_{corr}) \\ 0 & \text{for } t \ge T_1 + D_i/(0.0232\cdot i_{corr})\end{cases} \tag{2.11}$$

where n is the number of reinforcing bars, D_i is the initial diameter of the rebars, t is the elapsed time, T_1 is the corrosion initiation time, i_{corr} is the corrosion rate, and the diameter of the reinforcing steel bars at time t is given by:

$$D(t) = D_i - 0.0232\cdot i_{corr}\cdot(t - T_1) \tag{2.12}$$

Similar expressions were also given for the general case where reinforcement consists of bars of different diameters and which begin corrosion at different times. Note that the coefficient of i_{corr} in Eq. (2.12) (i.e. 0.0232) is derived from the application of Faraday's law, as shown in Eq. (2.7).

Enright and Frangopol (1998) proposed the time variant resistance of an element as the product of the initial resistance (R_o) and a resistance degradation function $g(t)$:

$$R(t) = R_o \cdot g(t) \tag{2.13}$$

The resistance degradation function $g(t)$ is expressed in terms of a single random variable k:

$$g(t) = 1 - kt^{\alpha} \tag{2.14}$$

where t is the elapsed time in years and α is a rate parameter. The initial resistance R_o is determined from the equations for nominal resistance in relevant design codes. The final

cumulative time-failure of a bridge element subjected to environmental attack, such as corrosion, is given by:

$$p_f\left(t_L\right)=1-\int_0^{\infty}\int_0^{\infty}\exp\left[-\lambda_{s_1}t_{\mathrm{L}}\left[1-\frac{1}{t_{\mathrm{L}}}\int_0^{t_{\mathrm{L}}}F_{s_1}\left\{r\cdot g\left(t\right)-s_2\right\}dt\right]\right]f_{s_2}\left(s_2\right)f_{R_0}\left(r\right)ds_2dr \quad (2.15)$$

where $p_f(t_L)$ is the cumulative time-failure probability from 0 to time t_L, S_1 is the time-variant (live) load, λ_{S1} and $F_{S1}(\cdot)$ are the mean occurrence rate and the cumulative distribution function of the time-variant (live) load, respectively, $g(t)$ is the resistance degradation function, S_2 is time-invariant (dead) load, $f_{S2}(\cdot)$ is the probability density function of the time-invariant (dead) load, and $f_{Ro}(\cdot)$ is the probability density function of the initial resistance.

A comprehensive probabilistic structural deterioration model was also developed by Stewart and Rosowsky (1998; 1998b) to calculate the probabilities of structural and serviceability failures (flexure and spalling limit states) for typical RC continuous slab bridges. Corrosion was considered to result from the application of de-icing salts and/or exposure to marine sea spray, and flexural (transverse) cracking. The model accounts for the random variability of the diffusion of chlorides, corrosion rates, concrete material properties, element dimensions, reinforcement placement, environmental conditions, and loads. As in the model of Enright and Frangopol (1998), Eq. (2.12), it is assumed that corrosion will lead to a uniform reduction in the cross-sectional area of the reinforcing steel; however, the deterioration is expressed in terms of a reduction in bar diameter $D(t)$:

$$D\left(t\right)=\begin{cases}D_i & t\le T_1\\ D_i-2\lambda\left(t-T_i\right) & T_i<t<T_i+\left(D_i/2\lambda\right)\\ 0 & t>T_i+\left(D_i/2\lambda\right)\end{cases} \quad (2.16)$$

where D_i is the initial diameter of the rebars, T_1 is the time to initiation, and λ is the corrosion rate (at a surface), which is approximated as $0.0116\cdot i_{corr}$ (mm/yr). The current density i_{corr} is taken as a uniformly distributed random variable (within the range of 1 ~ 2 μA/cm^2). It is hence assumed that the corrosion rate is constant once corrosion has been initiated, and that it is not affected by cover thickness, concrete quality or longitudinal cracking and spalling.

Pitting corrosion is neglected because the authors declare that since pitting is spatially distributed, it is unlikely that many bars will be affected by pitting, and therefore pitting corrosion will not significantly influence the structural capacity at any given cross-section. The time to longitudinal cracking and spalling is predicted using the Liu and Weyers (1998) model, which treats the concrete cover as a thick-wall cylinder subjected to the pressure generated by the build-up of corrosion products. Loss of bond was not considered because of the assumption that bond loss does not have a significant effect on the reliability of bridge elements in flexure.

Like the model proposed by Enright and Frangopol (1998), Stewart and Rosowsky (1998; 1998b) also recognized that the structural resistance is time-dependent ($R(t)$) and loads may occur randomly in time and intensity. The total bridge load is the sum of the dead and truck (live) loads. For multiple-lane bridges, the critical load effect occurs when two heavily loaded trucks are side-by-side. Given that the number of crossings of two heavily loaded fully correlated trucks per year is N and the truck weight is normally distributed, then the distribution of the heaviest truck weight w (annually) is simply:

$$F_n(w) = \left[\Phi\left(\frac{w - \mu_w}{\sigma_w} \right) \right]^N \tag{2.17}$$

where μ_w and σ_w are the statistical moments of truck live load and $\Phi(\,)$ is the standard normal cumulative distribution. Assuming that n independent load events (S_j) occur within the time interval (0, t_L) at deterministic time intervals t_j, then the cumulative probability that the structure fails (strength limit state) anytime during this time interval is given by:

$$p_f(t_L) = 1 - \Pr\left[\left(R(t_1) > S_1 \right) \cap \left(R(t_2) > S_2 \right) \cap \ldots \cap \left(R(t_n) > S_n \right) \right] \tag{2.18}$$

Equation (2.18) recognizes that the probability of failure is dependent on the prior load and resistance histories and not simply on the extreme load up to time t_L and resistance at time t_L, as assumed in time-invariant reliability analyses (Figure 2-13). For the serviceability limit state (longitudinal cracking and spalling), the probability of spalling p_s is given by:

$$p_s(t) = \Pr(t > T_{cr}) \tag{2.19}$$

where T_{cr} is the time to longitudinal cracking and spalling. Because Eqs. (2.18) and (2.19) cannot be expressed in closed form, Monte Carlo simulation was used to calculate the time-dependent probabilities of structural failure and spalling for annual increments over the lifetime of a bridge. The model was verified with field data and was used to perform a lifetime reliability analysis of a three-span RC slab bridge. It was concluded that the application of de-icing salts cause significant long-term deterioration and reduction in structural safety and that concrete cover and concrete compressive strength have the greatest influence on the probabilities of spalling and collapse.

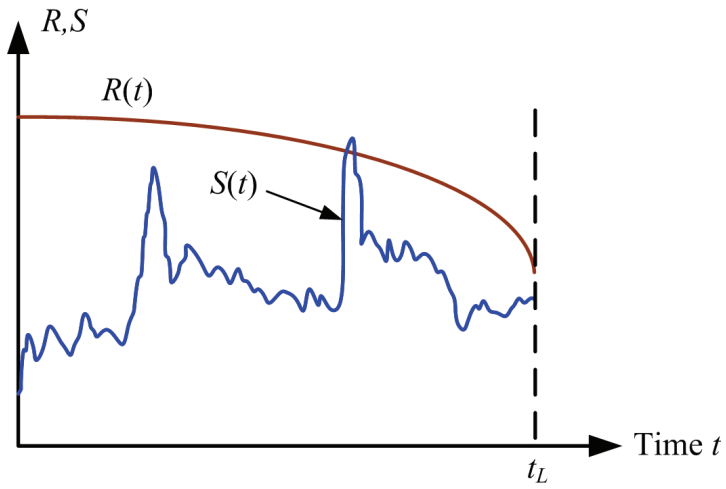

Figure 2-13: Realization of load effect $S(t)$ and resistance $R(t)$ (reproduced from Stewart et al. 1998b).

Vu and Stewart (2000) developed a structural deterioration reliability model to calculate probabilities of structural failure of RC slab bridges. This model is an extension of the Stewart and Rosowsky (1998) model described above. Improvements consist of more accurate corrosion initiation and propagation models that include the effect of durability specifications on time-variant corrosion rates, a time-variant loading model, and a shear failure limit state. To account for time-variant load effects, it was suggested that traffic loads and volume will continue to increase with time. Given that annual increases in trucks loads and heavy traffic (truck) volume are represented by λ_m and λ_v, respectively, then the time-variant cumulative distribution of the weight of the heaviest truck w (annually) is given by:

$$F_n(w,t) = \left[\Phi\left(\frac{w - \mu_w (1+\lambda_m)^t}{\sigma_w (1+\lambda_m)^t} \right) \right]^{N(1+\lambda_m)^t} \tag{2.20}$$

where, as in Eq. (2.17), t is time in years, μ_w and σ_w are statistical parameters of live load for a single truck, and Φ is the cumulative function of the standard normal distribution. Annual maximum truck loads are assumed statistically independent. As in the Stewart and Rosowsky model (1998), the cumulative probability of failure is given by Eq. (2.18). Likewise, the computational procedure in the analysis of RC slab bridges was carried out through Monte-Carlo simulation.

2.7 Gap in the State of the Art

A review of the literature highlights the need to account for corrosion-induced damage in the evaluation of the safety of corrosion affected RC beams. Experimental evidence has shown that the loss of cross-sectional area and the reduction of bond interaction between concrete and steel due to corrosion adversely affect the strength and ductility of RC flexural members. While the loss of steel cross section has been taken into account by most probabilistic models developed to estimate the reliability of such members, there has been limited effort to consider corrosion-induced decrease in bond strength. Furthermore, reliability models of RC beams subject to reinforcement corrosion are based on sectional analysis, ignoring the nonlinear effects of corrosion-induced damage. This work attempts at accounting for these effects by coupling nonlinear finite element modelling of corrosion-induced damage of RC beams with probabilistic analysis to estimate the time-dependent reliability of these members.

Chapter 3. A Stochastic Finite Element Analysis Framework

3.1 Introduction

The modelling, analysis, and design of RC structures are commonly performed with the assumption that values of the input parameters are deterministic. However, uncertainties in these values are always present, and consequently they should be considered as random variables.

The first mathematical formulations of the structural safety problem can be attributed to Mayer (1926), Wierzbicki (1936), and Streletzki (1947). They recognized that the load and resistance parameters are random variables and therefore, for each structure, there is a finite probability of failure. Their concepts were further developed by Freudenthal (1947; 1956). However, since the formulations involved convolution functions that were too difficult to evaluate by hand, the practical applications of reliability analysis were not possible until the pioneering work of Cornell and Lind in the late 1960s and early 1970s (Nowak and Szerszen 2000) wherein Cornell (1969) proposed a second moment reliability index while Hasofer and Lind (1974) formulated a format-invariant reliability index. An efficient numerical procedure for calculation of the reliability index was then formulated by Rackwitz and Fiessler (1978). Since then, and through many further contributions, the reliability methods reached a degree of maturity, becoming the basis for the development of new codes.

The first generation design standards, for example the Allowable Stress Design (ASD) approach, introduced the idea of deterministic safety factors, which were intended to reduce the likelihood of failure but without any way to quantify the actual levels of reliability in the structures designed according to such approach (Melchers 1987). By utilizing the ideas mentioned in the last paragraph, nominal safety factors have given way to the more rational

partial factor safety formats, such as the Load and Resistance Factor Design (LRFD) and Limit States Design (LSD) philosophies utilized in most current building codes and design standards. These have been increasingly underpinned by structural reliability theory.

The advent of performance-based engineering has placed an increased emphasis on realistic simulation of structural behaviour under complex loading mechanisms. Instead of the traditional prescriptive and non-transparent code rules aimed at ensuring life safety, next generation codes will include additional performance indicators, for example, amount of damage, monetary loss, and reduction in functionality (Koduru S.D. and Haukaas 2006). In addition, there remains an increasing demand for safety assessments outside of conventional code formats. Such assessments are frequently necessary for the design of critical or unique structures or for the determination of the remaining service life in existing structures, particularly where safety or economic considerations are significant. The time-dependent deterioration of RC structures due to corrosion of reinforcement is a particularly challenging problem and there exists a demand in the civil engineering community for lifecycle decision support tools dealing with this problem.

Accurate decision tools depend on comprehensive numerical modelling for realistic representation of non-linear structural behaviour. In addition, because uncertainty is present in every aspect of the analysis, the prediction of structural performance must be carried out within a reliability framework (Melchers 1987). In general, for realistic and hence typically complex structural and geotechnical infrastructure systems this is an enormous computational task. This follows easily when considering the coupling of advanced reliability analysis methods with complex structural analysis such as finite elements. The resulting methodologies are often referred to as Stochastic Finite Element Analysis (SFEA) or SFEA-based reliability methods.

Fundamentally, in SFEA-based methods, structural reliability analysis provide the basis for modelling and quantification of uncertainties and computation of probabilities, while the finite element method (Cook 1981; Bathe 1996; Zienkiewicz and Taylor 2000) provides the necessary computational approach for analyzing complex structures and continuum systems. The application of these two concepts in a closely integrated fashion is the basis of stochastic

finite element analysis, and results in a powerful tool for realistically dealing with practical engineering problems while accounting for system uncertainties. As with finite element analysis, SFEA methods are generally applicable to both linear and nonlinear structural problems (Haukaas and Kiureghian 2004). The phrase stochastic finite element analysis is loosely employed here to describe the explicit treatment of uncertainty in any system quantity within the framework of the finite element method. The fundamental concepts of structural reliability theory are introduced and discussed in Appendix A.

This chapter describes the development of a SFEA Framework for RC flexural members with corroding reinforcement. The merit of using SFEA is explained, and relevant methodologies are reviewed and evaluated for their applicability to time-dependent reliability analysis of RC structures. After considering the issues related to practical implementation of the various techniques, a SFEA Framework is proposed along with the rationale behind it. Finally, a case study which is used to illustrate the implementation of the proposed framework, as well as its constitutive components, is introduced.

3.2 Merit of Stochastic Finite Element Analysis

The probabilistic approach has a solid theoretical foundation and the advantage of the Bayesian methodology to separate aleatory and epistemic components of the uncertainty and to assess distributions of epistemic random variables. Aleatory (objective) uncertainty refers to an intrinsic variability of certain quantities, such as the wind pressure on a structure. By contrast, epistemic (subjective) uncertainty refers to a lack of knowledge about certain aspects of a system which, in contrast to aleatory uncertainty, can be reduced through additional information. Importance measures obtained from reliability analysis are invaluable in recognising the most important sources of reducible uncertainty (Eiermann, Ernst et al. 2005). This information provides guidance when seeking additional data and improved models. Although reliability analysis techniques are able to account for uncertainties in the design variables, and may be used to estimate the reliability, or its complement, the probability of failure, these methods fail to represent structural behaviour as realistically as possible and cannot be used when performance functions are not available in explicit form.

In other words, explicit reliability analysis of structures requires that the problem space can be represented with a closed-form function or equation. This is by far the greatest limitation of traditional reliability analysis.

Analogously, finite element analysis (FEA) is a powerful and well established methodology commonly used in all branches of engineering to analyze from relatively simple structures to very complex continuum systems. Finite element methods allow consideration of complicated geometric arrangements and constitutive relationships of the materials, realistic connection or support conditions, various sources of nonlinearity, and many load paths to failure. FEA provides good results for a set of assumed values of the input variables while completely ignoring the uncertainty in them (Haldar and Huh 2001).

Combining the desirable features of FEA together with reliability methods leads to the concept of stochastic finite element analysis. Stochastic finite element analysis is necessary to evaluate the reliability of complicated systems considering their behaviour as realistically as possible. It is parallel to the deterministic finite element method, but it incorporates uncertainties in the variables. Moreover, SFEA can be used when the limit state functions are implicit. Finally, the stochastic finite element method is inherently capable of dealing with spatially and temporally distributed system uncertainties through efficient incorporation of random fields. In the strict sense, the distinguishing feature of stochastic finite element analysis is that it involves the discretization of the parameter space of a random field of material properties, geometry, and/or loads (Orisamolu 1992). For completeness, a detailed literature review of random variables and fields, as well as the available analytical and numerical techniques for the discretization of random fields, is presented in Appendix B.

In the last decade, there has been considerable effort in the reliability assessment of RC members with corroding reinforcement. In general, these probabilistic assessments have utilized limit states based on sectional analysis where corrosion (either uniform or pitting corrosion) is accounted for only through a reduction of the cross sectional area of the reinforcing bars. However, reinforcement bond takes a primary role in the assessment of corrosion-induced damage of RC structures. The impact of bond loss due to corrosion on the load and deformation capacity of RC beams needs to be further studied by explicitly

accounting for the effect of corrosion location and corrosion length. The analysis of corroded flexural members at the section level with modified material and geometric properties to account for corrosion effects therefore does not give realistic predictions, because both corrosion-induced concrete cracking and bond loss lead to nonlinear behaviour of these members. It is for this reason that nonlinear finite element modelling of the effect of corrosion on structural behaviour of reinforced concrete RC flexural members is a better tool to capture and simulate the observed corrosion-induced phenomena. The SFEA framework developed as part of this research provides a novel and effective tool for probabilistic assessment of the safety of affected RC structures at different levels of damage.

3.3 Stochastic Finite Element Analysis Methodologies

The development of various methodologies for stochastic finite element analysis has been a very active and rapidly growing area of research over more than the last two decades. During this time remarkable progress has also been made in effective and practical implementations of SFEA, due in no small part, to the availability of affordable high speed computing technology. However, the idea of incorporating randomness in a finite element formulation has a longer history, particularly in the area of stochastic mechanics ((Matthies, Brenner et al. 1997), and (Schuëller 1997)).

In structural reliability analysis, the first merger between reliability methods and finite element analysis can be traced to Der Kiureghian and Taylor (1983). A number of notable contributions on the various methods of SFEA have since been presented, including those by Liu and Der Kiureghian (1991), Zhang and Ellingwood (1996), Zhang and Der Kiureghian (1997), Der Kiureghian and Zhang (1999), Sudret and Der Kiureghian (2000), Imai and Frangopol (2000), Haukaas and Der Kiureghian (2004), Nie and Ellingwood (2005), and Koduru and Haukaas (2006). In addition, the first books presenting specific SFEA approaches were introduced by Ghanem and Spanos (1991) and Kleiber and Hien (1992), while Haldar and Mahadevan (2000a) published the first comprehensive textbook on performing reliability analysis with the stochastic finite element method.

SFEA methodologies may be broadly divided into three categories, based on the essential philosophy, namely: (1) Simulation techniques (Monte Carlo, importance sampling methods, and variation reduction schemes), (2) response surface methods, and (3) sensitivity-based analysis (Haldar and Mahadevan 2000a). All these methods have certain advantages, disadvantages, and optimal applicability to a particular class of problems. For instance, direct Monte Carlo Simulation (MCS) is generally applicable to any type of problem involving random processes but tends to be impractical in SFEA due to the high computational costs associated with the large number of deterministic finite element analyses required to capture the low probabilities of failure encountered in structural systems. This is even more significant when analysing structural systems with many random variables or fields.

All three categories of SFEA methodologies mentioned above were thoroughly investigated as part of the research presented here. Although these categories can be further decomposed into specific analytical techniques, only the methods belonging to the third category, sensitivity-based analysis, are introduced separately. Therefore, the SFEA methodologies currently being researched can be classified into the following five groups:

1. **Simulation Methods**
2. **Second Moment methods**: (i) Perturbation-based SFEA approaches, and (ii) the Weighted Integral method;
3. **Spectral Stochastic Finite Element Method (SSFEM)**;
4. **Reliability-based SFEA methods**; and
5. **Response Surface Methods (RSM)**

With the exception of the Monte Carlo simulation and the weighted integral techniques, these methods are generally based on the combination of stochastic finite element discretization techniques and reliability methods.

A concise summary of the critical reviews and comparisons of these five methodologies is presented in Table 3-1. The focus of the reviews was on the applicability and practical implementations of the methodologies to SFEA of reinforced concrete elements, namely the advantages and disadvantages of each approach. A more detailed presentation

Table 3-1: Comparison of SFEA Methodologies

Methodology	Advantages	Disadvantages
Simulation	• Relatively easy to implement; • Adaptable to all types of problems described by both explicit and implicit performance functions; • Results can be obtained to any desired accuracy; • Accuracy benchmark for all other techniques.	• Very inefficient and impractical for low failure probabilities encountered in structural engineering applications (10^{-2} - 10^{-7}), thus prohibitive with FEA due to the large number of deterministic FE runs required; • Impractical for dealing with random fields.
Second Moment *Perturbation*	• Relatively simple to implement; • 1st-order perturbation method is practical for estimating the response variance; • Applicable to a wide range of problems at a low computational cost;	• Accurate results only for small parameter variability. Upper limit on COV strongly depends on the degree of nonlinearity (up to 20%); • While the results are distribution-free, MCS results must be obtained for specific distributions, hence dependent on assumed PDF in MCS; • The derivatives of $\boldsymbol{K}$ and $\boldsymbol{F}$ must be derived at least to 2nd-order (at element level before assembling the system) leading to intricate analytical formulae. Calculations can be time time-intensive while higher-order approximations are completely intractable.
Weighted Integral Method	• Allows determination of 2nd-order statistics for the response of a given input random field; • Upper bound on the response variance - independent of the correlation structure of the random field.	• Limited to elastic problems and small COV of the input; • Bounds on the response variance are difficult to compute in practice due to the complex expression of the response variability functions. • Excessively time consuming for large number of elements.
SSFEM	• Ideally suited to analysis involving random fields; • The response (vector of random nodal displacements) is cast as a series expansion in standard normal random variables. This can be interpreted as an 'intrinsic' representation of the random response, from which quantities such as statistical moments can be computed by post-processing (analytically or through simulation).	• Requires two discretizations of the stochastic partial differential equations governing the problem under consideration - the spatial and probabilistic domains; • Practically limited to linear problems. Material or geometrical non-linearity cannot be dealt with by SSFEA in its latest state of development. • The amount of computation required for a given problem is much greater than that of the equivalent deterministic.

Table 3-1: (concluded)

Methodology	Advantages	Disadvantages
		problem. Typically 15-35 coefficients are needed to characterize nodal displacements. • To date, no error estimator has been developed; • Accuracy of the method has not been established; • For lognormal random fields, even for a single variable, only an infinite number of terms in the expansion reproduce the lognormal characteristic. • Limited applicability to reliability problems involving small failure probabilities. The polynomial chaos expansion provides a global fit to each response quantity in the central region of the respective distribution, but poor in the tail regions. Because small-probability events are influenced by the tail regions of these the PDFs, accurate results cannot be expected for such problem.
Reliability-based SFEA (direct coupling of reliability and FEA)	• PDFs of the input random variables is used; • PDFs of the response quantities can be obtained; • The approach is estimated to reduce computation times by a factor equal to the number of random variables; • Particularly compatible with the algorithmic structure of existing FEA codes; • Reasonably straight forward to implement in linear FEA setting, where solution of the system can be obtained by inversion of the stiffness matrix and related techniques;	• For non-linear FEA, where the solution of the system is obtained in an iterative manner, the implementation of this approach is very challenging; • The majority of the successfully developed software utilizing this integrated SFEA methodology was in discrete mechanics (trusses, frames, etc.) and continua mechanics dealing with homogeneous problems such as plates, composite materials; • Although very promising, it has yet to be successfully applied to non-linear SFEA of RC structures.
Response Surfaces	• Accuracy comparable with direct coupling; • Response surfaces carefully generated, and checked at each step, always converge to the design point; • The computational cost of this approach is far less than the direct approach for a small number of random variables, typically 3-5.	• Requires stable, reliable, and validated component programs; • Generation of response surfaces can be time prohibitive for problems involving a large number of random variables and random fields; • Convergence must be checked to ensure valid results.

of each methodology, including the mathematical and theoretical developments, with references to source literature, is available in Appendix C (beginning on page 191). Based on this review, it can be reasonably stated that the most appropriate and efficient general methodology would be the reliability-based SFEA (direct coupling of reliability and FEA) approach. On the other hand, this strategy is the most difficult to implement in practice for non-linear, inelastic problems such as being considered in this work. Furthermore, a successful development of this approach for the said problem domain has not been achieved to date.

It is emphasized here that the development and implementation of the SFEA Framework, developed during this research, is not simply based on a review of the literature (as summarized in the previous table) but also on practical computational experimentation with the various strategies. These efforts are explained in section 3.4.

3.4 Strategies for Implementation of SFEA

In general, three options are currently available for an investigator aiming to implement the stochastic finite element method in research or engineering practice. These are:

(1) utilization of commercial, open source, and other SFEA software (if available);

(2) development of custom SFEA software, directly integrating non-linear finite element and reliability analyses; and

(3) development of a framework combining one or more finite element and reliability programs (commercial, open-source, or custom), as components linked through custom architectures and scripting.

All three strategies were thoroughly explored as part of this research and are discussed next.

3.4.1. Utilization of Existing SFEA Software

The existence and availability of de facto SFEA software was the first option considered at the outset of the research. The search involved traditional review of academic literature, internet searches, as well as formal and informal communications with researchers in the private and government R&D sectors. The results of this investigation identified several

computer software systems developed over the last two decades. These ranged from commercial software available for a license fee to open source resources available free of charge to the general public. The list of computer software given here is not exhaustive. For instance, programs developed in the Canadian private and government sectors, which are security classified, and/or are not applicable to the problem domain being investigated, are not presented. However, it can be stated that such software systems are in demand, are being developed, and are expected to play a major role in structural analysis and design, in civil, mechanical, and maritime engineering, in the near future.

Commercial Software:

At this time, a commercial SFEA software system, applicable to a broad spectrum of applications, is not available in the marketplace. However, fully integrated SFEA software designed for specific applications have been identified, and include the following proprietary programs:

1. **NESSUS** (Numerical Evaluation of Stochastic Structures under Stress), developed by the Southwest Research Institute, for NASA;
2. **CalREL-FEAP –** developed at the University of California, Berkeley;
3. **COSSAN** ("COmputational Stochastic Structural ANalysis"), developed at the Institute of Engineering Mechanics, University of Innsbruck, Austria (IfM)
4. **STRUREL -** developed and marketed by RCP GmbH, in Germany; an independent consultancy specialising in reliability and risk analysis of technical systems.

A detailed review of these SFEA programs is presented in Appendix D.1. The principal limitation of these software packages is their high licensing costs and, more importantly, lack of built-in concrete and RC element models. Development of such capabilities within these programs is generally as demanding as development from scratch. Thus, the above programs cannot be applied to SFEA of RC elements or structures in their current form.

Open Source Software (OSS) and Free Software:

Open-source software is computer software that is available in source code form, for which the source code and certain other rights, normally reserved for copyright holders, are provided under a software license that permits users to study, modify, and improve the software. Open source licenses often meet the requirements of the Open Source Definition (Opensource.org). Some open source software is available within the public domain. The principal benefit of OSS is the rapid development by a large number of distributed developers in a collaborative manner.

The only system falling in the open source category is OpenSees (Open System for Earthquake Engineering Simulation). OpenSees is a general-purpose deterministic finite element framework developed by a multi university team, lead by University of California, Berkeley (2000), under the sponsorship of the Pacific Earthquake Engineering Research (PEER) Center . Details of OpenSees functionality are summarized in Appendix D.2. During the course of this research, approximately three months were spent exploring the potential of using the OpenSees system for the SFEA of RC structures. Ultimately, the reliability analysis component initially developed for OpenSees is no longer functional, thus this system does not have any SFEA capability.

The category of free SFEA software contains only one program: **Rt** (Reliability tools). Rt is a new reliability software currently being developed at UBC under the supervision of Professor Haukaas (see Appendix D.2). Interfaces with programs such as Matlab and SAP2000 are underway. It is planned to link Rt with the finite element capabilities of OpenSees. Rt appears to be a very promising tool for SFEA and with time it is possible that it could be adapted for SFEA of RC structures. However, this capability is not yet available.

3.4.2. Development of Custom Integrated SFEA Software

The second option for the implementation of SFEA of RC structures is to develop custom software. According to studies in the literature, for example Der Kiureghian and Taylor (1983), Arnbjerg-Nielsen and Bjerager (1988), Mahadevan (1988), Liu and Der Kiureghian (1991), Haldar (2000), and Haukaas (2003), a fully integrated and coupled finite element

reliability analysis program is the most suitable approach for the analysis of discrete structural analysis problems, and to certain continuum structures due to its efficient ability of utilizing random fields. The statistical properties of the random variables are supplied as information additional to the finite element input data and the probabilistic analysis proceeds automatically with the reliability analysis controlling the finite element analysis. The user is therefore, spared the tedious task involved in the detailed description of the probabilistic model. Furthermore, the reliability-based approach to SFEA is particularly compatible with the algorithmic structure of existing FEA codes and is commonly considered to be the best strategy of all presently available methodologies. See Appendix C.4 for more detail.

Based on the literature review, significant effort was invested in pursuing this strategy in a piecewise manner, beginning with development of integrated SFEA software for the solution of discrete structural problems with random variables/fields. Given good understanding of matrix analysis of structures, basic familiarity with statistics and probability theory, and significant practical programming experience, it is reasonably straight forward to implement this approach to the linear-elastic structures. The solution of the system of linear equations can be obtained by inversion of the "stochastic" stiffness matrix and related FE techniques. For this purpose, a program called **SFEAP** (Stochastic Finite Element Analysis Program) was written in Microsoft Visual Basic 6 and Fortran90. The software utilized established linear FEA procedures modified for reliability analysis, and utilized the modified Rackwitz and Fiessler (1978) version of FORM. The program also included random field discretization routines for continuum problems. The results of reliability analysis on a portal frame with random material properties and loads, published in the book by Haldar and Mahadevan (2000a), were reproduced by SFEAP. Details of the frame problem, the input data, and analysis output files, as well as interpretation of the results are presented in Appendix E. The source code which consists of over 7,000 lines of code is not included in the Appendix to limit the total number of pages in this thesis.

The next step was to attempt extension of SFEAP to non-linear analysis of a basic continuum problem, typically a plate with a hole subjected to boundary stress, while randomness of the modulus of elasticity would be described by random field. Although this was accomplished

for the elastic case, extension to non-linear analysis was problematic due to the competing nature of the FE and reliability solver algorithms. This is the main challenge of implementing the fully integrated approach, as mentioned in Table 3.1 and as experienced by other researchers/developers in academia and the private sector, as mentioned in Appendices D.1 and D.2. Therefore, in the case of non-linear FEA, where the solution of the system is obtained in an iterative manner, the implementation of this approach is very challenging. Moreover, as already stated this approach has yet to be successfully applied to non-linear SFEA of reinforced concrete structures.

Taking into account the various constraints in knowledge, technological, economic, human resources, and practical, within a reasonable time frame, the approach was re-evaluated. Considering that the software systems described earlier were developed by large teams of researchers with significant financial and time investments the development of an integrated SFEA program from scratch, while replicating nonlinear FEA capabilities of commercial packages, is an overwhelming task. Although options involving less direct coupling approaches were also explored, including the writing of custom source code for large commercial packages such as **Abaqus** and modification of existing programs for which the access to source code was potentially available, it was decided that the third option, namely development of a framework linking validated reliability and nonlinear finite element analyses codes, is very promising.

3.4.3. Development of a SFEA Framework for Reinforced Concrete

The development of SFEA systems based on a combination of existing reliability and FEA programs can be achieved through various ways depending on the level of access to the inner workings of the individual programs. If the inner data structures and functionality of each software component are accessible through an Application Programming Interface (API) then it is possible to develop custom programs, or scripts, that may effectively link the components resulting in an indirectly integrated SFEA framework. This approach is less effective and efficient if some of the components do not offer APIs. In the case where none of the components provide a programming interface, the individual programs are referred to as “black boxes” or input-output models. In this case the only options are to apply simulation

techniques (such as Monte Carlo), response surface methodologies (RSM), or a combination of both. It has already been established that the simulation approach to SFEA is impractical for complicated non-linear problems where the failure probabilities are very low as is the case in the application presented here. Therefore, the SFEA framework for RC developed here is based on a RSM-based integration strategy.

3.5 The Proposed SFEA Framework

Following a critical evaluation of available reliability analysis and FEA software, two programs were selected. A schematic diagram of the proposed SFEA Framework is presented in Figure 3-1. The coupling of the nonlinear finite element analysis of reinforced concrete (NLFEARC) component with the reliability component is accomplished through the response surface method (RSM) briefly explained in Section 3.3 and expanded in detail in Chapter 6. Implementation specific to each component of the framework is briefly described next.

In principle, the NLFEARC component can be filled by any nonlinear FE program, such as Abaqus, ANSYS, etc. The program selected must fulfill the following criteria: (i) it must enable effective and accurate representation of RC (the material constitutive relationships for concrete and steel, as well as the interface between the two materials), (ii) it must be robust (computationally stable), and ideally, (iii) it must be mature and validated. In addition, a programming or scripting interface is very useful. Although a program like Abaqus offers concrete material models, it has been observed that these built-in models provide inadequate performance for the problem at hand particularly in the post-yielding behaviour. This is a serious issue, because reliability requires a stable FE solver and consistent results. This issue can probably be addressed through development of own concrete material models, which can be incorporated in such packages. However, this also requires very significant development, debugging, and validation/verification efforts. After careful consideration of various options, implementation of the NLFEARC component was fulfilled through the VecTor2 software

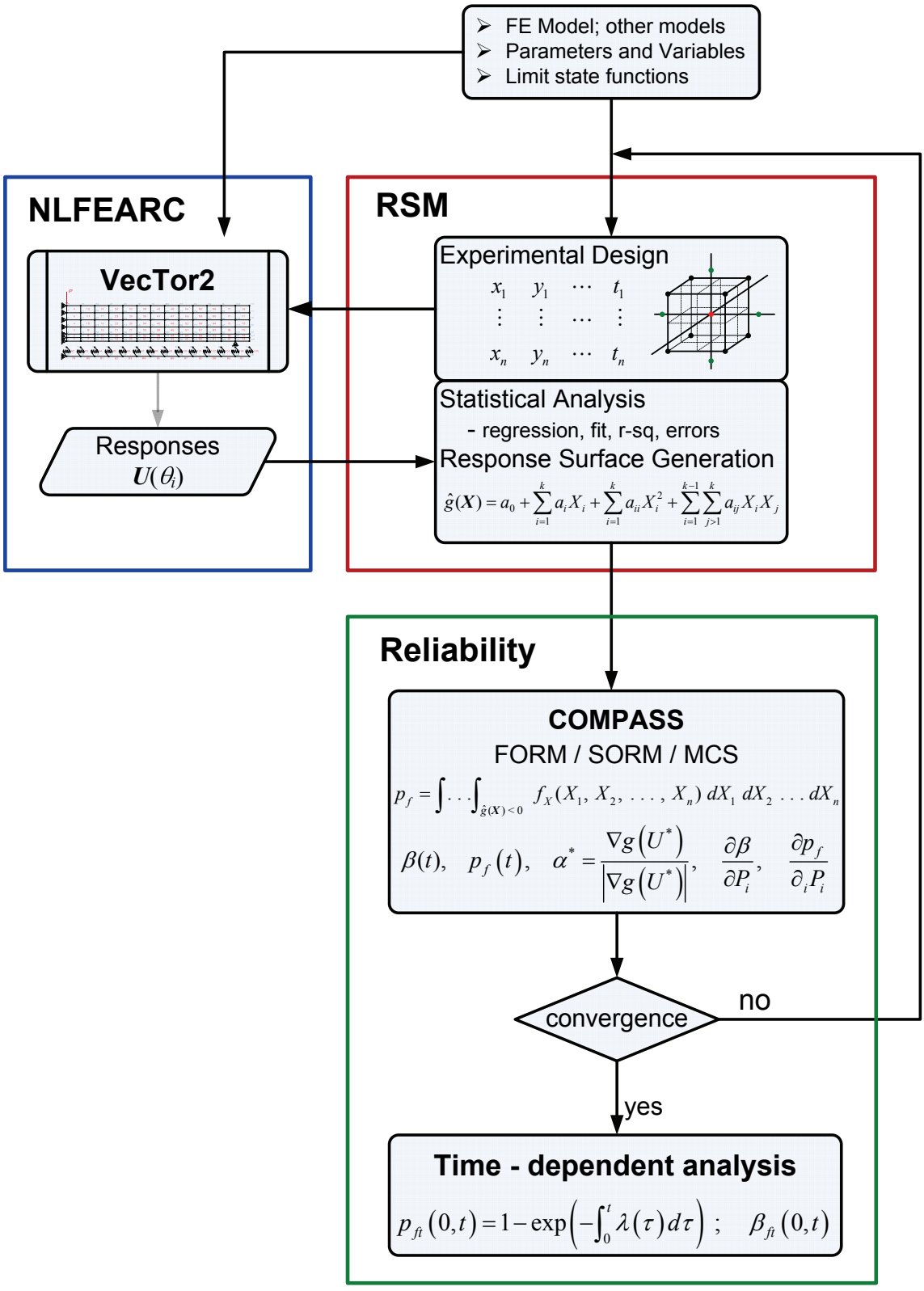

Figure 3-1: The proposed SFEA framework

developed by Professor Frank Vecchio at the University of Toronto (2002). VecTor2 is a comprehensive NLFEARC package dedicated to 2-dimensional analysis of RC structures. It best fulfills the above requirements as it has a wide selection of validated material models, allows modeling of the bond-slip mechanism, the solver is particularly stable, and comes with very useful pre- and post-processor programs. Details of the VecTor2 implementation are provided in Chapter 4, which describes the finite element and corrosion models used in this work.

The implementation of the reliability component is through a comprehensive component and system reliability software: COMPASS (COmputer Methods for Probabilistic Analyses of Structures and Systems). COMPASS is a general purpose software for the reliability and risk analysis of stochastic systems. The program was developed and is maintained, marketed, and supported by Martec Limited, an advanced engineering consultancy based in Halifax, Nova Scotia, Canada. It has been successfully applied to a broad range of scientific and engineering problems. It also provides a programming user interface allowing the analyst custom definition limit state functions among other functionalities. Details of the COMPASS program and application as part of the proposed framework are presented in Chapter 5, which deals with structural reliability analysis.

Implementation of the proposed framework was achieved by combining the VecTor2 software for the NLFEARC and COMPASS for the reliability analysis through the response surface method (RSM). The response surface approach was selected for the following reasons:

1. it does not require access to the source code of the reliability and FE programs (the case here) when the programs are used more like “black boxes”;
2. it gives accurate results for most problems and may be faster than the direct coupling when a small number of random variables is considered;
3. when it is not possible to implement the direct differentiation method (for instance, when a commercial finite element code is used); and
4. it is applicable to the most general problems and does not require the implementation of gradients in the finite element code.

Implementation of the framework involves the following general steps:

1. **Preparation for Analysis**
   (i) Finite element model; (ii) random variables; and (iii) limit state functions
2. **RSM 1 - Experimental design** – define test space and input variables x
3. **Deterministic FE analysis** – generate vector of responses y
4. **RSM 2 - Statistical analysis and generation of response surfaces**
5. **Reliability Analysis (COMPASS)** – instantaneous annual β, p_f, α
6. **Cumulative Probability of Failure** – time dependent

The computational procedure is carried out at each time step as follows:

1. An experimental design selects appropriate set of points in the design space so that an approximate representation of the limit state can be formed. The central composite design approach is used to generate design for the random variables to enter the finite element component. The initial range of values for each random variable is based on $\mu \pm \sigma$, where μ and σ respectively represent the mean and the standard deviation of each variable.
2. Nonlinear finite element analysis is carried out for each design experiment for the given time step.
3. Once the response values are generated through the deterministic finite element runs, they are returned to the RSM module for various statistical tests and regression analysis to generate the vector of coefficients that defines the limit state surface in terms of the input random variables.
4. Using the coefficients of the limit state response surface, the reliability software is used to compute the instantaneous probabilities of failure as well as the corresponding reliability indices for the given time step. FORM and SORM were used to compute these values.
5. The adaptive RSM is used to verify whether the results had converged to the correct failure point. Here, the values of the random variables at the new design point are used in place of the initial random variables at their mean values. The entire process is repeated, and the new design point is compared with the previous iteration. In general, the adaptive RSM scheme presented here requires only two to three cycles for convergence.

6. For a service life interval of t years, the time-dependent reliability, or probability of successful performance during the time period (0, t), is determined through post-processing of the annual reliability results generated in Step 4, by applying a conditional probability function known as the hazard rate.

The proposed SFEA methodology is original and unique in that it represents the first practical tool for the time-dependent reliability analysis of RC members wherein the corrosion induced deterioration mechanism (coupled reduction of reinforcement area and bond strength) is modelled explicitly. This is in contrast to the earlier approaches based on closed-form limit state functions derived from sectional analysis or design code formulae, most of which only considered the reduction of reinforcement area due to corrosion while ignoring the loss of bond. Bond deterioration was also ignored in the more sophisticated sectional analysis based methods in which the spatial distribution of steel area was modelled. The literature reveals only one previous study utilizing a finite element based approach to the reliability analysis of RC beams with corroding reinforcement. However, the methodology used requires the proprietary development of a fully integrated non-linear finite element and reliability code; it cannot be used with existing reliability and/or finite element software. Furthermore, all currently available practical applications of SFEA (commercial or open source) are limited to the analysis of discrete structural systems (trusses, frames, etc.) or simple homogeneous continuum problems (plates). Most of these applications are based on elastic finite element analysis, and none are applicable to reinforced concrete.

Chapter 4. Finite Element Analysis Module

4.1 Introduction

Finite element analysis (FEA) has become a widely used analysis and design tool in general engineering practice. Although non-linear finite element analysis is gradually gaining acceptance in the engineering community, the preponderance of finite element analyses in today's design practice is still linear analysis (Fish and Belytschko 2007). In stress analysis, for most analyses of operational loads, linear analysis is adequate as it is usually undesirable to have operational loads that can lead to non-linear material behaviour or large displacements. However, in the analysis and design of concrete structures subjected to extreme loads, displacements, and various deterioration mechanisms nonlinear analysis is required (Coronelli and Gambarova 2004).

Conservative methods that have been used to assess the effect of corrosion on the structural behaviour of RC members consist in the application of the limit states theory used in the design of new structures by modifying section and material properties to account for the deterioration (Rodriguez, Ortega et al. 1996; CONTECVET 2001; Lay, Schießl et al. 2003). The analysis of corroded flexural members at the section level with modified material and geometric properties to account for corrosion effects does not give realistic predictions, since corrosion-induced concrete cracking and bond loss lead to nonlinear behaviour of these members. Here, the assumptions of plane sections and perfect steel/concrete bond may no longer apply (Coronelli and Gambarova 2004). It is for this reason that nonlinear finite element modelling of the effect of corrosion on structural behaviour of RC flexural members is a better tool to capture and simulate the observed corrosion-induced phenomena, which includes (i) stiffness decay due to concrete cracking and loss of bond between the steel and the concrete; (ii) strength deterioration in bending and shear; (iii) transition from tension to

compression-triggered failures in critical sections; and, (iv) bond failure along the span and/or at beam ends (Dekoster, Buyle-Bodin et al. 2003; Coronelli and Gambarova 2004).

In this research, the modeling and analysis of RC beams subjected to corrosion-induced deterioration was carried out using VecTor2 (Wong and Vecchio 2002), a two-dimensional nonlinear finite element analysis program for reinforced concrete structures developed at the University of Toronto over the past 20 years. In comparison to other general, commercial off-the-shelf finite element packages, VecTor2 is a user-friendly and efficient finite element program, which is a quality critical to successful coupling with reliability analysis algorithms.

This chapter presents details of the finite element analysis component of the proposed SFEA framework shown in Figure 3-1. It discusses the implementation of a FE model for RC beams in which the bond strength-slip relationship is modified to account for corrosion. Validation is provided through comparison of the analyses carried herein with published results of load–deflection studies of RC beams. Mesh sensitivity studies are also discussed.

4.2 Corrosion Damage Model

Corrosion of steel reinforcement is modelled in this work through the decrease in the steel cross-sectional area and the reduction in bond strength at the steel/concrete interface. In the case of corroded reinforced concrete members, those effects are always coupled, and as such, it is not realistic to forecast the behaviour of corroded beams merely in terms of steel cross-section reduction. The aim of the corrosion model is thus to describe the separated and coupled effects of the reduction in bond strength and steel cross section.

4.2.1. Reduction in cross-sectional area of steel

The reduction in the reinforcing steel cross-sectional area due to corrosion is obtained by direct application of Faraday's law, Eq. (2.1), assuming all the anodic corrosion current is used up in the corrosion process (i.e., there is no loss of current in the form of heat). The area of a single reinforcing bar at time t, $A_s(t)$, due to a uniform reduction in cross-sectional area is given by:

$$A_s(t) = \frac{\pi}{4}\left(d_b(t)\right)^2 \tag{4.1}$$

where $d_b(t)$ is the reinforcing steel diameter at time t, obtained from Eq. (2.7). The rate of corrosion used to determine $A_s(t)$ is assumed to be constant over the time period during which reinforcement corrosion proceeds.

4.2.2. Reduction of bond strength

The general trend in the relationship between bond strength and degree of corrosion was discussed in Chapter 2. In spite of the apparent scatter reflected in experimental data, tests show the trend to be well defined for the evolution of bond strength with the corrosion level. According to research by Almusallam et al. (1996) and Cabrera (1996), bond strength changes qualitatively as indicated in Figure 2-7. An initial increase for limited corrosion levels (pre-cracking stage) is followed by a decrease, due to the splitting of the cover as a result of corrosion-induced cracking. According to Coronelli and Gambarova (2004), bond failure in corroded bars is mostly through splitting, for commonly used concrete covers and stirrup amounts, thus the parameters of the bond stress-slip relationship must be modified in order to reproduce such brittle behaviour.

To account for the loss of bond strength due to corrosion, the bond slip relation proposed by Eligehausen et al. (1983), and included in VecTor2, is modified here to incorporate the corrosion effects, as shown in Figure 4-1. Thus, the bond strength τ_{max} and the slip s_1 at the maximum bond stress and the softening branch, for the uncorroded bar, are reformulated as a function of the corrosion level, becoming $\tau_{max,residual}$, and slip s'_1. The post-peak behaviour includes cover splitting through the elimination of both the plateau and the frictional strength. Since no comprehensive models have been developed so far for the bars placed in an actual beam (Coronelli 2002), reference is made here to the empirical model proposed by Val et al. (1998) to predict bond-strength decay in corroded bars, as shown in Figure 4-2.

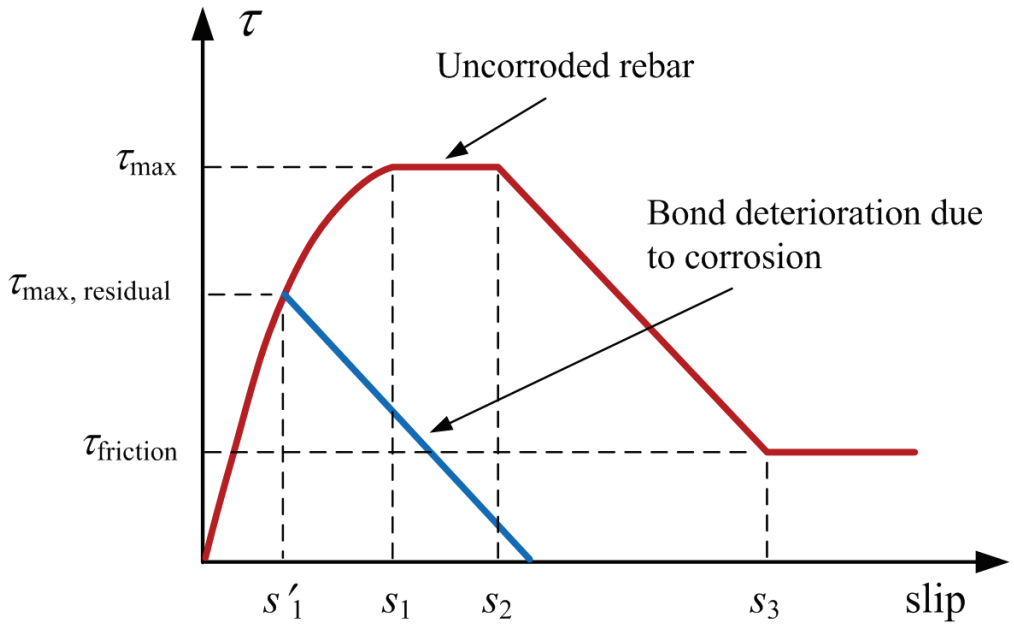

Figure 4-1: Bond stress – slip relationship according to Eligehausen model (adapted from Coronelli and Gambarova 2004).

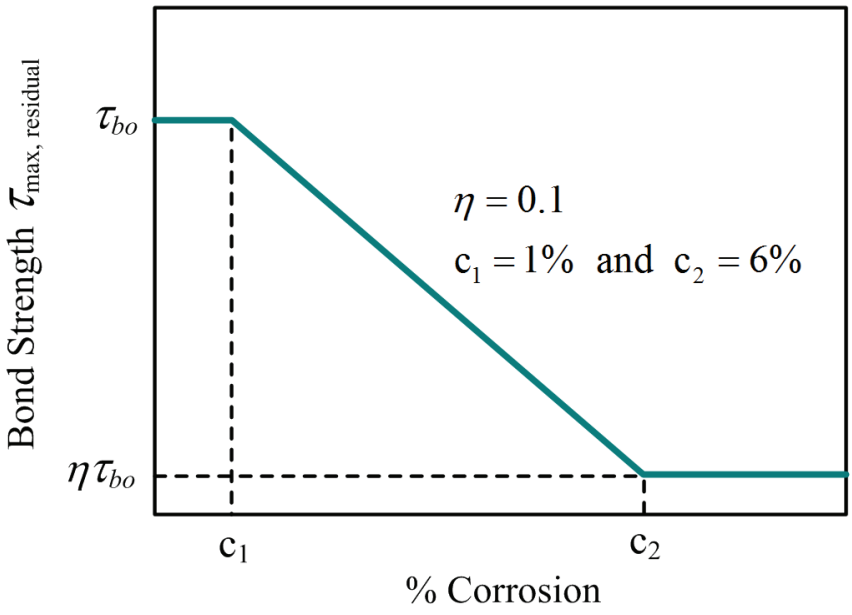

Figure 4-2: Assumed relationship for bond stress versus % corrosion (Val et al. 1998)

Based on the relationship between bond stress and percentage of corrosion, illustrated in Figure 4-2, and assuming uniform corrosion, the bond strength at time *t* can be estimated by the following expressions:

$$\tau_b(t) = \begin{cases} \tau_{bo} & c(t) \le c_1 \\ \tau_{bo}\left[1-(1-\eta)\dfrac{c(t)-c_1}{c_2-c_1}\right] & c_1 < c(t) \le c_2 \\ \eta\tau_{bo} & c(t) > c_2 \end{cases} \tag{4.2}$$

where τ_{bo} is the initial bond strength, c(t) is the percent corrosion at time t, and η is a factor for residual bond strength. Parameters c_1 and c_2 are taken as 1% and 6%, respectively (Val, Stewart et al. 1998). Based on experimental tests reported by Almusallam et al. (1996), the residual bond strengths range from 10% to 15% of the initial bond strength up to approximately 80% corrosion. The residual bond strength due to corrosion is assumed here to be 10%, hence η = 0.1. The percentage of corrosion c(t) in Eq. (4.2) can be calculated from $\Delta d_b(t)$ given on page 13 as:

$$c(t) = 100\left[1-\left(1-\frac{\Delta d_b(t)}{d_{bo}}\right)^2\right] \tag{4.3}$$

Thus, the loss of bond strength with time is coupled with the decrease in cross-sectional area of the reinforcement with time. The initial bond strength τ_{bo} is determined from Tepfers formula (Tepfers 1979):

$$\tau_{bo} = f_{ct}\left[\frac{c + d_{bo}/2}{1.664 d_{bo}}\right] \tag{4.4}$$

where f_{ct} is the tensile strength of concrete and c represents the minimum clear concrete cover for the longitudinal reinforcement. The bond strength at time t, for a particular level of corrosion (%), given by Eq. (4.2), provides the maximum residual bond strength ($\tau_{max,residual}$) in the modified bond-slip relationship illustrated in Figure 4-1.

4.3 Implementation in VecTor2

Finite element analysis of reinforced concrete beams were performed using the software finite element package VecTor2 (Wong and Vecchio 2002). VecTor2 is capable of modeling two-dimensional reinforced concrete membrane structures under monotonic, cyclic, and

reversed cyclic loading conditions. VecTor2 models the response of RC plane-stress members by using the Modified Compression Field Theory, MCFT (Vecchio and Collins 1986) and the Disturbed Stress Field Model, DSFM (Vecchio 2000), which treat cracked concrete as an orthotropic material with smeared and rotating cracks. The MCFT model is used here to simulate the behaviour of RC beams. The nonlinear algorithm implemented in VecTor2 is based on an incremental total load and iterative secant stiffness procedure. It must also be stated that VecTor2 has been undergoing extensive validation over the last nearly two decades, against a broad spectrum of practical engineering problems, for example Vecchio and Shim (2004).

Reinforced concrete is modelled in VecTor2 with 2-D triangular, rectangular, and quadrilateral elements for the concrete, while 1-D truss bar elements are used to represent reinforcing bars. The concrete elements can be associated with two types of reinforced concrete material: (i) plain concrete to represent the concrete cover, and (ii) concrete with smeared reinforcement to model the web region of the beam with well-distributed stirrup reinforcement. Figure 4-3 shows a two-dimensional finite element model of a simply supported RC beam. Because of symmetry in geometry and loading, only half of the beam is modelled. Support nodes are used at the line of symmetry to restrain the mesh in the *x*-direction while allowing translation in the *y*-direction.

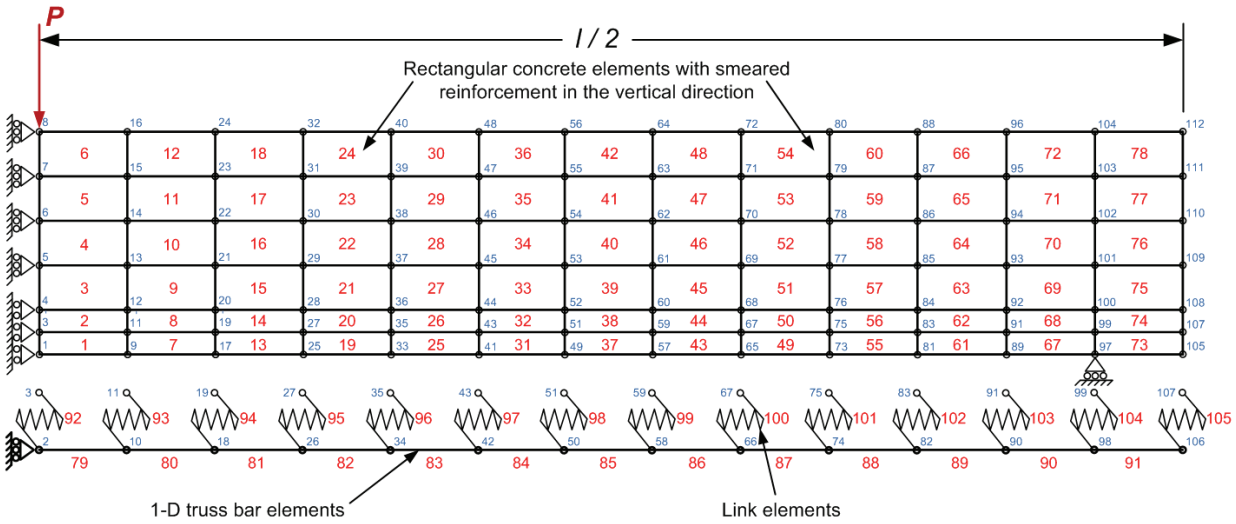

Figure 4-3: A 2-D finite element idealization of a simply supported RC beam

4.3.1. Elements

The finite element idealization of RC beams is accomplished by two-dimensional elements which lie in the *x*-*y* plane of the beam elevation, as shown in Figure 4-3. Plain concrete is modeled using plane stress rectangles shown in Figure 4-4a. Following the assumptions of the Timoshenko beam theory, the resulting stresses are assumed to be constant through the thickness of each element, and stresses in the *x*-*z* and *y*-*z* planes are ignored. The plane-stress rectangle is a four-node element with uniform thickness *t*. The element is defined by four node numbers in counter clockwise sequence, *i*, *j*, *k*, *l*. As each node translates in the *x* and *y* directions, the element has a total of eight degrees of freedom. The rectangle must be oriented isothetically, with its edges parallel to the *x* and *y* axes. Although the rectangle may assume any width and height, its accuracy degrades as the shape deviates from a square. As such, the aspect ratio best not exceed long to short side ratio of 3:2.

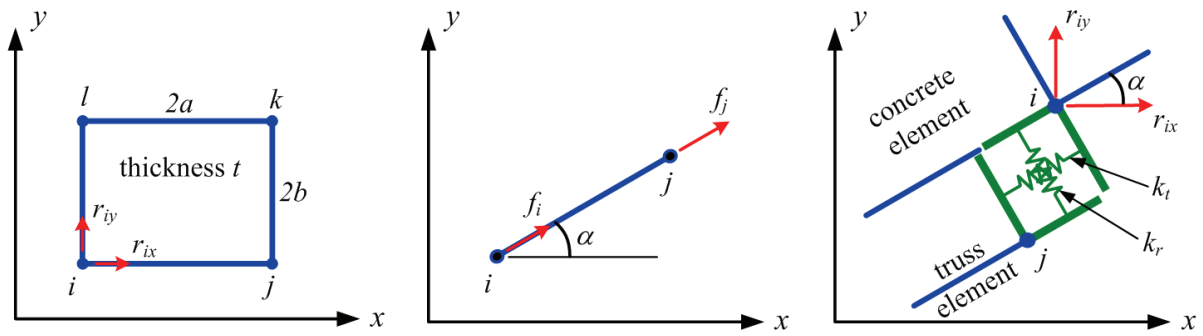

(a) Concrete (b) Steel Reinforcement (c) Link - Bond

Figure 4-4: Elements for concrete and steel reinforcement

Longitudinal steel reinforcement bars are modelled as one-dimensional (truss) elements assumed to deform by axial loading only. The truss bar element is a two-node element with uniform cross-sectional area, *A*, also shown in Figure 4-4b. The element is defined by two node numbers, *i*, *j*. As each node displaces in the *x* and *y* directions, the element has a total of four degrees of freedom. The truss element may assume any orientation α in the *x*, *y* coordinate system.

Transverse reinforcement (shear stirrups) is modelled by smearing the reinforcement in the concrete rectangular elements, where the element composite material stiffness matrix is the

sum of the concrete material stiffness matrix and the reinforcement component material stiffness matrices (Wong and Vecchio 2002). This approach is valid when shear reinforcement is well distributed along the web of the beam.

Bond slip is of particular importance in the analysis of RC structures with corroding reinforcement, because the expansion of corrosion products leads to cover cracking and, therefore, loss of bond strength. To account for the effects of bond loss and associated slip of reinforcement, as it is the case in the present work, explicit modeling of the bond-slip mechanism is required. This is accomplished here through the use of bond link elements, shown in green in Figure 4-4c. The bond link element connects one steel node with a corresponding concrete node, both occupying the same physical location in the undeformed configuration of the structure. Consequently, the use of this element in the finite element analysis of RC structures imposes the following restrictions: (a) the finite element mesh must be arranged so that a reinforcing bar is located along the edge of a concrete element, and (b) a double node is required to represent the relative slip between reinforcing steel and concrete. These restrictions arise from the fact that the stiffness of the bond link element is associated with the relative displacement between steel and concrete. Accordingly, the total displacement of both reinforcing steel and concrete is required at each node of the finite element mesh, so that the relative displacement and, consequently, the bond stress between steel and concrete can be determined. These requirements lead to a considerable increase in the number of degrees of freedom, not only because of the doubling of the number of nodes along the reinforcing steel bars, but also because the mesh has to be refined, so that the bars pass along the edges of concrete elements.

The link element in VecTor2 is a two-node, non-dimensional element. The element is defined by two different node numbers, *i* and *j*. Prior to slippage, the paired nodes must have the same coordinate; one node must be incident to a reinforced concrete element, and the other node must be incident to a discrete reinforcement element. Since each node displaces in the *x* and *y* directions, the element has a total of four degrees of freedom. The link element may be conceptualized as two-orthogonal springs, linking the reinforced concrete element and the discrete reinforcement element. One spring deforms tangentially to the discrete

reinforcement element, representing bond slip and bond stresses. The other spring deforms radially to the discrete reinforcement element, representing radial displacements and stresses.

4.3.2. Material models

The stress-strain response of concrete in uniaxial compression is described by the Popovics (1973) model for normal strength concretes and represented by the idealized stress-strain relationship shown in Figure 4-5a. Popovics' model reflects the higher stiffness and linearity of the ascending branch of the compression stress-strain curve and the reduced ductility of concretes when their compressive strength f'_c increases. This model is not modified to account for the effect of confinement provided by the stirrups.

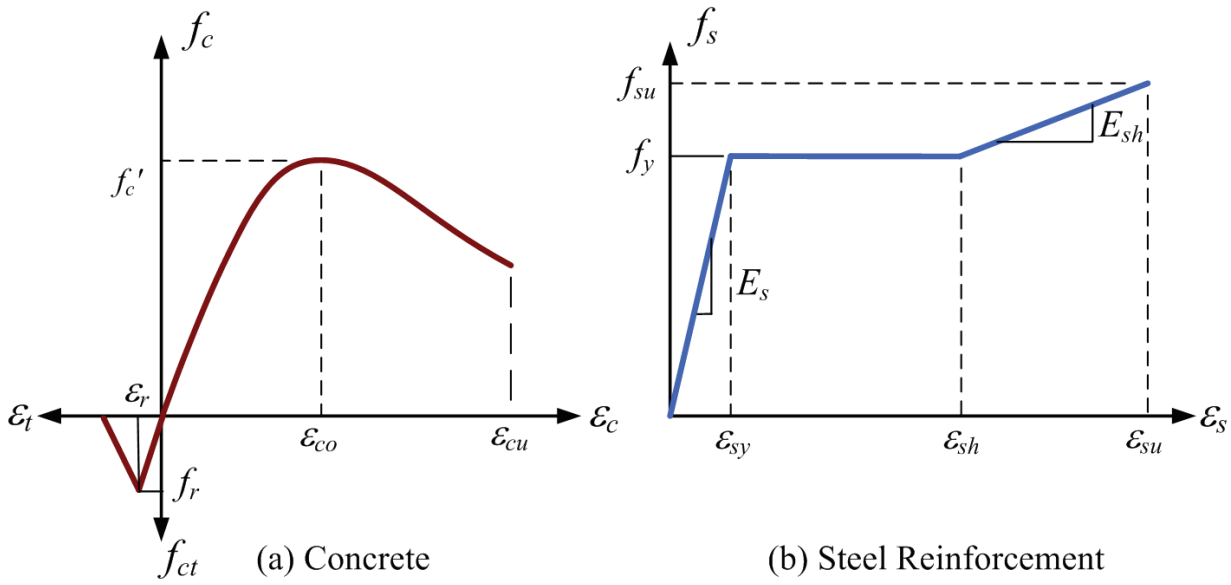

Figure 4-5: Material models for concrete and steel reinforcement

Prior to cracking, the concrete tensile response is assumed to be linear-elastic up to f_{cr}. The unconfined concrete tensile strength is represented by the relation in the CEB-FIP model, which is equivalent to the rupture modulus of concrete f_r defined in clause 8.6.4 of CSA A23.3-04 (2004):

$$f_{cr} = f_r = 0.6\lambda\sqrt{f_c'} \tag{4.5}$$

where λ is a modification factor for concrete density (λ = 1 for normal density concrete). After cracking, the average concrete tensile stresses are gradually decreased to account for tension stiffening. The tension stiffening model used is that proposed by Bentz (2000). The model, originally formulated for sectional analysis of reinforced concrete members, has been adapted for VecTor2 to account for two-dimensional stress conditions and the placement of smeared and discrete reinforcement.

The stress-strain relationship for the steel reinforcement shown in Figure 4-5b is idealized as a tri-linear elasto-plastic model formed by a linear-elastic branch, a yield plateau, and a linear strain-hardening branch until failure, described by Eq. (4.6). Figure 4-5b shows only the tensile (positive) part of the stress-strain model for reinforcing steel, but the same (negative) curve is implied for compression.

$$f_s = \begin{cases} \varepsilon_s E_s & |\varepsilon_s| \le |\varepsilon_y| \\ f_y & \varepsilon_y < |\varepsilon_s| \le \varepsilon_{sh} \\ f_y + E_{sh}(\varepsilon_s - \varepsilon_{sh}) & \varepsilon_{sh} < |\varepsilon_s| \le \varepsilon_u \\ 0 & \varepsilon_u < |\varepsilon_s| \end{cases} \tag{4.6}$$

Since one of the main objectives of this research is to account for the modification of bond slip by the effects of corrosion, the bond stress-slip relationship employed in this work is a user-defined model. VecTor2 allows the analyst to specify the bond model through a series of reference bond stress and slip values. This user defined bond stress-slip relationship was described in Section 4.2.2. and is based on Eligehausen's bond model (1983). For embedded bars, the bond model first determines the stress-slip relationship for two distinct cases: confined bars and unconfined bars. The stronger relationship for confined bars corresponds to pull-out type bond failure, whereas the relationship for unconfined bars corresponds to splitting failure. Since bond failure due to corrosion is associated to a splitting failure mode, due to corrosion-induced longitudinal cracking of the concrete cover, the bond stress-slip curve for unconfined bars is used here to simulate the slippage between the longitudinal reinforcement and the surrounding concrete. Figure 4-6 shows Eligehausen's model (1983)

as calculated by VecTor2 for a M30 bar with a clear cover of 50 mm and spacing between bars of 84 mm.

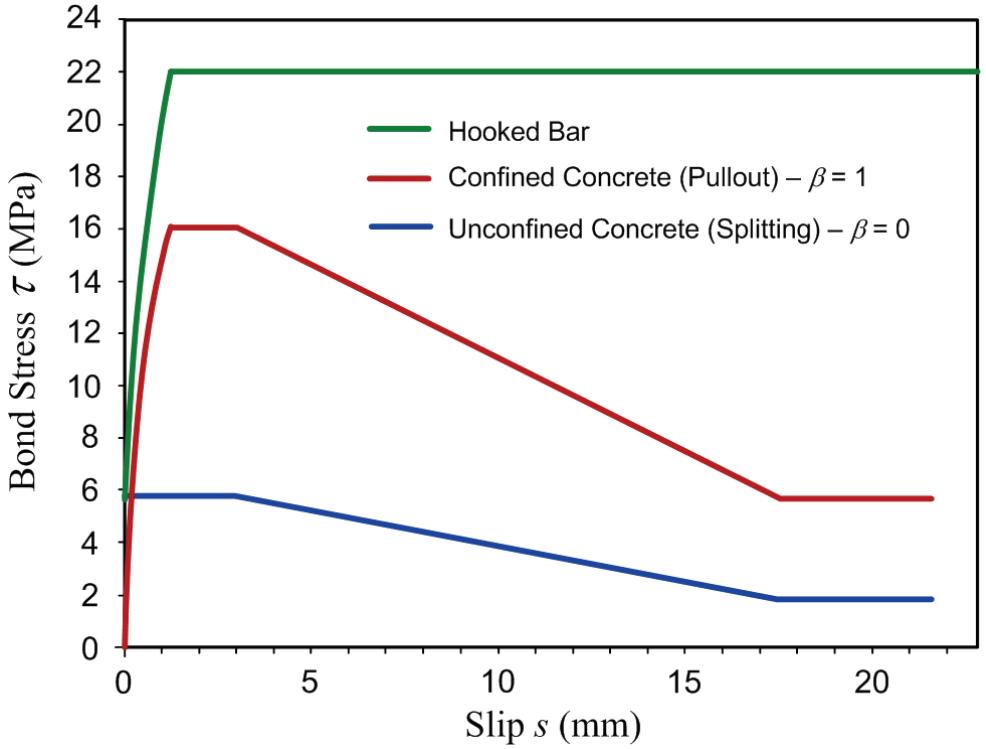

Figure 4-6: Bond - Slip Relationship based on Eligehausen's model (1983) as calculated in VecTor2

4.4 Finite Element Model Validation without Corrosion Damage

A number of correlation studies were conducted as part of the validation and verification of the finite element model of RC beams used in this research. Among these are results of experimental and numerical RC beam tests carried out at the University of Toronto (U of T) by Vecchio and Shim (2004). The U of T beams are nominally identical to the beams in the classic experimental tests by Bresler and Scordelis (1963), in terms of cross-section dimensions, amount and strength of reinforcement provided, and concrete compressive strength.

Only one representative example of these comparisons is presented here, that of U of T beam specimen A3, which approximately corresponds to beam A3 in the original Bresler and

Scordelis (1963) tests. The geometry, cross sectional dimensions, and material properties of beam A3 are presented in Figure 4-7. In all studies, the bond-slip effect was taken into account using the bond link element described in Section 4.3.1. These validation studies also aimed at identifying the effect of finite element mesh size on the results.

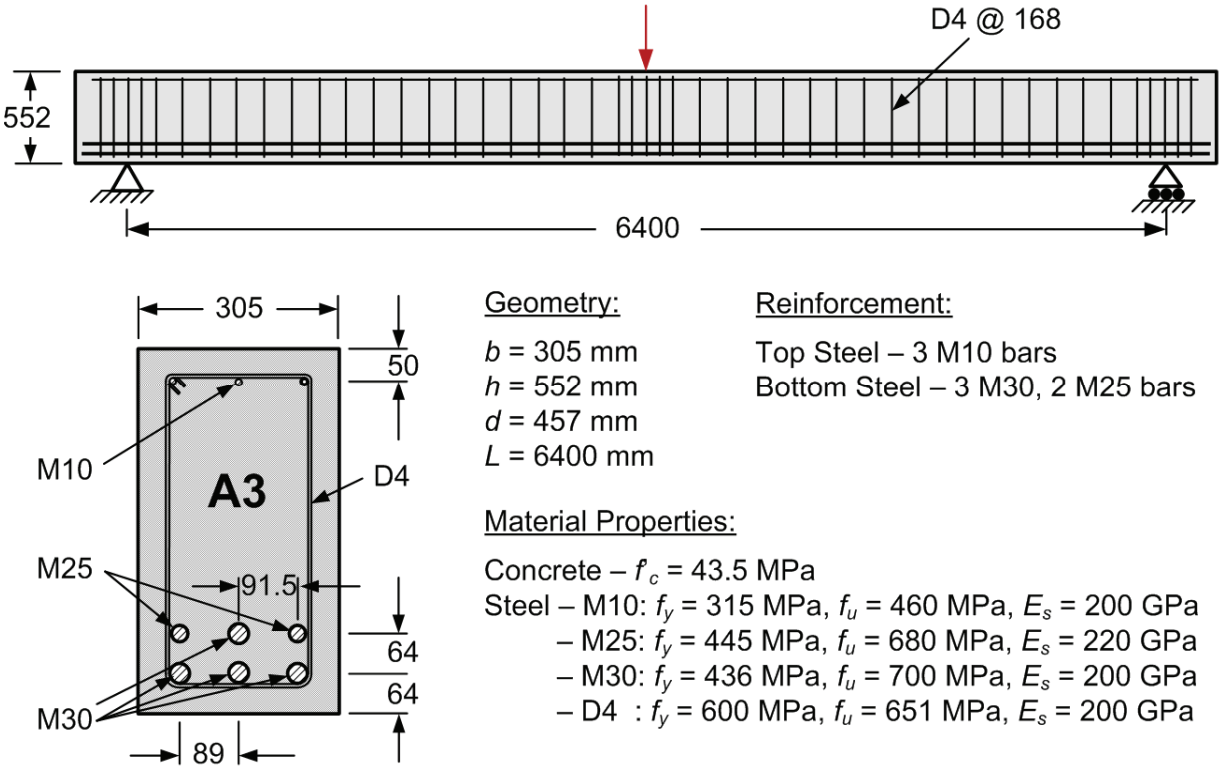

Figure 4-7: Details of U of T reinforced concrete beam A3

Figure 4-8 shows the finite element model of the U of T RC beam A3, as implemented in VecTor2. The finite element mesh in Figure 4-8 consists of 980 nodes, 759 4-node rectangular concrete elements with smeared reinforcement in the vertical direction to model the stirrups, 207 truss elements to represent the longitudinal compression and tension reinforcing bars, and 138 link elements to model the bond-slip behaviour at the steel/concrete interface.

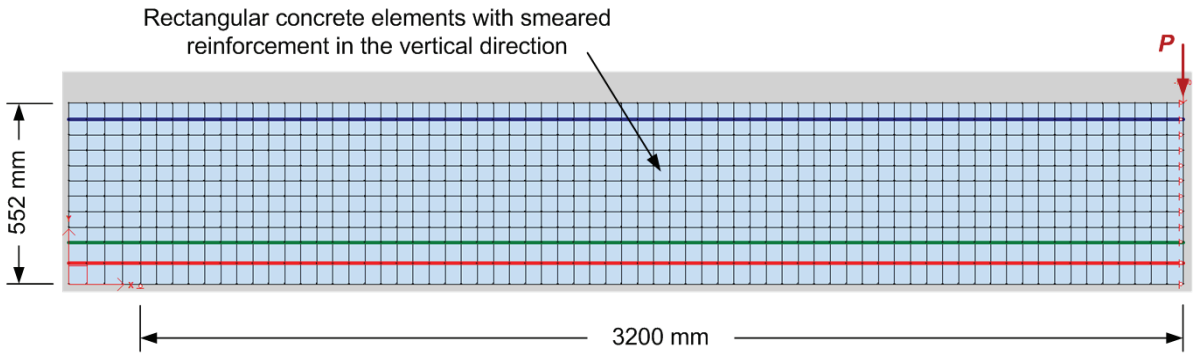

Figure 4-8: FE mesh for beam A3 implemented in VecTor2

Figure 4-9 presents a comparison of the numerical results with the experimental load-displacement response of RC beam A3. Both the strength and the stiffness are slightly overestimated using the finite element model. The ratio of the experiment-to-calculated strength is 0.95.

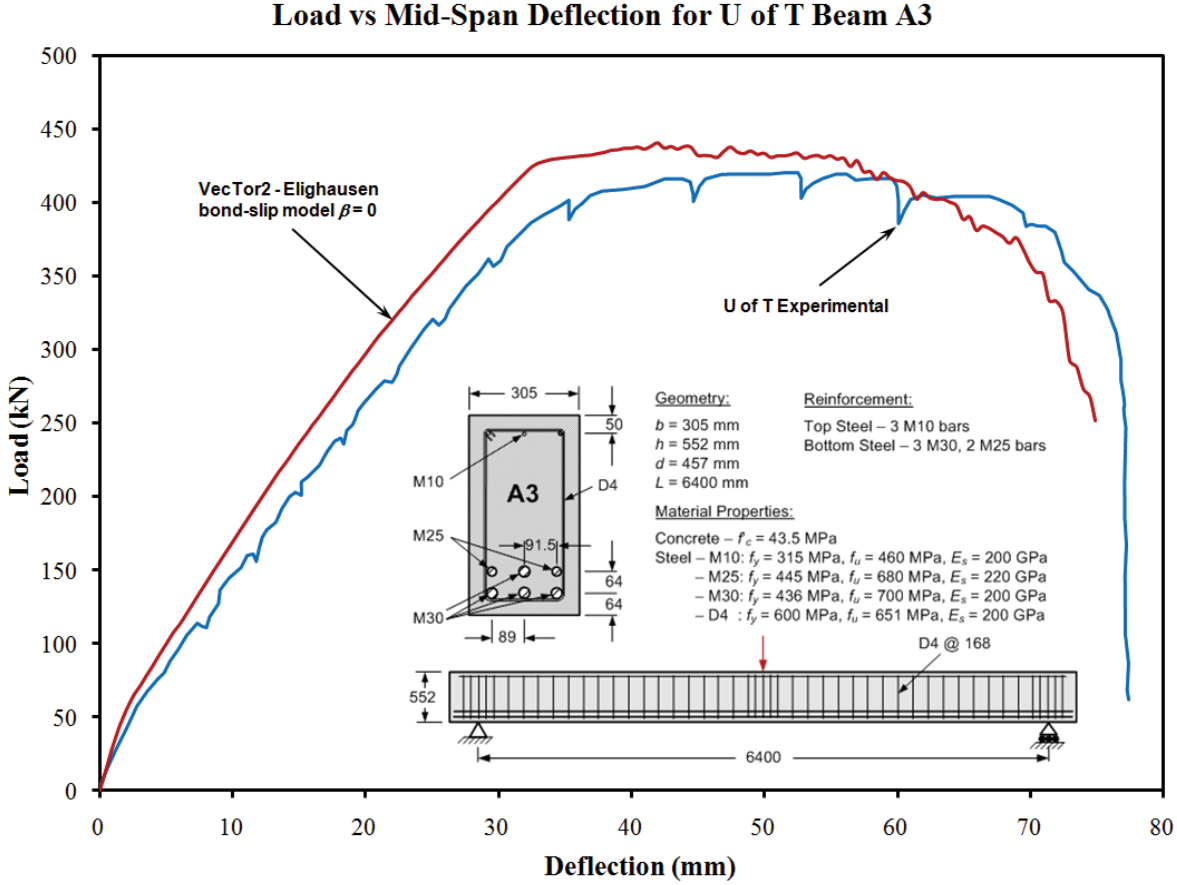

Figure 4-9: Load-deflection curve for UofT beam A3 obtained from VecTor2 analysis

In order to study the effect of finite element mesh size on the numerical results, three different mesh configurations were investigated: meshes of 10×50, 12×67 and 21×100 rectangular elements, as shown in Figure 4-10. The results indicate that they are not sensitive to mesh size. However, in order to compromise between computer execution time and mesh refinement, the 12×67 mesh discretization was chosen for the FE model of the RC beam used in this research.

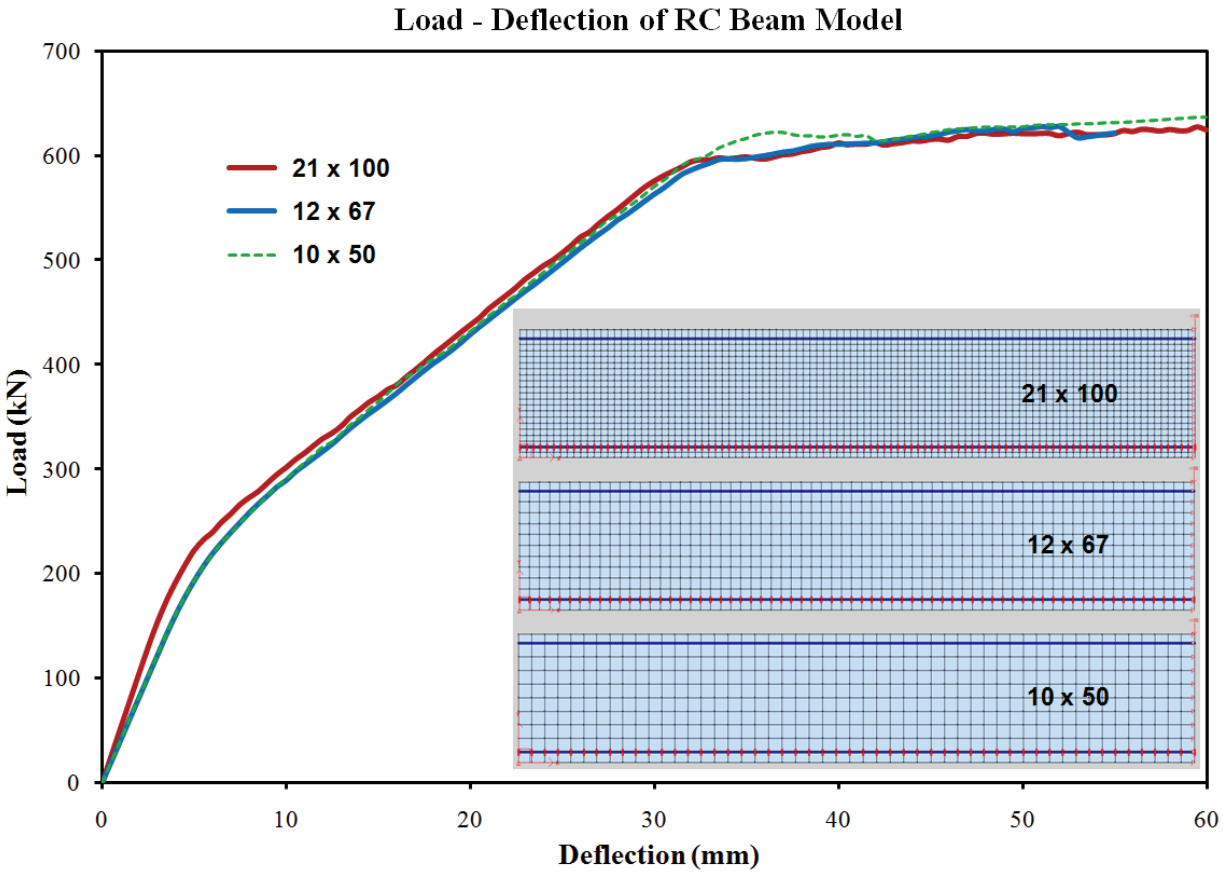

Figure 4-10: Load-deflection curves for different FE meshes obtained from VecTor2 analysis

4.5 Introduction to Case Study: Parking Garage Girder

To study how the time-dependent reliability of a RC beam is affected by corrosion of reinforcement, a representative example beam was designed. The problem selected for demonstration is a RC girder in a parking garage structure. Parking garage structures in

Canada are typically situated in aggressive corrosion environments. In parking structures, the concrete becomes chloride-contaminated when a mixture of de-icing chemicals (chlorides) and snow, carried into the garage on the underside of vehicles, is deposited on the driving surfaces and melts. In the absence of an effective waterproofing system, this chloride-contaminated water soaks into the concrete, with or without the presence of cracks, and eventually penetrates the concrete cover to the embedded steel. This is also the reason why prestressing does not prevent corrosion of embedded reinforcement even when cracking is almost completely eliminated.

In a survey of parking structures constructed before 1980, conducted by the Canada Mortgage and Housing Corporation (CMHC) (Bickley 1984), it was found that in some instances deterioration of unprotected structures became evident 5 years after construction, and thereafter the annual concrete cover delamination rate could be in the order of 3% of the floor area. Furthermore, major repairs were often needed within 10 years of construction. Even in the British Columbia lower mainland, where the use of de-icing chemicals is much lower than in many areas of Canada, older structures were in need of repair due to corrosion caused by de-icing chemicals (Bickley 1984).

Figure 4-11: Corrosion-induced damage in the soffit of girders in a parking garage structure in Ottawa

Corrosion-induced damage in parking garage structures is typically found in the top surfaces of the slabs, particularly in the absence of proper protective membranes or when existing membranes have not been appropriately maintained. Furthermore, corrosion of rebar and the resulting damage is also frequently observed on the tension side of girders and beams, as illustrated in Figure 4-11, found in a parking garage in Ottawa. Similar damage had been observed in many similar parking garages.

Figure 4-12 shows a partial plan view of a typical storey in a multilevel parking garage structure. It also shows the location and basic cross-sectional geometry of the RC girder used for the case study throughout the thesis – G2.

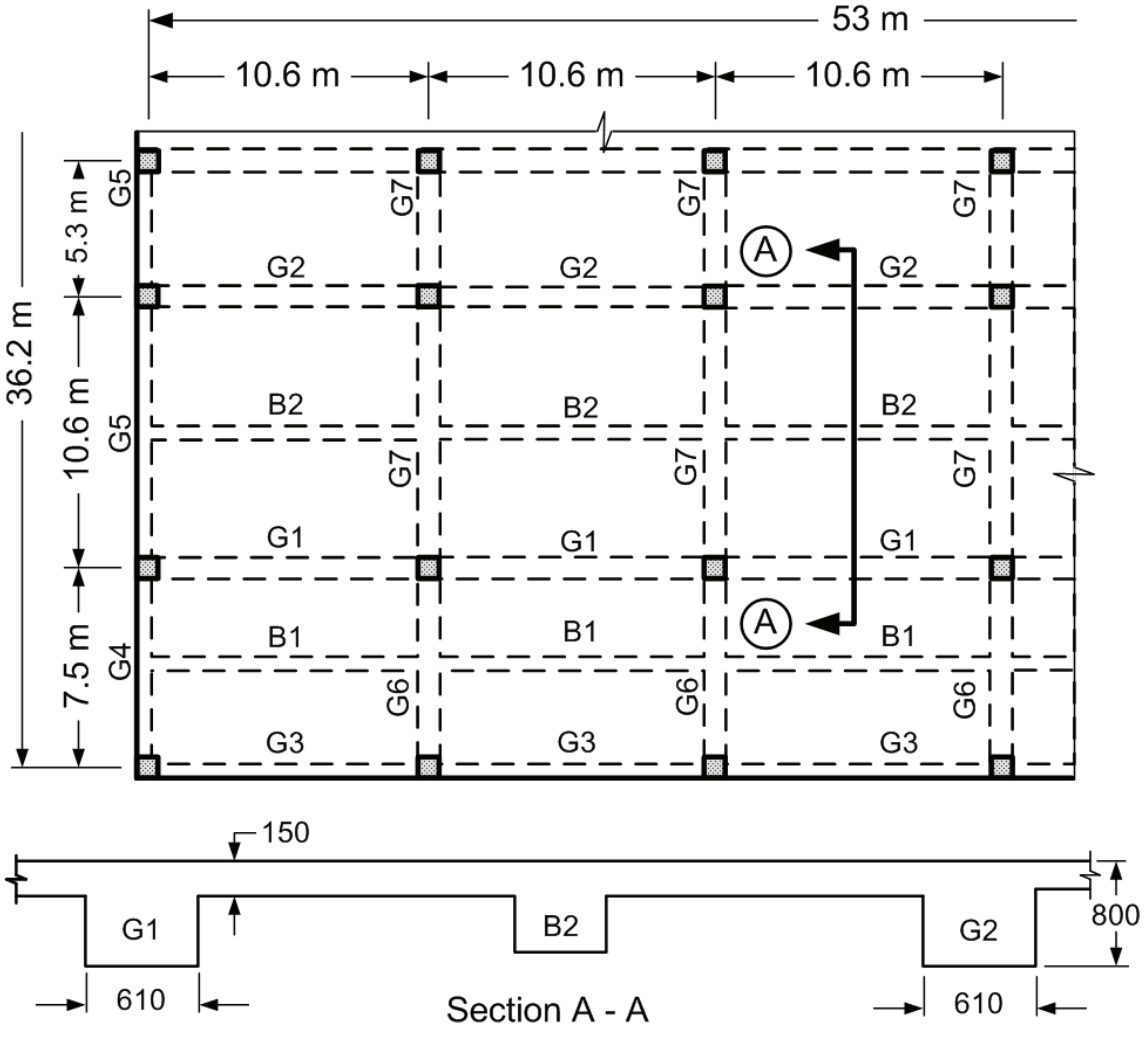

Figure 4-12: Typical parking garage structure and location of girder G2

Certain assumptions were made to simplify the SFEA analysis of girder G2, namely:

(i) the girder is assumed to be simply supported;

(ii) typical end support details are as illustrated in Figure 4-13 (the connection detail shown is for the purpose of the surface envelope requirements and thus, it does not provide significant structural end fixity / moment resistance); and

(iii) contribution of the slab to T-beam action is ignored, thus the cross section of girder G2 is assumed to be rectangular 610 mm × 800 mm through floor depth. The slab is thus part of the dead UDL.

Similar assumptions have been made by other investigators conducting reliability analyses of RC beams in office buildings, for example Stewart (2004; 2009), Val (2007), Stewart and Suo (2008), Stewart and Al-Harthy (2008). Assumption (ii) is conservative – the contribution of the slab to T-beam action would increase stiffness and flexural strength. The simplifying assumption (iii) was made for the benefit of the 2-D FEA model not for the closed form reliability analysis presented in Chapter 5, which could have been as easily carried out for a T-beam.

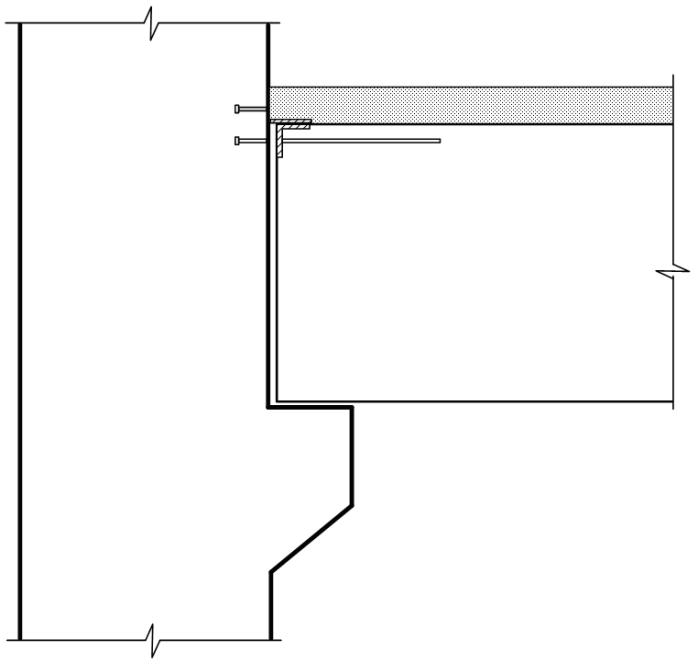

Figure 4-13: Details of the assumed end connection for girder G2

The girder was designed according to the provisions of the current Canadian Concrete Design Standard (CAN/CSA A23.3-04 2004) and the 3rd Edition of the Parking Structures

Standard (CAN/CSA S413-07 2007). The deterministic design parameters are summarized in Table 4-1.

Table 4-1: Nominal design parameters for RC girder G2

Geometry	Length l (mm)	Width b (mm)	Depth h (mm)	Clear cover c (mm)
	10 000	600	810	40
Material Properties	f_c' (MPa)	f_{ct} (MPa)	E_c (MPa)	
Concrete:	40	3.79	28 000	
	f_y (MPa)	E_s (MPa)	f_u (MPa)	
Reinforcing Steel:	430	200 000	680	
Loads	dead w_D (kN/m)	live (sustained) w_L (kN/m)		
	36	34		

The design live load w_L is determined from the specified vehicle design load of 6.0 kPa in CSA S413-07 (2007), used for passenger cars, SUVs, and light trucks, not exceeding 2700 kg. For parking garages restricted to passenger cars only the minimum design load is 2.4 kPa. Further, CSA S413 requires that vehicle design loads be determined from worst case load effects considering both uniformly distributed, and concentrated loads. The standard provides minimum concentrated design loads, and in many practical cases concentrated design loads actually produce the highest load effects. However, to simplify the analysis in this example, it was assumed that the uniform design load of 6.0 kPa governs.

For the parameters in Table 4-1, the design requires tension reinforcement consisting of 7 M30 bars at an effective depth d = 745 mm. Shear reinforcement consists of M10 stirrups spaced at 300 mm over 1350 mm from each end of the girder and 450 mm spacing elsewhere. The cross-sectional details, along with the design moments and flexural design capacities, are shown in Figure 4-14.

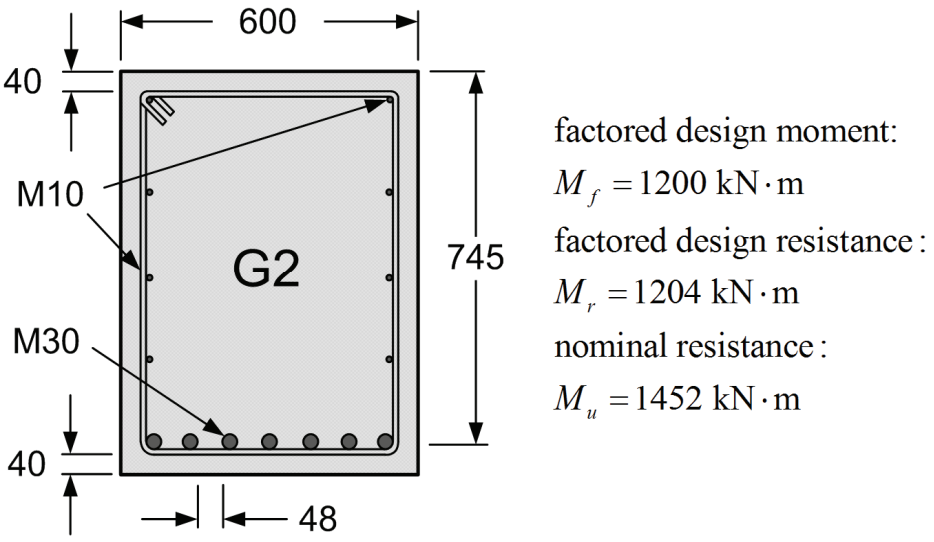

Figure 4-14: Cross-sectional design details for girder G2

4.6 Finite Element Model Validation with Corrosion Damage

A finite element model of the parking girder G2, presented in Section 3.2, was developed and implemented in the VecTor2 nonlinear FE software. Corrosion-induced deterioration was implemented by reducing the cross-sectional area of longitudinal tension reinforcement according to Eq. (4.1) and by reducing the bond strength of the link elements according to Eq. (4.2). Since the value of the corrosion rate i_{corr} cannot be input directly into VecTor2, the parameters in Eqs. (4.1) and (4.2) that depend on i_{corr} must be modified in the input of the FE model. The values in this case are the bar diameter and total cross-sectional area of all the longitudinal tension reinforcement. Likewise, the bond-slip model parameters for the **modified** Eligehausen model, the maximum bond stress $\tau_{max,\ residual}$, the slip at maximum bond stress s'_1, as well as the maximum slip value must also be set in the input prior to running the finite element analysis. Once these values are provided in VecTor2, special attention must be paid in selecting appropriate load/displacement parameters for the analysis (i.e., number of increments, step sizes, convergence limits, etc.) to ensure convergence, stability, and adequate resolution.

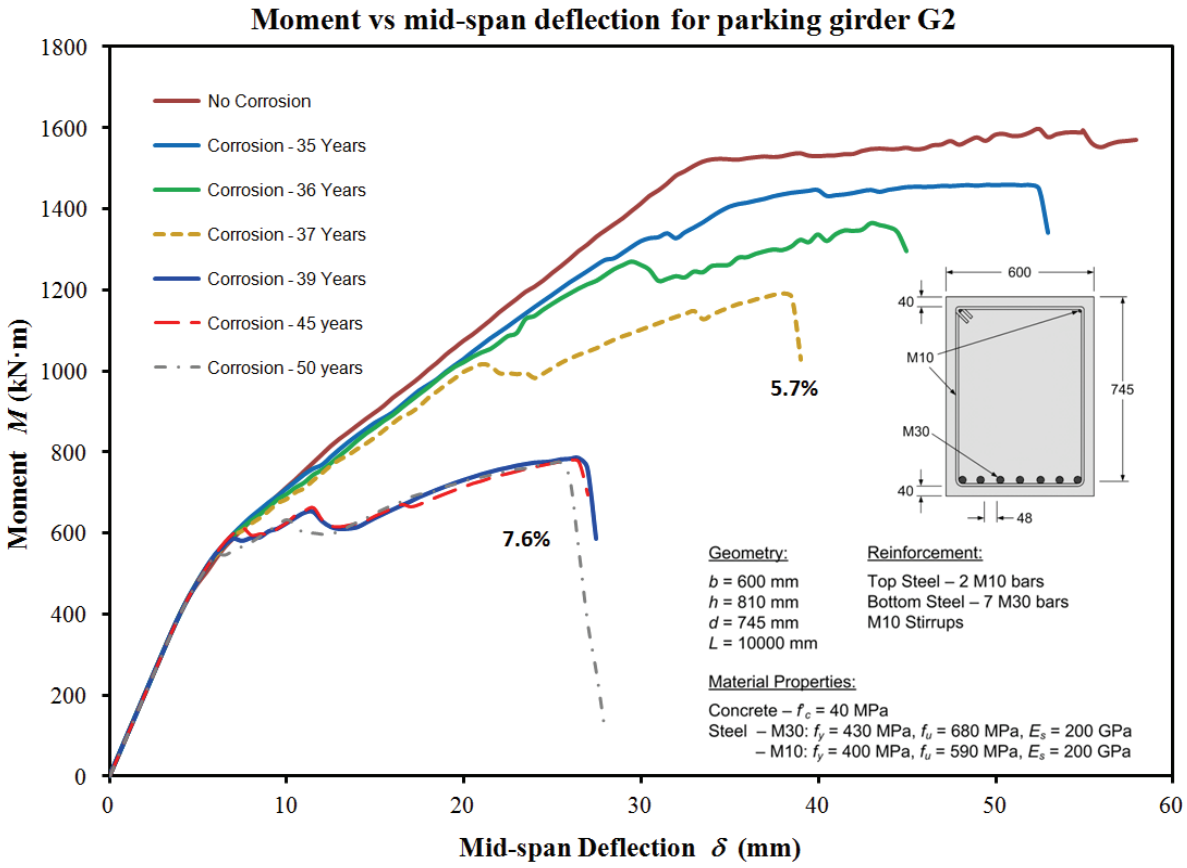

Figure 4-15: Moment-deflection curves for girder G2 for i_{corr} = 1 μA/cm^2 at various times and levels of corrosion (5.7% and 7.6%).

Figure 4-15 presents plots of the flexural strength degradation for the parking girder G2, at progressing points in time, due to uniform corrosion growth. The simulated behaviour includes the coupled effect of reduction of reinforcement area and progressive loss of bond strength as discussed. Validation of the FE model including corrosion-induced strength degradation could only be made in a qualitative sense due to the scarcity of available test data on corroded RC beams. However, the general trend in reduction of flexural capacity, as a function of percentage of steel area loss, can be observed in the few available tests, for example Almusallam et al. (1996) and Mangat and Elgarf (1999a), shown in Figure 4-16 on the next page. Note that the first reference is based on tests of RC slabs, while the latter presents results of accelerated corrosion tests of RC beams under extremely high rates of corrosion. Certainly, direct comparison is not possible, but the ratios of initial capacity at

various corrosion levels are roughly comparable in the case of the RC beam results for Mangat and Elgarf (1999a).

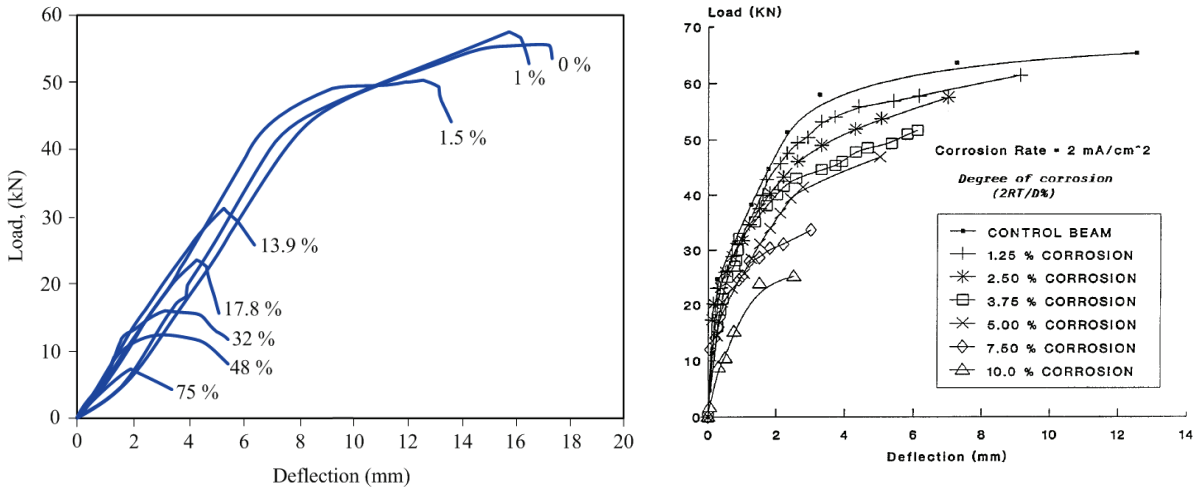

Figure 4-16: Load-Deflection curves for slabs (Almusallam, Al-Gahtani et al. 1996) and RC beams (Mangat and Elgarf 1999a) at various levels of corrosion

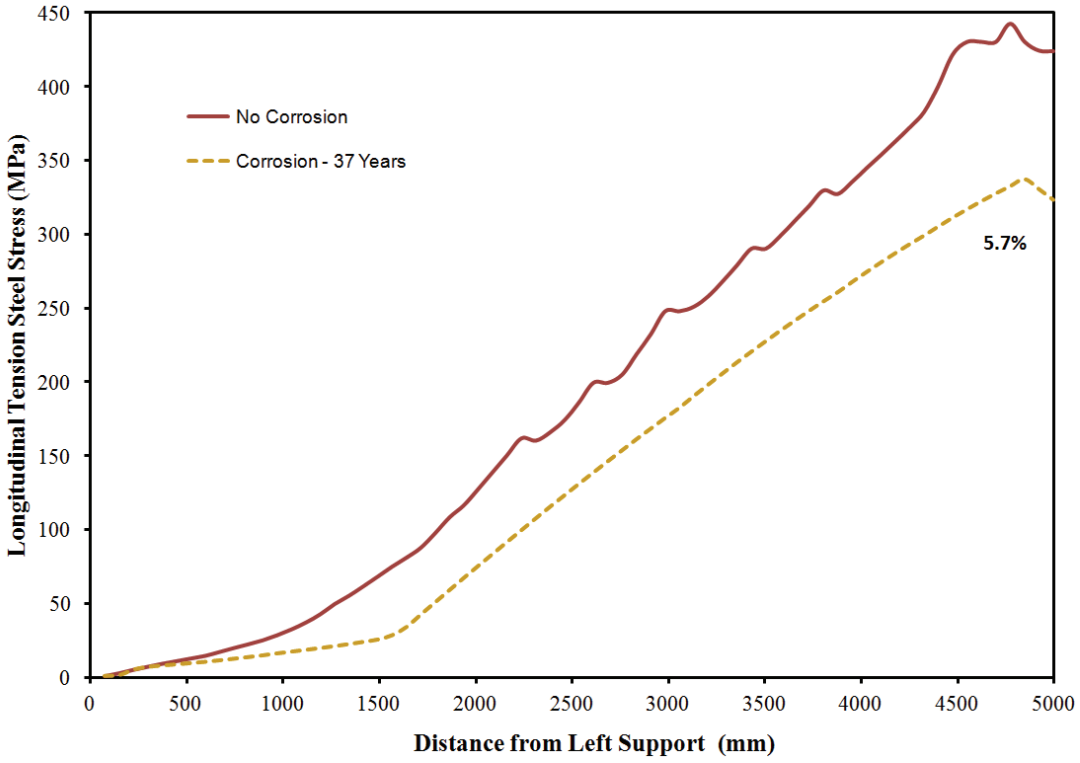

Figure 4-17: Longitudinal tension reinforcing steel stress along the RC beam span for no corrosion and 5.7% corrosion

As shown in Figure 4-17, the effect of corrosion on bond clearly reduces the capacity of the beam and prevents the tensile capacity of the longitudinal reinforcement to develop. This could not have been observed through sectional analysis, where only the reduced $A_s(t)$ could have been included in the calculations.

The principal concrete stress fields and corresponding crack directions for the RC girder G2 at t = 0 years and t = 37 years are compared in Figure 4-18 and Figure 4-19, respectively. Both figures show the principal compressive stresses and crack patterns in the girder at the same load level: a midspan moment M = 1150 kN·m. This load level corresponds to the ultimate moment capacity of the girder at t = 37 years and a corrosion level of 5.7%.

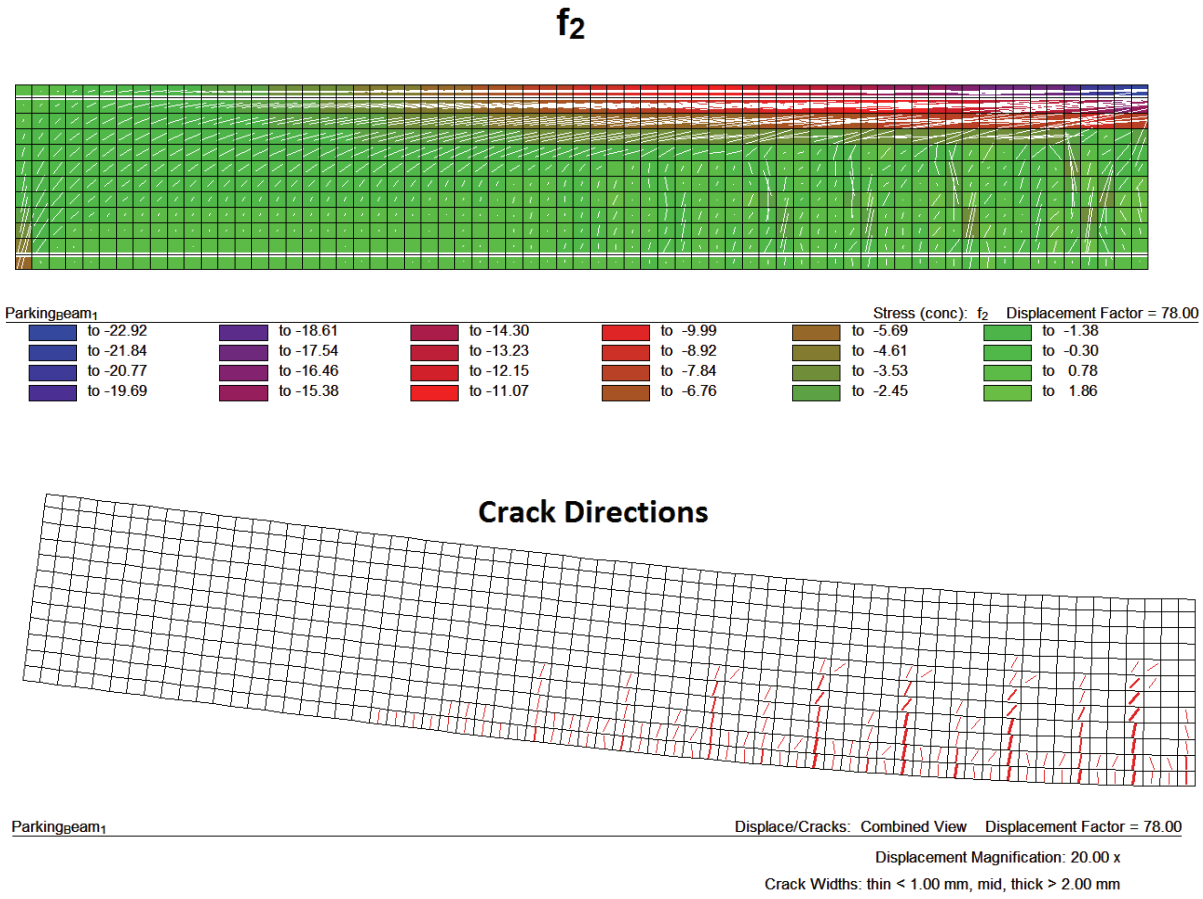

Figure 4-18: Principal concrete compressive stresses and crack directions for the RC beam in the absence of corrosion (t = 0 years, M = 1150 kN·m)

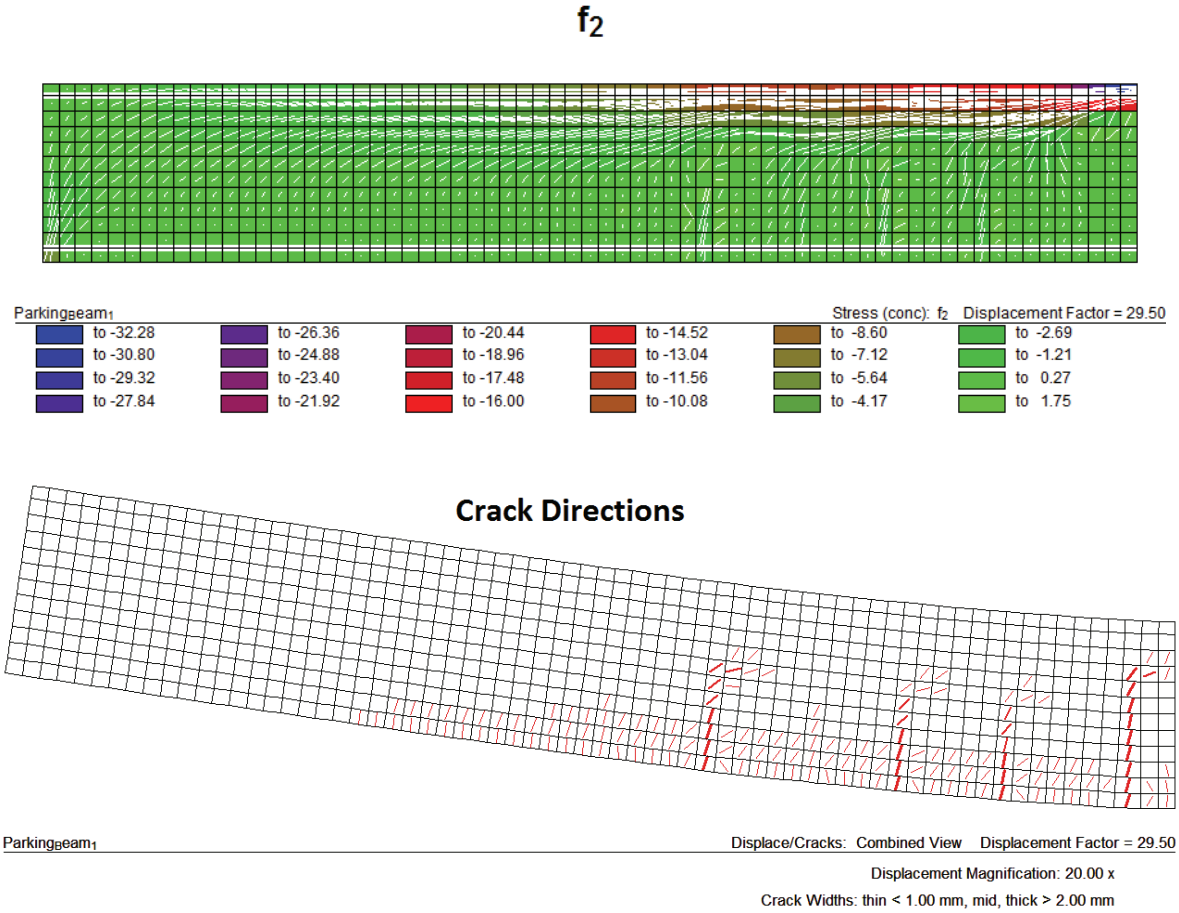

Figure 4-19: Principal concrete stresses and crack directions for the RC beam at 5.7% corrosion (37 years, $M = 1150$ kN·m $= M_u$)

As expected, at $t = 0$ years and no corrosion the beam displays ductile response with a maximum stress of 382 MPa in the tension reinforcement (no yielding), a maximum compressive stress of 23 MPa in the concrete, and a mid-span deflection of 22 mm. Yielding of the tension steel at the mid-span of the beam is initiated at a moment of 1550 kN·m corresponding to a deflection of 45 mm, while ductile failure occurs at 1610 kN·m and a maximum deflection of 70 mm. In contrast, at $t = 37$ years when the degree of corrosion in the tension steel reaches 5.7%, the maximum midspan deflection of the girder at failure is only 29 mm. Furthermore, in agreement with Figure 4-17, yielding of tension steel is never developed due to the severe reduction of composite action. The failure mechanism is therefore caused by the loss of bond at the mid-span of the girder. This observation is also

supported by comparing the crack patterns in Figures 4-18 and 4-19. For the uncorroded beam, Figure 4-18 shows crack development that is well distributed along the midspan region of the beam, which indicates typical composite action. However, as shown in Figure 4-19, the cracking in the girder at 5.7% corrosion is characterized by fewer and larger cracks spaced further apart, implying slippage of the tension steel and associated loss of bond.

Chapter 5. Structural Reliability Analysis Module

5.1 Introduction

Many sources of uncertainty are inherent in structural design, and thus absolute safety (zero probability of failure) can never be achieved. Consequently, structures must be designed to serve their functions with a finite probability of failure (Nowak and Collins 2000).

Society expects buildings, bridges, dams, and other structures to be designed to a "reasonable" level of safety. In engineering practice, these expectations are achieved by following code requirements specifying design values for minimum strength, maximum allowable deflections, and other criteria. Such criteria are commonly referred to as reliability-based design criteria, since they are implemented in a probabilistic context.

This chapter deals with the general concepts behind the application of structural reliability theory and reliability analysis methods, with emphasis on RC structures. These are then applied to the case study of the parking garage girder subjected to corrosion-induced deterioration, introduced in section 3.6, in the form of reliability analysis based on a closed-form limit state function.

5.2 Random Variables

The description of uncertainties in any reliability analysis is accomplished through the definition of random variables for the parameters known, or considered, to be significant. Detailed presentation of how uncertainties are represented through random variables and fields, and how these fields are used in SFEA, is provided in Appendix B. As mentioned there, for certain problems in reliability analysis the basic parameters are assumed to be spatially-invariant, allowing them to be represented by single-valued random variables. In

other cases, it is essential to consider some variables as being randomly distributed in space or time. In such cases the input data may need to be modeled by random fields or processes.

The random variables of significance in the reliability analysis of corroding RC beams include: (i) the applied dead and live loads; (ii) material properties of concrete and steel; (iii) geometric properties, included in Table 5-1; and, (iv) parameters related to corrosion. With some exceptions, in the limit state function $g(\boldsymbol{X}) = \boldsymbol{R} - \boldsymbol{S}$, the loads contribute to the demand component $\boldsymbol{S}$, the material properties and corrosion effects relate mainly to the capacity component $\boldsymbol{R}$, while geometric properties can figure in both.

Selection of the random variables for the current study is primarily based on the information available in the literature, summarized in Table 5-1. The random variables used in the analysis presented here are single random variables (not random fields/processes). This assumption is reasonable for the variables considered here for the following reasons:

1. The dead load can be assumed not to vary with time. This is also the case for vehicle loads in parking garages which are typically modeled as sustained live loads (not transient).
2. Material properties such as the compressive and tensile strength of concrete, as well as the concrete modulus of elasticity vary throughout the structure. However, the reliability analysis presented here is based on a closed-form limit state function based on utilizing the nominal flexural strength formula for RC beams. Therefore, spatial discretization of a random field cannot be implemented in this approach. For reinforcing steel properties, spatial variance is insignificant, therefore, a single random variable accounts for uncertainty between specimens.
3. Research shows that the rate of corrosion of steel rebar in RC structures exhibits very strong scatter, both spatially and temporally (Glass and Buenfeld 2000; Vu and Stewart 2000). As in the previous point, the current analysis approach cannot account for this variability. Further, characterization of the rate of corrosion with such complex and simultaneous variability in space and time is extremely difficult even if the current model could be utilized with random fields. Also, only uniform (generalized) corrosion is analyzed herein. It is therefore reasonable to represent the rate of corrosion with a single random variable.

Table 5-1: Typical values of random variables for RC structures and rates of corrosion

Variable	Description	Units	Mean	COV	PDF type	Source
i_{corr}	corrosion rate	$\mu A/cm^2$	1.0	0.30	Normal	Stewart et al. (2008)
			0.5	0.10	Normal	
			1.0	0.20	Normal	
			3.0	0.30	Normal	Val, Stewart, and Melchers (1998)
			5.0	0.40	Normal	
			10.0	0.50	Normal	
d	effective depth	mm	Nominal	0.03	Lognormal	Enright and Frangopol (1998), Nowak et al. (1994)
	to reinforcement		Nominal	0.05	Normal	Val, Stewart, and Melchers (1998)
			Nominal	0.02	Normal	Val (2008), Lu et al. 1994
d_{bo}	initial bar diameter	mm	Nominal	0.02	Lognormal	Enright and Frangopol (1999), Nowak et al. (1994)
f'_c	concrete strength	MPa	Nominal	0.18	Lognormal	Enright and Frangopol, 2001, Nowak et al. (1994)
			Nominal	0.18	Lognormal	Val (2008), Mirza, et al. 1979
f_y	steel yield strength	MPa	Nominal	0.10	Lognormal	Enright and Frangopol 2002, Nowak et al. (1994)
			Nominal	0.10	Lognormal	Val (2008); Mirza and McGregor (1979)
			Nominal	0.10	Normal	Val, Stewart, and Melchers (1998)
			Nominal	0.03	Normal	Stewart and Suo (2009)
w_D	uniform dead load	kN/m	Nominal	0.10	Gamma	Val (2008), Ellingwood et al. (1982)
			Nominal	0.10	Normal	Val, Stewart, and Melchers (1998)
			1.05 Nom	0.10	Gamma	Val (2008), Ellingwood et al. (1982)
w_L	uniform live load	kN/m	*Nominal*	*0.12*	*Gumbel*	
	(sustained)		0.30 Nom	0.60	Gamma	Val (2008), Chalk and Corotis (1980)

5.3 Limit States

Of interest in this research is the current lack of a durability limit state in current design codes. As mentioned in Chapter 1, a durability limit state is mentioned in the CAN/CSA A23.3-04 concrete design standard (2004) (referenced to CSA A23.1(2004) and CAN/CSA-S413 (2007)). However, it is merely a prescriptive specification on concrete mix design and minimum concrete cover thickness in RC members. It may be argued that in many cases durability concerns the serviceability of the structure, such as the functionality and aesthetic aspects, since if limits for necessary repairs or maintenance actions are exceeded, this is usually considered a serviceability problem. However, it should be noted that in cases where deterioration might go unobserved, the durability problem can be directly associated with an ultimate state (Vrouwenvelder and Schiessl 1999). For various reasons, cracking followed by corrosion might go undetected and collapse of the structure may occur. According to Vrouwenvelder and Schiessl, durability is always an aspect of either an ultimate or a serviceability limit state (1999).

Two limit states are considered as part of this research, namely flexural strength and midspan deflection of the RC girder.

5.3.1. Performance Function for Ultimate Limit State in Flexure

A limit state function is generally expressed in terms of the flexural capacity M_u, and the load effects due to applied dead and live load moments, M_{DL} and M_{LL}:

$$g(\boldsymbol{X})_{\text{Flexure}} = M_u - (M_{DL} + M_{LL}) = 0 \tag{4.7}$$

The flexural capacity of the RC beam M_u, is a function of the material, geometry, and the environmental load degradation mechanisms. The applied moments are also a function of the dead and live load random variables. If the above equation for M_u is available analytically the reliability problem may be analyzed directly. Hence, an analytical limit state function can be derived from the expression for nominal ultimate moment capacity in the CSA A23.3-04 design standard (2004), resulting in:

$$g(\boldsymbol{X})_{\text{Flexure}} = A_s \cdot f_y \left[d - \frac{A_s \cdot f_y}{2\alpha_1 f_c' b} \right] - \frac{(w_D + w_L) \cdot l^2}{8} \tag{4.8}$$

The limit state function for a flexural strength of RC beams given by Eq. (5.2), can be further extended to include the time dependent effects of corrosion. The uniform corrosion process considered here leads to a uniform reduction of reinforcement area, while effects of bond deterioration are ignored. The reduction of bar diameter due to corrosion as a function of time was derived in Chapter 4 and expressed by Eq.(4.1). Substituting this relationship into the formula for the area of a circle (bar area) results in:

$$A_s(t) = \frac{n\pi}{4}\left(d_{\text{b}} - 0.0232 \cdot i_{\text{corr}} \cdot t\right)^2 \tag{4.9}$$

Substituting Eq. (5.3) into Eq. (5.2) leads to the following limit state function:

$$g(\boldsymbol{X},t)_{\text{Flexure}} = A_s(t) \cdot f_y \left[d - \frac{A_s(t) \cdot f_y}{2\alpha_1 f_c' b} \right] - \frac{(w_D + w_L) \cdot l^2}{8} \tag{4.10}$$

Equation (5.4) now accounts for the loss of area of steel due to corrosion as a function of time.

For the stochastic finite element analysis, the flexural capacity M_u in Eq. (5.1) is obtained from the FE model (VecTor2), while the demand M is calculated from $(w_D + w_L)l^2/8$ within the reliability implementation in COMPASS. Thus Eq. (5.1) can be re-stated as:

$$\begin{aligned} g(\boldsymbol{X},t)_{\text{Flexure}} &= M_{FEA \cup RSM}(\boldsymbol{X}) - M_{REL}(w_D, w_L) \\ &= M_{\text{VecTor2} \cup RSM}(\boldsymbol{X}) - M_{\text{COMPASS}}(w_D, w_L) \end{aligned} \tag{4.11}$$

5.3.2. Performance Function for Serviceability Limit State

Similarly, the SLS can be expressed as:

$$g(\boldsymbol{X})_{\text{Deflections}} = \delta_{\max} - \delta \tag{4.12}$$

Here, the limit state function is a little different in that the capacity is represented by the maximum allowable deflection δ_{max}, which is a constant (span/360), while the demand δ is now obtained through the finite element model. The performance function can thus be rewritten as:

$$\begin{aligned} g(\boldsymbol{X})_{\text{Deflections}} &= \delta_{\max} - \delta_{FEA \cup RSM}(\boldsymbol{X}) \\ &= \frac{l}{360} - \delta_{\text{VecTor2} \cup RSM}(\boldsymbol{X}) \end{aligned} \tag{4.13}$$

5.4 Time-dependent Reliability Analysis

Time-dependent reliability analysis of structures is of interest for two main reasons:

1. Most of the loads acting on structures are time-dependent (time-parametered random processes); and
2. Material and strength properties of structural members/components are subject to variation over time due to degradation processes such as those caused by corrosion, fatigue, crack propagation, and creep.

For time-dependent problems, a general form of the limit state function can be expressed as:

$$g = g\left(\boldsymbol{X}(t)\right) \tag{4.14}$$

The failure probability is then given by:

$$p_f(t) = \int_{g(\boldsymbol{X}(t) \le 0)} f_{\boldsymbol{X}(t)}\left[\boldsymbol{X}(t)\right] d\boldsymbol{X}(t) \tag{4.15}$$

Equation (5.9) implies that the time-variant reliability problem is considerably more difficult than its time-invariant counterpart. First, the joint probability density function of the loading and strength parameters is continuously changing with time. Secondly, the failure surface and hence the domain of integration varies from time-to-time in general, and thus, the failure probability itself also changes with time.

For this class of reliability problems, the failure event constitutes the out-crossing of the vector process through the limit state surface $g = g\left(\boldsymbol{X}(t)\right) = 0$, as shown in Figure 5-1. The exact solution of this out-crossing probability problem is not available even for the simplest case of linear limit state function involving only stationary random processes.

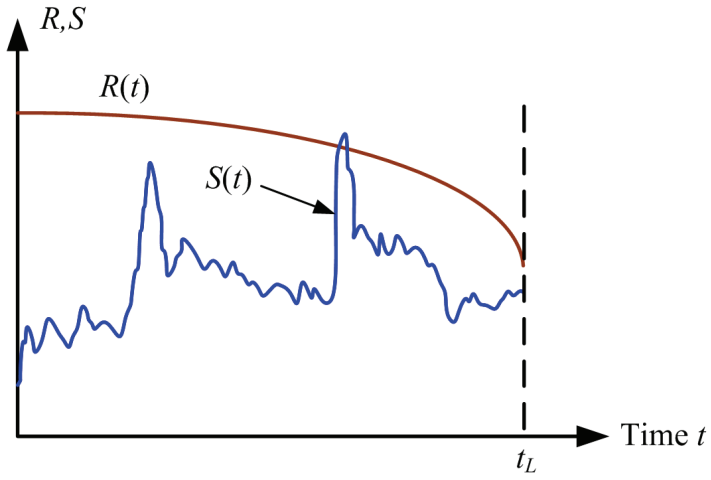

Figure 5-1: Realization of load effect $S(t)$ and resistance $R(t)$ (Stewart et al, 1998b).

In structural applications, particularly structural dynamics (e.g. wind engineering), the time dependent parameter is often the dynamic loads acting on a structure. The design practice is geared towards the determination of the maximum value of the load $z(t)$ in a given time period, T. Thus, the general reliability problem for this case may be stated as:

$$p_f = \mathrm{P}\left[\left(R(\boldsymbol{X}) - \max_T z(t)\right) \le 0\right] \tag{4.16}$$

In the above formulation, the maximum value of the load process $z(t)$ is a random variable, which is determined from the appropriate distribution function of the parent distribution. Extreme value analysis procedures (utilizing extreme value distributions) for achieving this are available. Hence, it should be possible to deal with Eq. (5.10) with a time-invariant random variable problem using the techniques for spatial random processes sections.

More sophisticated methods for time-dependent reliability analysis are available and perhaps applicable. Representing the vector of random variables as $z(t) = \left(\boldsymbol{X}(t)^T, \boldsymbol{y}(t)^T\right)^T$, where

$\boldsymbol{X}$ is the vector of time-independent random variables and $\boldsymbol{y}(t)$ is the vector of time-dependent random variables, the probability that failure occurs in the time interval [0, T] is:

$$p_f(t) = \int P\left[\min_{t\in[0,T]}\left(\boldsymbol{y}(t)\middle|\boldsymbol{X}\right) < 0\right] f_X(\boldsymbol{X})\, d\boldsymbol{X} \tag{4.17}$$

where $f_x(\boldsymbol{X})$ is the PDF of $\boldsymbol{X}$. An important step is to determine the conditional failure probability:

$$P(x_1) = P\left[\min_{t\in[0,T]}\left(\boldsymbol{y}(t)\middle|\boldsymbol{X}\right) < 0\right] \tag{4.18}$$

The conditional failure probability is the probability that the vector process $\boldsymbol{y}(t)$ is in the failure set at the beginning or during the time interval [0, T]. This failure probability is bounded in terms of the probability of failure at time $t = 0$, $p_{fp}(x_1)$, and the expected number of outcrossings, $N(x_1)$, into the failure domain by an expression proposed by Madsen and Tvedt (1990):

$$p_f(x_1) \le p_{f_o}(x_1) + N(x_1) = P\left[g\left\{x_1, x_2(0)\right\} \le 0\right] + \nu(x_1)T \tag{4.19}$$

where $\nu(x_1)$ is the mean outcrossing rate for the stationary random process. The conditional failure probability $p_f(x_1)$ may also be approximated as (Madsen and Tvedt 1990):

$$p_f(x_1) = \left[1 - p_{f_o}(x_1)\right] \exp\left[\frac{\nu(x_1)T}{1 - p_{f_o}(x_1)}\right] \tag{4.20}$$

The term p_{fo} may be calculated by a conventional time-independent reliability analysis method such as FORM, SORM, or FORM-based response surface analysis.

In the presence of degradation mechanisms, the ultimate strength of a RC structure $R(t)$ is a decreasing function of time, therefore, the probability of failure is also a function of time. By varying the time period $R(t)$ can be estimated. Furthermore, the instantaneous failure probability at any time t, defined by $P[R(t) < S(t)]$ without regard to survival of the structure in the previous years, can be obtained using Eq. (5.9).

However, successive yearly loading and decreasing values of yearly structure ultimate strength are dependent events and must be accounted for in reliability estimation. This can be accomplished by using time-dependent or progressive reliability estimates that are based on conditional probability theory. The hazard rate, or failure function strategy, is used herein. The progressive or time-dependent reliability, $\gamma_p(t)$, of a degrading RC structure can be expressed by:

$$\gamma_p(t) = \exp\left(-\int_0^t \lambda(\tau)\, d\tau\right) \tag{4.21}$$

where τ is the variable of integration, and $\lambda(t)$ is the conditional probability function referred to as the hazard rate by Ellingwood and Mori (1993) and is defined by $\lambda(t) = P$[failure between time t and $t + dt$ | no failure up to time t]. This implies independent annual failure probabilities. For continuous systems, the hazard rate is defined by Ang and Tang (1984) as:

$$h(t) = \frac{f(t)}{1 - F(t)} \tag{4.22}$$

where $f(t)$ is the joint probability density function and $F(t)$ is the joint cumulative density function. For discrete space with one year increment, the hazard function simply becomes:

$$h(t_i) = \frac{p_f(t_i)}{1 - \sum_{j=1}^{i-1} p_f(t_i - 1)} \tag{4.23}$$

Substituting Eq. (5.17) into Eq. (5.15) gives the time-dependent reliability. The time dependent failure probability is given by:

$$p_{ft}(t) = 1 - \gamma_p(t) \tag{4.24}$$

where the subscript *ft* is for time-dependent failure probability. Equation (5.18) is therefore used to estimate the progressive or time-dependent reliability.

The time-dependent reliability is determined through post-processing of the reliability results generated in COMPASS.

5.5 Implementation of Reliability Analysis in COMPASS

COMPASS (COmputer Methods for Probabilistic Analyses of Structures and Systems) is a general purpose software for the reliability and risk analysis of stochastic systems. The program was developed and is maintained, marketed, and supported by Martec Limited: an engineering consultancy based in Halifax, Nova Scotia, Canada.

The development of COMPASS was aimed at the practical application of probabilistic reliability analysis methods amongst professional engineers and scientists. COMPASS provides a platform for the application of advanced probabilistic concepts and methodologies (Liu, Orisamolu et al. 1999).

5.5.1. Overview of COMPASS Features and Capabilities

The principal features and capabilities of COMPASS consist of the following:

- Random variable definition;
- Component definition;
- System definition;
- First-order and second-order reliability methods (FORM/SORM);
- Simulation;
- Determination of reliability index β and corresponding probability of failure;
- Parameter sensitivity of first-order reliability index and failure probability;
- Parametric studies; and,
- System reliability analysis.

A set of random variables and constants can be created in the variable definition phase, which often represents the first step of a new reliability analysis. The definition of random variables requires specification of probability distributions and the associated statistical parameters. COMPASS has a built-in library of 16 commonly used probability distributions (Liu, Orisamolu et al. 1999). Correlations between random variables can be defined either through a correlation matrix or a pair wise specification of the correlation coefficient between two random variables. The use of correlations to describe statistical dependence is a

very practical approach to the probabilistic modelling of engineering parameters. The representation is exact for normal (Gaussian) variables and approximate (but reasonably accurate) for non-normal random variables (Liu, Orisamolu et al. 1999).

A component is the fundamental concept for the representation of performance or failure modes in probabilistic reliability analysis, and a set of components can be created and analyzed in COMPASS. Each component requires a limit-state function which is defined in terms of random variables that are chosen from the variable set defined previously. Although a library of explicit limit-state functions for several engineering applications is provided with COMPASS, for the research work presented here it was necessary to develop and implement custom performance functions. This was accomplished through development of user-programmed Fortran subroutines describing the limit-state functions of interest. The user-defined source code file contains all required limit-state functions and may be updated as required, thereby serving as the user's own library. The user defined file developed as part of the work presented here is attached in Appendix G. The file contains the Fortran source code for the explicit closed-form limit state functions used for the analysis presented here, as well as the general second-order response surfaces and implicit limit state functions used for SFEA shown in Chapters 6 and 7.

Most reliability analysis algorithms require the calculation of the gradients of limit-state functions. These are normally computed automatically in COMPASS using a numerical finite-difference method and in most cases the resulting gradients are sufficiently accurate. However, the user can also specify explicit gradient calculations through own Fortran subroutines.

The first-order reliability method (FORM) is one of the classes of algorithms available for reliability analysis in COMPASS. As described in Appendix A, the FORM procedures are based on the replacement of limit-state functions by tangent hyper-planes at design points in a transformed standard normal space. The design points are the points of maximum likelihood of failure (i.e. highest joint probability density) in the transformed normal space. These are also referred to as the most probable points (MPP) or failure point. A computation

of the distance from the origin to the MPP defines the reliability index β, and it is related to the failure probability p_f through Eq.(A.12).

COMPASS allows the choice of four FORM algorithms, including the Rackwitz/Ang/Tang algorithm, HL-RF algorithm, modified HL-RF algorithm, and an enhanced sequential quadratic programming (SQP) algorithm. For each of the FORM options, eight possible convergence criteria may be selected. FORM algorithms give exact solutions for linear limit-state functions.

COMPASS also includes algorithms for the second-order reliability method (SORM). This class of procedures is based on the replacement of the limit-state functions by hyperparaboloids fitted at design points in a transformed standard normal space. In general, SORM algorithms give more accurate results than FORM for nonlinear limit-state surfaces. Three SORM procedures (based on a curvature-fitting scheme for the hyperparaboloid approximation) are available in COMPASS. These include Breitung's asymptotic formula (Breitung 1984), Hohenbichler's asymptotic formula (Hohenbichler and Rackwitz 1988), and one based on the exact integral formula derived by Tvedt (1990). It should be noted that SORM results depend on FORM results. The SORM failure probability p_f, defined by Breitung's formula is given by Eq.(A.17).

Simulation schemes are also available in COMPASS for estimating the probability integral in reliability analysis. Both, the direct Monte Carlo Simulation scheme and Importance Sampling (IS) techniques are available in COMPASS for estimating the failure probability and reliability index for components and series systems. Parallel systems can be analyzed using only the direct Monte Carlo simulation scheme. The simulation of random variables covers all the types of PDFs in the COMPASS distribution library. The accuracy of direct Monte Carlo simulation depends heavily on the size of samples. Importance sampling aims at enhancing simulation efficiency by reducing sample size.

Computation of probabilistic sensitivity measures is an important part of modern reliability analysis. In many applications, the identification of the main sources of uncertainty which have significant influences on the reliability of a system is as important as the calculation of

failure probabilities. COMPASS has capabilities for computing several parameter sensitivity measures based on FORM results. COMPASS first computes the sensitivities of the distribution parameters and then computes the sensitivities of means and standard deviations. Since parameters in limit-state functions can be converted to distribution parameters by introducing fixed-valued variables, only capabilities for computing sensitivities with respect to distribution parameters, P_i are computed in COMPASS. These cover β and p_f sensitivities, namely:

$$\frac{\partial \beta}{\partial P_i} \quad \text{and} \quad \frac{\partial p_f}{\partial_i P_i} \tag{4.25}$$

Importance factors, α, are also computed, in which

$$\alpha^* = \frac{\nabla g\left(U^*\right)}{\left|\nabla g\left(U^*\right)\right|} \tag{4.26}$$

where g is the limit state function, U^* is the most probable point in the standard normal space (u-space), and ∇ is the gradient operator. Importance factors express the relative importance of the different sources of uncertainty associated with the basic random variables that define a problem.

Another important capability available in COMPASS is one for performing probabilistic parametric studies to evaluate how the reliability index β, or the failure probability p_f, varies with a selected limit-state parameter.

5.5.2. Application of COMPASS

The reliability analysis algorithms in COMPASS are directed toward the evaluation of the probability of failure, p_f corresponding to the generalized limit-state function $g(\mathbf{X})$ given by Eqs. (A.2) and (A.4). The probability of failure is defined by the multi-dimensional integral in Eq. (A.7), over the failure domain Ω represented as:

$$\Omega = \left\{ g\left(X_1, X_2, ..., X_n\right) < 0 \right\} \tag{4.27}$$

Thus, the analyst is responsible for defining the random variables, X_i, and the limit-state functions $g_i(\boldsymbol{X})$. Components may then be defined in terms of these limit-state functions and, in turn, systems may be defined in terms of the components.

The full version of COMPASS can be executed through a graphical user interface or in batch mode (command line prompt), which requires working directly with the ASCII format input files (Liu, Orisamolu et al. 1999). The version of COMPASS used in this research was limited to batch mode only. Results of an analysis are saved to text files which can be viewed directly or imported for processing into a spreadsheet program. The output files contain an echo of the user input as well as analysis results such as β, p_f, uncertainty importance factors, parametric sensitivities, number of reliability iterations required for convergence, number of Monte Carlo simulation samples, etc. In addition, the PDF or CDF of random variables may be plotted.

Customization of COMPASS

In order to permit the utilization of user-programmed limit-state functions or gradients for the user's applications, COMPASS is provided not only in executable code format, but also as object codes. Once the custom user defined subroutines have been developed, they can be compiled and linked with the other COMPASS object codes and libraries to generate a custom version of COMPASS. The version of COMPASS used in this work was customized by defining limit state functions for analysis of RC beams including limit state functions formulated in response surface methodology format (Appendix H). Note that cumulative, or time-dependent, probabilities of failure must be calculated analytically (post processing). COMPASS provides instantaneous values only.

5.6 Reliability Analysis of RC beams with corroding reinforcement

This section presents the details and results of the reliability analysis carried out for the example case study of the RC parking garage girder G2, introduced in section 3.6. The initial set of deterministic and random variables used in the analysis is presented in Table 5-2. The statistical parameters in the last column of the table are simply the values describing the

specific probability density function for each random variable calculated from the means and standard deviations, and can be found in the monograph by Haldar and Mahadevan (2000b), amongst many other.

Table 5-2: Initial set of variables for RC girder G2

No	Variable	units	PDF	μ	CoV	σ	PDF Param.
1	Corrosion rate - i_{corr}	$\mu A/cm^2$	Log-normal	1.0	0.30	0.3	0.0000E+00 0.2936E+00 -0.4309E-01
2	Bar diameter - d_b	mm	Normal	29.9	0.02	5.98	0.2990E+02 0.5980E+01
3	Steel yield strength - f_y	MPa	Log-normal	430	0.10	43.0	0.0000E+00 0.9975E-01 0.6059E+01
4	Concrete strength – f'_c	MPa	Log-normal	40	0.18	7.20	0.0000E+00 0.1786E+00 0.3673E+01
5	Section width - b	mm	Deterministic	600	---	---	---
6	Effective depth - d	mm	Log-normal	745	0.03	22.4	0.0000E+00 0.2999E-01 0.6613E+01
7	Dead load - w_D	kN/m	Normal	36	0.10	3.60	0.3600E+02 0.3600E+01
8	Live load - w_{Ls}	kN/m	Gamma	12.92	0.66	8.53	0.0000E+00 0.2778E+01 0.2723E+00
9	Number of bars - n	---	Deterministic	7	---	---	---
10	Beam span - L	mm	Deterministic	10000	---	---	---

The majority of the random variables in Table 5-2 have mean values equal to the design variables, and coefficients of variance, and PDFs based on representative values in the literature, as per Table 5-1. The exception is the live load, which in reliability analysis is normally represented by a sustained service live load (instantaneous distribution) and not the design load. The reason for this is that the design load is generally derived from a Type I extreme value distribution (Gumbel), representing the maximum load expected for a certain return period, as illustrated in Figure 5-2. The instantaneous distribution is typically modeled by a Gamma distribution with a mean and coefficient of variance related to the area of

influence of the live load. For the problem here, the mean value for w_L is assumed to be 0.38 of the design value.

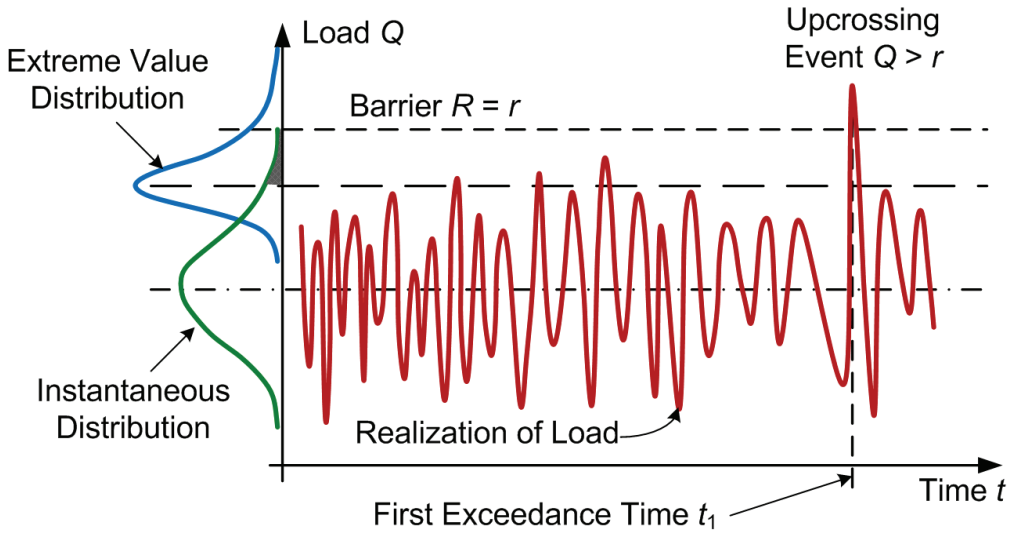

Figure 5-2: Realization of wind loading modeled as a continuous random process showing an exceedance of structural resistance and time to first exceedance.

In practice, some of the variables in reliability analysis may have insignificant impact on the calculation of the probability of failure and could be treated as deterministic parameters in order to optimize the computational effort. In some cases several deterministic calculations are sufficient to determine the sensitivity of the response to various input variables, allowing selection of a smaller number of the most significant variables. Determination of parameter sensitivity is inherent to reliability analysis techniques such as FORM.

For the variables in Table 5-2, the limit state function given by Eq. (5.4) can be restated as:

$$g\left(\left\{i_{corr}, d_b, f_y, f_c', d, w_D, w_L\right\}, t\right)_{\text{Flexure}} = A_s(t)\cdot f_y\left[d - \frac{A_s(t)\cdot f_y}{2\alpha_1 f_c' b}\right] - \frac{(w_D + w_L)\cdot l^2}{8} \quad (4.28)$$

The analysis was carried out for a time frame of 50 years, a reasonable lifespan for the given type of structure. For each year, the analysis included FORM (on average 6 iterations), direct Monte Carlo simulation (50 million cycles per year), and probabilistic sensitivity analysis. It is important to note the following three assumptions in the analysis:

1. Corrosion begins at time 0; there is no period for corrosion initiation;
2. The process runs without interruptions, such as maintenance repairs; and
3. Only uniform corrosion is considered; effects of pitting corrosion are not modeled.

5.6.1. Results of Reliability Analysis for the Initial Set of Variables

The time-dependent reliability of the girder G2 is shown in Figure 5-3, while the corresponding time-dependent probability of failure is displayed in Figure 5-4. Selected values of reliability index and probability of failure, both instantaneous and cumulative, for the case of corrosion, are presented in Table 5-3, below.

Table 5-3: Results of reliability analysis for RC beam study 2

Time (years)	Instantaneous		Time-dependent	
	$\beta(t)$	$p_f(t)$	$\beta(0, t)$	$p_f(0, t)$
1	3.96	3.74×10^{-5}	3.96	3.74×10^{-5}
2	3.96	3.83×10^{-5}	3.79	7.56×10^{-5}
3	3.95	3.92×10^{-5}	3.68	1.15×10^{-4}
:	:	:	:	:
:	:	:	:	:
23	3.83	6.47×10^{-5}	3.04	1.20×10^{-3}
24	3.82	6.63×10^{-5}	3.02	1.26×10^{-3}
25	3.82	6.79×10^{-5}	3.01	1.33×10^{-3}
:	:	:	:	:
:	:	:	:	:
49	3.67	1.23×10^{-4}	2.69	3.58×10^{-3}
50	3.66	1.26×10^{-4}	2.68	3.71×10^{-3}

The initial reliability index β of the girder was calculated to be 3.96 ($p_f = 3.7 \times 10^{-5}$). The target reliability index β_T, in the absence of corrosion, is approximately 2.89 ($p_f = 2.0 \times 10^{-3}$). These values are reasonable with respect to corresponding reliability indices obtained in

current design practice for RC beams designed for ductile failure in flexure, and a 50 year reference period (Nowak and Collins 2000). Taking into account the effect of reduction of reinforcement area due to uniform corrosion, the value of the reliability index β is reduced to 2.69 ($p_f = 3.6 \times 10^{-3}$), not significantly lower than in the absence of corrosion. This is due to the large initial diameter of the No. 30 bar subjected to the moderate rate of loss of 1μA/cm^2. Larger loss of reliability would be expected for beams reinforced with smaller diameter bar since the relative loss of steel section would be greater.

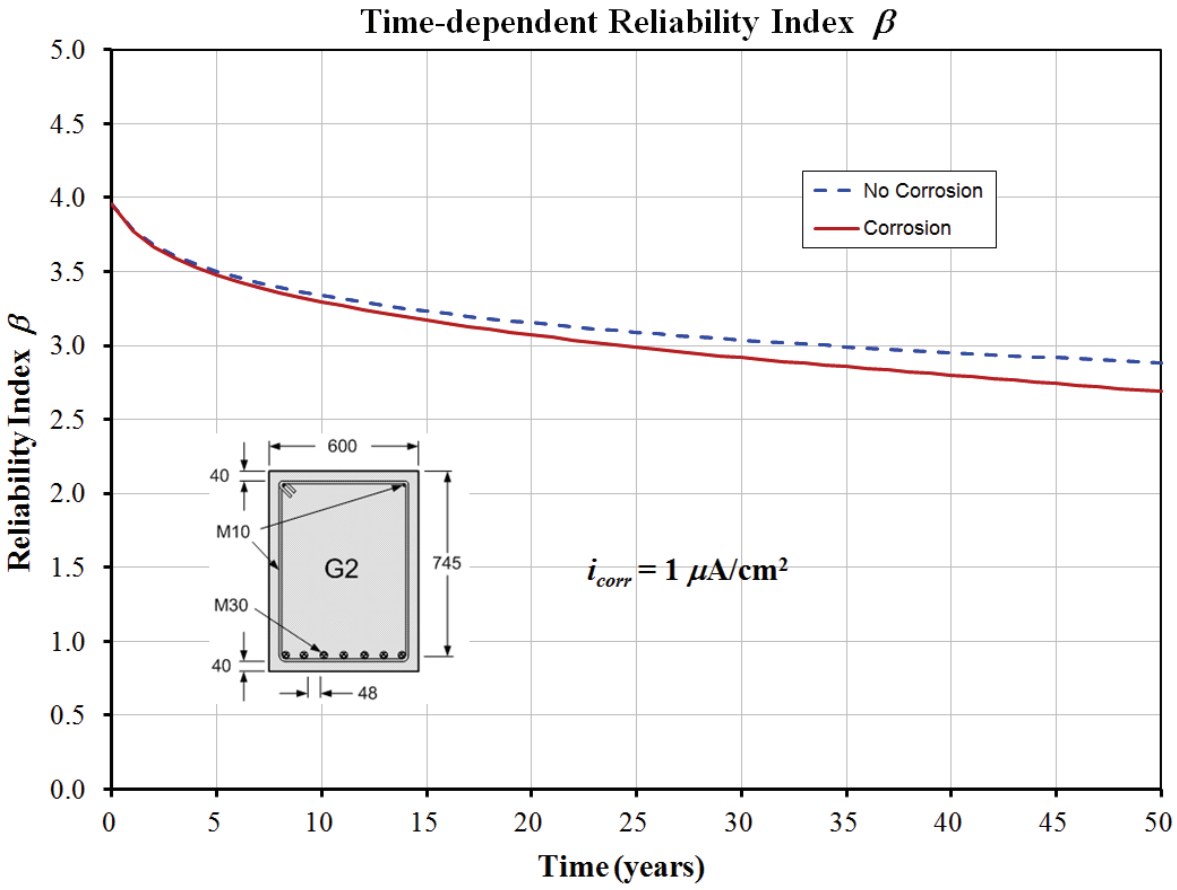

Figure 5-3: Time-dependent reliability index for RC girder G2 with and without the effect of corrosion-induced loss of bar area.

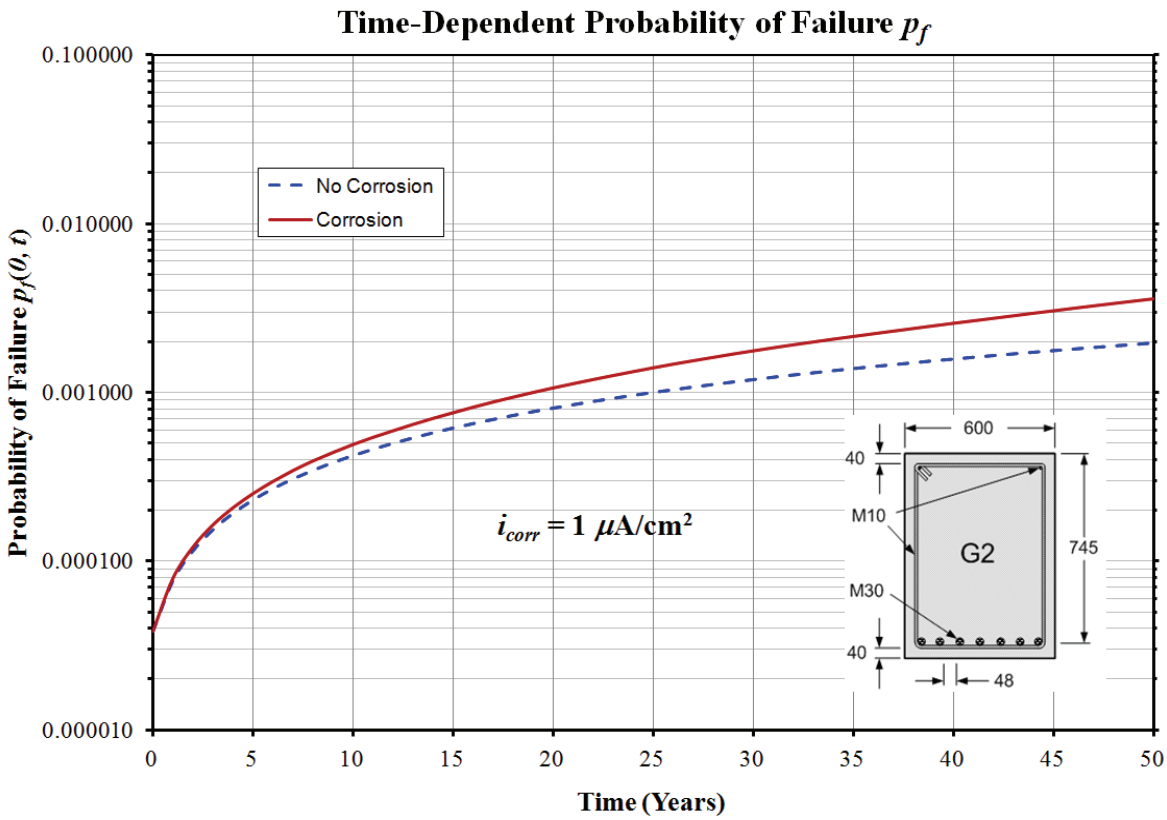

Figure 5-4: Time-dependent probability of failure for RC girder G2 with and without the effect of corrosion-induced loss of bar area (using FORM)

The above results compare well with other studies on the cumulative probability of failure of RC beams with corroding reinforcement. Examples include the pioneering works of Enright and Frangopol (1998), Stewart and Rosowsky (1998a; 1998b), Val and Stewart (1998), and later expanded by Stewart (2004; Stewart 2009), Val (2007), and Stewart and Al-Harthy (2008). Figure 5-5 shows cumulative probabilities of failure for RC Beams with spans of 8 metres, a corrosion rate of 1μA/cm^2, and for two bar diameters (16mm and 27mm), from work reported by Stewart and Al-Harthy (2008). The analysis considers also the effects of spatial distribution of corrosion rates. The analysis was carried on a limit state function similar to the one used here for girder G2. The authors utilized Monte Carlo simulation with a stepwise "survival" scheme to capture the time-dependent probabilities of failure. The results of time-dependent reliability analysis of girder G2 are very similar to the beam in presented in Figure 5-5 (non-spatial analysis and Y27 rebar). Although, the absolute values of the reliability index and corresponding probability of failure are different, the relative ratio

of the reliability index at 50 years to the initial is about 0.6 as it is for girder G2. The difference in absolute values of reliability indices between the two studies is due to the difference in the geometries, bar diameters, and loads between the respective beams. Precise reproduction Stewart and Al-Harthy's (2008) results would require knowledge of all design and modeling parameters used in their studies. However, this information was not available for this and the other studies referred to above. More significantly, the model of corrosion induced loss of steel area used by these authors includes a degradation factor accounting for the reduction in the ductility of the rebar as a function of the degree of corrosion present at any given time. The results are thus less comparable due to this assumption.

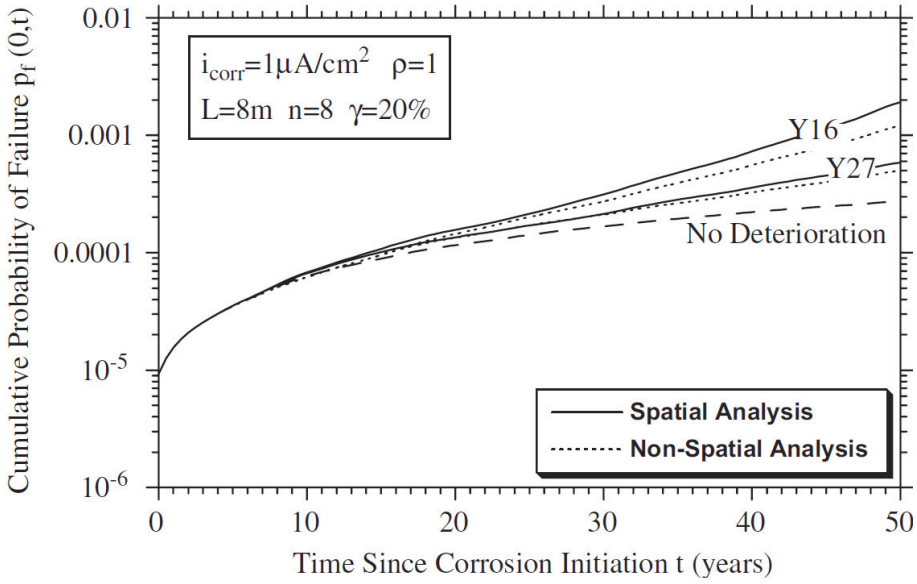

Figure 5-5: Cumulative probabilities of failure (Stewart and Al-Harthy 2008)

The reliability analysis of girder G2 also includes measures of the importance of each random variable with respect to the overall reliability or probability of failure. These measures are provided by importance factors, as shown in Figure 5-6, for the RC girder at 1 and 50 years. The importance factor indicates the relative contribution of each random variable to the total reliability, and it is useful for selecting the most relevant variables and eliminating those that have little impact on the probability of failure (screening). This information is particularly valuable when the reliability analysis is very computationally demanding. By removing the least significant variables (i.e., considering them as deterministic values), the analyst can optimize the numerical calculations. However, caution

should be exercised to ensure that importance factors are consistent over the region and/or time frame analyzed, since some variables may have low importance at one time and high importance at a later time. As Figure 5-6 illustrates, the relative importance of the basic variables does not change appreciably between 1 and 50 years. Also, the importance measures are specific to the problem at hand, due to the uncertainty description of the basic random variables, and should not be generalized.

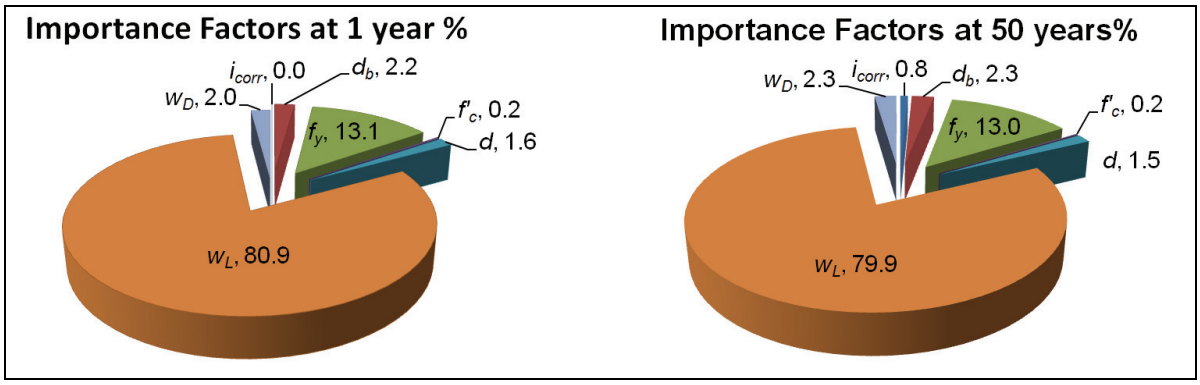

Figure 5-6: Importance factors at 1 and 50 years

The variables which can likely be considered as deterministic are: the dead load w_D, bar diameter d_b, effective depth d, and compressive concrete strength f'_c. As expected, the live load w_L and the yield strength of steel f_y have the greatest proportion of the reliability of the RC girder. Although the corrosion rate i_{corr} shows low importance, it is a fundamental variable here, and thus it must be retained as random. Furthermore, importance factors are not the only measure of the significance of random variables in a reliability problem. The analyst must also consider the sensitivities of the reliability index to the basic random variables.

The sensitivities of the random variables can be obtained from COMPASS in relation to the failure probability and reliability index. Referring to Eq. (5.19), it is possible to calculate the sensitivity of the reliability index, or of the failure probability, with respect to any of the probability distribution parameters. Sensitivities of the reliability index with respect to the mean measure of each basic random variable in the RC girder problem are summarized in Figure 5-7, at four time points in the 50 year period considered.

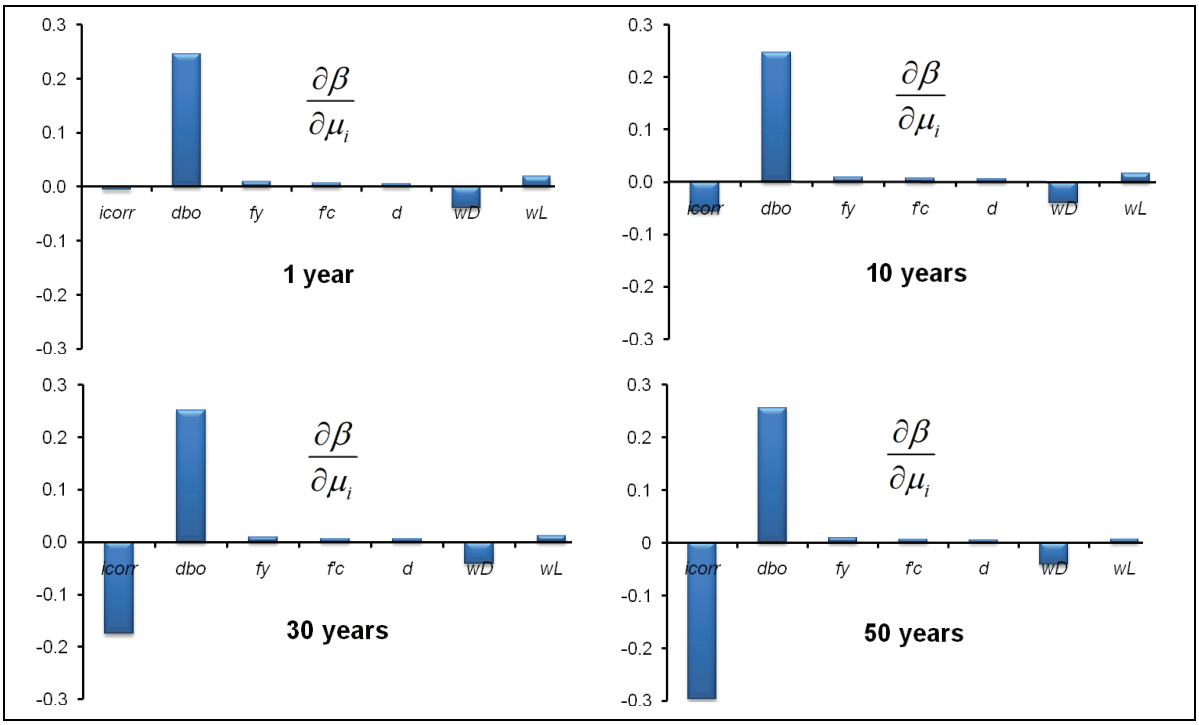

Figure 5-7: Sensitivities of the reliability index with respect to the mean values of the basic random variables

Sensitivity values, or gradients, complement the information provided by the importance factors. In contrast to the importance metrics, which provide the weighted contribution of each random variable to the reliability index and failure probability, sensitivities indicate how strongly fluctuations in the probabilistic parameters of a random variable impact the reliability index and probability of failure. Figure 5-7 shows that variability in the mean diameter of the reinforcing bars has the greatest impact on the reliability index throughout the life of the girder. This makes sense since small changes to rebar diameter impact the flexural strength of RC members. Since the diameters of manufactured rebars do not vary significantly, this measure further emphasizes the loss of diameter due to corrosion. As expected, the rate of corrosion also dominates the reduction of safety with time. In addition, rebar diameter is closely correlated to the corrosion rate. Both these variables show low importance but high influence on safety and reliability. Although, the live load and yield strength have the greatest proportion of the reliability index, their means do not impact it in this case. Of particular note are the variables that show low importance and low sensitivity

(f'_c, w_D, and d), further suggesting that if necessary, these variables could be treated as constants in subsequent analysis.

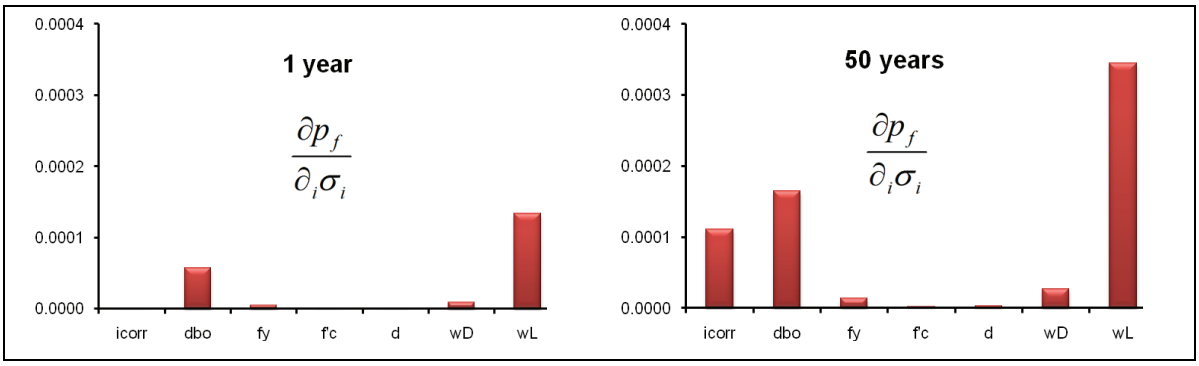

Figure 5-8: Sensitivities of failure probability with respect to the standard deviation values of the basic random variables

It is also very useful to examine the sensitivity of the reliability index to the standard deviation of the basic random variables, since scatter also has great influence on the measures of safety. Figure 5-8 illustrates the sensitivity of the probability of failure with respect to variance in the random variables. Although the mean measure of the live load suggests low influence on the reliability index, the failure probability is most sensitive to the large variance in the live load. Hence, together with its importance value the live load must remain as a random variable.

5.6.2. Results of Reliability Analysis for a Reduced Set of Variables

Based on the results of the above sensitivity studies, analysis of girder G2 was repeated for the case where only i_{corr}, w_L, and f_y are characterized as random variables and all other parameters are deemed to be deterministic. The limit state function thus becomes:

$$g\left(\left\{i_{corr}, f_y, w_L\right\}, t\right)_{\text{Flexure}} = A_s(t)\cdot f_y\left[d - \frac{A_s(t)\cdot f_y}{2\alpha_1 f_c' b}\right] - \frac{\left(w_D + w_L\right)\cdot l^2}{8} \qquad (4.29)$$

The time cumulative reliability index and probability of failure are plotted in Figure 5-9 and Figure 5-10, respectively.

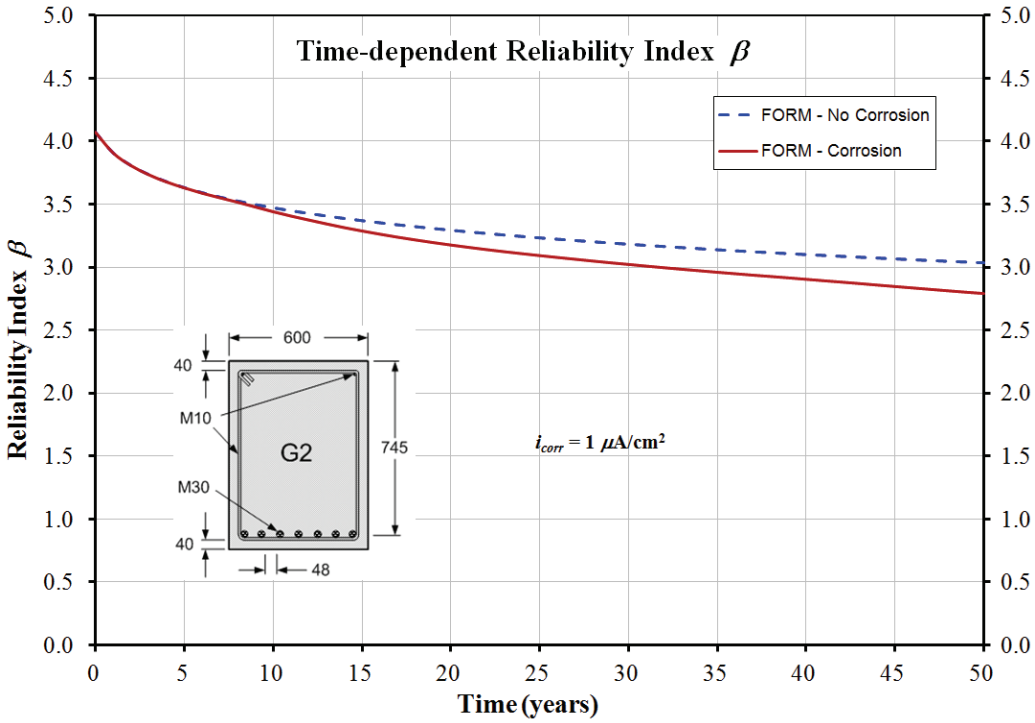

Figure 5-9: Time-dependent reliability index for RC girder G2 with and without the effect of corrosion-induced loss of rebar area

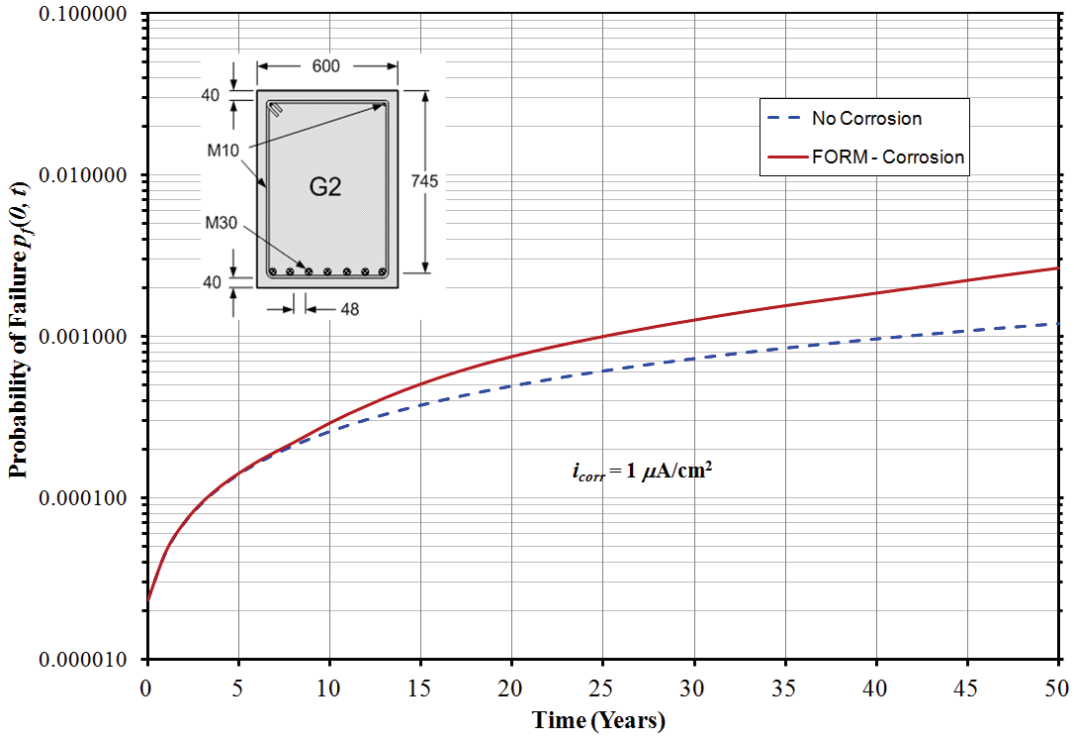

Figure 5-10: Time-dependent probability of failure for RC girder G2 with and without the effect of corrosion-induced loss of rebar area (using FORM)

Although the reliability analysis methodologies presented here are generally applicable to the analysis of structures, the results of these studies are specific to girder G2. For instance, it could be deduced that the uniform corrosion rate does not affect this girder very dramatically. However, a beam with different reinforcement bars, or other details like geometric proportions, dead to live load ratios, etc., might result in significantly different reliability measures. To illustrate the effect of higher rates of corrosion, girder G2 was re-evaluated for other corrosion rates, with results presented in Figure 5-11 for the cumulative reliability index. The resulting safety index at 50 years is reduced from 2.68 for a rate of 1 μA/cm^2 to 2.00 at 3 μA/cm^2. Of course the latter corrosion rate would be considered to be very high.

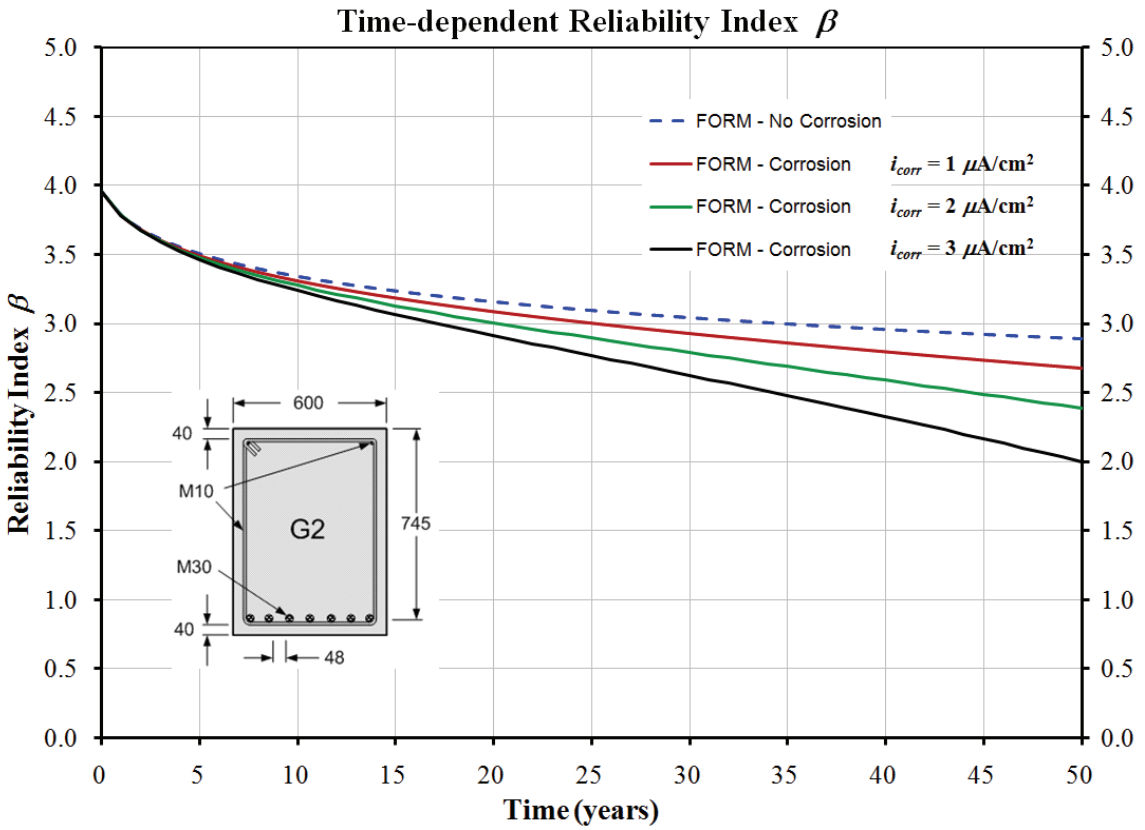

Figure 5-11: Time-dependent reliability index for RC girder G2 for various rates of corrosion (using FORM)

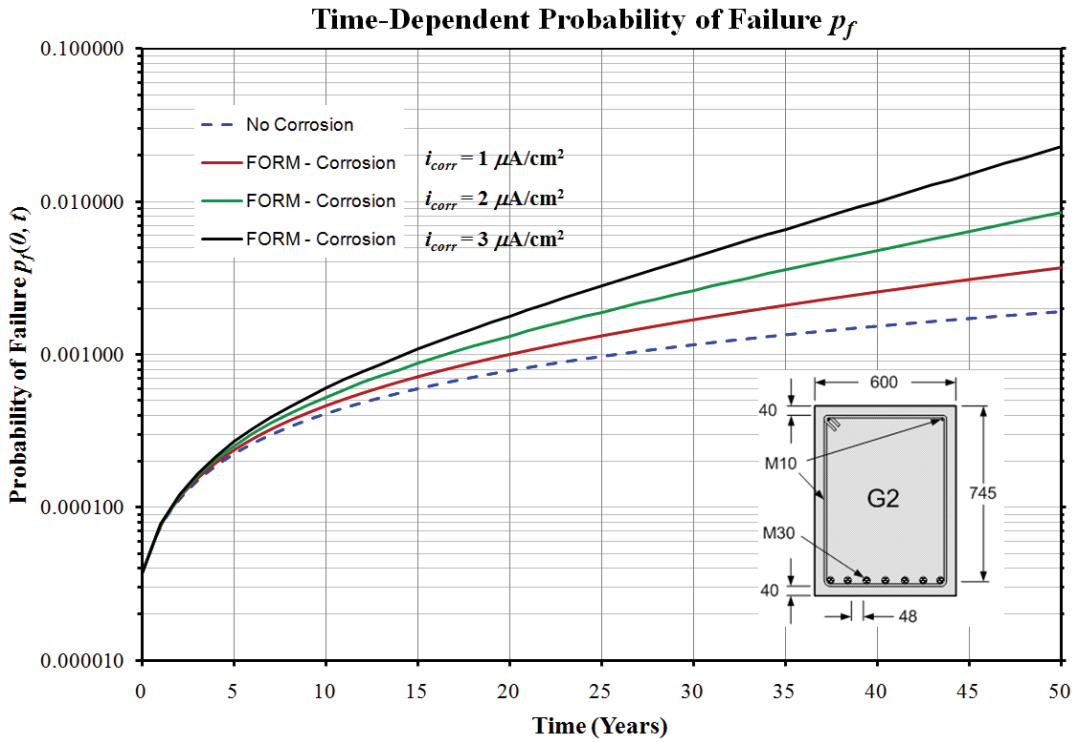

Figure 5-12: Time-dependent failure probability for RC girder G2 for various rates of corrosion (using FORM)

5.7 Random Variables and Limit State Functions for SFEA Analysis

The random variables relevant to the closed-form reliability analysis of RC beams were identified from relevant literature and optimized through on the basis of sensitivity analyses presented in section 5.6.1. The sensitivity studies included deterministic perturbation of the model parameters as well as reliability based sensitivity investigations obtained through COMPASS. For the flexural strength ultimate limit state (ULS) the critical random variables are: rate of corrosion i_{corr}, sustained live load w_L, and the yield strength of rebar f_y. For the deflections serviceability limit state (SLS), the random variables are: i_{corr}, w_L, and the compressive concrete strength f'_c. These parameters are also characterized by the single random variables (as opposed to random fields), as summarized in Table 5-2. As explained in section 5.6.1, this is a reasonable assumption for the random variables used to describe the sustained load, compressive strength of concrete, and rebar yield strength random variables. Because the corrosion rate of reinforcing steel is highly variable, both spatially and

temporally (Stewart 2004), it should ideally be represented by a random field. Indeed one of the primary strengths of SFEA lies in the ability to integrate the discretization of random fields as an inherent part of the methodology.

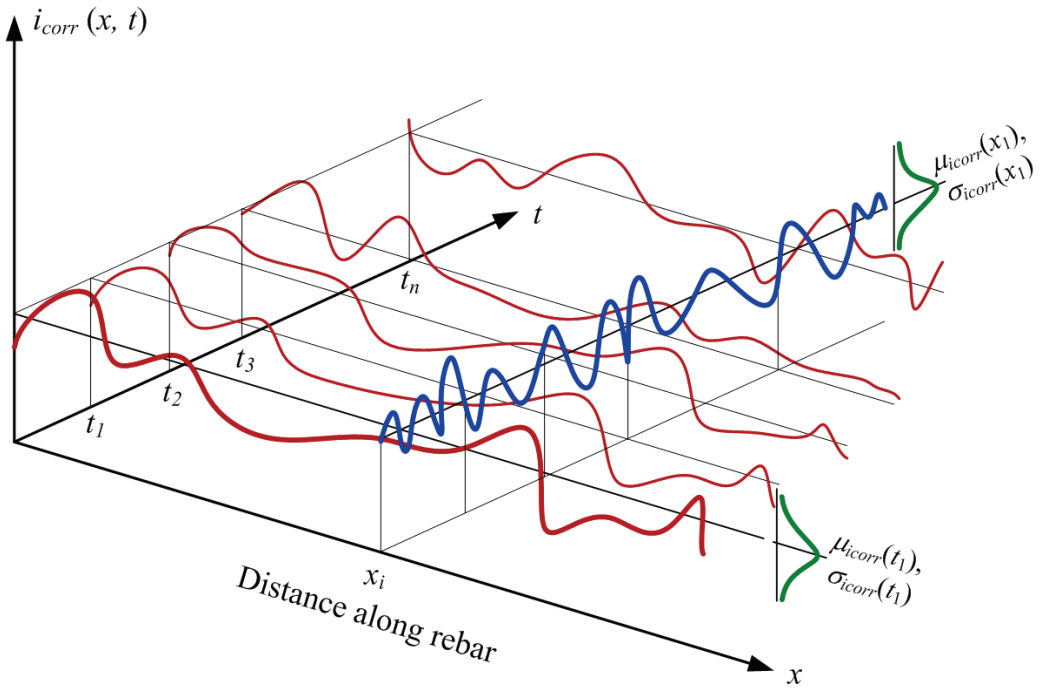

Figure 5-13: Idealization of the corrosion rate i_{corr} in space and time

An idealized random field description of the corrosion rate in space and time is shown in Figure 5-13. However, it must be emphasized that this is not a two-dimensional random field in space, but rather two random processes, one in space and one in time. For any point in time, the rate of corrosion varies along the embedded reinforcing bar. Similarly, at any bar location the corrosion rate changes with time as a function of chloride concentration, temperature, available oxygen, and other conditions. The techniques for discretization of random fields, presented in Chapter 3 and Appendix C, are relatively straight forward to implement for one and two dimensional fields in space. However that is not the case for the current problem involving spatial and temporal distribution of the corrosion rate. Clearly, this is a very difficult phenomenon to model even if experimental and/or field corrosion data are available. However, such information is seriously lacking in the literature and thus many

assumptions are necessary to account for the variability in the rate of corrosion while simultaneously keeping the problem computationally tractable.

The rate of corrosion at a point on the rebar fluctuates at short time intervals (daily) and likely increases over long time (years) as chloride concentrations and oxygen potentially increase due to progressive cracking and other deterioration mechanisms. However, in the absence of reliable data, it is assumed here that the rate of corrosion in the time domain is a stationary process which can be described with a single normally distributed random variable, as shown in Figure 5-13. Although the corrosion rates can also be highly variable spatially, it is unlikely that adjacent critical sections will have corrosion rates that are completely unrelated. If a section is experiencing a higher-than-average corrosion rate, there is a greater likelihood that adjacent sections are also experiencing elevated corrosion rates. This spatial interdependence between nearby rebar sections can be modeled using correlation coefficients. Research by Marsh and Frangopol (2008) on the reliability of RC slab bridges, incorporating simulated spatial and temporal corrosion rate data, used this approach to determine the effect of spatial correlation of corrosion rates. Spatial corrosion rate coefficients are 0 for uncorrelated, 0.5 for partially correlated, and 1 for perfectly correlated. As shown in Figure 5-14, the three different corrosion rate spatial correlation relationships appear to have little impact on the reliability of the slab deck. There is little distinction between the failure probabilities over time given assumptions of no correlation, partial positive correlation, and perfect correlation between adjacent critical section corrosion rates.

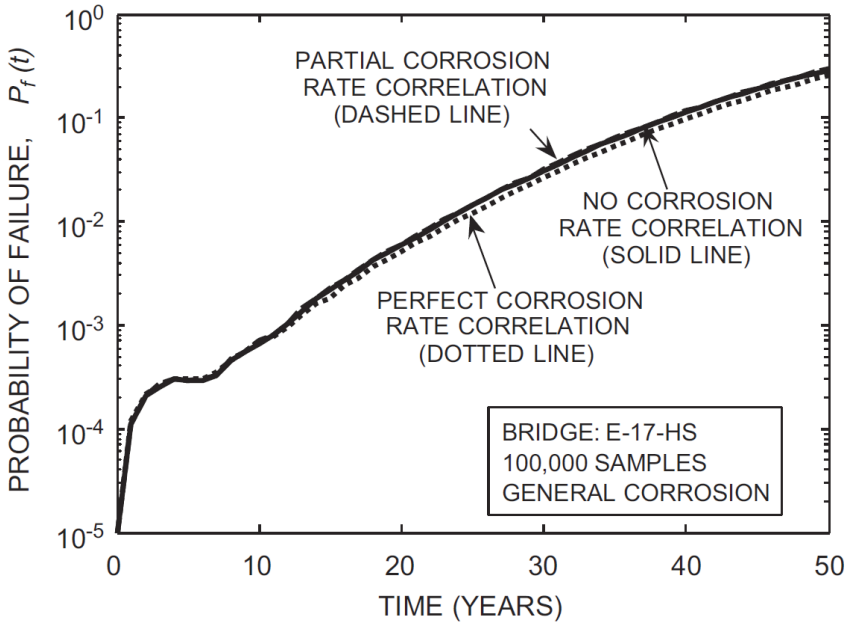

Figure 5-14: Time variation of probability of failure of RC deck for different spatial correlations of corrosion rate using improved reliability model and assuming general corrosion (Marsh and Frangopol 2008)

Marsh and Frangopol (2008) also studied the effect of spatial distribution of corrosion rates on the failure probability of the RC slab. A comparison between the reliabilities of failure predicted by spatially variant and spatially invariant analyses is presented in Figure 5-15. It can be observed that for general corrosion the probability of failure based on spatially invariant analysis is larger than the failure probability based on spatial variability. These results show that accounting for spatial variation of the corrosion rate is very important. However, in the absence of real sensor field data and because of the conservative probability of failure obtained by spatially invariant analysis, the corrosion rate along the rebar is also assumed to be characterized by a single normal random variable. Finally, by equating the spatially and temporally averaged rate of corrosion, it is assumed the rate of corrosion over space and time is thus represented by a single random variable (spatial and temporal variance is ignored).

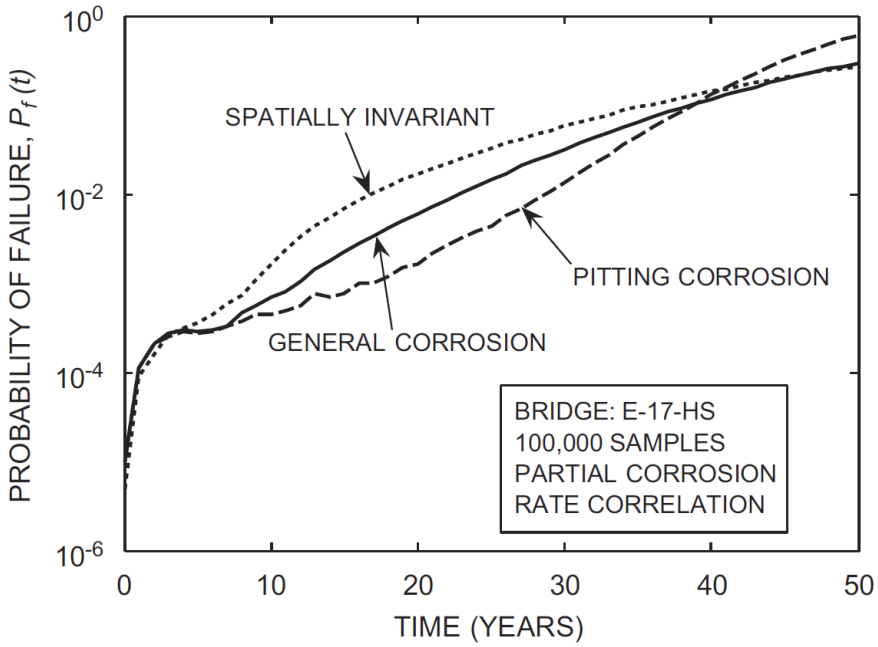

Figure 5-15: Time dependent probability of failure of RC deck based on spatially invariant and reliability models given partial positive spatial correlation of corrosion rates, and general and pitting corrosion models (Marsh and Frangopol 2008)

Hence, returning to the ultimate and serviceability limit states for SFEA-based analysis (ULS and SLS, respectively), as introduced in Eqs. (5.5) and (5.7), the same random variables are adopted as for the reliability analysis using the closed-from code based performance function, presented in section 5.6. This will also allow direct comparison of the results calculated through each approach and compare the effects of including bond loss. In the implicit function for ULS, i_{corr} and f_y are associated with the capacity only and w_L is part of the load term, thus Eq. (5.5) can be re-stated as:

$$\begin{aligned} g\left(i_{corr}, f_y, w_L\right)_{\text{Flexure}} &= M_{FEA\cup RSM}\left(i_{corr}, f_y\right) - M_{REL}\left(w_L\right) \\ &= M_{\text{VecTor2}\cup RSM}\left(i_{corr}, f_y\right) - M_{\text{COMPASS}}\left(w_L\right) \end{aligned} \tag{4.30}$$

In the function corresponding to the SLS the capacity is represented by the maximum allowable deflection δ_{max}, (span/360), while the demand δ is now obtained through the finite element model for all three random variables, i_{corr}, w_L, and f'_c. The performance function given by Eq. (5.7) is therefore rewritten as:

$$
\begin{aligned}
g\left(i_{corr}, f_c', w_L\right)_{\text{Deflections}} &= \delta_{\max} - \delta_{FEA \cup RSM}\left(i_{corr}, f_c', w_L\right) \\
&= \frac{l}{360} - \delta_{\text{VecTor2} \cup RSM}\left(i_{corr}, f_c', w_L\right)
\end{aligned}
\tag{4.31}
$$

The SFEA analysis is presented in Chapter 6 by demonstrating the application of the RSM functionality.

Chapter 6. Response Surface Module

6.1 Introduction

Response Surface Methodology (RSM) is a key element of the proposed SFEA framework, and hence, a more formal explanation is presented in this chapter. In the most general sense, RSM is a collection of statistical and mathematical techniques useful for developing, improving, and optimizing processes. It also has important applications in the design, development, and formulation of new products, improvement of existing product designs (Myers, Montgomery et al. 2009), and more recently in reliability analysis.

Initially, RSM was developed for models in biology and agriculture (Box, Hunter et al. 1978). However, over the last thirty years it has been applied to a large variety of problems in all branches of science and engineering as well as medicine, economics, and the social sciences. The most extensive applications of RSM are in the industrial world, particularly in situations where several input variables potentially influence some performance measure or quality characteristic of a product or process. This performance measure or quality characteristic is referred to as the response. It is typically measured on a continuous scale, although attribute responses, ranks, and sensory responses can also be used. Most real world applications of RSM involve more than one response. The input variables are subject to the control of the engineer or scientist, at least for purposes of a test or an experiment.

The field of response surface methodology consists of the experimental strategy for exploring the space of a process, empirical statistical modeling to develop an appropriate approximating relationship between the response and relevant variables, and optimization methods for finding the levels or values of the process variables that produce desirable values of the response.

6.2 Implementation of RSM in Reliability Analysis

In reliability analysis RSM can be defined as: a set of statistical and mathematical techniques designed to find the "best" value of the response considering the uncertainty or variations in the values of input variables (Khuri and Cornell 1996). However, instead of product or process optimization, the primary application of RSM in reliability analysis is in constructing explicit equations for performance (or limit state) functions which closely approximate the actual implicit performance function $g(\boldsymbol{X})$. As previously defined, $\boldsymbol{X}$ is a vector containing all load and resistance-related input random variables. Response surface methodology can also be used to obtain the structural response statistics, that is, the mean and coefficient of variation of the response (Haldar and Mahadevan 2000a).

In this work, RSM is used to generate explicit limit state functions which represent the response obtained from the nonlinear finite element model of a RC beam. This approximate, or surrogate, limit state function is then used to calculate the reliability using any of the techniques normally used in reliability analysis in problems where the limit state function is known explicitly. Usually, an iterative strategy needs to be employed for its implementation.

Based on the work by Huh and Haldar (2001), the essential components of basic RSM are:

1. **Degree of Polynomial** to be used to represent the performance function;
2. **Construction of a response surface**
3. **Experimental region and codified variables**;
4. **Experimental Design** - selection of sampling or design points; and
5. **Determination of the centre point**.

These topics are discussed in the following sections.

6.2.1. Degree of Polynomial in Performance Function

A limit state function $g(\boldsymbol{X})$ is called the true performance function, and is generally unknown a priori, and perhaps very complicated. It is assumed to be a continuous function of the individual random variables X_i, where $\boldsymbol{X} = \{X_1, \ldots, X_n\}$ is a vector of basic random variables.

Successful application of the response surface methodologies is critically dependent upon the experimenter's ability to develop a suitable approximation of $g(\boldsymbol{X})$. A low-order polynomial over some relatively small region of the independent variable space might be appropriate. In many cases, either a first-order or a second-order model is used. For the case of n independent variables, a first-order model can be expressed as:

$$\hat{g}(\mathbf{X}) = a_0 + a_1 X_1 + a_2 X_2 + \ldots + a_n X_n \tag{6.1}$$

The first-order model is likely to be appropriate when the analyst is interested in approximating the true response surface over a relatively small region of the independent variable space in a location where there is little curvature. The form of the first-order model in Equation (6.1) is often referred to as a main effects model, because it includes only the main effects of the variables X_i. If interaction between some or all of these variables is suspected, it must be included as follows:

$$\hat{g}(\mathbf{X}) = a_0 + a_1 X_1 + a_2 X_2 + a_{12} X_1 X_2 + \ldots \tag{6.2}$$

Often the curvature in the true response surface is strong enough that the first-order model (even with the interaction term included) is inadequate. A second-order model will likely be required in these situations. For the case of two variables, the second-order model is

$$\hat{g}(\mathbf{X}) = a_0 + a_1 X_1 + a_2 X_2 + a_{12} X_1 X_2 + a_{11} X_1^2 + a_{22} X_2^2 \tag{6.3}$$

This model would likely be useful as an approximation to the true response surface in a relatively small region around where there is substantial curvature in the true response function. However, caution must be exercised higher order response surfaces are notoriously susceptible to multiple co-linearities. Fortunately, identification and correction of this phenomenon is not difficult once the analyst become familiar with RSM.

The second-order model is widely used in response surface methodology for several reasons. Among these are the following:

1. It is very flexible and it can take on a wide variety of functional forms; it will often work well as an approximation to the true response surface.

2. It is easy to estimate the parameters a_i in the second-order model. The method of least squares can be used for this purpose.
3. There is considerable practical experience indicating that second-order models work well in solving real response surface problems.

Considering the nonlinear response of structures, the exact performance function can be approximated with a second-order polynomial function $\hat{g}(\boldsymbol{X})$, which for n random variables can be expressed as:

$$\hat{g}(\mathbf{X}) = a_0 + \sum_{i=1}^{k} a_i X_i + \sum_{i=1}^{k} a_{ii} X_i^2 + \sum_{i=1}^{k} \sum_{j=1, j\neq i}^{k} a_{ij} X_i X_j \tag{6.4}$$

In the context of reliability analysis, X_i is the ith random variable, k is the total number of random variables present in the problem, and coefficients $\boldsymbol{a} = \{a_o, a_i, a_{ii}, a_{ij}\}$ corresponding to the constant, linear, square, and cross terms respectively, are to be determined. The number of coefficients to be estimated for Eqn. (6.4) is $p = (k + 1)(k + 2)/2$. If cross terms are ignored then $p = 2k + 1$. Equation (6.4) can also be derived from a second order Taylor series expansion.

Sudret and Der Kiureghian (2002) proposed that a limited number of evaluations of the limit state function (i.e. number of finite element runs) are required to build the surface. The reliability analysis can then be performed by means of the analytical expression given by Eq. (6.4) instead of the true limit state function. This approach is particularly attractive when simulation methods such as importance sampling (Bucher and Bourgund 1990) are used to obtain the reliability results.

Since the limit state function $g(\boldsymbol{X})$ consists of two components, namely the resistance $R(\boldsymbol{X})$ and the load effect $S(\boldsymbol{X})$, where $g(\boldsymbol{X}) = R(\boldsymbol{X}) - S(\boldsymbol{X})$, a response surface can also be generated separately for either of these components instead of for the total limit state function. This is very useful in cases where, for instance, each component is a function of different random variables and one wishes to separate the response surfaces to study the components individually.

6.2.2. Construction of the Response Surface

The determination of the unknown coefficients $\boldsymbol{a} = \{a_o, a_i, a_{ii}, a_{ij}\}$ is generally performed by the least-square method. After choosing a set of fitting points $\{\boldsymbol{X}^k, k = 1, ..., N\}$, for which the exact value $y^k = g(\boldsymbol{X}^k)$ is computed, the following error is minimized with respect to $\boldsymbol{a}$:

$$\mathrm{err}(\boldsymbol{a}) = \sum_{k=1}^{N} \left(y^k - \hat{g}\left(\boldsymbol{X}^k\right) \right)^2 \tag{6.5}$$

Recasting Eq. (6.4) in the form:

$$\hat{g}(\boldsymbol{X}) = \left\{1, X_i, X_i^2, X_i X_j\right\}^T \cdot \left\{a_o, a_i, a_{ii}, a_{ij}\right\} \equiv \mathbb{Z}^T\left(\boldsymbol{X}^k\right) \cdot \boldsymbol{a} \tag{6.6}$$

the least-square problem becomes:

$$\text{Find } \boldsymbol{a} = \text{Argmin} \left\{ \sum_{k=1}^{N} \left(y^k - \mathbb{Z}^T\left(\boldsymbol{X}^k\right) \cdot \boldsymbol{a} \right)^2 \right\} \tag{6.7}$$

According to Faravelli (1989), solution of the above problem may be formulated as:

$$a = \left(\mathrm{Z}^T \cdot \mathrm{Z}\right)^{-1} \mathrm{Z}^T \cdot \boldsymbol{y} \tag{6.8}$$

where Z is the matrix whose rows are the vectors $\mathbb{Z}\left(\boldsymbol{X}^k\right)$ in Eq. (6.6) and $\boldsymbol{y}$ is the vector whose components are $y^k = g\left(\boldsymbol{X}^k\right)$.

The various response surface methods proposed in the literature differ only in the terms retained in the polynomial expression (6.4) (e.g. with or without cross terms), and the selection of the coordinates of the fitting points $\{\boldsymbol{x}^k, k = 1,..., N\}$, i.e., the experimental design used in the regression analysis (Sudret and Kiureghian 2000). It is emphasized that $N \geq n$ (number of fitting points ≥ number of random variables) is required to be able to solve Eq. (6.8). Furthermore, the fitting points have to be chosen in a consistent way in order to obtain independent equations (i.e. an invertible $\mathrm{Z}^T \cdot \mathrm{Z}$), and must be bound within the

independent data range to be valid. In other words, the results (response) cannot be extrapolated beyond this data range.

6.2.3. Experimental Region and Coded Variables

For efficient and accurate construction of a performance function, the experimental region should he kept to a minimum (Khuri and Cornell 1996). The uncertainty in the random variables can be used to define the experimental region. The region or bounds for each input variable X_i is often specified as

$$X_i^{\text{region}} = X_i^C \pm h_i \sigma_{X_i} x_i \tag{6.9}$$

where X_i^C and σ_{X_i}, are the centre point and standard deviation of a random variable X_i, respectively, h_i is an arbitrary factor used to define the region, and x_i is the coded variable.

The coded variable can be defined as

$$x_i = \frac{X_i - X_i^C}{h_i \sigma_{X_i}} \qquad i = 1,\ 2,\ \ldots,k \tag{6.10}$$

The value of h_i is generally considered to be between 1 and 3. From Equation (6.10), it is clear that the value of a coded variable at the centre point is zero. The transformation of random variables to coded variables facilitates the evaluation of the coefficients in Equation (6.4) (Snee 1973).

6.2.4. Experimental Design

In experimental design, the sets of values of the random variables are selected within the experimental region to analyze a structure deterministically to evaluate the coefficients of the performance function $g(\mathbf{X})$. The number of design points should be kept to a minimum to increase the computational efficiency but must be at least equal to the number of coefficients p needed to define a performance function. Efficient location of design points around the centre point, discussed next, is essential in the accurate construction of the performance function.

To construct performance functions containing second-order polynomials, the available procedures for experimental design can be divided into two categories: **classical design** and **saturated design**.

Classical Design

In the classical design approach, responses are first calculated at specified design points and then a regression analysis is carried out to formulate the performance function. In this approach, one of the conceptually simpler designs is factorial design, in which the response values are estimated for each variable sampled at equal intervals. In order to fit a second order surface for n input variables, the sampling points must have at least three levels for each variable, leading to 3^n factorial design. Factorial design considers all possible combinations of the sampling points, thus clearly, it is computationally more demanding. For example, constructing a second order response surface for 4 variables leads to 81 combinations, and therefore, requires 81 runs of FE element code.

Box and Wilson (1951) introduced a more efficient approach for fitting second order surfaces, known as central composite design (CCD). This approach does not require the use of a complete three-level factorial experiment. Instead, it is built on a complete 2^n factorial design, augmented with centre points, and two axial points on the axis of each random variable at a distance α from the centre point. For clarification, assuming a planar representation of the experimental region, CCD can be schematically shown as in Figure 6-1.

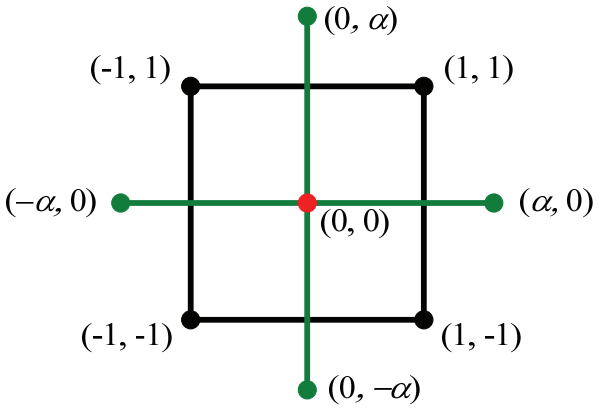

Figure 6-1: Central Composite Design

Values of α can range from 1, resulting in the axial values appearing at the edge of each side, to $\alpha = \sqrt[4]{2^n}$ in order to make the design rotatable. The centre points are often replicated in order to improve the precision of the experiment. The actual 3 level (n = 3) CCD is illustrated in Figure 6-2. The total number of design points in CCD is $N = 2^n + 2n + 1$; N is much larger than the number of coefficients $p = (n + 1)(n + 2)/2$ to be estimated. Regression analysis can then be used to estimate the coefficients of the performance function.

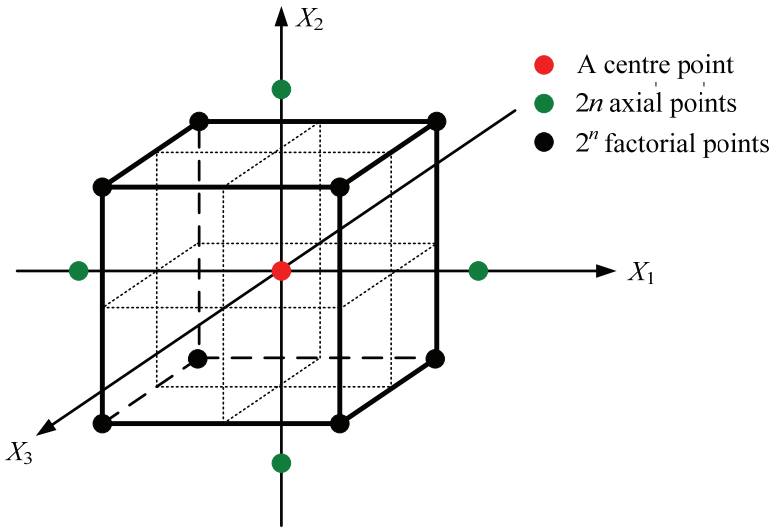

Figure 6-2: Central Composite Design using full second order polynomial with cross terms for n =3

Other experimental design methods, such as Box-Behnken design (1960), have also been used in response surface-based reliability analysis (Fox 1993). The central composite design is the experimental approach used to generate the surrogate response surfaces in this work.

Saturated Design

Saturated design consists of only as many design points as the total number of coefficients necessary to define a polynomial representing the performance function. The unknown coefficients are obtained by solving a set of linear equations, without conducting any regression analysis. The design can be used for second-order polynomials with and without cross terms. For second-order polynomials without cross terms, the total number of required design points is $2n + 1$, where n is the number of random variables. For second-order polynomials with cross terms, the total number of required design points is $(n + 1)(n + 2)/2$.

Clearly, saturated design is far more efficient than CCD. On the other hand, CCD is far more accurate. Considering both computational efficiency and accuracy, a mixture of the two models may be desirable in certain situations. A simple example of the application of the RSM approach is presented in Appendix F.

6.2.5. Determination of the Centre Point

The centre point around which the design points are selected plays an important role in the construction of the performance function. Determining the location of the centre point is not a simple task, and a systematic iterative approach is necessary. Information on the reliability index and the coordinates of the corresponding checking point, obtained from the FORM analysis, can be used to select the centre point. (Bucher and Bourgund 1990) suggested the iterative linear interpolation scheme for this purpose, discussed next.

Since the location of the centre point is unknown at the beginning of the iteration, the centre point is initially assumed to be located at the mean values of the random variables X_i's. This point is denoted as $\boldsymbol{x}_{C_1}$, and it will produce a performance function $\hat{g}_1(\boldsymbol{X})$. A linear interpolation scheme can then be used to select the next centre point as:

$$\boldsymbol{x}_{C_2} = \boldsymbol{x}_{C_1} + \left(\boldsymbol{x}_{D_1} - \boldsymbol{x}_{C_1}\right) \times \frac{g\left(\boldsymbol{x}_{C_1}\right)}{g\left(\boldsymbol{x}_{C_1}\right) - g\left(\boldsymbol{x}_{D_1}\right)} \quad \text{if} \quad g\left(\boldsymbol{x}_{D_1}\right) \geq g\left(\boldsymbol{x}_{C_1}\right) \tag{6.11}$$

or

$$\boldsymbol{x}_{C_2} = \boldsymbol{x}_{D_1} + \left(\boldsymbol{x}_{C_1} - \boldsymbol{x}_{D_1}\right) \times \frac{g\left(\boldsymbol{x}_{D_1}\right)}{g\left(\boldsymbol{x}_{D_1}\right) - g\left(\boldsymbol{x}_{C_1}\right)} \quad \text{if} \quad g\left(\boldsymbol{x}_{D_1}\right) < g\left(\boldsymbol{x}_{C_1}\right) \tag{6.12}$$

Another performance function can then be constructed by considering design points around the new centre point $\boldsymbol{x}_{C_2}$. The iteration process needs to be continued until all the random variables at the centre point converge to a preselected criterion. For each random variable, the difference between two successive iterations can be limited, for example to 1%, giving the required convergence criterion. It generally takes only 2 to 3 iterations to satisfy this convergence criterion (Huh and Haldar 1999). The iteration scheme is shown graphically in Figure 6-3.

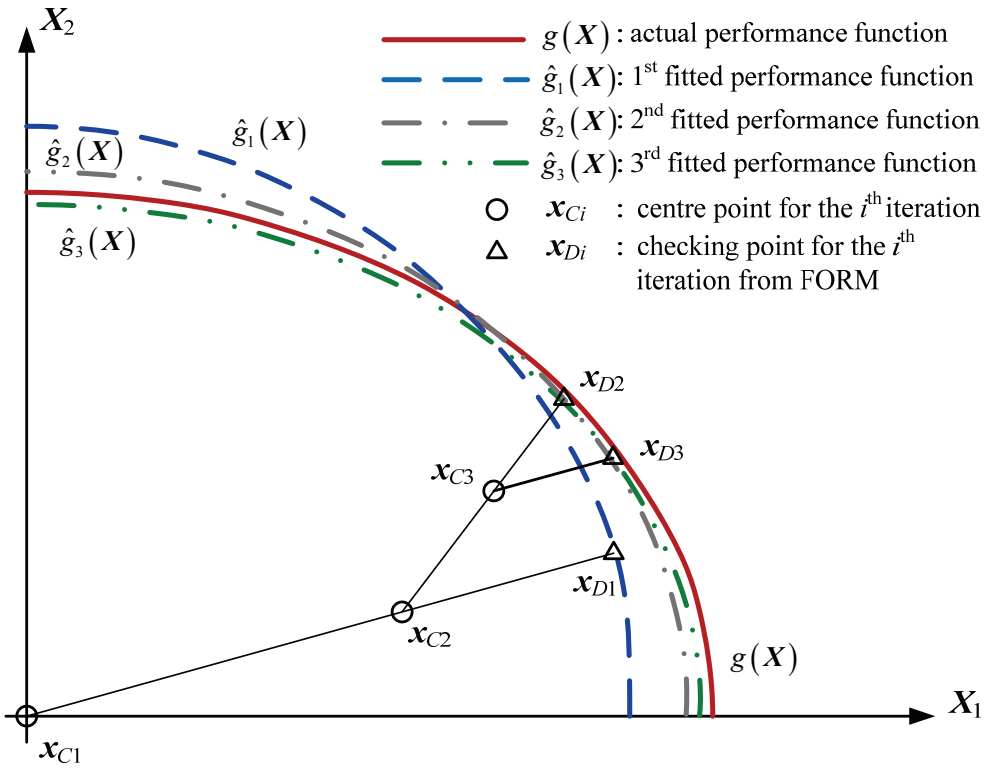

Figure 6-3: Iterative linear interpolation scheme (adapted from Huh and Haldar, 2001)

The concept behind the construction of the performance function using RSM is simple. However, considering computational efficiency and accuracy, the implementation of a basic RSM scheme in the reliability evaluation of nonlinear systems could be impractical. If an RSM scheme needs to be implemented, the number of random variables needed to construct the response surface should be kept to a minimum. This can be accomplished using sensitivity analysis. Furthermore, a mixture of the CCD and saturated design models may need to be implemented for efficient construction of an RSM. A computationally efficient model, such as saturated design, can be used in the first (n - 1) iterations, and the more accurate model, CCD, can be used at the last iteration.

6.3 RSM Algorithm

Structural reliability is always calculated with respect to a limit state function. The RSM-based algorithm is capable of estimating reliability considering both the strength and serviceability limit states. The steps required for estimating reliability are:

1. An initial centre point is selected to start the iteration at the mean values of all the random variables.
2. The experimental design model is chosen considering the type of polynomial, number of random variables, and computational efficiency.
3. Deterministic analysis of the structure is carried out at all the design points according to the model selected in step 2 using a nonlinear finite element model.
4. The surrogate performance function $\hat{g}(\boldsymbol{X})$ is derived by evaluating the coefficients in Equation (6.4).
5. Using the performance function thus generated, the reliability index is calculated satisfying a convergence criterion and the corresponding coordinates of the checking point using FORM, SORM, or simulation.
6. The information on the sensitivity obtained in Step 5 can be used as the basis for removal of less sensitive random variables from the analysis or by treating these values as deterministic constants at their mean values.
7. The coordinates of the new centre point to be used in subsequent iterations are then derived by using the linear interpolation scheme given by Equations (6.11) or (6.12).
8. Steps 2 through 7 are repeated until the coordinates of the centre point for all random variables converge to a preselected tolerance criterion. This completes the first (n -1) iterations.
9. A polynomial and corresponding experimental design model is finally selected considering accuracy for the final iteration.
10. The final response surface is constructed.
11. The reliability index is finally calculated.

6.4 RSM: Case Study

6.4.1. RSM 1 – Experimental Design

The analysis begins with experimental design, which is a key element of the response surface component of the framework as per Figure 3-1. The objective of the experimental design, as outlined in this chapter, is to select appropriate set of points in the design space so that an approximate representation of the limit state can be formed. For this purpose, the central composite design (CCD) approach was used to generate design for the two random variables i_{corr} and f_y, with 5 central, 4 axial, and 4 corner points. The initial range of values for each random variable was based on $\mu \pm \sigma$. Thus the range for i_{corr} is (0.7 -1.0 -1.3) μA/cm^2, and for f_y (387 – 430 – 473) MPa. As mentioned earlier, the live load does not enter the FE capacity calculations; hence the stochasticity of w_L is handled directly in COMPASS. The 13 combinations based on CCD are shown in Columns 2 and 3 of Table 6-1. These are the random variables which enter the finite element component.

6.4.2. Deterministic Finite Element Analysis

Using the nonlinear FE model for girder G2, 13 runs are required, one for each experiment. One of the challenges with this is that the FE model does not use i_{corr} directly, therefore the parameters which depend on the rate of corrosion must be set in the FE model. The values in this case are the bar diameter and total cross-sectional area of all tension rebar (Columns 4 and 5 in Table 6-1). In addition, the bond-slip model parameters for the modified Eligehausen model, the maximum bond stress, the slip at maximum bond stress, and the maximum slip value, are shown in Columns 6 through 8. Once these values are provided in VecTor2, along with all other constant parameters, the code can be executed for each case. Special attention must be paid in selecting appropriate load/displacement parameters for each run (i.e. number of increments, step sizes, convergence limits, etc.) to ensure convergence, stability, and adequate resolution. The output flexural capacities, from the deterministic VecTor2 trials, are given in the last column of Table 6-1.

Table 6-1: Random variables and related input parameters for t = 25 years

run	i_{corr}	f_y	$d_b(t)$	$A_s(t)$	τ_{bu}	s	s_{max}	M_u
#	μA/cm^2	MPa	mm	mm^2	MPa	mm	mm	kN·m
1	0.7	473	29.49	4782.50	3.436	0.03177	15.5042	1646.97
2	0.7	387	29.49	4782.50	3.436	0.03177	15.5042	1353.76
3	0.7	430	29.49	4782.50	3.436	0.03177	15.5042	1497.66
4	1.0	430	29.32	4726.24	2.416	0.01318	10.9044	1479.47
5	1.0	430	29.32	4726.24	2.416	0.01318	10.9044	1479.47
6	1.0	430	29.32	4726.24	2.416	0.01318	10.9044	1479.47
7	1.0	430	29.32	4726.24	2.416	0.01318	10.9044	1479.47
8	1.0	430	29.32	4726.24	2.416	0.01318	10.9044	1479.47
9	1.0	387	29.32	4726.24	2.416	0.01318	10.9044	1340.17
10	1.0	473	29.32	4726.24	2.416	0.01318	10.9044	1616.39
11	1.3	473	29.14	4670.31	1.403	0.00339	6.3317	1587.53
12	1.3	430	29.14	4670.31	1.403	0.00339	6.3317	1454.04
13	1.3	387	29.14	4670.31	1.403	0.00339	6.3317	1308.90

6.4.3. RSM 2 – Statistical Analysis and Generation of Response Surfaces

Once the response values are generated through the deterministic finite element runs, they are returned to the RSM component for various statistical tests, the regression analysis used to generate the response surface for the given set of values and the coefficients which define the response surface. The statistical tests that should be considered are:

i. Correlations between the input and response values, and interactions between input variables;
ii. Lack of fit, R^2, pure error, standard error, and F-values (ANOVA);
iii. Normal plots of residuals, predicted vs actual, Box-Cox; and
iv. Surface / contour plots may be helpful.

Surface plots can be difficult to understand when involving many random variables, since only the response to two values can be visualized in three dimensions. Above that only partial views are possible, which are difficult to interpret. Since in this case M_u is a function of only two variables, i_{corr} and f_y, a response surface can be generated very easily, as shown in Figure 6-4. The surfaces are for the 25 and 37-year time points, and the diagram underlines how significantly curvature can vary depending on the experimental values and behaviour. The earlier surface shows negligible curvature and can be represented with a linear response

function, whereas, in contrast, the second surface is quadratic. Surface plots also help with identifying the trend in the response due to changes in the input variables, and occasionally locations of significant regions.

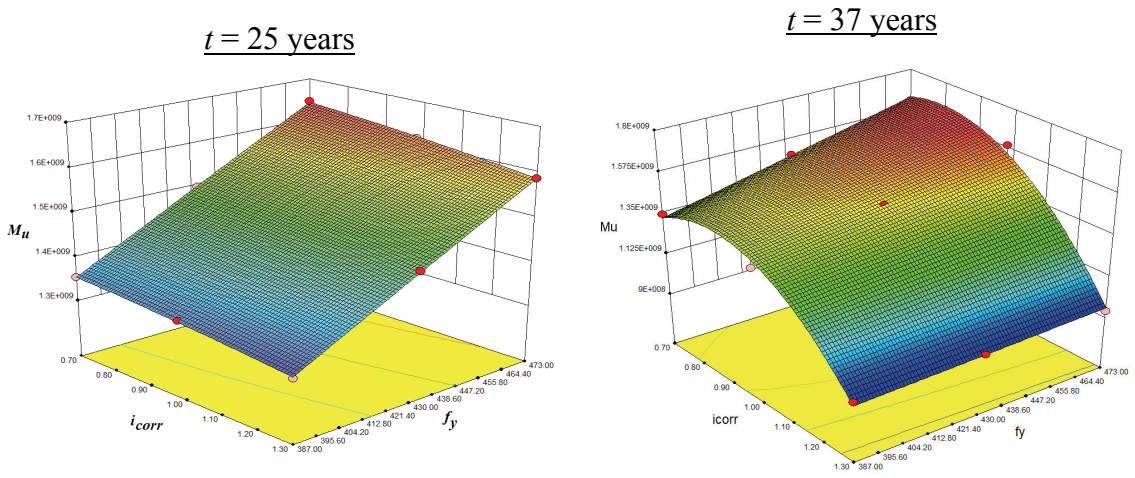

Figure 6-4: Response surfaces for M_u as a function of i_{corr} and f_y at $t = 25$ and 37 years

The statistical analysis, linear regressions, and plots can be performed using the built-in math functions and procedures in spreadsheets, such as Microsoft Excel. Mathematical software, for instance Matlab, make RSM quite straight forward, as other dedicated statistical packages, provided the user understands what the results mean.

The regression analysis generates the vector of coefficients that defines the surface in terms of the input random variables. These coefficients define the equation of the response surface, which for girder G2 at $t = 25$ years, is given by:

$$\begin{aligned}\hat{M}_u = &-1.523\times10^8 + 1.2374\times10^8 i_{corr} + 4.2062\times10^6 f_y \\ &- 2.8256\times10^5 \left(i_{corr}\cdot f_y\right) - 4.2207\times10^7 i_{corr}^2 - 740.2 f_y^2\end{aligned} \tag{6.13}$$

Comparison between the values of flexural capacity M_u, generated by the FE model, and the values $\hat{M}_u$, predicted by the response surface given by Eq. (6.13), is summarized in Table 6-2. The maximum error difference is 0.25%. For the highly nonlinear surfaces the maximum error at some points does not exceed about 10% in the worst case. It is important to note that the equation is only valid for the range of values used in its construction, and it should not be

relied upon for extrapolated response values. Substituting Eq. (6.13) into Eq. (5.1) results in the limit state function for the reliability analysis in COMPASS. The Fortran source code for implementation of the RSM based limit state functions in COMPASS can be found in Appendix H.

Table 6-2: Comparison of actual response M_u with response surface $\hat{M}_u$ for t = 25 years

run	M_u	$\hat{M}_u$	$M_u - \hat{M}_u$	*Error*
#	kN·m	kN·m	kN·m	%
1	1646.97	1644.00	2.975	0.181
2	1353.76	1354.02	0.259	0.019
3	1497.66	1500.38	2.716	0.181
4	1479.47	1479.52	0.051	0.003
5	1479.47	1479.52	0.051	0.003
6	1479.47	1479.52	0.051	0.003
7	1479.47	1479.52	0.051	0.003
8	1479.47	1479.52	0.051	0.003
9	1340.17	1336.81	3.361	0.251
10	1616.39	1619.50	3.106	0.192
11	1587.53	1587.40	0.131	0.008
12	1454.04	1451.07	29.14	0.204
13	1308.90	1312.00	29.14	0.237

Detailed statistical analyses of the above ULS response surfaces for t = 25 and 37 years are presented in Appendix G.

6.4.4. Analysis for the SLS – maximum allowable deflections

The analysis proceeds in the same manner, although it is somewhat more computationally demanding. In this case three random variables, i_{corr}, w_L, and f'_c (corrosion, load, and material property) are all required on the demand side of the limit state function, increasing the number of experimental design points, and the number of FE input parameters that depend on these three variables. As summarized in Table 6-3, VecTor2 computes the initial concrete elasticity E_c and the tensile strength of concrete based on the values of concrete compressive strength. As for flexural strength runs, reinforcement diameters and areas, and the bond-slip

relationship parameters also had to be entered directly, since these parameters depend on the rate of corrosion.

For the experimental design, using a minimum CCD scheme required at least 16 points to define the response surface of the SLS. This design results in larger regression errors; however, due to computational demands, it was deemed acceptable. Comparison between the deflections generated from the FE analysis and those predicted by the surrogate response function given by Eq. (6.14) are presented in Table 6-4.

$$\begin{aligned}\hat{\delta} = &- 6.567 + 22.991\, i_{corr} + 9.577\times10^{-2} f_c' + 0.8638\, w_L \\ &- 5.0521\times10^{-2}\left(i_{corr}\cdot f_c'\right) - 1.3466\times10^{-2}\left(i_{corr}\cdot w_L\right) - 6.1972\times10^{-3}\left(f_c'\cdot w_L\right) \\ &- 9.993\, i_{corr}^2 - 1.926684\times10^{-3} f_c'^2 - 3.6522\, w_L^2\end{aligned} \quad (6.14)$$

Table 6-3: Random variables and related input SLS parameters for t = 25 years

run	i_{corr}	f'_c	w_L	f_{ct}	E_c	$d_b(t)$	$A_s(t)$	τ_{bu}	δ_L
#	μA/cm^2	MPa	kN/m	MPa	MPa	mm	mm^2	MPa	mm
1	0.7	32.8	4.39	3.44	27500	29.250	4703.83	1.825	7.906
2	0.7	47.2	4.39	4.12	31521	29.250	4703.83	2.186	6.240
3	0.7	40.0	12.92	3.79	29602	29.250	4703.83	2.015	9.546
4	0.7	32.8	21.45	3.44	27500	29.250	4703.83	1.825	15.029
5	0.7	47.2	21.45	4.12	31521	29.250	4703.83	2.186	12.461
6	1.0	40.0	4.39	3.79	29602	28.972	4614.71	0.495	6.842
7	1.0	32.8	12.92	3.44	27500	28.972	4614.71	0.449	13.385
8	1.0	40.0	12.92	3.79	29602	28.972	4614.71	0.495	11.471
9	1.0	40.0	12.92	3.79	29602	28.972	4614.71	0.495	11.471
10	1.0	47.2	12.92	4.12	31521	28.972	4614.71	0.538	9.755
11	1.0	40.0	21.45	3.79	29602	28.972	4614.71	0.495	16.150
12	1.3	32.8	4.39	3.44	27500	28.694	4526.45	0.495	8.025
13	1.3	47.2	4.39	4.12	31521	28.694	4526.45	0.495	6.252
14	1.3	40.0	12.92	3.79	29602	28.694	4526.45	0.495	11.995
15	1.3	32.8	21.45	3.44	27500	28.694	4526.45	0.495	15.366
16	1.3	47.2	21.45	4.12	31521	28.694	4526.45	0.495	12.032

Table 6-4: Comparison between the deflections computed by the FEA with values predicted by the response surface equation, at t = 25 years

δ	$\hat{\delta}$	δ_u	$g = \delta_u - \delta$	$\hat{g} = \delta_u - \hat{\delta}$	$\lvert g - \hat{g} \rvert$	Error
mm	mm	mm	mm	mm	mm	%
7.906	7.457	27.78	19.872	20.321	0.449	2.21
6.240	5.696	27.78	21.538	22.081	0.544	2.46
9.546	10.455	27.78	18.232	17.322	0.909	5.25
15.029	15.283	27.78	12.749	12.495	0.254	2.03
12.461	12.291	27.78	15.317	15.487	0.170	1.10
6.842	7.852	27.78	20.936	19.925	1.010	5.07
13.385	12.801	27.78	14.393	14.977	0.584	3.90
11.471	11.604	27.78	16.307	16.174	0.133	0.82
11.471	11.604	27.78	16.307	16.174	0.133	0.82
9.755	10.207	27.78	18.023	17.571	0.452	2.57
16.150	15.007	27.78	11.628	12.771	1.143	8.95
8.025	8.228	27.78	19.753	19.550	0.203	1.04
6.252	6.031	27.78	21.526	21.746	0.221	1.01
11.995	10.953	27.78	15.783	16.825	1.042	6.19
15.366	15.943	27.78	12.412	11.835	0.577	4.87
12.032	12.515	27.78	15.746	15.263	0.483	3.16

Clearly, the approximate limit state function for serviceability is more complex and with larger curvature, as reflected by the larger % error. However, the maximum error is only 9%.

Chapter 7. SFEA Framework: Analysis of the Case Study Results

7.1 Introduction

A general stochastic finite element framework for the analysis of RC beams with corroding reinforcement was proposed in Chapter 3. As represented schematically in Figure 3.5, the framework is an integration of nonlinear finite element software (VecTor2) and a reliability program (COMPASS) through a response surface methodology. These components were individually introduced and described in Chapters 4, 5, and 6, respectively. Direct application of each part was also presented through relevant example problems and, where possible, validation.

The purpose of this chapter is to present and explain the implementation of the proposed SFEA framework to the reliability analysis of RC beams subjected to the effects of reinforcement corrosion over time. The corrosion-induced damage includes the effects of two deterioration mechanisms: the reduction of reinforcement cross-sectional area and the loss of bond between the rebar and surrounding concrete. The results of application of the framework to the Case Study of an RC parking garage girder, introduced in Chapter 3, are reported and compared with the most relevant experimental and numerical studies available in the literature.

7.2 Results of SFEA-based Reliability Analysis

The proposed framework was implemented in the reliability analysis of parking girder G2, over a 50 year design life, while accounting for the effects of corrosion-induced reduction of reinforcement area and degradation of bond strength.

7.2.1. Ultimate Limit State – Flexural Strength of RC girder G2

The annual (instantaneous) reliability and its corresponding probability of failure for RC girder G2 are plotted in Figure 7-1 and Figure 7-2, respectively. For the first 25 year period the decrease in the reliability index is quite unremarkable and typical of degradation of RC beams caused by the gradual and uniform reduction of rebar area. The rapid loss of reliability between 25 and 30 years is caused by the breakdown of bond between the steel and surrounding concrete, particularly in the mid-span region of the girder. Once the residual

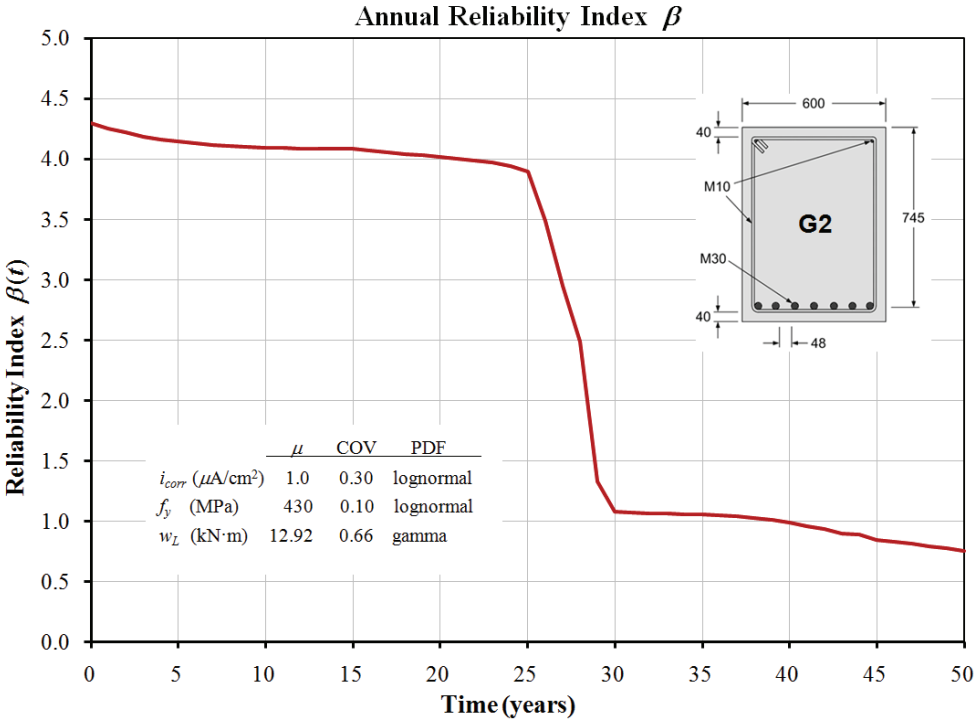

Figure 7-1: Annual reliability index for RC girder G2

bond strength is reached, the reliability of the girder, beyond the 30 year mark, continues at a gradual rate similar to the initial 25 year period. This behaviour is also governed by the loss of steel section. However, the time-dependent reliability and probability of failure must be calculated to account for the cumulative survival of the system. The instantaneous annual probabilities of failure are required to calculate the time-dependent probability of failure using the methodology referred to in Section 5.4. The cumulative reliability is illustrated in Figure 7-3, while the associated cumulative failure probability is shown in Figure 7-4. For comparison, the figures also include the cumulative curves for the case when bond-slip effects are ignored.

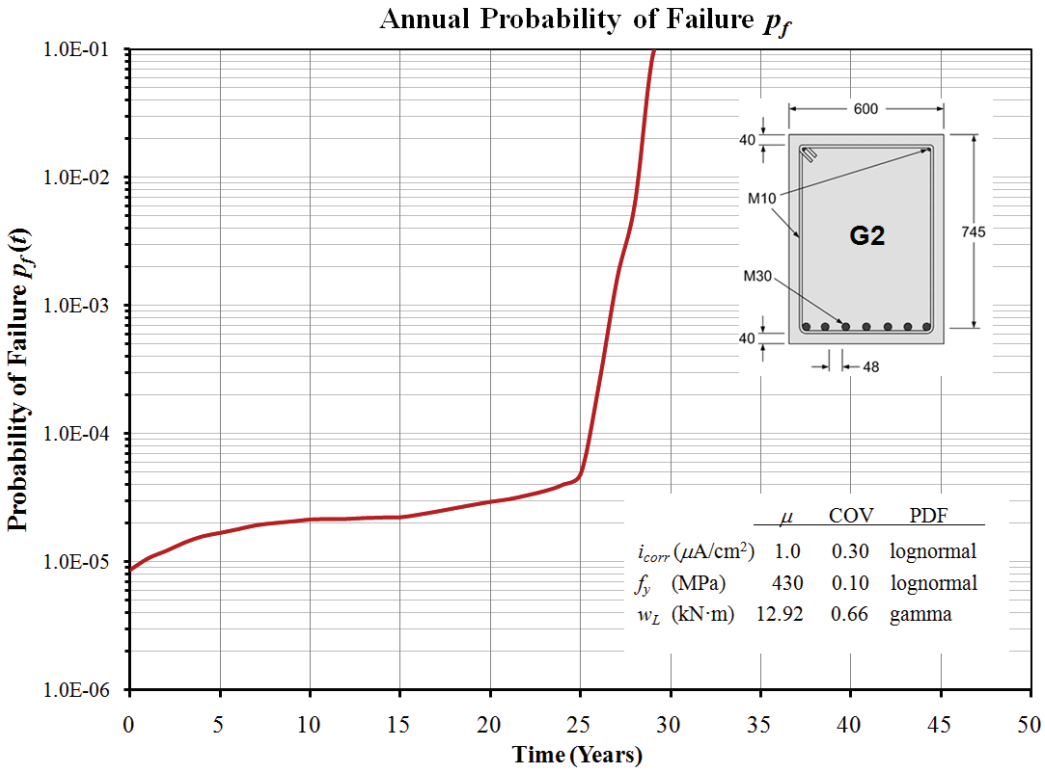

Figure 7-2: Annual probability of failure for RC girder G2

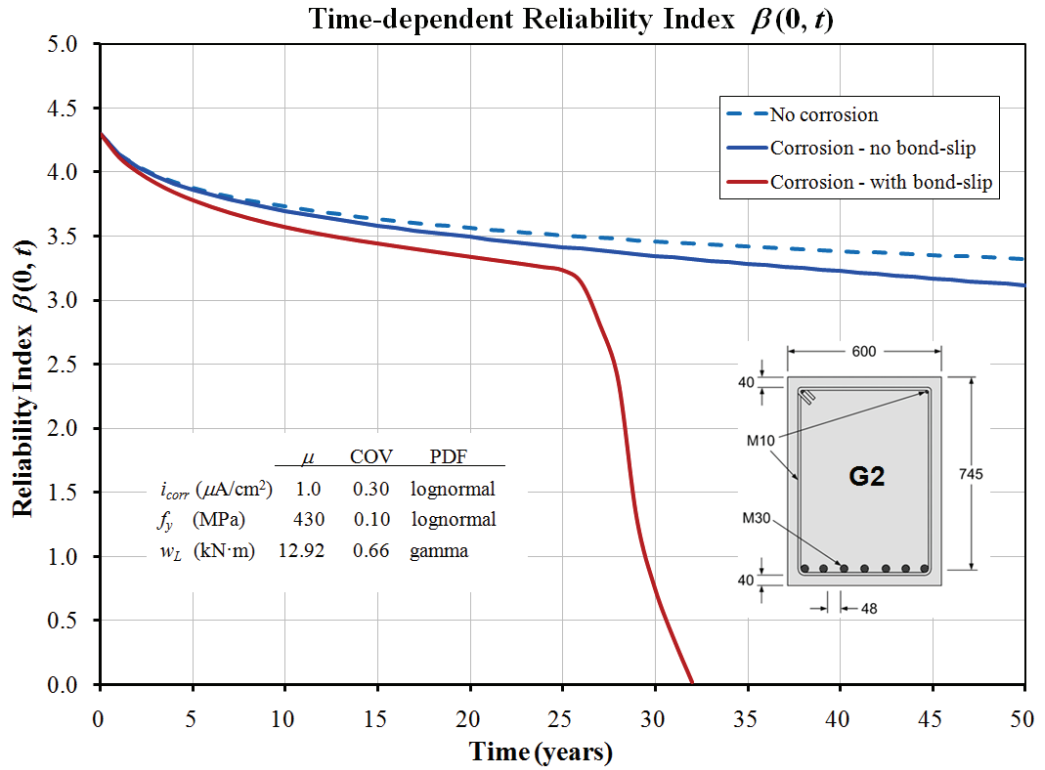

Figure 7-3: Time-dependent reliability index for RC girder G2

Ignoring the effects of corrosion, the target reliability for RC girder G2 is $\beta_T = 3.32$, based on the SFEA approach, which is of the order expected for code based design. Accounting only for the uniform reduction of rebar section, and ignoring the effects of bond deterioration, the time-dependent reliability at the end of life is 3.12 ($p_f = 9.155 \times 10^{-4}$). This rather small decrease in reliability is due to the fact that the initial diameter of each M30 rebar (29.9 mm) is relatively large, and with a corrosion penetration rate of 0.0161 mm/year (corresponding to the mean i_{corr} = 1 μA/cm^2), the residual diameter is 28.7 mm. The same penetration rate in M25 and smaller bars would result in a more significant decrease in the reliability index. In addition, as reported by Stewart (2004; 2009), Stewart and Al-Harthy (2008), and Val (2007), who also accounted for the spatial effects of pitting corrosion, the reliability in terms of flexural and shear strength, is further decreased depending on the density and distribution of pits. In those studies, deterioration of bond strength was not considered.

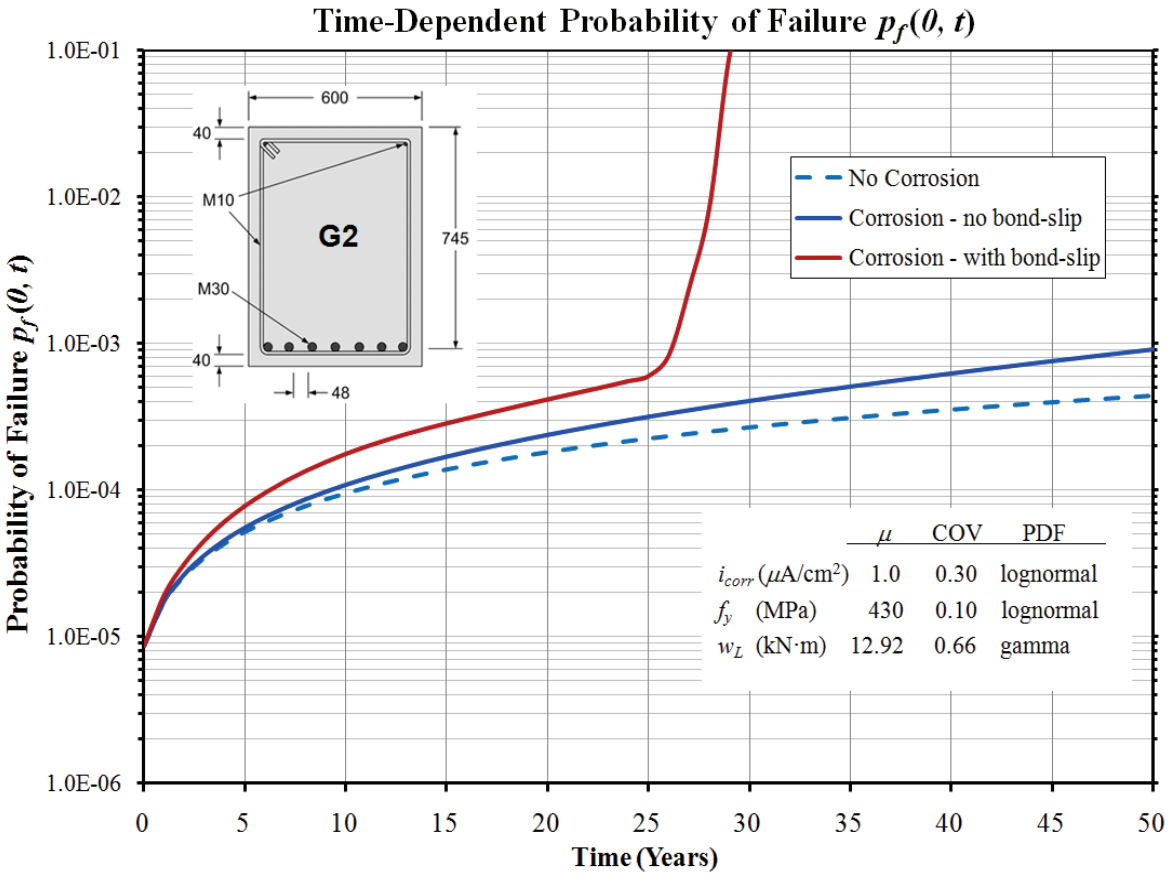

Figure 7-4: Time-dependent probability of failure for RC girder G2

Nevertheless, as discussed in Chapter 2, the deterioration of RC structures is not due as much to the reduction of flexural strength, as a result of rebar area loss, as to the products of corrosion exerting stresses in the concrete matrix (Cabrera 1996), which lead to the loss of bond strength. Thus, referring to the curves representing corrosion effects that include both the loss of steel area and the degradation of bond strength, the cumulative probability of failure is significantly higher than when bond-slip mechanisms are ignored. The results show that corrosion does not affect the girder reliability significantly for about 25 years after its initiation (Figure 7-3). Taking into account the conservative assumptions in the example problem, i.e. (i) all tension reinforcement assumed is subjected to uniform corrosion, and (ii) the nearly complete loss of bond in the span between the corroded reinforcement and concrete, indicates that there is a rather long period of time even after the initiation of corrosion before it will affect the reliability of the girder significantly, as measured in terms of the ultimate limit state in flexure. However, after this period the girder reliability deteriorates rapidly. In the example presented here, the probability of failure at $t = 25$ years $p_f = 9.155 \times 10^{-4}$ increases to $p_f = 0.1$ at just over $t = 29$ years. Also, during the 1 to 25 year period the reliability is lower than when bond deterioration is ignored in the analysis.

This trend appears to be in sharp contrast to the results obtained by Val et al. (1998) in their pioneering work. Their research is particularly significant to the present study, because it represents the first application of finite element-based reliability analysis to RC structures in general, and more importantly, RC structures affected by the corrosion of reinforcement. The method they employed includes a nonlinear finite element structural model and probabilistic models for traffic loads, corrosion propagation, bond characteristics, and material properties. Reliability was estimated in terms of the reliability index using FORM and Monte Carlo simulation. The methodology was applied to calculating reliabilities for a deteriorating simple-span RC slab bridge for ultimate strength and serviceability limit states. For the ultimate limit state, the time-dependent reliability of the bridge is illustrated in Figure 7-5.

As is evident in Figure 7-5, no noticeable strength degradation occurs during the initial 50 year period, followed by rapid decrease in the flexural strength due to pitting corrosion. Although the strength loss due to general corrosion is initiated at about the same time, the rate of the degradation is much smaller. As a result the authors concluded that the complete

loss of bond has a relatively insignificant effect on bridge reliability in flexure (ULS). Clearly, the same conclusion cannot be reached based on the results obtained here (Figure 7-3), where uniform corrosion leads to very rapid deterioration of flexural strength. However, the difference between the results reported here and those of Val et al. (1998) can be explained by comparing the assumptions and the finite element implementations of the reinforcement and bond-slip models in the two studies. While Val et al. (1998) did not provide details of the FE mesh used in their study, the authors assumed that for general corrosion all bond is lost between the concrete and the corroded reinforcement in the bridge span except in regions near the abutments. This is analogous to allowing general corrosion only in the midspan of the beam and possibly explicit modeling of anchorage effects in the support zones. In actual simply supported RC beams, the tension steel is anchored by hooking the rebar in the support area. Furthermore, bond strength is enhanced by the effects of loading in the support zone and confinement provided by the shear reinforcement.

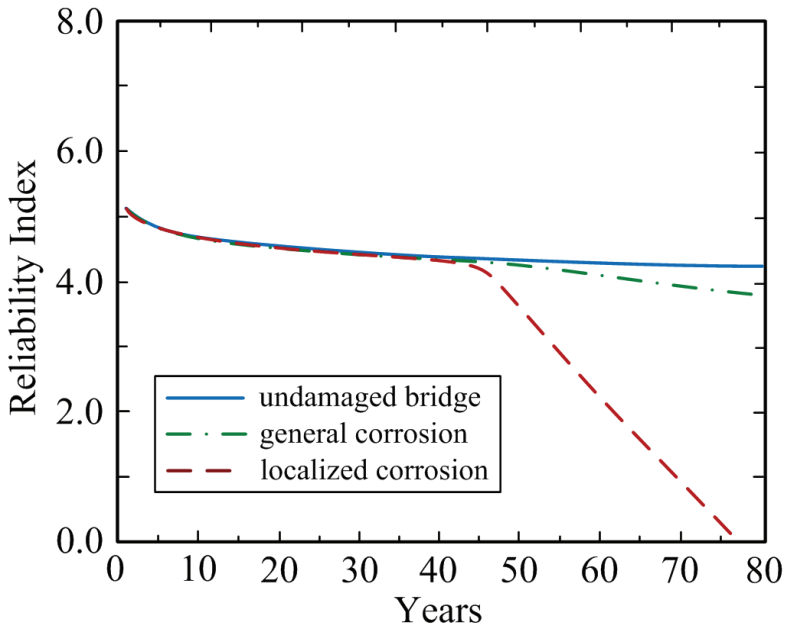

Figure 7-5: Time-dependent reliability index for RC bridge beam for ultimate limit state, adapted from Val and Stewart (1998)

In the current research it is assumed that uniform corrosion occurs along the rebar elements over the entire span of the girder. More importantly, in the finite element model, reduction of bond strength is also assumed to occur along the entire girder. In light of these assumptions the results obtained here are in general agreement with recent experimental and analytical

studies in which the effects of corrosion location and corrosion lengths were explicitly considered. For example Chung et al. (2008) carried out experimental and analytical evaluations of 70 simply supported concrete slabs reinforced with corroded and uncorroded bars, subject to four-point loading. The primary variables were the bond length and the corrosion level which ranged from 0% to 9% area loss. The results indicate that flexural capacity begins to drop significantly as soon as the loss in bar area exceeds 4%, while by the time area loss of rebar reaches 9%, the reduction of flexural strength is substantial for all specimens tested regardless of the corrosion length. This agrees with the predictions obtained in the current numerical studies as illustrated in Figure 4-4. These results confirm the hypothesis that bond deterioration is a major contributor to the reduction of moment capacity (Chung, Najm et al. 2008).

Complimentary conclusions were also reached by Bhargava et al. (2008) who observed that corroded beams failed in flexure, due to the loss of bond at the longitudinal reinforcement interface, whereby the bond between longitudinal reinforcement and concrete is transferred to the beam ends. The moment resistance of the corroded beams is hence controlled by the anchorage (bond) of the bars and not by the yielding of fully bonded tensile reinforcement at failure (Mangat and Elgarf 1999a).

More recently, Cousin and Martín-Pérez (2010) reported the results of experimental research on the effects of corrosion on pre-tensioned pre-stressed beams subjected to sustained four point loading. The authors reported that up to 60% of the loading capacity is lost at higher degrees of corrosion while at lower corrosion rates the loading capacity is decreased up to 60% if the corrosion affects the anchorage length. Conversely, no significant decrease of the loading capacity was observed when the anchorage zone was not affected by corrosion (i.e corrosion occurs in the midspan region). This set of experiments demonstrates that the location of corrosion along the prestressing strands has a strong influence on the loading capacity of the beams (Cousin and Martín-Pérez 2010).

7.2.2. Serviceability Limit State – Deflection of RC girder G2

The serviceability limit state considered is given in terms of a deflection limit for the RC parking girder for transient live vehicle loads. The deflection is calculated as the deflection under total load minus the deflection under dead load only (i.e. instantaneous live load). In the

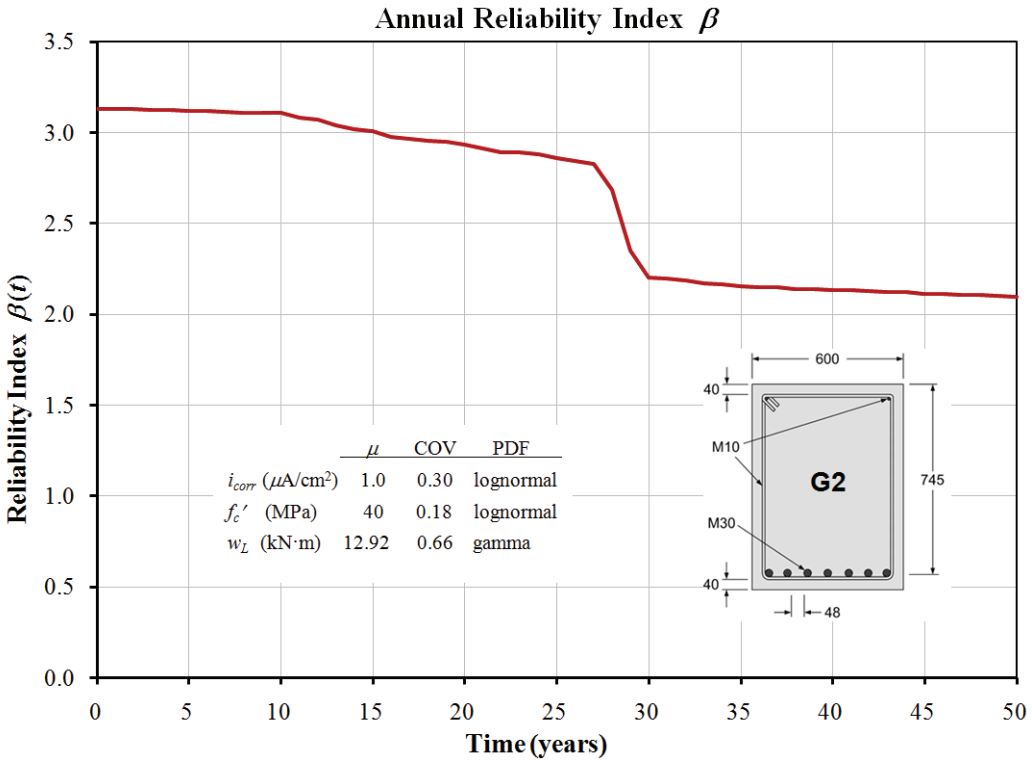

Figure 7-6: Annual reliability index for RC girder G2

context of this limit state, the design parameters that influence the girder flexural stiffness will have an effect on the girder reliability. These are the moduli of elasticity of concrete E_c and steel E_s, and parameters controlling cracking of the concrete and its behaviour after cracking, which include the concrete tensile strength f_{ct}. Uncertainties associated with these parameters were not explicitly considered. However, the tensile strength, modulus of elasticity, and compressive strength of concrete are mutually dependent. Since in the FE model, E_c and f_{ct} are calculated from the values of the compressive strength f_c', and f_c' is a random variable, uncertainty in the other two parameters is accounted for implicitly. The reliability index and the corresponding annual probability of failure for RC girder G2 are respectively shown in Figure 7-6 and Figure 7-7, for an assumed service life of 50 years.

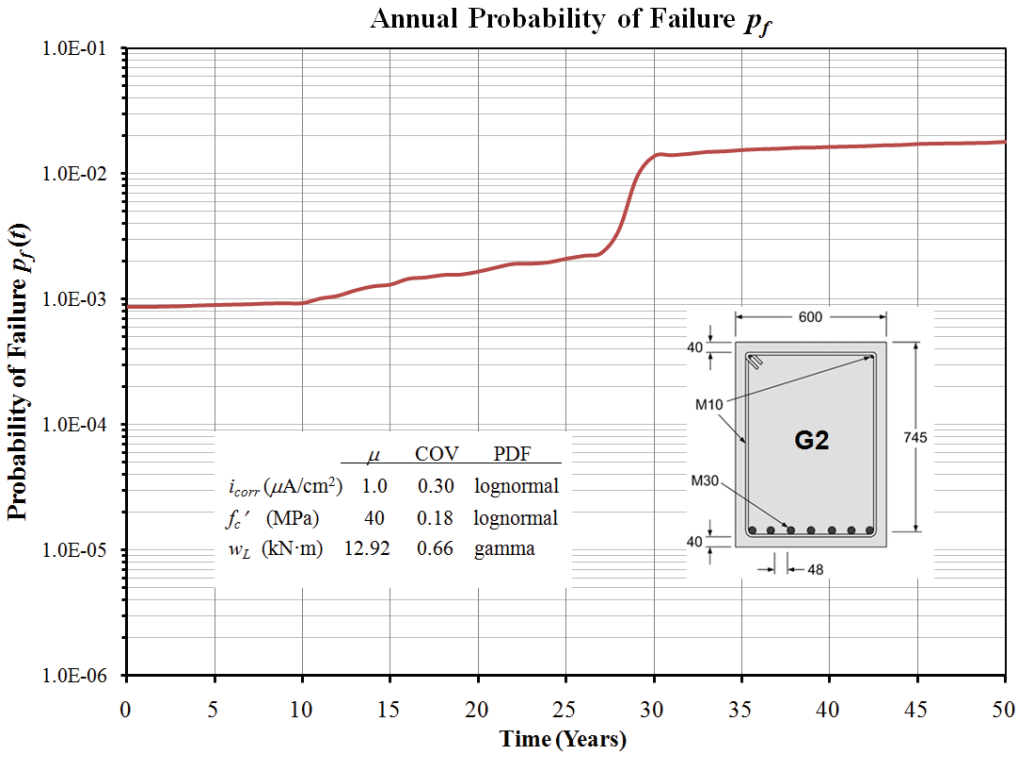

Figure 7-7: Annual probability of failure for RC girder G2

The results indicate that general corrosion leads to a very significant decrease in the reliability of the girder for the serviceability limit state (deflection). This is mainly due to the decrease in bond strength between the concrete and the corroded reinforcement, whereas reduction of the cross-sectional area of the reinforcement has an insignificant effect on serviceability reliability. The annual reliability index decreases rapidly between 27 and 30 years for the example girder. Beyond the 30th year, once the bond strength reached its residual value, further corrosion growth seems to have an insignificant impact on the reliability of the example girder. This trend is in overall agreement with the results reported by Val et al. (1998) for the serviceability limit state, as shown by Figure 7-8. The magnitude of the drop in the reliability index is essentially the same for both cases. Figure 7-8 also shows that pitting corrosion does not have a significant influence on the reliability of RC beams for SLS.

The time-dependent reliability index for RC girder G2, with and without the effects of general corrosion, is shown in Figure 7-9. In the absence of corrosion, the target reliability is $\beta_T = 1.7$ at $t = 50$ years. This is a typical value of performance for deflection SLS at the end

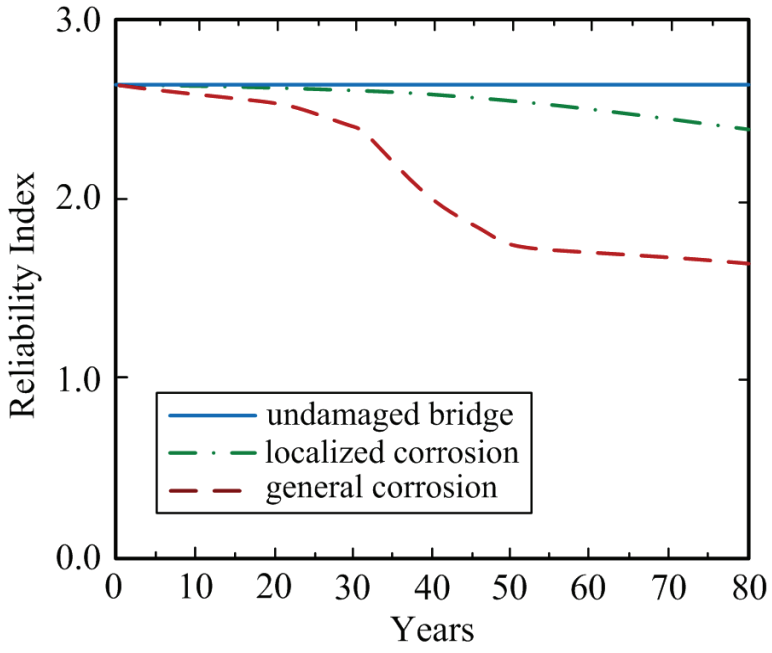

Figure 7-8: Annual reliability index for serviceability limit state, adapted from Val and Stewart (1998)

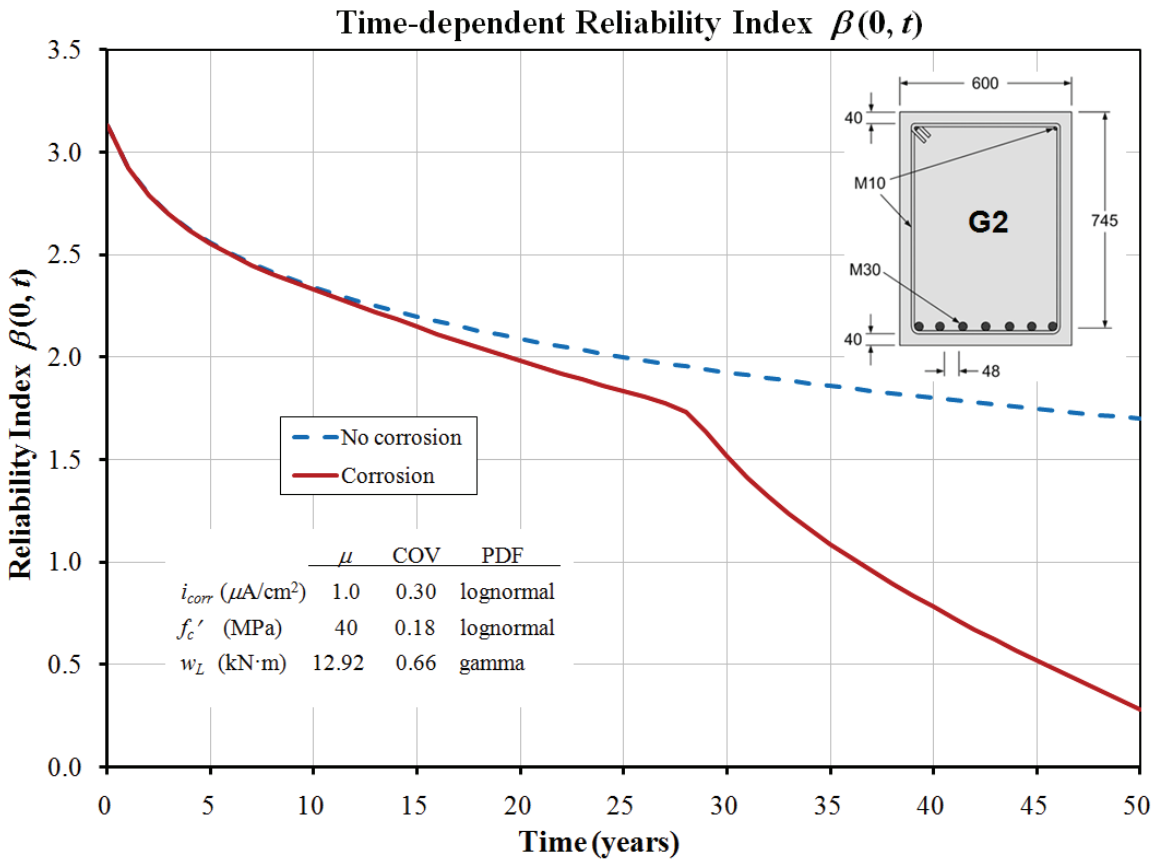

Figure 7-9: Time-dependent reliability index for RC girder G2

of service life. The reliability for deflections is not noticeably affected during the first 10 years, and only moderately up to about 27 years. Beyond this point in time, the reliability of the girder is significantly reduced, as the bond strength in the mid-span of the beam is transferred to the end regions of the girder, reaching a probability of failure of p_f = 0.4, meaning that there is a 40% likelihood of exceeding the deflection limit of l/360 by the end of service life. As with the annual reliability index, the time-dependent results correlate well with those of Val et al. (1998), as shown in Figure 7-10. The differences between the results are only due to the details and design parameters specific to the example problems, as well as the details in the respective finite element models.

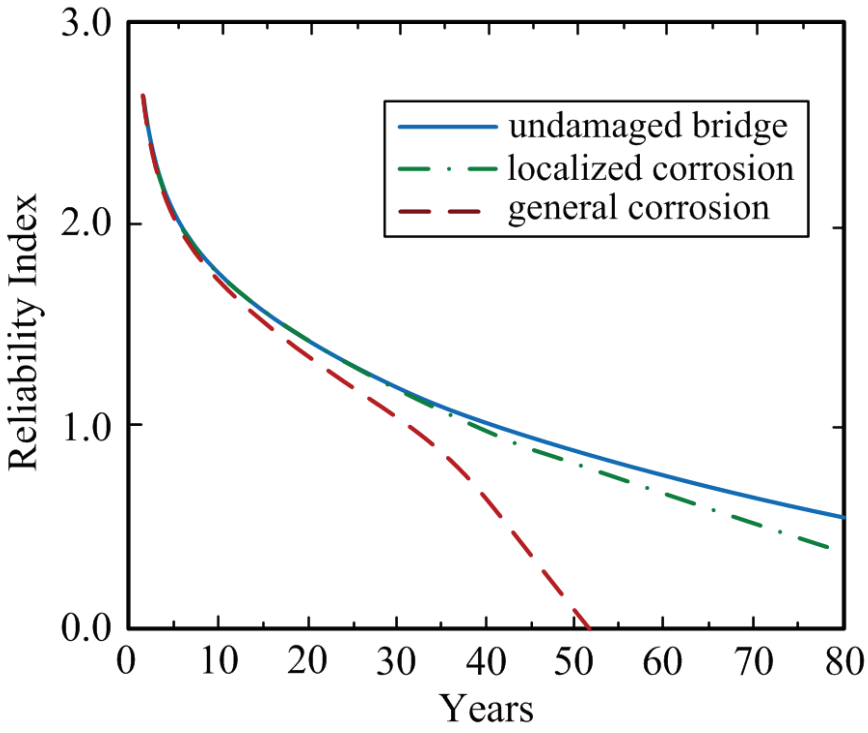

Figure 7-10: Time-dependent reliability indices for serviceability limit state, adapted from Val and Stewart (1998)

The time-dependent SLS probability of failure for the RC parking girder example is shown in Figure 7-11. The probability of failure at the end of service life, mainly due to the effects of uniform corrosion-induced degradation, is an order of magnitude higher than in the absence of corrosion.

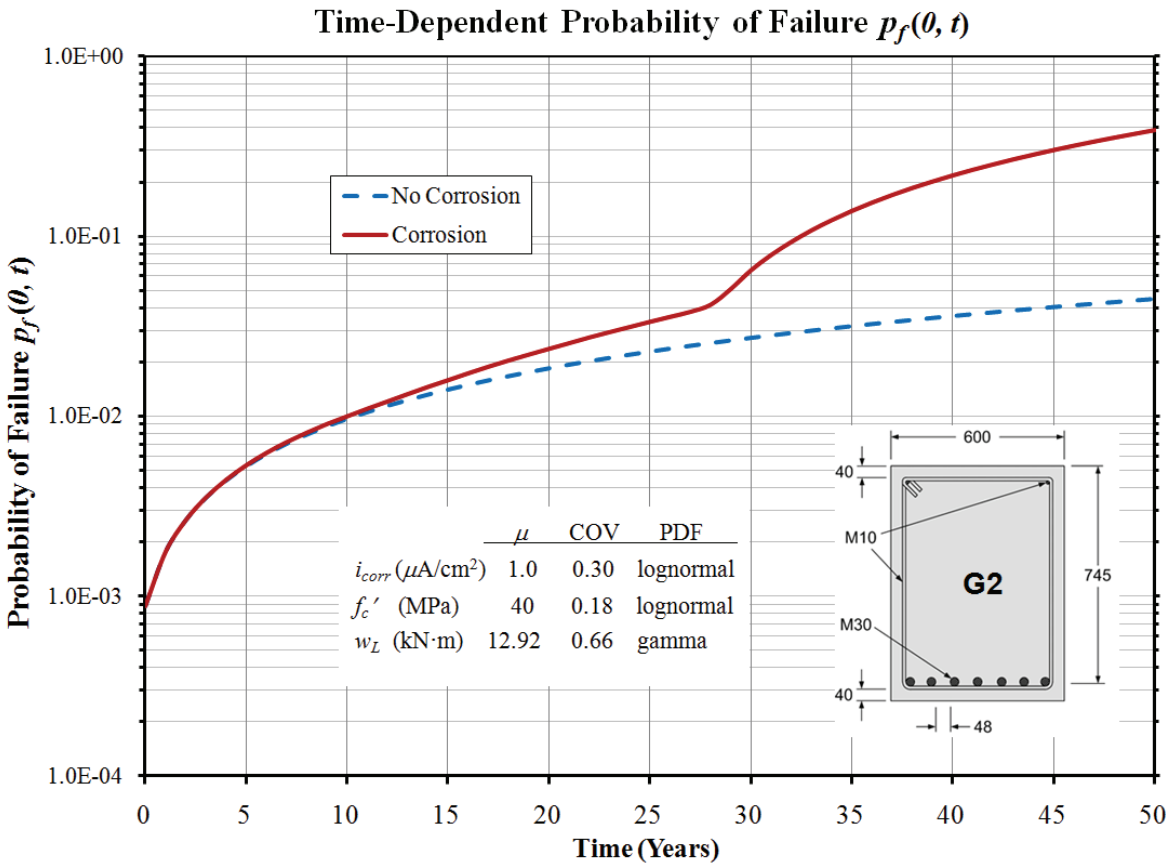

Figure 7-11: Time-dependent probability of failure for RC girder G2

7.3 Summary of the Results

The results presented in the preceding sections are based on the SFEA of a specific example problem. While these results cannot be generalized to the time-dependent reliability of an entire spectrum of RC beam problems, the results are expected to be representative of a typical RC beam affected by corrosion, where the effects of bond strength loss are included. Furthermore, the results reported in the preceding sections show that for the serviceability limit state, uniform corrosion has a very significant influence on the reliability of RC beams, mainly because of the gradual reduction of bond strength along the length of reinforcement. A similar conclusion can also be reached for the ultimate limit state, provided that general corrosion leads to a complete loss of bond in the anchorage reinforcement region (pullout failure).

The results presented in this section demonstrate that the proposed SFEA framework can be used for the time-dependent reliability analysis of RC structural elements. Furthermore, in conjunction with experimental research, which is essential for the validation and verification of the finite element modeling component, the framework could be used in lifecycle management studies and as part of partial safety factor calibration in the development of durability design standards and codes. General discussion of this research project, conclusions, and recommendations for further research are presented in Chapter 8.

Chapter 8. Closure

8.1 General

Rebar corrosion is the most serious deterioration mechanism affecting the performance of RC structures throughout the world (Hansson et al., 2007; Rostam, 2003). Over time the damage caused by corrosion leads to loss of strength, serviceability and functionality, and ultimately affects the structural safety. The costs of maintaining, repairing, or replacement of affected structures are extremely high. Given the limited resources of infrastructure authorities and owners, a need clearly exists for the optimal allocation of resources for design, construction, inspection, and maintenance. However, current RC design standards are mainly concerned with structural performance, without an explicit attempt to evaluate the effect of deterioration mechanisms, such as reinforcement corrosion, over long periods of time. Since current structural design practice is primarily based on the limit states philosophy, wherein the performance of a structure is checked against various limiting conditions at appropriate load levels, it follows that the same framework can be applied to durability design in order to integrate it with the former.

The objective of the research reported here was to develop a Stochastic Finite Element Analysis Framework applicable to time-dependent reliability analysis of RC beams affected by corrosion-induced deterioration. The proposed framework integrates nonlinear finite element and reliability analyses through an iterative response surface methodology. In this approach, nonlinear finite element analysis provides the computational approach necessary for analyzing complex continuum systems, while methods of structural reliability analysis allows modeling and quantification of uncertainties, and computation of response probabilities. Furthermore, response surface methodologies facilitate the integration of FEA and reliability methods when these components are provided by commercial software. This

particular SFEA strategy was chosen after careful consideration of computational efficiency, development effort, accuracy, and practical applicability to the specific problem domain: the time-dependent reliability analysis of RC beams affected by corrosion-induced degradation mechanisms, including the gradual reductions of reinforcement cross-sectional area and the bond strength between the concrete and corroded reinforcement.

Effective implementation of the framework was demonstrated through numerical studies of a simply-supported RC girder with tension reinforcement subjected to the effects of uniform corrosion. The framework proved to be a promising research tool for the prediction of time-dependent reliability, determination of the most relevant design variables, and the analysis of how uncertainties in these variables impact the performance of RC beams subjected to corrosion of flexural reinforcement. The case study represents only a demonstration of the application of the SFEA and thus in term of result it can only identify further areas of experimental and numerical research.

8.2 Discussion of Results and Conclusions

Ultimate Limit State – Flexural Strength

The results of numerical studies reported here show that the impact of moderate to severe rate of uniform corrosion on the reliability of RC beams with longitudinal reinforcement of M30 or larger is not significant when considering only the gradual reduction of tension steel area. For the RC girder modeled here, the reliability index at 25 years is 2.6% lower than in the absence of corrosion. Accounting for both the reduction of rebar area and the progressive loss of bond strength between the corroding tension reinforcement and surrounding concrete, indicates a relative reduction of reliability of 8%. However, over a 50 year reference design life, the reliability of the RC girder deteriorates very rapidly between 25 and 30 years. This abrupt loss of reliability is caused by the breakdown of bond between the steel and concrete along the entire span of the girder, including the anchorage zones. Once the residual bond strength is reached, the reliability of the girder continues to decrease at a gradual rate similar to the initial 25 year period. This observation is in contrast to numerical studies of RC beams subjected to general corrosion where bond loss is assumed to occur only in the midspan

region but not near the beam ends. Nonetheless, the results obtained in this research are in agreement with recent experimental and numerical studies in which the effects of corrosion location and corrosion lengths were explicitly considered, confirming that bond deterioration is a major contributor to the reduction of flexural strength capacity, and thus reliability. Furthermore, the results from the case study suggest that flexural resistance of corroded RC beams is controlled by the anchorage (bond) of the bars and not by the yielding of fully bonded tensile reinforcement at failure. This is significant since the end regions can be severely corroded due to chloride, moisture, and oxygen access at connections and expansion joints.

Serviceability Limit State - Deflections

Similarly, the results of the SFEA of the example RC parking garage girder indicate that general corrosion leads to a very significant decrease in the reliability in terms of maximum deflections. This loss of serviceability was shown to be predominantly caused by the loss of bond strength, whereas the effect of reduction of the cross-sectional area of reinforcement was found to be insignificant. The probability of failure at the end of service life, due to the effects of uniform corrosion induced degradation is observed to be approximately an order of magnitude higher than in the absence of corrosion. The general trend in the time-dependent reliability for deflections is also very similar to that for flexural strength. These conclusions are in agreement with recent experimental and numerical studies reported in the literature.

The Proposed SFEA Framework

The proposed computational framework facilitates performance and reliability predictions of RC beams affected by corrosion. Combined with acceptable limiting performance criteria for RC beams and limit states, the SFEA model may be used as a basis for development of rational criteria for serviceability and strength requirements for reinforced concrete beam elements subjected to reinforcement corrosion. The application of the proposed framework can not only serve as a tool for the reliability assessment of existing structures, but also as a complementary tool for planning and optimisation of future experimental studies by establishing an a priori parameter sensitivity (even though some are difficult to control in

physical experimentation). Accurate performance evaluation of corrosion-prone structures could allow extension of service life, where appropriate, and may contribute to a more consistent safety level across structures. This would improve the efficient use of scarce resources, and minimize the impact of indirect costs through optimised inspection, maintenance and repair works.

In summary, the following conclusions are postulated based on the limited numerical results generated in this research:

(1) Reduction of the steel area of reinforcement has only a marginal effect on the reliability of RC beams in terms of the flexural strength (ULS), particularly for larger bar diameters.
(2) The load-deflection response is significantly affected by the deterioration of bond strength (flexural strength and stiffness). This indicates that bond damage should be considered for the ULS reliability predictions of corroded beams for general corrosion (along the entire length of the tensile steel).
(3) Explicit modelling of bond deterioration is essential for realistic reliability assessment in both the ultimate and serviceability limit states.
(4) Limitations of conventional sectional analysis methods in advanced reliability assessment and performance prediction studies are underscored. Hence the need for SFEA based models presented herein.
(5) The onset of longitudinal cracking as an end-of-service-life criterion may be not a realistic target for assessment of the remaining life of in-service structures. Perhaps potentially better criteria is quantification of corrosion-induced damage in terms of residual bond capacity.
(6) Stochastic finite element analysis is necessary to evaluate the reliability of complicated systems considering their behaviour as realistically as possible especially when explicit limit state functions are not available.
(7) Successful implementation of this SFEA framework requires that the reliability and FEA software used are stable, robust, and validated. At this time, RSM appears to be

the best method for integrating existing commercial software, especially when access to the source code is not available.

(8) The results presented in this section demonstrate that the proposed SFEA framework can be used for the time-dependent reliability analysis of RC structural elements. In conjunction with experimental research the proposed framework could be used in lifecycle management studies and as part of partial safety factor calibration in the development of durability design standards and codes.

8.3 Recommendations for Future Research

Based on the findings of this study, the following recommendations for future work are listed:

SFEA Framework

- Implementation of spatial discretization of the random fields: the stochastic finite element method is inherently capable of dealing with spatially and temporally distributed system uncertainties through efficient incorporation of random fields. In the strict sense, the distinguishing feature of stochastic finite element analysis is that it involves the discretization of the parameter space of random fields. This is particularly important for modeling the uncertainty in the rate of corrosion.
- Development of a programmer's interface between the COMPASS and VecTor2 components would allow rapid FORM/SORM/IS/RSM functionality and much faster direct Monte Carlo simulation. VectTor2 is recommended because of stability, comprehensive capability, specificity to modeling and analysis of RC structures, and extensive validation with experimental research. Similarly, COMPASS is a fast, validated, powerful, and relatively straight forward to modify and extend. This functionality also favours the capability of dealing with random fields.
- Extension to system reliability analysis which would allow consideration of various evolving failure mechanisms and limit state functions simultaneously (shear, etc.). A performance function can be defined in terms of engineering demand parameters,

damage measures, or decision variables. Estimation of the probability of the defined failure event poses a component reliability problem. However, failure according to one performance criterion may not constitute failure of an entire structural system. It is therefore of interest to define system reliability problems as sets of components and rules, as to which combinations of component failures constitute system failure. This would allow comprehensive time-dependent reliability analysis of situations where, for example, corrosion of transverse steel leads to brittle shear failure in advance of yielding of flexural reinforcement.

Corrosion Damage Model

- Verification of the bond-slip as a function of corrosion level model.
- Extension of the model to include the effects of pitting corrosion.
- Concrete compression failure - the impact of corrosion in the compressive region cannot be readily isolated.
- Inclusion of the effects of transverse steel confinement on the residual bond performance of corroded longitudinal reinforcement.
- Further investigation on the interaction between corrosion expansion and incurred damage.

Probabilistic durability design of RC beams

- Inclusion of shear ULS and implementation of multiple failure mode analysis (system reliability).
- Partial safety factor calibration work in support of research to develop durability based limit-state design.
- Extensive numerical service life studies of a full spectrum of RC beam types (short/deep beams, different dead/live load ratios, various reinforcement configurations, etc.) using the proposed SFEA Framework.

Experimental Research

- Experimental data related to RC corrosion (regimes, rates, and damage mechanisms), essential to modeling and analysis, and the development of lifecycle tools is seriously lacking in the literature. Most of the available data comes from accelerated corrosion testing often on scale structural elements. This is understandable given the time required to conduct corrosion testing in real time. However, a promising solution is to obtain data from in-service structures (predominantly bridges) instrumented for monitoring and collection of real-time corrosion data. The number of such structures is still extremely small and sensor data is currently difficult to obtain. Nevertheless, this is a particularly promising source of valuable corrosion data for realistic modeling, analysis, and evaluation of RC structures subjected to reinforcement corrosion.

References

Ahmad, S. (2003). "Reinforcement corrosion in concrete structures, its monitoring and service life prediction - a review." Cement and Concrete Composites **25**(4-5): 459-471.

Al-Hammoud, R., K. Soudki, et al. (2010). "Bond analysis of corroded reinforced concrete beams under monotonic and fatigue loads." Cement and Concrete Composites **32**(3): 194-203.

Al-Sulaimani, G. J., I. A. Kaleemullah, et al. (1990). "Influence of corrosion and cracking on bond behaviour and strength of reinforced concrete members." ACI Structural Journal **87**(2): 220-231.

Allen, D. E. (1991). "Limit states criteria for structural evaluation of existing buildings." Canadian Journal of Civil Engineering **18**: (pp. 995–1004).

Almusallam, A. A., A. S. Al-Gahtani, et al. (1996). "Effect of reinforcement corrosion on flexural behavior of concrete slabs." Journal of Materials in Civil Engineering **8**(3): 123-127.

Amleh, L. and S. Mirza (2008). "Framework for durability-based design for concrete-steel bond against corrosion." Journal of Materials in Civil Engineering **20**(10): 678-681.

Anders, M. and M. Hori (1999). "Stochastic finite element method for elasto-plastic body." International Journal of Numerical Methods in Engineering **46**(11): 1897-1916.

Andersen, J. E. (2006). Structural Health Monitoring Systems, Jacob Egede Andersen.

Andrade, C. and C. Alonso (1996). Durability design based on models for corrosion rates. The Modelling of Microstructure and Its Potential for Studying Transport Properties and Durability. H. Jennings, J. Kropp and K. Scrivener. The Netherlands**:** 473-492.

Ang, A. A.-H. and W. H. Tang (1984). Probability Concepts in Engineering Planning and Design, Volume II: Decision, Risk and Reliability, John Wiley and Sons.

Arnbjerg-Nielsen, T. and P. Bjerager (1988). Finite Element Reliability Method with Improved Efficiency by Sensitivity Analysis. Proceedings of the Joint ASME / ISES Applied Mechanics and Engineering Sciences Conference. **93:** (pp. 15-25).

ASCE. (2009). "Report card for America's infrastructure." Retrieved September 1, 2010, from http://apps.asce.org/reportcard/2009/grades.cfm.

Ballim, Y. and J. C. Reid (2003). "Reinforcement corrosion and the deflection of RC beams - an experimental critique of current test methods." Cement and Concrete Composites **25**(6): 625-632.

Bathe, K. J. (1996). Finite Element Procedures, Prentice-Hall, Inc.

Batis, G. and E. Rakanta (2005). "Corrosion of steel reinforcement due to atmospheric pollution." Cement and Concrete Composites **27**(2): 269-275.

Beard, M. D., M. J. S. Lowe, et al. (2003). "Ultrasonic Guided Waves for Inspection of Grouted Tendons and Bolts." ASCE Journal of Materials in Civil Engineering **15**(3): 212–218.

Bentz, E. C. (2000). Sectional Analysis of Reinforced Concrete Members, Ph.D. Thesis, University of Toronto.

Berto, L., P. Simioni, et al. (2008). "Numerical modelling of bond behaviour in RC structures affected by reinforcement corrosion." Engineering Structures **30**(5): 1375–1385.

Bhargava, K., A. K. Ghosh, et al. (2008). "Suggested empirical models for corrosion-induced bond degradation in reinforced concrete." ASCE Journal of Structural Engineering **134**(2): (pp. 221-230).

Bickley, J. A. (1984). Parking Structure Deterioration: A Survey and Analysis of its Extent and Influencing Factors, The Research Division, Policy Department and Research Sector, Canada Mortgage and Housing Corporation, Ottawa. **Volume 1**.

Bielewicz, E., Gorski, J., and Walukiewicz, H. (1991). Random Fields: Digital Simulation and Applications in Structural Mechanics. Computational Stochastic Mechanics. P. D. Spanos, and Brebbia, C.A., Computational Mechanics Publications and Elsevier Applied Science.

Bolomey, J. (1927). Durcissement des Mortiers et Betons, Bulletin Technique de la Suisse Romande, 16, 22, and 24.

Borgard, B., C. Warren, et al., Eds. (1990). Mechanisms of Corrosion of Steel in Concrete. Corrosion Rates of Steel in Concrete. ASTM STP 1065.

Box, G. E. P. and D. W. Behnken (1960). "Some new three level designs for thestudy of quantitative variables." Technometrics **2**(4): 455-475.

Box, G. E. P., W. G. Hunter, et al. (1978). Statistics for Experimenters, John Wiley & Sons , New York, USA.

Box, G. E. P. and K. B. Wilson (1951). "On the experimental attainment of optimum conditions." Journal of the Royal Statistical Society **B-13**: 1-38.

Breitung, K. (1984). "Asymptotic approximation for multi-normal integrals." ASCE Journal of Engineering Mechanics **110**(3): (pp. 357–366).

Brennan, D., U. Akpan, et al. (2001). Random Field Modelling of Rainfall Induced Soil Movement. Halifax, Martec Ltd.**:** 83pp.

Bresler, B. and A. C. Scordelis (1963). "Shear strength of reinforced concrete beams." Journal of American Concrete Institute **60**(1): (pp. 51-72).

Broomfield, J. P. (2007). Corrosion of Steel in Concrete - Understanding, investigation and repair, 2nd Edition. London, E & FN Spon Press.

Bucher, C. G. and U. Bourgund (1990). "A fast and efficient response surface approach for structural reliability problems." Structural Safety **7**(1): 57-66.

Cabrera, J. G. (1996). "Deterioration of concrete due to reinforcement steel corrosion." Cement & Concrete Composites **18**: 47-59.

CAC (1995). Concrete Design Handbook, Cement Association of Canada, Rexdale (Toronto).

Cairns, J. and S. Millard (1999). Reinforcement corrosion and its effect on residual strength of concrete structures. Structural Faults and Repair-99. M. C. Forde. Edinburgh, Engineering Technics Press.

Cairns, J., G. A. Plizzari, et al. (2005). "Mechanical properties of corrosion-damaged reinforcement." ACI Materials Journal **102**(4): 256-264.

CAN/CSA A23.1-04 (2004). Concrete Materials and Methods of Concrete Construction, Canadian Standards Association International, Rexdale, ON**:** (232 pp.).

CAN/CSA A23.3-04 (2004). Design of Concrete Structures, Canadian Standards Association, Rexdale, ON**:** (232 pp.).

CAN/CSA S413-07 (2007). Parking Structures, 3rd Edition, Canadian Standards Association (124pp.)

Capozucca, R. (1995). "Damage to reinforced concrete due to reinforcement corrosion." Construction and Building Materials **9**(5): 295-303.

Castel, A., R. François, et al. (2000). "Mechanical behaviour of corroded reinforced concrete beams - Part 1: experimental study of corroded beams." Materials and Structures **33**: 539-544.

Chalk, P. and R. B. Corotis (1980). "A Probability model for design live loads." ASCE Journal of Structural Engineering **109**(4): (pp. 858-874).

Chung, L., J.-H. J. Kim, et al. (2008). "Bond strength prediction for reinforced concrete members with highly corroded reinforcing bars." Cement and Concrete Composites **30**(7): 603-611.

Chung, L., H. Najm, et al. (2008). "Flexural behavior of concrete slabs with corroded bars." Cement & Concrete Composites **30**: (pp. 184-193).

CONTECVET (2001). A validated Users Manual for Assessing the Residual Service Life of Concrete Structures, Geocisa & Instituto Eduardo Torroja.

Cook, R. D. (1981). Concepts and Applications of Finite Element Analysis, John Wiley & Sons.

Cornell, C. A. (1969). A normative second-moment reliability theory for structural design. Solid Mechanics Division, University of Waterloo, Waterloo, Ontario, Canada.

Cornell, C. A. (1969). "A probability-based structural code." Journal of the American Concrete Institute **66**: 974-985.

Coronelli, D. (2002). "Corrosion cracking and bond strength modeling for corroded bars in reinforced concrete." ACI Structural Journal **99**(3): 267-276.

Coronelli, D. and P. Gambarova (2004). "Structural assessment of corroded reinforced concrete beams: modeling guidelines." Journal of Structural Engineering **130**(8): 1214-1224.

Cousin, B. and B. Martín-Pérez (2010). Chloride ingress in pre-tensioned prestressed concrete beams and the effect of corrosion on their structural behaviour. Sixth International Conference on Concrete under Severe Conditions, Environment & Loading (CONSEC '10), Mérida, Yucatán, México, CRC Press/Balkema Taylor & Francis Group.

Cousin, B. and B. Martín-Pérez (2010). Chloride ingress in pre-tensioned prestressed concrete beams and the effect of corrosion on their structural behaviour. Sixth International Conference on Concrete under Severe Conditions, Environment & Loading (CONSEC '10). M. Castro-Borges, Sakai, Gjorv, and Banthia, eds. Mérida, Yucatán, México, CRC Press/Balkema Taylor & Francis Group, London**:** (pp. 247-256).

Cruse, T. A., Burnside, O.H., Wu, Y.-T., Polch, E.Z., and Dias, J.B. (1988). "Probabilistic structural analysis methods for select space propulsion system structural components (PSAM)." Computers and Structures **29**(5): 891-901.

CSA A23.3-04 (2004). Design of concrete structures, Canadian Standards Association, Mississauga, ON, Canada. **CSA A23.3-04**.

CSA S408-11 (2011). Guidelines for the development of limit states design standards, Canadian Standards Association, Mississauga, ON, Canada. **CSA S408-11**.

Dekoster, M., F. Buyle-Bodin, et al. (2003). "Modelling of the flexural behaviour of RC beams subjected to localised and uniform corrosion." Engineering Structures **25**(10): 1333-1341.

Deodatis, G. (1991). "The weighted integral method, I: stochastic stiffness matrix." Journal of Engineering Mechanics **117**(8): 1851–1864.

Deodatis, G. and M. Shinozuka (1991). "The weighted integral method, II: response variability and reliability." Journal of Engineering Mechanics **117**(8): 1865–1877.

Der Kiureghian, A. and J. B. Ke (1988). "The Stochastic Finite Element Method in Structural Reliability." Probabilistic Engineering Mechanics **3**(2): 83-91.

Der Kiureghian, A. and R. L. Taylor (1983). Numerical methods in structural reliability. 4th International Conference on Applications of Statistics and Probabillity in Structural and Soil Engineering (ICASP4). Florence, Italy.

Der Kiureghian, A. and Y. Zhang (1999). "Space-variant finite element reliability analysis." Computer Methods in Applied Mechanics and Engineering **168**(1-4): (pp. 173-183).

Det Norske Veritas (2002). Proban, DNV Software, Norway.

Ditlevsen, O. (1996). Dimension reduction and discretization in stochastic problems by regression method, CRC Mathematical Modelling Series.

DuraCrete (2000). The European Union - Brite EuRam III, DuraCrete - Probabilistic performance based durability design of concrete structures, Final Technical Report of Duracrete project, Document BE95-1347/R17, May 2000.

Eiermann, M., O. G. Ernst, et al. (2005). Computational Aspects of the Stochastic Finite Element Method. Proceedings of ALGORITMY 2005.

Eligehausen, R., E. Popov, et al. (1983). Local Bond Stress-Slip relationship of Deformed Bars under Generalized Excitations, Report No. UCB/EERC-83/23, Earthquake Engineering Center, University of California, Berkeley.

Ellingwood, B. R. and Y. Mori (1993). "Probabilistic methods for condition assessment and life prediction of concrete structures in nuclear plants." Nuclear Engineering and Design **142**: (pp. 155-166).

Ellingwood, B. R. e. a. (1982). "Probability-based load criteria: load factors and load combinations." Journal of the Structural Division, ASCE **108**(5): (pp. 978-997).

Enright, M. P. and D. M. Frangopol (1998). "Probabilistic analysis of resistance degradation of reinforced concrete bridge beams under corrosion." Engineering Structures **20**(11): 960-971.

Enright, M. P. and D. M. Frangopol (1998). "Probabilistic Analysis of Resistance Degradation of Reinforced Concrete Bridge Beams under Corrosion." Engineering Structues, Elsevier **20**(11): 960-971.

Enright, M. P. and D. M. Frangopol (1999). "Reliability-based Condition Assessment of Deteriorating Concrete Bridges Considering Load Redistribution." Structural Safety **21**: 159-195.

Fang, C., K. Lundgren, et al. (2004). "Corrosion influence on bond in reinforced concrete." Cement and Concrete Research **34**(11): 2159-2167.

Faravelli, L. (1989). "A Response Surface Method for Reliability Analysis." ASCE Journal of Engineering Mechanics **115**(12): 2763-2781.

Fenton, G. A. and E. H. Vanmarcke (1990). "Simulation of Random Fields via Local Average Subdivision." ASCE Journal of Engineering Mechanics **116**(8): 1733-1749.

Fiessler, B., H. J. Neumann, et al. (1979). "Quadratic limit states in structural reliability." ASCE Journal of Engineering Mechanics **105**(4): (pp. 661–676).

Fish, J. and T. Belytschko (2007). A First Course in Finite Elements, John Wiley & Sons, Ltd., England.

Fox, E. P. (1993). Methods of integrating probabilistic design within an organization's design system uding Box-Behnken matrices. 34th AIAA/ASME/ASCE/AHS/ASC Structures, Structural Dynamics and Materials Conference.

Frangopol, D. M. and K. Maute (2003). "Life-cycle reliability-based optimization of civil and aerospace structures." Computers & Structures **81**(7): (pp.397–410).

Freudenthal, A. M. (1947). "The safety of structures." Transactions of ASCE **112**: (pp. 125–180).

Freudenthal, A. M. (1956). "Safety and the probability of structural failure." Transactions of ASCE **121**: (pp. 1337–1397).

Freudenthal, A. M., J. M. Garrelts, et al. (1966). "The analysis of structural safety." Journal of the Structural Division, ASCE **92**(1): (pp. 267–325).

Ghanem, R. and R. Kruger (1996). "Numerical Solution of Spectral Stochastic Finite Element Systems." Computer Methods in Applied Mechanics and Engineering **129**(3): 289–303.

Ghanem, R. and P. D. Spanos (2003). Stochastic Finite Elements: a spectral approach, Springer, New York.

Ghanem, R. G. (1999). "The nonlinear gaussian spectrum of lognormal stochastic processes and variables." Journal of Applied Mechanics, ASME **66**(4): 964-973.

Ghanem, R. G. and V. Brzakala (1996). "Stochastic finite element analysis of randomly layered media." Journal of Engineering Mechanics **122**(4): 361-369.

Ghanem, R. G. and D. Ghiocel (1996). A comparative analysis of FORM/SORM and polynomial chaos expansion for highly nonlinear systems. 11th ASCE Specialty Conference on Engineering Mechanics. Y. Lin., and Su, T. Fort Lauderdale, FL.**:** 535-538.

Ghanem, R. G. and P. D. Spanos (1991). "Spectral stochastic finite-element formulation for reliability analysis." Journal of Engineering Mechanics **117**(10): 2351–2372.

Glass, G. K. and N. R. Buenfeld (2000). "Chloride-induced corrosion of steel in concrete." Progress in Structural Engineering and Materials **2001**(2): 448-458.

Grigoriu, M. (1992). Application of the Sampling Theorem to the Representation of Random Fields. Sixth Specialty Conference. Y. K. Lin. Structural and Geotechnical Engineering Divisions, ASCE Engineering Mechanics**:** 33-36.

Haldar, A. and J. Huh, Eds. (2001). Reliability Analysis of Structures Subjected to Dynamic Loadings Using Nonlinear SFEM. International Union of Theoretical and Applied Mechanics (IUTAM), Nonlinearity and Stochastic Structural Dynamics, Kluwer Academic Publishers.

Haldar, A. and S. Mahadevan (2000a). Reliability Assessment Using Stochastic Finite Element Analysis, John Wiley & Sons, Inc., New York, (342pp).

Haldar, A. and S. Mahadevan (2000b). Probability, Reliability, and Statistical Methods in Engineering Design, John Wiley & Sons, Inc., (320 pp.).

Handa, K. and K. Andersson (1981). Application of finite element methods in the statistical analysis of structures. Proceedings of the Third International Conference in Structural Safety and Reliability, ICOSSAR'81**:** (pp. 409–420).

Hansson, C. M. Poursaee, A., and Jaffer, S.J. (2007) "Corrosion of Reinforcing Bars in Concrete", R&D Serial No. 3013, Portland Cement Association, Skokie, Illinois, USA, (33 pp).

Hasofer, A. M. and N. C. Lind (1974). "Exact and Invariant Second-Moment Code Format." ASCE Journal of Engineering Mechanics **100**(1): 111-121.

Haukaas, T. (2003). Finite Element Reliability and Sensitivity Methods for Performance-Based Engineering. PhD Thesis, University of California, Berkeley.

Haukaas, T. and A. D. Kiureghian (2004). Finite Element Reliability and Sensitivity Methods for Performance-Based Earthquake Engineering. PEER Report 2003/14, Pacific Earthquake Engineering Research Center, University of California Berkeley**:** (258 pp.).

Hisada, T. and S. Nakagiri (1985). Role of the Stochastic Finite Element Method in Structural Safety and Reliability. 4th International Conference on Structural Safety and Reliability (ICOSSAR '85). A. H.-S. A. I. Konishi, and M. Shinozuka,. Kobe, Japan**:** (pp. 385-394).

Hohenbichler, M. and R. Rackwitz (1988). "Improvement of Second-order Reliability Estimates by Importance Sampling." ASCE Journal of Engineering Mechanics **114**(2).

Hornet, P., Pendola, M., and Lemaire, M. (1998). "Failure probability calculation of an axisymmetrically cracked pipe under pressure and tension using a finite element code." PVP, Fatigue, Fracture and Residual Stresses **373**: 3-7.

Huh, J. and A. Haldar (1999). Reliability Analysis Under Dynamic Loadings. 8th International Conference on Applications of Statistics and Probability (ICASP8-1999). December, 1999**:** 789-796.

IfM. (2010). "COSSAN." Institut für Mechanik, University of Innsbruck, Austria Retrieved August, 2010, from http://mechanik.uibk.ac.at/softwaredevelopment.

Imai, K. and D. M. Frangopol (2000). "Response Prediction of Geometrically Nonlinear Structures." ASCE Journal of Structural Engineering **126**(11): (pp. 1348-1355).

INTES. (2010). "PERMAS." INTES Ingenieurgesellschaft für technische Software mbH, Stuttgart, Germany Retrieved August, 2010, from http://www.intes.de/.

J. Cairns, J., Pantazopoulou, S.J., Noghabai, K., and Rodriguez, J. (2000). Bond of corroded reinforcement. Bond of Reinforcement in Concrete, *fib* Bulletin 10**:** 187-215.

Khuri, A. I. and J. A. Cornell (1996). Response Surfaces – Designs and Analyses. New York, NY, Dekker, Inc.

Kleiber, M. and T. D. Hien (1992). The Stochastic Finite Element Method: basic perturbation technique and computer implementation, John Wiley & Sons Ltd., England.

Koduru S.D. and Haukaas, T. (2006). "Uncertain reliability index in finite element reliability analysis." Int. J. Reliability and Safety **1**(1/2): 77–101.

Lawrence, M. (1987). "Basis Random Variables in Finite Element Analysis." International Journal for Numerical Methods in Engineering **24**: 1849-1863.

Lay, S., P. Schießl, et al. (2003). Lifecon Deliverable D 3.2 - Service Life Models, Technical Research Centre of Finland (VTT)**:** 169.

Lemaire, M., Ed. (1997). Finite element and reliability: combined methods by surface response. Probamat-21st Century, Probabilities and Materials: Tests, Models and Applications for the 21st century, Kluwer Academic Publishers.

Li, C. C. and A. Der Kiureghian (1993). "Optimal discretization of random fields." Journal of Enginering Mechanics **119**(6): 1136-1154.

Li, C. C. and A. D. Kiureghian (1992). An Optimal Discretization of Random Fields, University of California at Berkeley, California.

Liu, P. L. and A. Der Kiureghian (1986). "Multivariate Distribution Models with Prescribed Marginals and Covariances." Probabilistic Engineering Mechanics **1**(2): (pp. 105-112).

Liu, P. L. and A. Der Kiureghian (1991). "Finite Element Reliability of Geometrically Nonlinear Uncertain Structures." ASCE Journal of Engineering Mechanics **117**(8): 1806-1825.

Liu, P. L. and A. D. Kiureghian (1991). "Finite element reliability of geometrically nonlinear uncertain structures." ASCE Journal of Engineering Mechanics **117**(8): (pp. 1806-1825).

Liu, P. L. and A. D. Kiureghian (1991). "Optimization Algorithms for Structural Reliability." Structural Safety **9**: 161-177.

Liu, P. L., H. Z. Lin, et al. (1989). CalREL, University of California, Berkeley, CA.

Liu, Q., I. R. Orisamolu, et al. (1999). COMPASS, Version 1.4, User's Manual, Martec Limited, Halifax, NS.

Liu, T. and R. E. Weyers (1998). "Modeling the dynamic corrosion process in chloride contaminated concrete structures." Cement and Concrete Research **28**(3): 365-379.

Liu, W. K., T. Belytschko, et al. (1986a). "Probabilistic finite elements for non linear structural dynamics." Computer Methods in Applied Mechanics and Engineering **56**(pp. 61–86).

Liu, W. K., T. Belytschko, et al. (1986b). "Random field finite elements." International Journal of Numerical Methods in Engineering **23**(10): (pp. 1831–1845).

Liu, Y. and R. E. Weyers (1998). "Modelling the time-to-corrosion cracking in chloride contaminated reinforced concrete structures." ACI Materials Journal **95**(6): 675-681.

López, W. and J. González (1993). "Influence of the degree of pore saturation on the resistivity of concrete and the corrosion rate of steel reinforcement." Cement and Concrete Research **23**(2): 368-376.

Madsen, H. O. and L. Tvedt (1990). "Methods for Time-dependent Reliability and Sensitivity Analysis." ASCE Journal of Engineering Mechanics **116**(10): 2118-2135.

Mahadevan, S. (1988). Stochastic finite element-based structural reliability analysis and optimization. Ph.D. Thesis, Georgia Institute of Technology.

Malumbela, G., Moyo, P. (2012), and Alexander, M. "Longitudinal strains and stiffness of RC beams under load as measures of corrosion levels." Engineering Structures **35**(2): 215-227

Malumbela, G., Alexander, M., and Moyo, P. (2009). "Steel corrosion on RC structures under sustained service loads – A critical review." Engineering Structures **32**(11): 2518-2525

Mangat, P. S. and M. S. Elgarf (1999a). "Flexural strength of concrete beams with corroding reinforcement." ACI Structural Journal **96**(1): 149-158.

Mangat, P. S. and M. S. Elgarf (1999b). "Bond characteristics of corroding reinforcement in concrete beams." Materials and Structures **32**: 89-97.

Marsh, P. S. and D. M. Frangopol (2008). "Reinforced concrete bridge deck reliability model incorporating temporal and spatial variations of probabilistic corrosion rate sensor data." Reliability Engineering & System Safety **93**(3): 394-409.

Martín-Pérez, B. (1999). Service Life Modelling of R.C. Highway Structures Exposed to Chlorides Ph.D. thesis, University of Toronto.

Matthies, H. G., C. Brenner, et al. (1997). "Uncertainties in probabilistic numerical analysis of structures and solids - stochastic finite elements." Structural Safety **19**: 283–336.

Mayer, M. (1926). Die Sicherheit der Bauwerke. Berlin, Springer-Verlag.

Maymon, G. (1993). "Probability of Failure of Structures without a Closed-Form Failure Function." Computers & Structures **49**(2): (pp. 301-313).

McKenna, F., G. L. Fenves, et al. (2002). Open System for Earthquake Engineering Simulation, http://opensees.berkeley.edu/, Pacific Earthquake Engineering Research Center, Berkeley, CA.

Melchers, R. E. (1987). Structural Reliability Analysis and Prediction, Ellis Horwood Limited, West Sussex, England.

Mirza, S. A. and J. G. MacGregor (1979). "Variabilityof mechanical propertries of reinforcing bars." Journal of the Structural Division, ASCE **105**(ST5): (pp. 921-937).

Myers, R. H., R. C. Montgomery, et al. (2009). Response Surface Methodology: Process and product optimization using designed experiments, 3rd Edition, John Wiley& Sons, Inc., New Jersey, USA, (704pp).

Nie, J. and B. R. Ellingwood (2005). "FE-based structural reliability assessment using efficient directional simulation." ASCE Journal of Engineering Mechanics **131**(3): (pp. 259-267).

Nowak, A. S. and K. R. Collins (2000). Reliability of Structures, McGraw-Hill Higher Education, New York.

Nowak, A. S. and M. M. Szerszen (2000). "Structural reliability as applied to highway bridges." Progress in Structural Engineering and Materials, **2**(2): 218-224.

Nowak, A. S., A. S. Yamani, et al. (1994). "Probabilistic models for resistance of concrete bridge girders." ACI Strucural Journal **91**(3): 269–276.

Opensource.org. "The Open Source Definition." Retrieved Sept.15, 2010, from http://www.opensource.org/osd.html.

Orisamolu, I. R. (1992). Technical Considerations in the Development and Application of Stochastic Finite Element Methodologies for Structural Reliability Analysis.

Orisamolu, I. R. and Q. Liu (1993). Stochastic Finite Element Methods for Structural Reliability Analysis, Contractor Document (Martec Limited), Defence Research Establishment Atlantic**:** (174pp.).

Orisamolu, I. R., Q. Liu, et al. (1992). Probabilistic Reliability Analysis Using General Purpose Commercial Computer Programs.

Page, C. L. (2007). Corrosion and protection of reinforcing steel in concrete. Durability of Concrete and Cement Composites. C. L. Page and M. M. Page. England, Woodhead Publishing Limited and CRC Press LLC**:** 136-186.

Palsson, R. and M. S. Mirza (2002). "Mechanical response of corroded steel reinforcement of abandoned concrete bridge." ACI Structural Journal **99**(2): 157-162.

Pendola, M., Mohamed, A., Lemaire, M., and Hornet, P. (2000). "Combination of finite element and reliability methods in nonlinear fracture mechanics." Reliability Engineering & System Safety **70**(1): 15-27.

Poirion, F. (1993). "Numerical Simulation of Homogeneous Non-Gaussian Random Vector Fields." Journal of Sound and Vibration **160**(1): (pp. 25-42).

Popovics, S. (1973). "A Numerical Approach to the Complete Stress-Strain Curve of Concrete." Cement and Concrete Research **3**(5): pp. 583-599.

Rackwitz, R. and B. Fiessler (1978). "Structural Reliability under Combined Load Sequences." Computers & Structures **9**: 489-494.

RCP. (2010). "STRUREL." RCP Consult GmbH, Reliability Consulting Programs, Munich, Germany Retrieved August, 2010, from http://www.strurel.de. .

Reh, S., F. Bohm, et al. (1991). First Order Reliability Analysis Using Stochastic Finite Element Methods. First International Conference on Computational Stochastic Mechanics, Corfu, Greece, Computational Mechanics Publications, Southampton, U.K.

Rodriguez, J., L. M. Ortega, et al. (1997). "Load carrying capacity of concrete structures with corroded reinforcement." Construction and Building Materials **11**(4): 239-248.

Rodriguez, J., L. M. Ortega, et al. (1996). Corrosion of reinforcement and service life of concrete structures. Durability of Building Materials and Components 7. C. Sjöström. London, UK. **1:** 117-126.

Rosenblatt, M. (1952). "Remarks on a multivariate transform." Annals. Math. Statist. **23**: (pp. 470–472).

Rostam, S. (2003). "Reinforced concrete structures – shall concrete remain the dominating means of corrosion prevention?" Materials and Corrosion **54**(6): 369 - 378.

Schuëller, G. I. (1997). "A State-of-the-Art Report on Computational Stochastic Mechanics." Journal of Probabilistic Engineering Mechanics **12**(4): 197–321.

Schuëller, G. I. (2007). "On the treatment of uncertainties in structural mechanics and analysis." Computers and Structures **85**(5-6): 235–243.

Schueller, G. I. and R. Stix (1987). "A critical appraisal of methods to determine failure probabilities." Structural Safety **4**: (pp. 293–309).

Shinozuka, M. and G. Deodatis (1991). "Simulation of Stochastic Processes by Spectral Representation." Applied Mechanics Reviews **44**(4): 191-203.

Shinozuka, M. and F. Yamazaki (1988). Stochastic Finite Element Analysis: An Introduction, Elsevier Applied Science, New York.

Snee, R. D. (1973). "Some aspects of nonorthogonal data analysis: PartI, developing prediction equations." Journal of Quality Tech. **5**: 67-79.

Spanos, P. D. and R. Ghanem (1989). "Stochastic Finite Element Expansion for Random Media." ASCE Journal of Engineering Mechanics **115**(5): 1035-1053.

SRI (1991). NESUSS, Southwest Research Institute, San Antonio, Texas.

Stewart, M. G. (2004). "Spatial variability of pitting corrosion and its influence on structural fragility and reliability of RC beams in flexure." Structural Safety **26**: 453-470.

Stewart, M. G. (2009). "Mechanical Behaviour of Pitting Corrosion of Flexural and Shear Reinforcement and its Effect on Structural Reliability of Corroding RC Beams." Structural Safety **31**(1): (pp. 19-30).

Stewart, M. G. and A. Al-Harthy (2008). "Pitting corrosion and structural reliability of corroding RC structures: Experimental data and probabilistic analysis." Reliability Engineering & System Safety **93**(3): 373-382.

Stewart, M. G. and D. V. Rosowsky (1998). "Time-dependent reliability of deteriorating reinforced concrete bridge decks." Structural Safety **20**(1): 91-109.

Stewart, M. G. and D. V. Rosowsky (1998a). "Time-dependent reliability of deteriorating Reinforced Concrete Bridge Decks." Structural Safety **20**(1): 91-109.

Stewart, M. G. and D. V. Rosowsky (1998b). "Structural safety and serviceability of concrete bridges." Journal of Infrastructure Systems **4**(4): 146-155.

Stewart, M. G. and Q. Suo (2008). Effect of spatially variable corrosion damage on strength and time-dependent reliability of RC beams. First International Symposium on Life-Cycle Civil Engineering (IALCCE'08). Lake Como, Italy 10-14 June, 2008, Taylor & Francis Group**:** p. 239-245.

Stewart, M. G. and Q. Suo (2009). "Extent of spatially variable corrosion damage as an indicator of strength and time-dependent reliability of RC beams." Engineering Structures **31**(1): 198-207.

Streletzki, N. S. (1947). Statistical Basis for Evaluation of the Structural Safety Factor. Stroizdat, Moscow.

Sudret, B. and A. Der Kiureghian (2002). "Comparison of Finite Element Reliability Methods." Probabilistic Engineering Mechanics **17**: 337-348.

Sudret, B. and A. D. Kiureghian (2000). Stochastic finite element methods and reliability: A state-of-the-art report, University of California Berkeley.**:** 189.

Takada, T. (1991). Galerkin Method to Analyze Systems with Stochastic Flexural Rigidity. Computational Stochastic Mechanics, Proceedings of the First International Conference, Computational Mechanics Publications and Elsevier Science Publishers**:** 511-522.

Tastani, S. P. and S. J. Pantazopoulou (2007). "Behavior of corroded bar anchorages." ACI Structural Journal **104**(6): 756-766.

Taylor, R. L. (2010). "FEAP." Department of Civil and Environmental Engineering, University of California, Berkeley, CA Retrieved August, 2010, from http://www.ce.berkeley.edu/rlt/feap.

Tepfers, R. (1979). "Cracking of concrete cover along anchored deformed reinforcing bars." Magazine of Concrete Research **31**(106): 3-12.

Tuutti, K. (1982). Corrosion of Steel in Concrete. Stockholm, Swedish Cement and Concrete Research Institute**:** 469.

Tvedt, L. (1990). "Distribution of quadratic forms in normal space application to structural reliability." ASCE Journal of Engineering Mechanics **116**(6): (pp. 1183–1197).

UBC. (2010). "InRisk, Rt." Retrieved September 1, 2010, from http://www.inrisk.ubc.ca/software.htm.

University of California, B. (2000). "OpenSees - Open System for Earthquake Engineering Simulation." Retrieved 2006 - Present, from http://opensees.berkeley.edu/.

Val, D. V. (2007). "Deterioration of strength of RC beams due corrosion and its influence on beam reliability." ASCE Journal of Structural Engineering **133**(9): (pp. 1297–1306).

Val, D. V., M. G. Stewart, et al. (1998). "Effect of reinforcement corrosion on reliability of highway bridges." Engineering Structures **20**(11): 1010-1019.

Val, D. V. and P. A. Trapper (2008). "Probabilistic evaluation of initiation time of chloride-induced corrosion." Reliability Engineering & System Safety **93**(3): 364-372.

Vanmarcke, E. H. (1983). Random Fields: Analysis and Synthesis, MIT Press, Cambridge, Massachusetts.

Vanmarcke, E. H. and M. Grigoriu (1983). "Stochastic Finite Element Analysis of Simple Beams." ASCE Journal of Engineering Mechanics **109**(5): 1203-1214.

Vanmarcke, E. H., Schinozuka, M., Nakagiri, S., Schuëller, G.I., and Grigoriu, M. (1986). "Random Fields and Stochastic Finite Elements." Structural Safety **3**: 143-166.

Vecchio, F. J. (2000). "Disturbed stress field model for reinforced concrete: formulation." ASCE Journal of Structural Engineering **126**(9): 1070-1077.

Vecchio, F. J. (2002). VecTor2, Nonlinear finite element analysis program of reinforced concrete, University of Toronto.

Vecchio, F. J. and M. P. Collins (1986). "The modified compression field theory for reinforced concrete elements subject to shear." ACI Journal **83**(2): 219-231.

Vecchio, F. J. and W. Shim (2004). "Experimental and analytical re-examination of classic concrete beam tests." ASCE Journal of Structural Engineering **130**(3): (pp. 460-469).

Vrouwenvelder, A. and P. Schiessl (1999). Durability aspects of probabilistic ultimate limit state design, HERON. **44:** (pp. 19-30).

Vu, K. A. T. and M. G. Stewart (2000). "Structural reliability of concrete bridges including improved chloride-induced corrosion models." Structural Safety **22**(4): 313-333.

Wierzbicki, W. (1936). Safety of Structures as a Probabilistic Problem. (Technical Review) Przeglad Techniczny (in Polish), Warsaw, Poland.

Wong, P. S. and F. J. Vecchio (2002). VecTor2 & Formworks User's Manual**:** 232pp.

Woodward, R. and F. Williams (1988). Collapse of the Ynys-Gwas bridge, West Glamorgan. Proc., Institution of Civil Engineers. London. **84:** 635–669.

Yamazaki, F., and Shinozuka, M. (1990). "Simulation of Stochastic Fields by Statistical Preconditioning." ASCE Journal of Engineering Mechanics **116**(2): 268-287.

Yamazaki, F. and M. Shinozuka (1988). "Digital Generation of Non-Gaussian Stochastic Fields." ASCE Journal of Engineering Mechanics **114**(7): 1183-1197.

Yoon, S., K. Wang, et al. (2000). "Interaction between loading, corrosion, and serviceability of reinforced concrete." ACI Materials Journal **97**(6): 637-644.

Zhang, J., and Ellingwood, B. (1996). "SFEM for Reliability of Structures with Material Nonlinearities." ASCE Journal of Structural Engineering **122**(6): 701-704.

Zhang, J. and B. Ellingwood (1994). "Orthogonal series expansion of random fields in reliability analysis." ASCE Journal of Engineering Mechanics **120**(12): 2660-2677.

Zhang, Y. and A. Der Kiureghian (1997). Finite Element Reliability Methods for Inelastic Structures, University of California, Berkeley.

Zienkiewicz, O. C. and R. L. Taylor (2000). The Finite Element Method, Butterworth-Heinemann.

Appendix A – Fundamental Concepts of Reliability Theory

A.1 Introduction

A means of defining performance criteria is essential when applying methods of reliability analysis in performance-based engineering. This is accomplished by so called performance functions. In structural reliability analysis the term **failure** is used to denote an event which does not meet a performance criterion. While the methodology to compute estimates of the probability of failure is at a mature stage for a range of performance functions, it may not be an obvious task as to how to define what constitutes failure (Haukaas and Kiureghian 2004).

A performance function can be defined in terms of engineering demand parameters, damage measures, or decision variables. Estimation of the probability of the defined failure event poses a component reliability problem. However, failure according to one performance criterion may not constitute failure of an entire structural system. It is therefore of interest to define system reliability problems as sets of components and rules, as to which combinations of component failures constitute system failure.

Performance functions for structural components are commonly denoted by $g(\boldsymbol{X})$, where $\boldsymbol{X}$ is a vector of basic random variables, $\{X_1, X_2, \ldots X_n\}^T$. The vector of random variables may consist of individual random variables for simple mechanical or structural elements, where the spatial variation of the variable is assumed constant, or it may contain discretized random fields for more complex continuum structures. The dependence on $\boldsymbol{X}$ can be implicit and through structural response quantities. However, $g(\boldsymbol{X})$ must be a continuous and differentiable function of $\boldsymbol{X}$, at least in the realizable domain of $\boldsymbol{X}$. The numerical value of the performance function distinguishes the failure state from the safe state (Figure A-1):

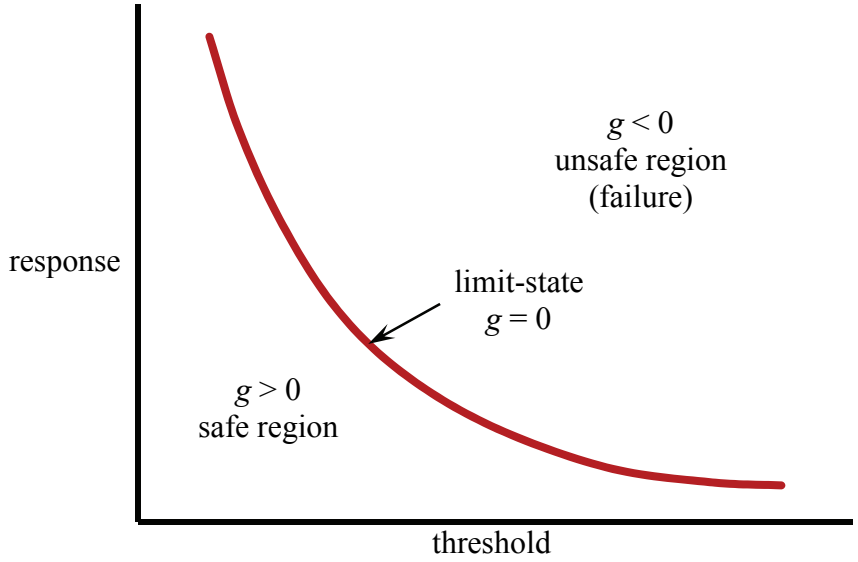

Figure A-1: Concept of the limit-state

When the uncertain response quantity exceeds the specified threshold, the performance function takes on a negative value and failure is implied. Note that both the specified threshold and the computed response can be functions of the random variables $\boldsymbol{X}$.

The primary concern in structural reliability analysis is to estimate probabilities of failure to achieve predefined performance. In the simplest case of one performance function, the component reliability problem is formulated as

$$p_f = \int_{g(\boldsymbol{X})\le 0} f(\boldsymbol{X})\, dX \tag{A.1}$$

where p_f is the probability of failure, $g(\boldsymbol{X})$ is the performance function and $f(\boldsymbol{X})$ is the joint probability density function (PDF) of $\boldsymbol{X}$. Note that the integration is over the set of random variables $\boldsymbol{X}$, which in finite element reliability analysis can be very large. Closed-form solutions of Eq. (A.1) are unavailable except for a few special cases. For this reason, a number of methods have been developed for the purpose of solving the integral approximately. Broadly, these include first- and second-order reliability methods (FORM/SORM), sampling techniques, response surface methods, and numerical integration schemes. In the context of SFEA the various methods of solving the convolution integral were introduced in section 39 and detailed in Appendix C.

With respect to design standards, performance functions are related limit states. Thus, a limit state is defined as the boundary between desired and undesired performance of a structure, as illustrated in Figure A-1. This boundary is generally represented mathematically by a limit state function, also referred to as a performance function. Once the limit state functions are formulated, and the relevant system uncertainties characterised through appropriate probability density functions, it is possible to compute the probability of failure for the given problem. Several methods are available to determine the failure probabilities.

A.2 Limit States

In order to compute the failure probability, it is necessary to formulate a limit state function $g()$ as a function of the basic random variables, represented by the vector $\boldsymbol{X}$, as follows:

$$g(\boldsymbol{X}) = g(X_1, X_2, \ldots, X_n) \tag{A.2}$$

The limit state function relates the basic random variables to structural response. The structural response may be nominally described by two variables, one related to the demand, or load effects on the structure $\boldsymbol{S}$, and the other related to the capacity, or resistance of the structure, $\boldsymbol{R}$. Both $\boldsymbol{R}$ and $\boldsymbol{S}$ are in turn functions of the basic random variables related to resistance and loads, respectively. Using this notation, Eq. (A.2) may be expressed as:

$$g(\boldsymbol{R}, \boldsymbol{S}) = \boldsymbol{R} - \boldsymbol{S} = R\left(x_1^r, x_2^r, \ldots, x_n^r\right) - S\left(x_1^s, x_2^s, \ldots, x_m^s\right) \tag{A.3}$$

Defining failure as the state when the load effects exceed a structure's capacity ($\boldsymbol{S} > \boldsymbol{R}$) implies that design requirements have not been satisfied and the corresponding point located is in the failure region. Conversely, when the demand is less than the capacity ($\boldsymbol{S} \leq \boldsymbol{R}$), design requirements have been satisfied and this condition corresponds to a point located in the safe region of the variable space. As mentioned earlier, the limit state can be seen as the boundary between the safe and failure regions ($\boldsymbol{S} = \boldsymbol{R}$) in the design space. Thus, returning to the generalized notation in Eq.(A.3), the limit state function is a function of the random parameters such that:

$$
\begin{aligned}
g(X_1, X_2, \ldots, X_n) > 0 &\quad : \text{ safety} \\
g(X_1, X_2, \ldots, X_n) = 0 &\quad : \text{ limit state} \\
g(X_1, X_2, \ldots, X_n) < 0 &\quad : \text{ failure}
\end{aligned}
\tag{A.4}
$$

Traditionally, in engineering practice, structural reliability analysis considers the following three types of limit states:

1. Ultimate Limit States (ULS) – related to the loss of load-carrying capacity. These modes of failure include: exceeding the moment or shear capacity, crushing of concrete in compression, loss of overall stability, etc.
2. Serviceability Limit State (SLS) – related to user's comfort, gradual deterioration, or maintenance costs. They may or may not be related to structural integrity and generally include: excess deflection, excess vibration, permanent deformation, and cracking. Although cracking in itself does not necessarily affect the structural performance of concrete structures, it can lead to steel corrosion, spalling of concrete cover, and enhanced chloride penetration.
3. Fatigue Limit States (FLS) – related to the accumulation of damage and eventual loss of strength or failure under repeated loads.

A.3 Probability of Failure

Of special interest in reliability assessment is the failure probability, p_f. Having defined the concept of limit state functions, it is now possible to formulate the means of determining failure probabilities. The vectors $\boldsymbol{R}$ and $\boldsymbol{S}$ in the limit state function, Eq.(A.3), respectively represent various resistance and load variables, which may be random or deterministic.

It is difficult to satisfy the basic design requirements in the presence of uncertainty. Figure A-2 shows the simple case for the two single random variables R and S, their randomness described by their respective means, μ_S and μ_R; standard deviations, σ_S and σ_R; and corresponding probability density functions (PDFs), $f_S(s)$ and $f_R(r)$.

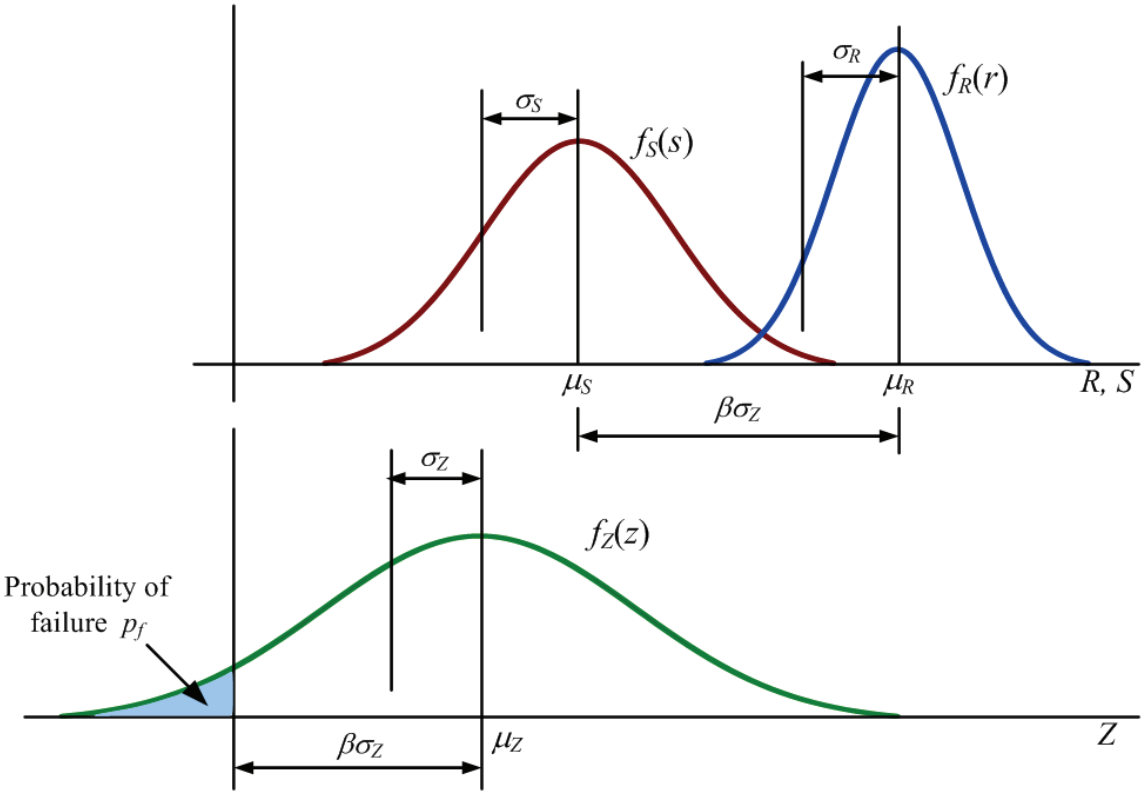

Figure A-2: Probabilistic performance concept.

In the load and resistance factor design (LRDF) concept, used in most current concrete and steel design standards, partial safety factors are applied to both the resistance and the loads. Referring to Figure A-2, where the uncertainties in the load and resistance variables are expressed in the form of the probability density functions (PDF), the probability of failure is composed of all possible combinations of $S = s_i$ and $R < q_i$, which can be summarized as:

$$p_f = \sum P\left[\left(S = s_i\right) \cap \left(R < r_i\right)\right] = \sum P\left(R < S \middle| S = s_i\right) P\left(S = s_i\right) \tag{A.5}$$

For continuous random variables, Eq. (A.5) is rewritten as:

$$p_f = \int_{-\infty}^{+\infty} F_R(s_i) f_S(s_i) ds \tag{A.6}$$

where $F_R(s)$ is the cumulative distribution function (CDF) of R evaluated at s. The failure domain is represented by the region of overlap between the two curves, shown as the shaded region in Figure A-2. This area of overlap depends on three factors (Haldar et al., 2000):

1. The relative positions of the two curves: As the distance between the two curves increases, reducing the overlap area, the probability of failure decreases. The positions of the curves may be represented by the means (μ_R and μ_S) of the two variables.
2. The dispersion of the two curves: If the two curves are narrow, then the area of the overlap, and hence the probability of failure will also be lower. The dispersion may be characterized by the standard deviations (σ_R and σ_S) of the two variables.
3. The shapes of the two curves: The shapes are represented by the probability density functions $f_R(r)$ and $f_S(s)$.

The objective of safe design in deterministic design procedures is achieved by selecting the design variables in such a way that the area of overlap between the two curves is minimized, so that the underlying risk is not compromised within the constraints of economy (Frangopol and Maute 2003).

Although evaluation of the probability of failure given by Eq. (A.6) appears relatively straight forward, it is actually difficult to evaluate the integral in practice. This becomes more apparent when rewriting Eq. (A.6) according to the general definition of limit state function, given by Eq. (A.1), as:

$$p_f = \int \ldots \int_{g(\boldsymbol{X}) < 0} f_{\boldsymbol{X}}(X_1, X_2, \ldots, X_n)\, dX_1\, dX_2 \ldots dX_n \tag{A.7}$$

where $f_{\boldsymbol{X}}(X_1, X_2, \ldots, X_n)$ is the joint probability density function (JPDF) for the basic random variables and the integration is performed over the failure region, that is, $g(\boldsymbol{X}) < 0$. Equation (A.7) is the fundamental equation of reliability analysis.

The difficulty in using Eq. (A.7) in engineering practice is quite clear. Specifically, the joint probability density function is rarely available in an analytical form. Further, the dimension of the design space is usually quite large, to the extent that the requisite integration can seldom be carried out either analytically or numerically (Schueller and Stix 1987). Also, actual realizations of $\boldsymbol{X}$ are often scarce and do not permit inference about their joint distribution beyond their joint second order moments (Ghanem and Spanos 1991).

Evaluation of the convolution integral given by Eq. (A.7) requires numerical integration techniques, the accuracy of which is often strongly inadequate (Nowak and Collins 2000). In practice, the probability of failure is calculated indirectly using the various reliability analysis procedures, including FORM and SORM, as well as simulation, discussed in section 0. In addition, the concept of a **reliability index** is used to quantify structural reliability.

A.4 Reliability Index

Given the computational and theoretical difficulties associated with evaluation of the probability of failure, it became desirable to introduce a standard measure for reliability analysis. Such a measure would be based on readily available second moment properties of the random variables involved and would reflect a measure of safety of a system. The reliability index was introduced as an attempt to meet these needs.

As stated by Ghanem and Spanos (2003): "the basic idea behind the reliability index concept is the fact that the less uncertainty there is concerning the limit state of a system, the safer the system is. In other words, the greater the mean of the limit state relative to its standard deviation, the less likely is the response to wander beyond this state". The reliability index was first defined by Freudenthal (1947; Freudenthal 1956) and subsequently extended by Freudenthal et al. (1966), Cornell (1969), and Melchers (1987) as follows:

$$\beta = \frac{\langle M \rangle}{\sigma_M} \tag{A.8}$$

where M denotes the safety margin, which is the difference between the resistance and the load effects; $\langle M \rangle$ denotes its expected value, and σ_M its standard deviation. Representing the difference given by M with $Z = R - S$, leads to $\langle M \rangle = \mu_Z$ and $\sigma_M = \sigma_Z$. Therefore, the reliability index may be rewritten as:

$$\beta = \frac{\mu_Z}{\sigma_Z} = \frac{\mu_R - \mu_S}{\sqrt{\sigma_R^2 + \sigma_S^2}} \tag{A.9}$$

If the random variables $\boldsymbol{X}$ are Gaussian and the limit state function given by Eq. (A.4) equation reference goes hereis linear in its arguments, the safety margin will have a Gaussian distribution. Also, β as defined by Eq. (A.9) is then equal to the distance from the origin to the hyperplane representing the limit state.

For nonlinear limit states, the standard deviation of the safety margin is related to higher order moments of the system random variables, which often are not known. In order to use β, as given by Eq. (A.9), the limit state surface is usually linearized using the first term in a Taylor series about some point in the design space. In this context, it is well known that the mean value μ_Z does not represent the best linearization point (Ghanem and Spanos 2003). Furthermore, if a function $g(\boldsymbol{X})$ satisfies Eq. (A.4), so does any function that is a power of $g(\boldsymbol{X})$, as well as any function that shares the same zeros with $g(\boldsymbol{X})$. This is the well-known lack of invariance problem (Haldar and Mahadevan 2000a).

The invariance issue was resolved by Hasofer and Lind (1974) by introducing a new reliability index defined by:

$$\beta_{HL} \equiv \min_{x \in g(\boldsymbol{X})} \sqrt{\left(x - \langle \boldsymbol{X} \rangle\right)^T C_X^{-1} \left(x - \langle \boldsymbol{X} \rangle\right)} \tag{A.10}$$

where C_X is the covariance matrix of the design variables X_i, and β_{HL} is known as the Hasofer-Lind reliability index. Given a set X_i, β_{HL} is uniquely determined as the shortest distance to the limit state surface. Thus, it is seen that the optimal point for the linearization of the limit state function is the point on that surface that is closest to the mean value after the design variables have been transformed to a set of uncorrelated variables.

A deficiency of the Hasofer-Lind index is a lack of comparativeness associated with the fact that any surface that is tangent to the failure surface at the design point has the same β_{HL}. (Haldar and Mahadevan 2000a). Transforming the design variables to a new set having the Gaussian distribution using the Rosenblatt transformation (1952) resolves this issue. When the failure surface is a hyperplane given by Eq. (A.2), the Hasofer-Lind index coincides with the previously defined index given by Eq. (A.9). The design point obtained in this way can

be shown to be the point of maximum failure likelihood when the design variables are uncorrelated and Gaussian (Shinozuka and Yamazaki 1988).

Given the reliability index, for Gaussian variables, the failure probability may be approximated by the expression

$$P_f \approx \Phi\left(-\beta_{HL}\right) = 1 - \Phi\left(\beta_{HL}\right) \tag{A.11}$$

where Φ is the normal probability function. Equation (A.11) is exact for linear limit states and becomes approximate for nonlinear limit states. Figure A-3 illustrates graphically the relationship between probability of failure and the reliability index.

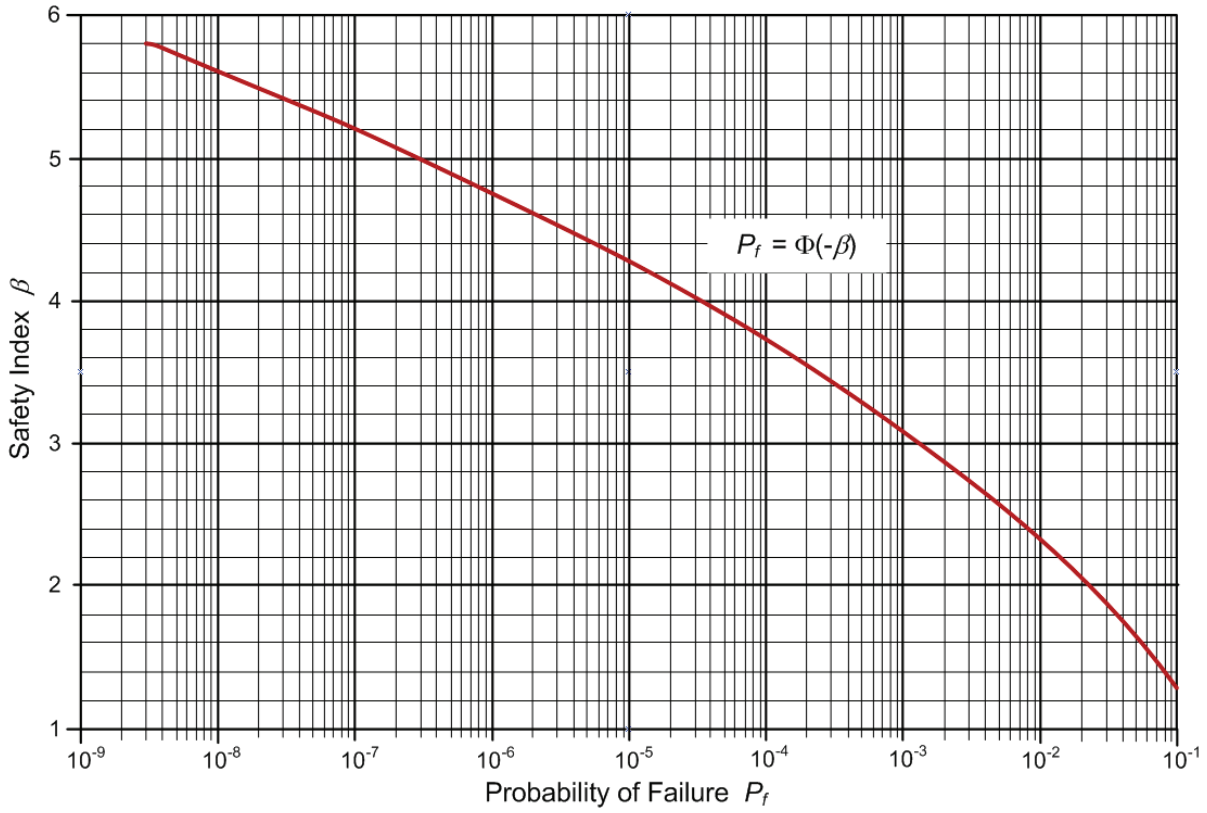

Figure A-3: Relationship between reliability index and probability of failure

A.5 Methods of Reliability Analysis

The various methodologies for stochastic finite element analysis were introduced in Chapter 3 and detailed in Appendix C. Many of the SFEA methods utilize one or more well established reliability analysis techniques, such as the first-order reliability method (FORM). These techniques are briefly discussed in the following sections.

A.5.1. First-Order Second-Moment Method (FOSM) and Advanced FOSM (AFOSM)

The FOSM, also referred to as the *mean value first-order second-moment* (MVFOSM) method in the literature, derives its name from the fact that it is based on a first-order Taylor series approximation of the performance function linearized at the mean values of the random variables, and because it uses only second-moment statistics (means and covariances) of the random variables. Information about the type of distribution is not used in FOSM. The original formulation by Cornell (1969) uses the simple two-variable approach of the previous sections, in which $g(\boldsymbol{X}) = Z = R - S$.

Assuming that R and S are statistically independent normally distributed random variables, the value Z is also a normal random variable. Using the definition of reliability index in Eq.(A.9), the probability of failure in terms of the safety index is obtained by:

$$p_f = 1 - \Phi(\beta) \tag{A.12}$$

Of course, this formulation was generalized for the case of many random variables, $Z = g(\mathbf{X}) = g(X_1, X_2, \ldots, X_n)$. This approach was used to derive earlier design codes. However, as explained in the previous section (A.4), the exact probability of failure can only be obtained in a few cases (i.e. for normally distributed, uncorrelated random variables, and linear limit state functions). Furthermore, this formulation suffers from the invariance problem described earlier. As a result it is rarely used in current practice; this problem was resolved by AFOSM which is instead used in practice.

AFOSM is simply the extension of FOSM, introduced by Hasofer and Lind (1974), utilizing the improvements to the reliability index as introduced in section A.4. The method eliminates the invariance problem, and it uses information on the type of distribution, provided that the

random variables are transformed from the original distribution to an equivalent normal distribution and correlated random variables are converted to uncorrelated random variables. The AFOSM method was used to derive the partial safety factors in some LFRD design codes. Furthermore, the AFOSM served as the basis for development of the FORM algorithm derived by Rackwitz and Fiessler (1978), described next.

A.5.2. First-Order Reliability Method (FORM)

As with AFOSM, reliability analysis using FORM is also carried out in the non-correlated standard Gaussian space, after applying the Rosenblatt transformation. The problem is considered as an optimization problem with one constraint and may be written in the following form:

$$\text{Minimize } \beta = \|\boldsymbol{Y}\|, \text{ subject to } g(\boldsymbol{Y}) = 0 \tag{A.13}$$

where β is the reliability index, $\boldsymbol{Y}$ is the vector of variables, and $g(\boldsymbol{Y})$ is the limit state function transformed to the non-correlated standard Gaussian space. The index β can be considered as the smallest distance from the origin of the reference system in the variable space to the limit state function. The intersection between vector $\boldsymbol{Y}$ and the limit state surface $g(\boldsymbol{Y}) = 0$ is defined as the design point, where $\|\boldsymbol{Y}\|$ has its minimum value. The coordinates of the design point, also referred to as the most probable failure point (MPP), will be contained in a vector denoted by $\boldsymbol{Y}^*$. As before, the failure probability p_f is approximately related to the reliability index through Eq. (A.12).

FORM is used to solve the optimization problem given by Eq. (A.13) by a sequence of approximations to find the coordinates of the design point in the non-correlated Gaussian space. The main advantage of this method is that it does not require solution of the limit state equation at each iteration step. Instead it uses a Newton-Raphson type recursive formula to find the design point (Haldar and Mahadevan 2000a). This is particularly useful in case of complicated nonlinear performance functions, which in most practical problems are not available in closed form (implicit limit state functions).

Basically, in the FORM approach the performance function is linearized at each iteration point. However, instead of solving the limit state equation explicitly for the performance index β, it uses the derivatives to find the next iteration point. For a non-linear performance function the k^{th} iteration point, $\boldsymbol{x}_k^*$ is given by:

$$\boldsymbol{x}_{k+1}^* = \frac{1}{\left|\nabla g\left(\boldsymbol{x}_k^*\right)\right|^2}\left[\nabla g\left(\boldsymbol{x}_k^*\right)^{\mathrm{t}}\, \boldsymbol{x}_k^* - g(\boldsymbol{x}_k^*)\right]\nabla g\left(\boldsymbol{x}_k^*\right) \tag{A.14}$$

Here, $\nabla g(\boldsymbol{x}_k^*)$ is the gradient vector of the performance function at the k^{th} iteration point. For each iteration point a new value of the performance index is also calculated. The algorithm is repeated until convergence, satisfying some criteria, for example:

$$\begin{aligned} &1.\ \text{If } \left|\boldsymbol{x}_k^* - \boldsymbol{x}_{k-1}^*\right| \le 0.001,\ \text{stop.} \\ &2.\ \text{If } \left|g\left(\boldsymbol{x}_k^*\right)\right| \le 0.001,\ \text{stop.} \end{aligned} \tag{A.15}$$

A.5.3. Second-Order Reliability Method (SORM)

The computations required for reliability analysis of problems with linear limit state equations are relatively simple. However, the limit state might be nonlinear either due to the nonlinear relationship between the random variables in the limit state equation. A linear limit state in the original space becomes nonlinear when transformed to the standard normal space (which is where the search for the minimum distance point is conducted) if any of the variables is non-normal. Also, the transformation from correlated to uncorrelated variables might induce nonlinearity. If the joint probability density function of the random variables decays rapidly as one moves away from the minimum distance point, then the first-order estimate of failure probability is quite accurate. If the decay of the joint PDF is slow and the limit state is highly nonlinear, then it is advisable to implement a higher-order approximation for the failure probability computation.

Considering the two limit states shown in Figure A-4, one linear and one nonlinear, both have the same minimum distance point but the failure domains are different for the two cases. FORM analysis will result in the same reliability estimate for both cases, although it is

apparent that the failure probability of the nonlinear limit state should be less than that of the linear limit state due to the difference in the failure domains. This due to the curvature of the nonlinear limit state being ignored in the FORM approach, which uses only a first-order approximation at the minimum distance point. Thus, the curvature of the limit state around the minimum distance point determines the accuracy of the first-order approximation in FORM.

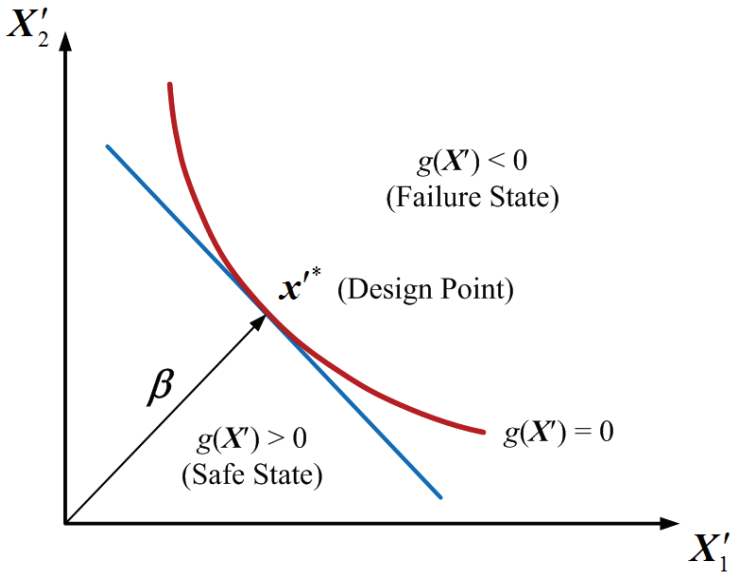

Figure A-4: Linear and nonlinear limit states

The curvature of any equation is related to the second-order derivatives with respect to the basic variables. Thus, the second-order reliability method (SORM) improves the FORM result by including additional information about the curvature of the limit state. The second-order Taylor series approximation to a general nonlinear function $g(X_1, X_2, \ldots, X_n)$ at the value $\left(x_1^*, x_2^*, \ldots, x_n^*\right)$ is

$$g(X_1, X_2, \ldots, X_n) = g\left(x_1^*, x_2^*, \ldots, x_n^*\right) + \sum_{i=1}^{n}\left(x_i - x_i^*\right)\frac{\partial g}{\partial X_i} + \frac{1}{2}\sum_{i=1}^{n}\sum_{i=1}^{n}\left(x_i - x_i^*\right)\left(x_j - x_j^*\right)\frac{\partial^2 g}{\partial X_i \partial X_j} + \ldots \tag{A.16}$$

where the derivatives are evaluated at the design point of X_i.

In the case of reliability analysis, the second-order approximation to $g(\boldsymbol{X})$ is constructed in the space of standard normal variables, at the minimum distance point. In the Taylor series approximation given in Eq. (A.16), FORM ignores the terms beyond the first-order term (involving first-order derivatives), and SORM ignores the terms beyond the second-order term (involving second-order derivatives).

The SORM approach was first explored by Fiessler et al. (1979) using various quadratic approximations. A simple closed-form solution for the probability computation using a second-order approximation, p_{f2} was given by Breitung (1984) using the theory of asymptotic approximations as

$$p_{f2} = \Phi(-\beta)\prod_{i=1}^{n-1}(1+\beta\kappa_i)^{-\frac{1}{2}} \tag{A.17}$$

where κ_i denotes the principal curvatures of the limit state at the minimum distance point, and β is the reliability index calculated using FORM. Breitung showed that this second-order probability estimate asymptotically approaches the first-order estimate as β approaches infinity, if $\beta\kappa_i$ remains constant.

Breitung's SORM method uses a parabolic approximation, that is, it does not use a general second-order approximation. It ignores the mixed terms and their derivatives in the Taylor series approximation in Eq. (A.16). Also, as mentioned earlier, it uses the theory of asymptotic approximation to derive the probability estimate. The asymptotic formula is accurate only for large values of β, which is the case for practical high-reliability problems. However, if the value of β is low, the SORM estimate could be inaccurate. Tvedt (1990) developed two alternative SORM formulations to address these problems. Tvedt's method uses a parabolic and a general second-order approximation to the limit state, and it does not use asymptotic approximations.

Appendix B – Random Variables and Fields

B.1 Representation of Uncertainties: Random Variables and Fields

B.1.1. General

The parameters of a classical finite element model are selected deterministically. In a stochastic finite element model the characterization of uncertainty in such parameters becomes an important task (Haukaas and Kiureghian 2004). In structural reliability problems which assume the basic structural parameters to be discrete, the parameters may be represented by single-valued random variables. This assumption is valid for quantities that are concentrated at discrete points in space, such as concentrated loads, stiffnesses of joints and supports, and in cases a material property that does not change along a rebar, for example the yield strength of steel. In this case each random variable would be described by an appropriate probability density function, the mean and the variance based on statistical procedures.

Throughout this thesis a single real random variable is denoted by X. For continuous random variables, the PDF of X is represented by $f_X(x)$, while the cumulative distribution function (CDF) is denoted by $F_X(x)$. The mean, variance, and n^{th} moment of X are:

$$\mu \equiv E[X] = \int_{-\infty}^{\infty} x f_X(x)\, dx \tag{B.1}$$

$$\sigma^2 = E\left[(X-\mu)^2\right] = \int_{-\infty}^{\infty} (x-\mu)^2 f_X(x)\, dx \tag{B.2}$$

$$E\left[X^n\right] = \int_{-\infty}^{\infty} x^n f_X(x)\, dx \tag{B.3}$$

where $E[\cdot]$ refers to the mathematical expectation. This one-dimensional definition can be expanded to multi-dimensional cases, as shown in Figure B-1a. Furthermore, the covariance of two random variables X and Y is:

$$\mathrm{Cov}\left[X,Y\right] = E\left[\left(X-\mu_X\right)\left(Y-\mu_Y\right)\right] \tag{B.4}$$

In the case of a joint PDF of these two variables, $f_{X,Y}(x, y)$, Eq. (B.4) can be rewritten as:

$$\mathrm{Cov}\left[X,Y\right] = \int_{-\infty}^{\infty}\int_{-\infty}^{\infty}\left(x-\mu_X\right)\left(y-\mu_Y\right) f_{X,Y}\left(x,y\right) dxdy \tag{B.5}$$

Most structural parameters are distributed in space, rather than being concentrated at a point. Examples include distributed loads, material properties (Young's modulus, ultimate strength of concrete, etc.), and geometric properties (width, thickness, etc.) that vary over the length of a beam, the area of a plate, and so forth. Consequently, such quantities should not be expressed by single random variables, but rather as random processes or random fields.

A random field is herein denoted by $\chi(\boldsymbol{x})$ representing a collection of random variables indexed by a continuous parameter $\boldsymbol{x}\in\Omega$, where Ω is an open set describing the system geometry. This implies that for a specific value of $\boldsymbol{x}$, say $\boldsymbol{x} = \boldsymbol{x}_o$, $\chi(\boldsymbol{x}_o)$ is a random variable. Furthermore, a random field can be *univariate* or *multivariate* depending on whether the quantity $\chi(\boldsymbol{x})$ attached to $\boldsymbol{x}$ is a random variable or a random vector. A *random vector* is simply a collection of random variables, denoted here by $\boldsymbol{X} = \{X_1, X_2, \ldots X_n\}^T$. A random field is Gaussian if any vector $\{\chi(\boldsymbol{x}_1), \ldots, \chi(\boldsymbol{x}_n)\ \}$ is Gaussian. A Gaussian field is completely defined by its mean $\mu(\boldsymbol{x})$, variance $\sigma^2(\boldsymbol{x})$, and autocorrelation coefficient $\rho(\boldsymbol{x}, \boldsymbol{x}')$ functions. Furthermore, it is homogeneous if the mean and variance are constant and ρ is only a function of their relative distance in space or time (i.e. $\boldsymbol{x}' - \boldsymbol{x}$).

A random field is a generalization of the concept of random process. Hence, in a random process, the joint probability density function also refers to a collection of random variables, or more precisely, a collection of PDFs, $X_1(x)$, $X_2(x)$, …, $X_n(x)$. Each function represents a sample (realization) of a deterministic function $\chi(\boldsymbol{x})$, where $\boldsymbol{x}$ is an independent variable (Haldar and Mahadevan 2000a). The variable $\boldsymbol{x}$ could for example denote time increments, or perhaps space coordinates along the length of a beam, while $\chi(\boldsymbol{x})$ could represent a material property such as compressive strength of concrete. Hence the ensemble of all realizations of $X_i(x)$ is a random process, while its variation at a particular cross-section is a random variable. Figure B-1b, shows an example of a one-dimensional temporal random process (i.e.

statistical variation along one dimension only). Thus, random fields may also be thought of as multi-dimensional, spatially fluctuating collection of random processes.

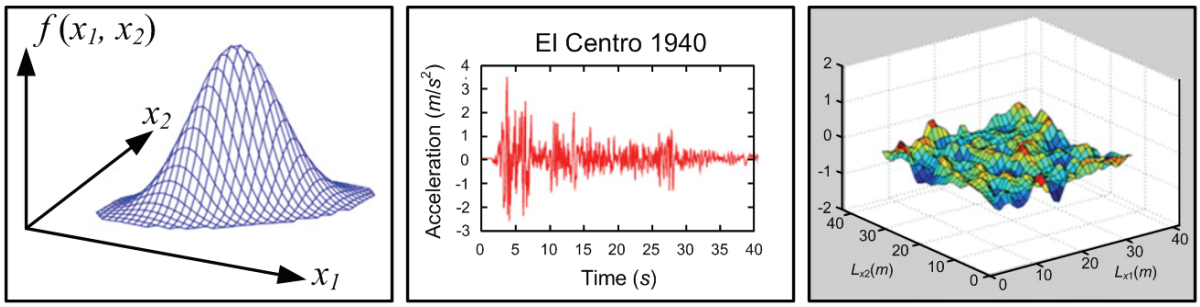

(a) Random Variable (b) Random Process (c) Random Field

Figure B-1: Quantification of Randomness (adapted from Schuëller, (2007))

Random fields are typically used to represent physical systems that have attributes which exhibit complex patterns of spatial and/or temporal variations. They provide the basis for predicting system response and performance. Examples of random fields include wind pressure fluctuations on area-like structures, or more relevant here, corrosion current densities along the length of steel reinforcement inside a reinforced concrete structure over time. A schematic sketch of a random field is given in Figure B-1c.

A detailed exposition of the theory of random fields and their engineering applications is provided in the monograph by Vanmarcke (1983).

B.1.2. RC Beams with Corroding Reinforcement

Ideally, to assess the effect of corrosion-induced mechanical damage on the structural integrity of RC Beams, a rational and systematic procedure that fully accounts for all the spatial and temporal variability inherent in corrosion rate and the resulting reduction of reinforcement area and ductility should be developed. Such a capability can be provided by adopting a random field based probabilistic modelling and analysis strategy ((Vanmarcke and Grigoriu 1983) and (Orisamolu, Liu et al. 1992)). The random field modelling approach is ideally suited for the representation of this complex spatial random phenomenon. Random fields offer an important mathematical framework through which a meaningful representation of parameters defined over a given domain can be modeled. In particular, a random field

approach can efficiently account for different severity and variability levels for corrosion intensity in the spatial domain via partitioning of a non-homogeneous random field representation into multiple homogeneous segments (each segment having a distinct correlation structure and set of statistical parameters). Furthermore, the correlation structure, which is derived during the random field characterization, can be used to measure the degree of similarity in behaviour (or properties) associated with any two points in the field. The main source of data to be used to characterize the corrosion random field is the existing experimental literature.

Support for the development of a spatial and temporal model of the corrosion process is motivated by an interest in adopting probabilistic methodologies for assessing the impact of corrosion damage on the structural integrity of RC beams. In the past corrosion damage assessment criteria were largely based on overly conservative empirical or semi-empirical methods. In contrast, adopting a probabilistic mechanics based approach for performing residual strength assessment on damaged (or degraded) RC beams provides a number of clear advantages over other more conventional techniques.

This section has dealt with random field description of uncertainties in structural system parameters. In general, implementation of spatial and temporal uncertainties in SFEA requires that random fields be discretized into sets of correlated random variables. Hence, random fields must first be transformed into vectors of individual random variables. Similar to the finite element discretization of a structure, issues of accuracy vs. computational effort are encountered in the case of random field discretization. Several techniques for the discretization of the random fields are summarized in the next section.

B.2 Discretization of Random Fields

For SFEA based structural reliability analysis, discretization is required to transform the spatial and/or temporal distribution of a random field to "point" values, i.e. random variables. A discretization procedure is the approximation of $\chi(\cdot)$ by $\hat{\chi}(\cdot)$ defined by means of a finite set of random variables $\boldsymbol{X}$:

$$\chi(x) \xrightarrow{\text{Discretization}} \hat{\chi}(x) = \mathfrak{F}[x, X] \tag{B.6}$$

The resulting reliability model then becomes of the (generally correlated) random variable type, for which the vast majority of existing computational algorithms for reliability analysis were designed for. In this case, the primary statistics of the random variables required for the reliability analysis are the mean values and the covariance matrix, which are obtained from the discretization process.

The available discretization techniques may be broadly classified into four groups:

1. **Spatial Average Discretization**;
2. **Point Discretization**: (i) mid-point and nodal-point methods, (ii) interpolation method, and (iii) optimal linear estimation (OLE);
3. **Series Expansion**: (i) Karhunen-Loève expansion (KL), (ii) orthogonal series expansion (OSE), and (iii) expansion optimal linear estimation (EOLE);
4. **Simulation**.

In the spatial averaging and point discretization methods, the domain of the random field is discretized into a mesh of random field elements (not necessarily coinciding with the finite element mesh) and the value for each element is described by a single random variable. In series expansion methods, the random field is exactly represented as a series involving random variables and deterministic spatial functions. The approximation is then obtained as a truncation of the series (Sudret and Kiureghian 2000). Hence, in essence, explicit discretization of the domain of the field is avoided, and instead series expansion methods are used to model the field as a series of shape functions with random coefficients. In the fourth group computer simulation is used to generate discretized random fields. Detailed reviews of several discretization methods can be found in Li and Der Kiureghian ((1992) and (1993)), Ditlevsen (1996), Matthies et al. (1997), Sudret and Der Kiureghian (2000), and most recently Schuëller (2007). The procedures pertaining to each of the groups of techniques listed above are summarized in the following sections.

B.2.1. The Spatial Average Method

The theory of local averages of homogeneous random scalar fields over rectangular domains is well established. A detailed discussion on the subject was provided by Vanmarcke in his textbook (1983) and forms the basis of the spatial averaging method.

The spatial averaging method (Vanmarcke and Grigoriu 1983) uses the local average of the field over a random field element to represent the random quantity for the element. Provided a mesh of the structure is available, it defines the approximated field in each element as a constant being computed as the average of the original field over the element. For the random field $\chi(\boldsymbol{x})$, the discretized value for an element i is given by a random variable:

$$X_i = \frac{1}{\Omega_e} \int_{\Omega_e} \chi(\boldsymbol{x}) d\Omega_e, \qquad \boldsymbol{x} \in \Omega_e \tag{B.7}$$

where Ω_e, is the domain of the element. Hence, the approximated random field $\hat{\chi}(\cdot)$ is entirely defined by a random vector $\boldsymbol{X} = \{X_1,\ldots,X_n\}^T$ where n is the number of elements. The mean μ and covariance matrix $\tilde{\boldsymbol{V}}_{XX}$ of $\boldsymbol{X}$ are obtained from the mean and covariance function of $\chi(\boldsymbol{x})$ over the domain Ω_e. For homogeneous fields and rectangular elements whose edges are parallel to the coordinate axes, expressions for the covariances of the discretized variables X_i in terms of the autocovariance function of $\chi(\boldsymbol{x})$ were derived by Vanmarcke (1983).

According to Der Kiureghian and Ke (1988), the spatial averaging method yields accurate results (even for coarse meshes) for Gaussian random fields. However, it has two major shortcomings in the context of application to SFEA. First, for a two-dimensional or three-dimensional continuum of arbitrary shape, it is not always possible to discretize the domain into rectangular elements. Several approximation schemes that have been suggested in the literature to deal with cases involving non-rectangular elements are known to introduce errors in the computed covariance matrix. These errors may lead to very inaccurate reliability results and are indeed capable of causing the reliability algorithms to breakdown in some cases (Liu and Der Kiureghian 1991). The second drawback of the spatial averaging method is

that the probability distribution of X_i is difficult or impossible to obtain, except when the underlying random field is Gaussian, in which case X_i is also Gaussian (Matthies, Brenner et al. 1997). Essentially, therefore, the use of this method is restricted to Gaussian fields.

B.2.2. Point Discretization Methods

The ***Midpoint*** and ***Nodal-point methods*** are two point discretization methods which represent the uncertainties of a random field by the values at some specific points. In the midpoint method (Der Kiureghian and Ke, (1988), Hisada and Nakagiri, (1985)), the element random variable is defined as the value of the random field at the centroid of the element. Hence, the randomness in a random field element *i* is represented by the random variable:

$$X_i = \boldsymbol{X}\left(x_i\right), \qquad \boldsymbol{x} \in \Omega_e \tag{B.8}$$

in which,

$$x_i = \frac{1}{N}\sum_{j=1}^{q} x_j^d \tag{B.9}$$

are the coordinates of the centroid, where q is the number of nodes of the random field element, and x_j^d are the nodal coordinates. The approximated random field $\hat{\boldsymbol{\chi}}(\cdot)$ is defined by the random vector $\boldsymbol{X} = \left\{X\left(\boldsymbol{x}_1\right),...,X\left(\boldsymbol{x}_q\right)\right\}^T$. The mean μ and covariance matrix $\tilde{\boldsymbol{V}}_{XX}$ are obtained from the mean, variance and autocorrelation coefficient functions of $\boldsymbol{\chi}(\cdot)$ evaluated at the element centroids.

The nodal-point method represents the random field in terms of the values at the nodal points of the finite element mesh. In this method, the randomness of the field at node *i* is also represented by Eq. (B.8), where

$$x_i = x_i^d \tag{B.10}$$

are the coordinates of node *i*.

In both the midpoint and the nodal-point methods, the mean, variance, and marginal distribution of X_i are the same as those of the process at point x_i. The correlation coefficient matrix of X_i is directly computed in terms of the auto-correlation coefficient function of the random field,

$$\rho_{X_i X_j} = \rho_{XX}\left(x_i x_j\right) \tag{B.11}$$

and the joint distribution for any set of X_i is given by the specified distribution of the random field.

As pointed out by (Der Kiureghian and Ke 1988), the midpoint method tends to over represent the variability of the field within each element, and it does not provide as accurate a result as the spatial averaging method for a coarse random field mesh. However, these point discretization methods have three advantages. First, no complicated computations are required for the covariance matrix and the method is easy to implement. Second, the correlation coefficient matrix obtained by Eq. (B.11) is always positive-definite, provided a valid autocorrelation function is specified. Hence, the numerical stability problem arising in the spatial averaging method does not exist in this case. Most importantly, the distribution information on the discretized variables X_i is retained and the method is not restricted to Gaussian random fields.

The Interpolation Method

The approach employed in the interpolation method, introduced by Liu et al. (1986b) represents the random field in terms of an interpolation rule involving a set of deterministic shape functions and the random nodal values of the field. Sudret and Kiureghian (2000), appropriately refers to this approach as the ***Shape Function Method***. The random field $\chi(\boldsymbol{x})$ is discretized into q random variables, X_i, $i = 1, ..., q$. The value at an arbitrary point is obtained by the following interpolation rule:

$$\hat{\chi}\left(\boldsymbol{x}\right) = \sum_{i=1}^{q} N_i\left(\boldsymbol{x}\right)\chi\left(\boldsymbol{x}_i\right), \qquad \boldsymbol{x} \in \Omega_e \tag{B.12}$$

where q is the number of element nodes and N_i are the polynomial shape functions associated with the element. Thus, the approximated field is obtained from $\boldsymbol{X} = \left\{\chi\left(\boldsymbol{x}_1\right),...,\chi\left(\boldsymbol{x}_q\right)\right\}^T$, where $\boldsymbol{x}_i$ is the set of nodal coordinates of the mesh. The shape functions N_i need not be the same as the finite element interpolation functions for the displacement field. Since the choice of the q nodal points and shape functions is arbitrary, the interpolation method constitutes a

class of random field discretization methods. In particular, it may be seen that if the nodes are chosen to be the centroids of the random field elements and the shape functions are assumed to be unity inside each element and zero elsewhere, the interpolation method becomes identical to the midpoint method described in the last section.

The mean and covariance of the approximated field $\hat{\boldsymbol{\chi}}(\cdot)$ are, respectively:

$$E\left[\hat{\boldsymbol{\chi}}(\boldsymbol{x})\right] = \sum_{i=1}^{q} N_i(\boldsymbol{x})\,\mu(\boldsymbol{x}_i) \tag{B.13}$$

$$\mathrm{Cov}\left[\hat{\boldsymbol{\chi}}(\boldsymbol{x}), \hat{\boldsymbol{\chi}}(\boldsymbol{x}')\right] = \sum_{i=1}^{q}\sum_{j=1}^{q} N_i(\boldsymbol{x})\,N_j(\boldsymbol{x}')\,\mathrm{Cov}\left[\boldsymbol{\chi}(\boldsymbol{x}_i), \boldsymbol{\chi}(\boldsymbol{x}_j)\right] \tag{B.14}$$

Each realization of $\hat{\boldsymbol{\chi}}(\cdot)$ is a continuous function, which is an advantage over the midpoint method.

Liu et al. (1986b) further suggested a method to reduce the number of random variables X_i. The random vector $\boldsymbol{X}$ is transformed into an uncorrelated random vector $\boldsymbol{C}$ by:

$$\boldsymbol{C} = \boldsymbol{\Phi}^T \boldsymbol{X} \tag{B.15}$$

such that the covariance matrix of $\boldsymbol{C}$, i.e. $\tilde{\boldsymbol{V}}_{CC}$, is diagonal. The orthogonalization matrix $\boldsymbol{\Phi}$ is obtained by solving the eigenproblem:

$$\tilde{\boldsymbol{V}}_{XX} \cdot \boldsymbol{\Phi} = \boldsymbol{\Phi} \cdot \boldsymbol{\Lambda} \tag{B.16}$$

where $\boldsymbol{\Lambda}$ is the eigenvalue matrix containing the variances of $\boldsymbol{C}$. Liu et al. (1986b) noted that a good approximation of the random field can be obtained by retaining only the C_i with large variables, thus reducing the number of random variables. It should be emphasized, however, that this reduction is only applicable to Gaussian random fields. This is because the distribution of $\boldsymbol{C}$ is generally unknown or difficult to obtain unless $\boldsymbol{X}(t)$ is Gaussian.

The Optimal Linear Estimation* (OLE) *Method

The OLE technique for random field discretization was introduced by Li and Der Kiureghian (1992). For a random field defined in a domain Ω_e, the approximated field $\hat{\chi}(\cdot)$ is defined by a linear function of the nodal values $\boldsymbol{X} = \{\chi(\boldsymbol{x}_1), ..., \chi(\boldsymbol{x}_q)\}^T$ in the form:

$$\hat{\chi}(\boldsymbol{x}) = a(\boldsymbol{x}) + \sum_{i=1}^{q} b_i(\boldsymbol{x}) X_i = a(\boldsymbol{x}) + b^T(\boldsymbol{x}) \cdot \boldsymbol{X} \tag{B.17}$$

where q denotes the number of nodal points in the domain. The functions $a(\boldsymbol{x})$ and $b_i(\boldsymbol{x})$ are determined optimally by minimizing the variance of the error $\mathrm{Var}\left[\chi(\boldsymbol{x}) - \hat{\chi}(\boldsymbol{x})\right]$. The minimization is subject to the condition that $\hat{\chi}(\boldsymbol{x})$ is an unbiased estimator in the mean, that is,

$$E\left[\chi(\boldsymbol{x}) - \hat{\chi}(\boldsymbol{x})\right] = 0 \tag{B.18}$$

which results in the representation:

$$\hat{\chi}(\boldsymbol{x}) = \mu(\boldsymbol{x}) + \tilde{\boldsymbol{V}}^T_{\chi(x)X} \tilde{\boldsymbol{V}}^{-1}_{XX} (\boldsymbol{X} - \mu_X) \tag{B.19}$$

Here, $\boldsymbol{X}$ denotes the vector of nodal values (random variables) and $\tilde{\boldsymbol{V}}^T_{\chi(x)X}$ denotes an $N \times 1$ vector containing the covariances of $\boldsymbol{X}$.

Li and Der Kiureghian (1993) carried out exhaustive comparisons of the above spatial average and point discretization methods in terms of discretization errors, through studies involving varying grid and element sizes. They concluded that OLE provides better results than the interpolation (shape function) method in all cases. This is not surprising given that OLE is basically an interpolation approach, where the shape functions are not prescribed polynomials, but rather the optimal functions to minimize the variance of the error. Other results comparing the approximated correlation structure to the initial one is also given by Li and Der Kiureghian (1993). In all cases, OLE leads to better accuracy in the discretization than the mid-point, nodal-point, spatial average and interpolation methods, and its efficiency can be further improved by using eigenvalue expansion. Furthermore, the OLE method can also be applied to problems involving non-Gaussian random fields by utilizing the Nataf

model of Liu and Der Kiureghian (1986). The Nataf model assumes that a transformed process $z(t)$ can always be found such that

$$\boldsymbol{X}(\boldsymbol{x}) = \Phi^{-1}\left[F\left(z(\boldsymbol{x})\right)\right] \tag{B.20}$$

where Φ is the standard normal cumulative distribution function. The key to the superior accuracy and efficiency of this method lies in the utilization of shape functions that take the correlation structure of the random field into account. Therefore, the OLE approach is currently the best point discretization technique for random fields in SFEA, where it is always desirable to represent a random field with as few random variables as possible.

B.2.3. Series Expansion Methods

The discretization methods presented up to now involved a finite number of random variables having a straightforward interpretation: point values or local averages of the original field (Sudret and Kiureghian 2000). They can be viewed as the expansions of each realization of the approximated random field. The methods presented in this section aim at expanding any realization of the original random field over a complete set of deterministic functions. The discretization results from truncating the obtained series after a finite number of terms. Several series expansion methods have been implemented over the past two decades in SFEA. These include the Karhunen-Loève expansion technique (KL), the orthogonal series expansion (OSE), and the expansion optimal linear estimation (EOLE) approach, as summarized below.

The Karhunen-Loève Expansion

The Karhunen-Loève method, also referred to as the kernel expansion method (Spanos and Ghanem 1989), employs orthogonal expansion to decompose a one-dimensional random field. The random field is expanded into the sum of its mean function and a single series:

$$\chi(\boldsymbol{x}) = \mu_X(\boldsymbol{x}) + \sum_{i=0}^{\infty} X_i \sqrt{\lambda_i}\varphi_i(\boldsymbol{x}) \tag{B.21}$$

where X_i are random coefficients independent of $\boldsymbol{x}$, and λ_i and $\varphi_i(\boldsymbol{x})$ are the eigenvalues and eigenfunctions of the covariance kernel, respectively. The latter are obtained as the solutions of the eigenvalue problem:

$$\int_{\Omega} \mathrm{Cov}\left(\boldsymbol{x}, \boldsymbol{x}'\right) \varphi_i\left(\boldsymbol{x}'\right) d\Omega_{x'} = \lambda_i \varphi_i\left(\boldsymbol{x}\right) \tag{B.22}$$

The kernel Cov(·,·) in Eq. (B.22), being an autocovariance function, is bounded, symmetric, and positive definite. Thus the set of $\{\varphi_i\}$ forms a complete orthogonal basis of Ω. The series in Eq. (B.21) are truncated after the first few dominant terms just as in the basis random variable method. Since this series has a zero mean and the eigenfunctions are orthogonal, the random coefficients X_i have properties similar to the basis random variables. Details of this method are extensively discussed and exemplified in the now classic monograph by Ghanem and Spanos (2003), first published in 1991.

One major obstacle of this method is the difficulty in solving the eigenvalue problem in Eq. (B.22) for arbitrary geometries and boundary conditions. Equation (B.22) can be solved analytically only for a few autocovariance functions and simple geometries of Ω. Detailed closed-form solutions for triangular and exponential covariance functions for one-dimensional homogeneous fields can be found in Spanos and Ghanem (1989). However, as noted by Liu and Der Kiureghian (1991), this is a particularly challenging task if the method is to be extended to two-dimensional or three-dimensional random fields. In those situations, and for complex geometries, the integral eigenvalue problem has to be solved numerically, adding significant computational overhead.

According to Sudret and Der Kiureghian (2000), it should be possible for general geometries, to embed Ω in a square-shape volume and use the latter to solve the eigenvalue problem in a closed form. However, to date, there is no evidence in the literature that this assertion has been explored. Last, it should be noted that both series expansion methods described above are strictly applicable only to Gaussian random fields by virtue of the central-limit theorem. Therefore, they are only appropriate for second-moment analysis or for reliability analysis when the random fields are truly Gaussian.

The Orthogonal series expansion **(OSE)**

Although the Karhunen-Loève expansion provides an efficient representation of random fields, it requires solution of an integral eigenvalue problem in Eq. (B.22) to determine the complete set of orthogonal functions $\{\varphi_i, i = 1, \ldots\}$. If an analytical solution is not available, as is usually the case, these functions have to be computed numerically. The orthogonal series expansion method, as proposed by Zhang and Ellingwood (1994), does not require solution of the eigenvalue problem given in Eq. (B.22), since it provides a complete set of orthogonal functions.

Defining $\{h_i(\boldsymbol{x})\}_{i=1}^{\infty}$ as a set of orthogonal functions (Zhang and Ellingwood (1994), and assuming the basis to be orthonormal, results in:

$$\int_{\Omega} h_i(\boldsymbol{x}) h_j(\boldsymbol{x}) d\Omega = \delta_{ij} \quad \text{(Kronecker Delta)} \tag{B.23}$$

For a random field $\chi(\boldsymbol{x}, \theta)$ with a mean function $\mu(\boldsymbol{x})$ and an autocovariance function $C_{\chi\chi}(\boldsymbol{x}, \boldsymbol{x}')$, any realization of the field can be expanded over Ω by means of the orthogonal functions $\{h_i(\boldsymbol{x})\}_{i=1}^{\infty}$. By considering all possible outcomes of the field, the coefficients in the expansion become random variables, leading to the following expansion:

$$\chi(\boldsymbol{x}, \theta) = \mu(\boldsymbol{x}) + \sum_{i=1}^{\infty} X_i(\theta) h_i(\boldsymbol{x}) \tag{B.24}$$

where $X_i(\theta)$ are random variables with a mean of zero. Applying the properties of orthogonal functions, it can be shown that:

$$\boldsymbol{X}_i(\theta) = \int_{\Omega} \left[\chi(\boldsymbol{x}, \theta) - \mu(\boldsymbol{x}) \right] h_i(\boldsymbol{x}) d\Omega \tag{B.25}$$

$$\left(\tilde{\boldsymbol{V}}_{XX} \right)_{kl} \equiv E\left[\boldsymbol{X}_k \boldsymbol{X}_l \right] = \int_{\Omega} \int_{\Omega} \boldsymbol{C}_{XX}(\boldsymbol{x}, \boldsymbol{x}') h_k(\boldsymbol{x}) h_l(\boldsymbol{x}') d\Omega_{\boldsymbol{x}} d\Omega_{\boldsymbol{x}'} \tag{B.26}$$

If $\chi(\cdot)$ is Gaussian, Eq. (B.25) proves that $\{\boldsymbol{X}_i\}_{i=1}^{\infty}$ are zero-mean Gaussian random variables, possibly correlated. If they are correlated, it is possible to transform them into an

uncorrelated standard normal vector $\boldsymbol{\xi}$ by performing a spectral decomposition of the covariance matrix $\tilde{\boldsymbol{V}}_{XX}$:

$$\tilde{\boldsymbol{V}}_{XX} \cdot \boldsymbol{\Phi} = \boldsymbol{\Phi} \cdot \boldsymbol{\Lambda} \tag{B.27}$$

where $\boldsymbol{\Lambda}$ is the diagonal matrix containing the eigenvalues λ_i of $\tilde{\boldsymbol{V}}_{XX}$ and $\boldsymbol{\Phi}$ is a matrix whose columns are the corresponding eigenvectors. The random vector $\boldsymbol{X}$ is related to $\boldsymbol{\xi}$ by:

$$\boldsymbol{X} = \boldsymbol{\Phi} \cdot \boldsymbol{\Lambda}^{1/2} \cdot \boldsymbol{\xi} \tag{B.28}$$

By denoting the coordinates of the k^{th} eigenvector by $\left\{\Phi_i^k, i = 1,...,n\right\}$, where n is the number of truncated terms, each random variable in $\boldsymbol{X}$ can be obtained from Eq. (B.28) by:

$$X_i = \sum_{k=1}^{n} \Phi_i^k \sqrt{\lambda_k}\, \xi_k \tag{B.29}$$

Substituting Eq. (B.29) in Eq. (B.24) leads to the following expansion:

$$X_i = \mu(\boldsymbol{x}) + \sum_{i=1}^{n} \left(\sum_{k=1}^{n} \Phi_i^k \sqrt{\lambda_k}\, \xi_k \right) h_i(\boldsymbol{x}) = \mu(\boldsymbol{x}) + \sum_{k=1}^{n} \sqrt{\lambda_k}\, \xi_k \left(\sum_{i=1}^{n} \Phi_i^k h_i(\boldsymbol{x}) \right) \tag{B.30}$$

Introducing the following notation: $\varphi_k(\boldsymbol{x}) = \sum_{i=1}^{n} \Phi_i^k h_i(\boldsymbol{x})$; Eq. (B.30) simplifies to:

$$\hat{\boldsymbol{X}}(\boldsymbol{x}) = \mu(\boldsymbol{x}) + \sum_{k=1}^{n} \sqrt{\lambda_k}\, \xi_k \varphi_k(\boldsymbol{x}) \tag{B.31}$$

The above equation is clearly an approximate Karhunen-Loève expansion of the random field $\boldsymbol{X}(\cdot)$ as seen by comparing with Eq. (B.21). Furthermore, by comparing the above developments with the numerical solution of the eigenvalue problem associated with the autocovariance function – Eq. (B.22), Zhang and Ellingwood (1994) concluded that the OSE method using a complete set of orthogonal functions $\left\{h_i(\boldsymbol{x})\right\}_{i=1}^{\infty}$ is strictly equivalent to the Karhunen-Loève expansion in the case when the eigenfunctions $\varphi_k(\boldsymbol{x})$ of the autocovariance function $\boldsymbol{C}_{XX}$ are approximated by using the same set of orthogonal functions $\left\{h_i(\boldsymbol{x})\right\}_{i=1}^{\infty}$.

The Expansion Optimal Linear Estimation **(EOLE)**

The expansion optimal linear estimation method proposed by Li and Der Kiureghian (1993), is an extension of the OLE method (section B.2.2) using a spectral representation of the vector of nodal variables $\boldsymbol{X}$.

If $\boldsymbol{X}(\cdot)$ is assumed to be Gaussian, the spectral decomposition of the covariance matrix $\tilde{\boldsymbol{V}}_{XX}$ of $\boldsymbol{X} = \{\chi(\boldsymbol{x}_1), \ldots, \chi(\boldsymbol{x}_N)\}$ is:

$$\boldsymbol{X} = \mu_X + \sum_{i=1}^{N} \sqrt{\lambda_i}\,\xi_i \varphi_i \tag{B.32}$$

where $\{\xi_i,\ i = 1,\ \ldots,\ N\}$ are independent standard normal variables and $(\lambda_i,\ \varphi_i)$ are the eigenvalues and eigenvectors of the covariance matrix $\tilde{\boldsymbol{V}}_{XX}$, verifying:

$$\tilde{\boldsymbol{V}}_{XX}\varphi_i = \lambda_i \varphi_i \tag{B.33}$$

Substituting Eq. (B.32) in Eq. (B.17) and solving the OLE problem results in:

$$\hat{\boldsymbol{X}}(\boldsymbol{x}) = \mu(\boldsymbol{x}) + \frac{1}{\sqrt{\lambda_i}} \sum_{i=1}^{N} \xi_i \varphi_i^{\,T} \tilde{\boldsymbol{V}}_{\chi(x)X} \tag{B.34}$$

As in the Karhunen-Loève expansion, the series can be truncated after n terms, the eigenvalues λ_i being sorted first in descending order.

The variance of the error for EOLE is:

$$\mathrm{Var}\left[\chi(t) - \hat{\chi}(t)\right] = \sigma^2(\boldsymbol{x}) - \sum_{i=1}^{n} \frac{1}{\lambda_i} \left(\varphi_i^{\,T} \tilde{\boldsymbol{V}}_{\chi(x)X}\right)^2 \tag{B.35}$$

As in OLE and KL, the second term in the above equation is identical to the variance of $\hat{\chi}(\boldsymbol{x})$, thus EOLE also always under-represents the true variance. Due to the form of Eq. (B.35) the error decreases monotonically with n, the minimal error being obtained when no

truncation is made ($n = N$). This allows automatic definition of the cut-off value n for a given tolerance in the variance error.

B.2.4. Simulation Methods

Digital simulation is a well known and powerful technique for solving complex engineering problems involving random variation. Assuming that a deterministic solution method is available, the simulation technique consists of repeatedly generating sets of observations of all the random variables or functions involved in the calculation, solving the deterministic problem associated with each set of the observations, and evaluating appropriate statistics of response and performance measures.

Shinozuka has developed and advocated the use of Monte Carlo simulation techniques in the field of engineering mechanics over the last four decades. A synopsis of his works in this regard is well documented in an article co-authored with Deodatis (1991). In particular, Yamazaki and Shinozuka (1988) proposed an interactive procedure to simulate non-Gaussian stochastic fields and later introduced statistical preconditioning to reduce the sample size in another work (1990).

Fenton and Vanmarcke (1990) presented a method of generating realizations of a discrete "local average" Gaussian random process using a local average subdivision technique. One of the advantages cited by the authors is the suitability for finite element models that employ efficient low-order interpolation functions, in which each local average becomes an element property. However, no structural applications of this technique have been reported in the open literature.

Other contributions in connection with the application of simulation schemes for modelling and discretization of random fields include the works of Bielewicz et al. (1991) on non-homogeneous scalar fields, Grigoriu (1992) on the application of the sampling theorem, and Poirion (1993) on the simulation of non-Gaussian fields.

A major disadvantage of simulation schemes is the enormous amounts of computation times associated with their application. For large structures or very complex elements analysed in great detail these procedures are impractical.

Appendix C – Description of SFEA Methodologies

C.1 Simulation Methods

The direct Monte Carlo Simulation method was used in many early works in stochastic finite element analysis (Brennan, Akpan et al. 2001). In this "brute force" approach, deterministic analysis is carried out using the finite element method for a series of parameters generated in accordance with their respective probability distributions. The desired statistics of the response quantities, such as the mean, variance, and exceedance probabilities, are then evaluated based on the generated sample. Applications of this procedure can be found, among many others, in Vanmarcke et al. (1986) and Takada (1991). The analysis may be accomplished quite easily by developing custom software or simply through the application of commercial FEA software, used as a black box, to generate the response quantities for a given vector of random variables.

Direct MCS works on the basis of random selection of actual values of each of the variables, running the finite element analysis for these values, and deciding if the structure fails. This is repeated N times. The estimate for the failure probability is then given by the number of failures divided by N.

More precisely, the process described in Eq. (A.1) can be stated as follows:

$$p_f = \int \cdots \int I\left[g\left(\boldsymbol{X}\right) < 0\right] f_{\boldsymbol{X}}\left(\boldsymbol{X}\right) d\boldsymbol{X} \tag{C.1}$$

or, in discrete form

$$p_f = \frac{1}{N}\sum_{j=1}^{N} I\left[g\left(X_j\right) \le 0\right] \tag{C.2}$$

where $I[\ ]$ is an indicator function defined such that $I[\vartheta] = 1$ if the expression represented by ϑ is "true" and zero otherwise. X_j represents the jth observation of random samples selected from $f_X(\ )$.

To apply Eq.(C.2) a discrete set of values is chosen for each of the random variables in the problem. This set is termed X_j. For each such set, the limit state function (i.e., $g(X_j)$) is evaluated. If it is violated (i.e., if the structure fails) the sum in Eq. (C.2) is incremented by one. Otherwise no action is taken. The process is repeated N times and the sum in Eq. (C.2) counts the number of failures n. The ratio n/N is an estimate of the probability of failure. In theory as $N \rightarrow \infty$, the approximation in Eq. (C.2) improves asymptotically. Values for X_j can be obtained from appropriate subroutines on many computers or can be generated from a set of random numbers.

MCS has the advantage that it is adaptable to all types of problems described by implicit performance functions, and the results can be obtained to any desired accuracy. However, since the failure probabilities for most structural systems are very low (typically on the order of 10^{-2} – 10^{-7}) the direct MCS process is clearly inefficient. In addition, for problems involving many random variables or random fields this procedure is typically extremely expensive, since a large number of solutions is needed to obtain reliable results. Although using a combination of Monte-Carlo simulation and deterministic finite element programs to calculate reliability is relatively straight forward, if the deterministic analysis is time-consuming (i.e. numerous finite elements and hundreds or more of simulation cycles), this approach is impractical. For example, assume that it takes 1 minute to complete a single run of a particular finite element model, where the probability of failure to be estimated is thought to be about 1 in 10,000. A rough estimate of the number of simulation runs required to capture a desired failure probability is: 100/estimated p_f (Maymon 1993). Hence, to capture a failure probability of only 10^{-4} requires approximately 1 million runs of the model, which corresponds to almost 2 years of continuous single processor time. This fact does not account for possible computer crashes and the massive amounts of data and output which needs to be managed. Even if the model is executed in a parallel computing environment the analysis is still prohibitively expensive. Furthermore, the reliability levels often sought in

structural systems can be two or even three magnitudes higher than the level in the above example. Therefore, for problems involving large structures, complicated structural elements (reinforced concrete), and/or large numbers of random variables, the direct Monte Carlo simulation approach is currently impractical and is of limited practicality.

Other schemes have been proposed to improve the efficiency of the Monte Carlo simulation method. Shinozuka and Yamazaki (1988) have introduced the Neumann MCS expansion technique. Computation time for this technique is reduced, since only the mean stiffness matrix needs to be decomposed with this formulation. Furthermore, the MCS approach can be significantly improved using variance reduction techniques (Haldar and Mahadevan 2000a) such as importance sampling (IS), Latin Hypercube Sampling (LHS), antithetic variables, stratified sampling, and others.

In importance sampling, Eq. (C.2) is replaced by:

$$p_f = \frac{1}{N}\sum_{j=1}^{N}\left\{ I\left[g\left(X_j\right) \le 0 \right] \frac{f_X\left(\hat{v}_j\right)}{h_V\left(\hat{v}_j\right)} \right\} \tag{C.3}$$

where $h_V(\ )$ is termed the importance sampling probability density function. The samples are now $\hat{v}_j$, taken from $h_V(\ )$ rather than from $f_X(\ )$. This has the advantage that $h_V(\ )$ can be selected by the investigator. Good choices of $h_V(\ )$ can considerably reduce the number of sample vectors $\hat{v}_j$ required for a good estimate of p_f, thereby significantly reducing computation times.

A robust choice for $h_V(\ )$ is a multi-normal distribution with independent components and with standard deviations of approximately 1 to 2 times those corresponding to $\boldsymbol{X}$. Ideally the mean is placed at the point of maximum likelihood in the failure domain. This point may have to be found by trial and error. Fortunately, there is a reasonable degree of latitude in estimating this point without having much effect on the estimate of p_f. SFEA analysis based on coupling of FEA with variance reduction techniques like importance sampling is a promising approach for the analysis of RC elements.

C.2 Second Moment Methods

Second moment analysis aims at characterizing second-order statistical moments (the means and variances of response quantities - displacements, strain and stress components, etc.) from those of the input variables. The perturbation method, first introduced by Handa and Andersson (1981), Hisada and Nakagiri (1985), and Liu et al., (1986a, 1986b), as well as the weighted integral method, introduced by Takada (1990), Deodatis (1991), and Deodatis and Shinozuka (1991) fall into this category.

C.2.1. Perturbation-Based SFEA Approach

The perturbation approach to probabilistic structural analysis was introduced more than two decades ago (Haldar and Mahadevan 2000). Initial applications were directed at the study of the eigenvalue problems related to the free vibration of structures with stochastic mass and stiffness matrices and the solutions of linear static problems involving loading and system stochasticity. The works of Handa and Anderson (1981) and Hisada and Nakagiri (1985) are amongst the earliest examples of application of this approach to structural safety and reliability analysis. In these works, SFEA was applied for the evaluation of the reliability index and design point within the framework of the Advanced First-Order Second Moment (AFOSM) method, discussed in Chapter 5.

Considering the well-known finite element equation for quasi-static linear problems:

$$\boldsymbol{K}\boldsymbol{U} = \boldsymbol{F} \tag{C.4}$$

where $\boldsymbol{K}$ is the global stiffness matrix, $\boldsymbol{U}$ is the vector of nodal displacement, and $\boldsymbol{F}$ is the global nodal load vector, the stochastic quantities can be expressed as:

$$\boldsymbol{K} = \boldsymbol{K}_o + \Delta\boldsymbol{K} \tag{C.5}$$

$$\boldsymbol{U} = \boldsymbol{U}_o + \Delta\boldsymbol{U} \tag{C.6}$$

$$\boldsymbol{F} = \boldsymbol{F}_o + \Delta\boldsymbol{F} \tag{C.7}$$

where $\boldsymbol{K}_o$, $\boldsymbol{U}_o$ and $\boldsymbol{F}_o$ are considered to represent the deterministic components, while the increments (perturbations) $\Delta\boldsymbol{K}$, $\Delta\boldsymbol{U}$, and $\Delta\boldsymbol{F}$ correspond to the stochastic parts of $\boldsymbol{K}$, $\boldsymbol{U}$, and $\boldsymbol{F}$, respectively. Substituting Eq. (C.5) through (C.7) into Eq. (C.4) leads to:

$$\left[\boldsymbol{K}_o + \Delta\boldsymbol{K}\right]\left[\boldsymbol{U}_o + \Delta\boldsymbol{U}\right] = \left[\boldsymbol{F}_o + \Delta\boldsymbol{F}\right] \tag{C.8}$$

Neglecting the product ($\Delta\boldsymbol{K}\Delta\boldsymbol{U}$) in the expansion and separating the deterministic and stochastic parts of Eq. (C.8) results in:

$$\boldsymbol{K}_0\boldsymbol{U}_0 = \boldsymbol{F}_0 \tag{C.9}$$

and

$$\boldsymbol{K}_o\Delta\boldsymbol{U} = \Delta\boldsymbol{F} - \Delta\boldsymbol{K}\boldsymbol{U}_o \tag{C.10}$$

Equation (C.10) represents the finite element solution at the deterministic expansion point. By iteratively solving this equation, the second-order variation of the response may be computed.

A more rigorous and general formulation of the perturbation approach can be constructed from a Taylor series expansion, which also paves the way for higher-order approximations. The stiffness matrix in Eq. (C.5) may be expanded about a deterministic reference point as:

$$\boldsymbol{K} = \boldsymbol{K}_o + \sum_{i=1}^{n} \boldsymbol{K}_i'\left(x - x_i\right) + \frac{1}{2}\sum_{i=1}^{n}\sum_{j=1}^{n} \boldsymbol{K}_{ij}'\left(x - x_i\right)\left(x - x_j\right) \tag{C.11}$$

where $\boldsymbol{K}_i'$ and $\boldsymbol{K}_{ij}'$ are the first-order and second-order partial derivatives of the stiffness matrix with respect to the basic variables $\boldsymbol{X}$. The displacement and load vectors in Eqs. (C.6) and (C.7) may be expanded in a similar fashion and the response computed as previously described.

When the mean state is chosen as the expansion point the approach is referred to as the mean-centred perturbation approach. Application of mean-centred perturbation results in the computation of reliability indices according to the First Order Second Moment (FOSM) approach of structural reliability analysis (see Chapter 5). In the AFOSM, however, the performance function is expanded not about the mean values of the basic variables, but

about the most probable failure point. Hisada and Nakagiri (1985) utilized this approach and also presented a second-order perturbation formulation in reference.

A notable feature of the formulations is that the stiffness matrix is inverted only once in contrast to simulation or response surface methods, in which many inversions of the stiffness matrix are required. The key to successful solution using the perturbation approach is the ability to compute and assemble partial derivative matrices for stiffness, displacements, and loads. Second-order approximations are obviously more accurate than the first-order approximations. However, these involve the computation and assembly of second-order partial derivative matrices.

Numerous applications of the perturbation approach have been reported in the open literature. Prominent in this connection are the works of Liu et al. (1986a), (1986b), in which, using interpolation/shape function discretization (section B.2.2), applications were investigated for static linear and nonlinear structural dynamics and a variational formulation of probabilistic finite elements was established. These problems included wave propagation in one dimensional elasto-plastic bar with random yield stress (Liu, Belytschko et al. 1986b), and static plane stress response of a cantilever beam (*ibid*).

Although the formulation of the perturbation approach is mathematically elegant, its application to reliability analysis has several disadvantages. The mean-centred perturbation method suffers from the well known invariance problem associated with FOSM reliability analysis. Furthermore, the perturbation methods do not use the distribution information about the basic random variables, even when it is available (Haldar and Mahadevan 2000a). This is a serious limitation, even in the exceptional cases in which all the variables are normally distributed; the choice of Gaussian distributions is questionable when describing material properties that are positive in nature. The method is also not capable of producing accurate results when there are large variations in the random variables defining a problem. In studies by Liu et al. (1986a), results compared well with Monte Carlo simulations, however, the coefficient of variation was limited to about 10%. Nevertheless, it must be noted that the Monte Carlo results by its very nature must be obtained for specific distributions. In that

sense, the comparison is dependent on the assumed distributions used in the Monte Carlo analysis.

C.2.2. The Weighted Integral Method

Under certain conditions, discretization of the random fields in SFEA may be completely avoided through the application of the weighted integral method, introduced by Deodatis (1991). It was applied by Deodatis and Shinozuka (1991) for the calculation of the response variability and reliability of stochastic frame structures and the calculation of the response variability of simple two-dimensional stochastic systems.

In the context of linear elasticity, the main idea is to consider the element stiffness matrices as basic random quantities. Using standard finite element notations, the stiffness matrix associated with a given element occupying a volume Ω_e is given by:

$$\boldsymbol{k}^e = \int_{\Omega_e} \boldsymbol{B}^T \boldsymbol{D} \boldsymbol{B} \, d\Omega_e \tag{C.12}$$

where $\boldsymbol{D}$ represents the elasticity matrix, and $\boldsymbol{B}$ is the strain matrix. Essentially, the method assumes that the elasticity matrix $\boldsymbol{D}$ can be expressed as a product of a scalar univariate random field $\chi(x)$ and a deterministic matrix $\boldsymbol{D}_o$, that is:

$$\boldsymbol{D}(x) = \left[1 + \chi(x)\right] \boldsymbol{D}_o \tag{C.13}$$

where $\boldsymbol{D}_o$ is the mean value and $\chi(x)$ is a zero-mean process. Considering this form of the elasticity matrix, Eq. (C.12) can be reformulated as:

$$\boldsymbol{k}^e = \boldsymbol{k}_o^e + \Delta \boldsymbol{k}^e, \quad \text{where } \Delta \boldsymbol{k}^e = \int_{\Omega_e} \chi(\boldsymbol{x}) \boldsymbol{B}^T \boldsymbol{D}_o \boldsymbol{B} \, d\Omega_e \tag{C.14}$$

Then, due to the polynomial nature of the strain matrix $\boldsymbol{B}$, the stochastic element stiffness matrix can be written as:

$$\boldsymbol{k}^e = \boldsymbol{k}_o^e + \sum_{i=1}^{n} X_i \Delta \boldsymbol{k}_i^e \tag{C.15}$$

where n denotes the number of distinct polynomial terms in the coordinates x in the matrix product $\boldsymbol{B}^T\boldsymbol{B}$, $\boldsymbol{k}_o^e$ and $\Delta\boldsymbol{k}_i^e$ are deterministic matrices, and X_i are random variables defined by:

$$X_i = \int_{\Omega_e} P_i(x)\,\boldsymbol{\chi}(\boldsymbol{x})\,\mathrm{d}\Omega_e \tag{C.16}$$

in which $P_i(x)$ denotes the i^{th} distinct polynomial term in the coordinates x. The random variables X_i are interpreted as weighted integrals for all elements and completely define the SFE problem without the need to discretize the random fields. According to Deodatis and Shinozuka (1991), a truss element requires only 1, a two-dimensional beam element 3, and a plane stress quadrilateral element 3 such weighted integrals and associated matrices.

The global stochastic stiffness matrix is obtained by assembling the individual contributions of the element stiffness matrices over N elements of the system. In the context of the perturbation method, expansion of the response may be obtained from a 1st-order Taylor series expansion of the vector of nodal displacements $\boldsymbol{U}$. Assuming that loads are deterministic, the nodal response vector is given by:

$$\boldsymbol{U} = \boldsymbol{U}_o - \sum_{e=1}^{N}\sum_{i=1}^{n} X_i^e \boldsymbol{K}_o^{-1} \cdot \frac{\partial \boldsymbol{K}}{\partial X_i^e} \cdot \boldsymbol{U}_o \tag{C.17}$$

while the covariance matrix of the response is then:

$$\mathrm{Cov}\left[\boldsymbol{U},\ \boldsymbol{U}\right] = \sum_{e_1=1}^{N}\sum_{e_2=1}^{N}\sum_{i_1=1}^{n}\sum_{i_1=1}^{n} \boldsymbol{K}_o^{-1} \cdot \frac{\partial \boldsymbol{K}}{\partial X_{i_1}^{e_1}} \cdot \boldsymbol{U}_o \cdot \boldsymbol{U}_o^T \cdot \frac{\partial \boldsymbol{K}^T}{\partial X_{i_2}^{e_2}} \left(\boldsymbol{K}_o^{-1}\right)^T \cdot \mathrm{Cov}\left[X_{i_1}^{e_1}, X_{i_2}^{e_2}\right] \tag{C.18}$$

The major advantage of this procedure has been cited as the circumvention of the restriction (in random field discretization) that the finite element size has to be a fraction of the correlation distance of the stochastic field involved in the problem. It is claimed that the method does not use any particular discretization scheme for the random field. However, as pointed out by Matthies et al. (1997), the weighted integral method is actually mesh-dependent. The original random field is projected onto the space of polynomials involved in the strain matrices $\boldsymbol{B}$, that is, basically onto the space spanned by the shape functions of the finite elements. Moreover, if the correlation length of the random field is small compared to

the size of integration domain Ω_e, the accuracy of the method is questionable. This has been illustrated by Zhang and Der Kiureghian (1997) on the example of an elastic rod in tension, having constant cross-section and random Young's modulus. The shape functions usually employed for elements with constant properties (e.g. prismatic beams with constant Young's modulus and cross-section) do not yield good results when these properties are rapidly varying in the element. The method is limited to elastic structural mechanics problems. Although extension of the method to nonlinear problems was claimed by Deodatis and Shinozuka (1991), such derivations seem to be unavailable in the literature. Furthermore, the method assumes a Gaussian random field, which is a serious drawback in reliability analysis where probabilities are sensitive to tails of the underlying distributions.

From a computational point of view, the assumption of a product form assumed in Eq. (C.13) is generally difficult to realize in practice. By making use of the first-order perturbation method, it is limited to relatively small coefficients of variation of the input. The bounds on the response variance are difficult to compute in practice, due to the complex expression of the response variability functions given in Eqs. (C.17) and (C.18). The method is very time consuming for systems having a large number of elements.

C.3 The Spectral Stochastic Finite Element Method (SSFEM)

Ghanem and Spanos (1991), (2003), developed a systematic approach for formulating and discretizing partial differential equations (PDEs) with random data known as the Spectral Stochastic Finite Element Method. This probably constitutes the first systematic Galerkin approximation in deterministic and random variables. The results of a SFEM approximation allow one to compute a large variety of statistical information, such as moments of the solution as well as the probability of certain events related to the PDEs through post processing.

The spectral stochastic finite element method is an approach well suited to analysis involving random fields (Sudret and Der Kiureghian 2002). SSFEM is based on two successive discretizations of the system of stochastic PDEs governing the problem under consideration,

one in the spatial domain and one in the probabilistic domain: (1) a spatial discretization similar to the one used in classical finite element analysis, i.e. involving a mesh of the structure and shape functions, and (2) a probabilistic discretization of the random field(s) representing the uncertain properties of the constitutive material or loads. The response is cast using any of the three series expansion methods described earlier (KL, OSE, or EOLE). This can be interpreted as an intrinsic representation of the random response, from which quantities such as statistical moments can be computed by post-processing, either analytically or by simulation. As shown by Sudret et al., (2000), and summarized in section B.2.3, all three discretization methods lead to a representation of the Gaussian random field in the form:

$$\hat{\boldsymbol{\chi}}(\boldsymbol{x}) = \mu(\boldsymbol{x}) + \sum_{i=1}^{M} \boldsymbol{\chi}_i(\boldsymbol{x})\,\xi_i \tag{C.19}$$

where $\{\xi_i,\ i = 1,\ \ldots,\ M\}$ are the standard normal random variables, $\{\boldsymbol{\chi}_i(\boldsymbol{x}),\ i = 1,\ \ldots,\ M\}$ are deterministic functions depending on the correlation structure of the field, and N represents the number of terms used in the series expansion.

In classical finite element analysis, the basic response quantity is the vector of nodal displacements. In SSFEM, due to the introduction of a random field as an input, the basic response quantity is a random vector of nodal displacements $\boldsymbol{U}$, whose probabilistic content is not known in advance. Each component U^i is expanded over the so called polynomial chaos (Sudret and Der Kiureghian 2002):

$$U^i = \sum_{j=0}^{P-1} U_j^i \Psi_j\left(\{\xi_k\}_{k=1}^{M}\right) \tag{C.20}$$

where $\{\xi_k,\ k = 1,\ldots,\ M\}$ denote the standard normal variables appearing in the discretization of the input random field given by Eq. (C.19), $\Psi_j\left(\{\xi_k\}_{k=1}^{M}\right)$ are multidimensional Hermite polynomials defined by means of the ξ_i variables, and P is the order of expansion. The latter is connected to the number of random variables M (order of the expansion of the random field) and the highest order p of the polynomials Ψ_j by:

$$P = \sum_{k=0}^{p} \binom{M+k-1}{k} \quad \left(\text{binomial coefficient}\right) \tag{C.21}$$

Using classical notation, the finite element method for static problems in linear elasticity eventually yields a linear system of size $N \times N$ (N being the number of degrees of freedom):

$$\boldsymbol{K}\boldsymbol{U} = \boldsymbol{F} \tag{C.22}$$

where $\boldsymbol{F}$ is the deterministic load vector, and where the global stiffness matrix $\boldsymbol{K}$ is obtained after assembling the element stiffness matrices $\boldsymbol{k}^e$:

$$\boldsymbol{K} = \sum_e \boldsymbol{k}^e, \qquad \boldsymbol{k}^e = \int_{\Omega_e} \boldsymbol{B}^T \boldsymbol{D}\boldsymbol{B}\, d\Omega_e \tag{C.23}$$

If it is assumed that the Young's modulus of the material is a random field, then the elasticity matrix at point $\boldsymbol{x}$ can be written as:

$$\boldsymbol{D}(\boldsymbol{x}) = \boldsymbol{X}(\boldsymbol{x})\boldsymbol{D}_o \tag{C.24}$$

where $\boldsymbol{D}_o$ is a constant deterministic matrix corresponding to a unit value of the Young's modulus. Substituting Eq. (C.24) in Eq. (C.23) yields the stochastic stiffness matrix:

$$\boldsymbol{K}(\theta) = \sum_e \boldsymbol{k}^e(\theta) = \sum_e \int_{\Omega_e} \boldsymbol{B}^T \boldsymbol{D}_o\, \boldsymbol{\chi}(\boldsymbol{x})\boldsymbol{B}\, d\Omega_e \tag{C.25}$$

By discretizing the random field $\boldsymbol{\chi}(\boldsymbol{x})$ in Eq. (C.25) according to the model in Eq.(C.19), the stochastic stiffness matrix takes the form:

$$\boldsymbol{K} \approx \boldsymbol{K}_o + \sum_{i=1}^{M} \boldsymbol{K}_i \xi_i \tag{C.26}$$

where the mean- and weighted stiffness matrices $\mathbf{K}_0$ and $\mathbf{K}_i$ are given by:

$$\boldsymbol{K}_o = \sum_e \boldsymbol{k}_o^e = \sum_e \int_{\Omega_e} \mu(\boldsymbol{x})\boldsymbol{B}^T \boldsymbol{D}_o \boldsymbol{B} d\Omega_e \tag{C.27}$$

$$\boldsymbol{K}_i = \sum_e \boldsymbol{k}_i^e = \sum_e \int_{\Omega_e} X_i(\boldsymbol{x})\boldsymbol{B}^T \boldsymbol{D}_o \boldsymbol{B} d\Omega_e \tag{C.28}$$

By collecting the terms in Eq. (C.27) in a vector form, the random vector of nodal displacements is expanded over the polynomial chaos with P coefficient vectors $\{\boldsymbol{U}_o,...,\boldsymbol{U}_{P-1}\}$. These coefficients are computed using the well known Galerkin method for minimizing the residual in the equilibrium equation, leading to:

$$\begin{bmatrix} \boldsymbol{K}_{00} & \cdots & \boldsymbol{K}_{0,P-1} \\ \boldsymbol{K}_{10} & \cdots & \boldsymbol{K}_{1,P-1} \\ \vdots & & \vdots \\ \boldsymbol{K}_{P-1,0} & \cdots & \boldsymbol{K}_{P-1,P-1} \end{bmatrix} \begin{bmatrix} \boldsymbol{U}_0 \\ \boldsymbol{U}_1 \\ \vdots \\ \boldsymbol{U}_{P-1} \end{bmatrix} = \begin{bmatrix} \boldsymbol{F} \\ 0 \\ \vdots \\ 0 \end{bmatrix} \tag{C.29}$$

where $\left\{\boldsymbol{K}_{jk} = \sum_{i=0}^{m} c_{ijk}\boldsymbol{K}_i, j,k = 0,...,P-1\right\}$ and $c_{ijk} = E\left[\xi_i \Psi_j \Psi_k\right]$ (mathematical expectation of products).

Essentially, the characterization of the random vector of nodal displacements in SSFEM is reduced to solving a linear system of size ($N \times P$), where N is the number of degrees of freedom of the structure, and P is the order of expansion of the response. In application, P is usually in the range 10^{-5}, which means that the above system of equations can be quite large, even for small size problems. Specific methods for efficiently solving this system of equations have been proposed by Ghanem and Kruger (1996).

The basic response quantity produced by SSFEM is the random vector of nodal displacements, cast as an expansion over the polynomial chaos. As in deterministic finite element analysis, the stochastic quantities such as stress in each Gauss point can be derived in terms of the random nodal displacements. Thus, any limit-state function involving these response quantities can be given an analytical expression in terms of standard normal random variables, while the probability of failure and response statistics can be obtained through any of the well established reliability methods (FORM/SORM) or simulation, through post-processing of the SSFEM results. The accuracy achieved in the SSFEM analysis depends on the accuracy of the representation of the limit-state function in terms of the expanded response quantities.

In the past, SSFEM has been applied to various kinds of problems including two-dimensional elasticity (Ghanem and Spanos 2003) and soil mechanics (Ghanem and Brzakala 1996), while the first attempt to include material non-linearity can be found in the work of Anders and Hori (1999). In these applications, the authors computed the coefficients of the series expansion of the response, and mean and standard deviation of various response quantities, without evaluating reliability. It had been shown that SSFEM is very effective for second moment analysis. The use of the probabilistic response expressions for reliability analysis of highly non-linear systems has been presented in Ghanem and Ghiocel (1996).

SSFEM has limited applicability to reliability problems involving small failure probabilities. Reasonable estimation of the probability of failure is only possible for probabilities larger than 1/1000 ($p_f > 10^{-3}$). The polynomial chaos expansion provides a global fit to each response quantity, which may be good in the central region of the respective distribution, but very poor in the tail regions. Since small-probability events are influenced by the tail regions of these probability distributions, accurate results from SSFEM cannot be expected for such problems. This limitation is more severe for problems involving random fields with short correlation lengths or large coefficients of variation (i.e. Cov > 0.1). It is evident that higher-order terms in the SSFEM expansion are necessary in order to accurately compute the tail ends of the joint probability distributions. In terms of computing efficiency, when using SSFEM, the CPT increases extremely rapidly with the order of the polynomial chaos expansion. However, higher orders of the polynomial chaos expansion would lead to an enormous amount of computation time. Thus, the method can be applied efficiently only when a small number of terms is used to describe the random field accurately. When more than two or three terms are used in the discretization of the random field, the computational time with a high-order polynomial chaos expansion rapidly increases and becomes prohibitive. Similar conclusions can be reached for the case of lognormal input random fields investigated by Sudret and Der Kiureghian (2000), using the discretization scheme proposed by Ghanem (1999). However, the computation cost for a given choice of expansion order and number of terms is even greater than in the Gaussian case. This is due to the fact that the input random field is discretized using the polynomial chaos as well, which requires more terms than the series expansion used in the Gaussian case. Nevertheless, it must be noted that

these conclusions do not invalidate the effectiveness of SSFEM for second-moment analysis. Furthermore, SSFEM might be effective in providing a good approximation to the central region of the probability density function of a response quantity.

C.4 The Reliability-Based SFEA Method

In essence, reliability-based SFEA entails the merger between finite element analysis and reliability methods such as the FORM, SORM, and importance sampling. The first merger between reliability analysis and the finite element method was presented by Der Kiureghian and Taylor (1983). Early efforts in the reliability-based approach focused on static analysis of linear elastic structures with random properties. Liu and Der Kiureghian (1991) proposed a general framework for finite element reliability analysis based on FORM and SORM. This work represents the first application of the finite element method in conjunction with SORM with non-Gaussian random fields and with system reliability analysis. Arnbjerg-Nielsen and Bjerager (1988), Mahadevan (1988), and Haldar (2000) have also developed and implemented a reliability-based SFEM approach and applied it to the modelling of frame structures.

The reliability approach has a significant advantage over the perturbation approach in that information about the distribution of the random variable is used. Furthermore, in the reliability approach, the probability density function of the response variable (not just second moment statistics) can be obtained. Since the computation of response gradients is a key operation in the implementation of this procedure, the use of the adjoint method has been recommended for this operation (Reh, Bohm et al. 1991). This technique is estimated to be capable of reducing computation times by a factor equal to the number of random variables.

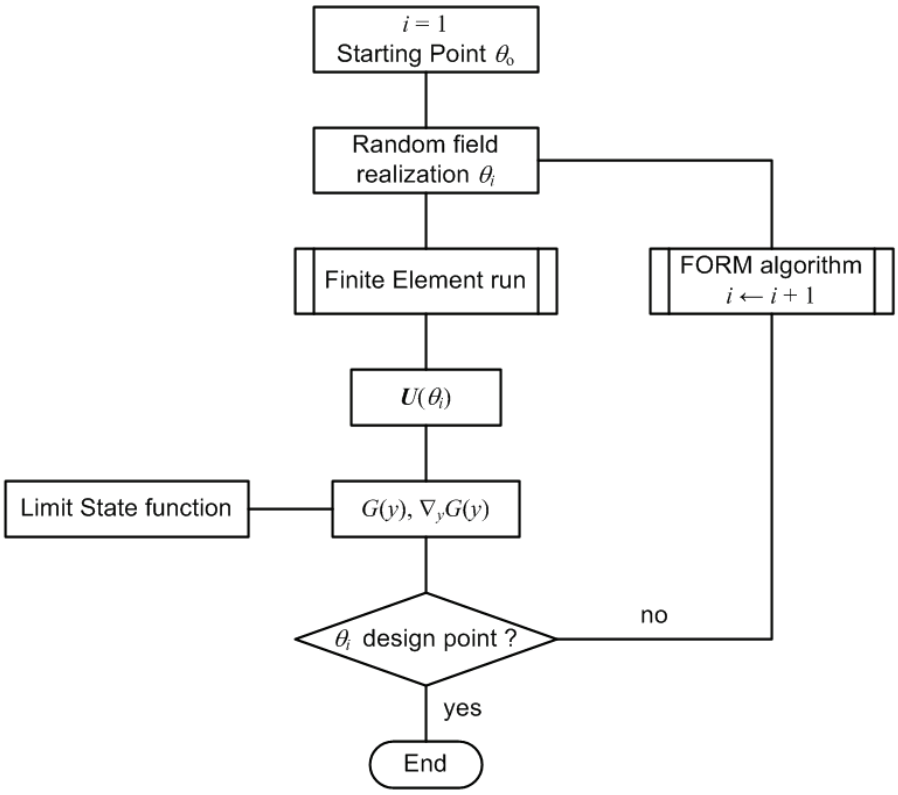

Figure C-1: Direct coupling between a reliability code and a finite element code (adapted from Sudret and Der Kiureghian (2002))

The reliability-based approach to SFEA is especially compatible with the algorithmic structure of existing FEA codes and is commonly considered to be the best strategy of all presently available methodologies. Figure C-1 illustrates a very general algorithm for direct coupling of the FE and reliability methodologies. It is reasonably straight forward to implement in a linear FEA setting, where the solution of the system can be obtained by inversion of the stiffness matrix and related techniques. However, in the case of non-linear FEA, where the solution of the system is obtained in an iterative manner, the implementation of this approach is very challenging. The majority of the successfully developed software utilizing this integrated SFEA methodology was in discrete mechanics (trusses, frames, etc.) and continua mechanics dealing with homogeneous problems such as plates, composite materials. One such example is the reliability analysis extension of the OpenSEES software; see Haukaas (2003). Although this is a very promising approach, it has yet to be successfully applied to non-linear SFEA of continuum reinforced concrete structures.

C.5 Response Surface Methods

The response surface method is a classical statistical technique in which a complex (computer) model is approximated by a functional relationship relating the output quantities and the basic input variables (Myers, Montgomery et al. 2009). In other words, a surrogate response surface is generated which, ideally, closely approximates the actual response surface. The approximation is usually based on polynomial functions, and often linear or quadratic response functions are applied. Adopting the simpler response functions allows an efficient repeated computation as may be needed in simulations or parameter studies in structural reliability analysis. This is because the approximation to the response surface rather than the original limit state function is used in the calculation of failure probabilities.

The concept of response surface methods has been used when approximating costly to compute and/or non-differentiable limit state functions. Within the framework of the stochastic finite element method, the steps required for the implementation of the response surface technique were described by Faravelli (1989). This involves the application of regression analysis to obtain the polynomial coefficients involved in the representation of the limit state function using the results of several numerical experiments.

The explicit representation of the limit state function $g(\boldsymbol{X})$, for the quadratic approximation for example, takes the form:

$$\hat{g}\left(\boldsymbol{X}\right) = a_0 + \sum_{i=1}^{k} a_i X_i + \sum_{i=1}^{k} a_{ii} X_i^2 + \sum_{i=1}^{k-1} \sum_{j>1}^{k} a_{ij} X_i X_j \tag{C.30}$$

where k is the number of basic random variables (X_i), and the coefficients a are to be determined from numerical experiments. This expression can also be derived from Taylor series of the corresponding order.

The works of Schüeller et al. (1997) and Bucher and Bourgund (1990) are among earlier efforts at promoting the application of response surface methods. Also, Ghanem and Spanos (1990) proposed a Galerkin-based response surface approach, in which the surface is approximated by its projection onto a complete set of polynomials that are orthogonal to the Gaussian measure (Brennan, Akpan et al. 2001).

In general, a limited number of evaluations of the limit state function (i.e. number of finite element runs) are required to build the surface. Reliability analysis can then be performed on the analytical expression generated by Eq. (C.30) instead of the true limit state function. Furthermore, adaptive response surface methodologies can be used for highly non-linear surfaces. These techniques are called adaptive because of successive refinement until convergence around the design point (Lemaire (1997). The up-to-date approach consists of generating quadratic response surfaces iteratively, where the center point converges to the design point. After convergence, any reliability method (FORM, SORM or importance sampling) can be applied with the response surface.

Hornet et al. (1998) and Pendola et al. (2000) proposed a benchmark problem in nonlinear fracture mechanics; crack initiation in a steel pipe submitted to internal pressure and axial tension. Various finite element codes (for example ANSYS and Abaqus) were used together with established reliability software, such as PROBAN (Det Norske Veritas 2002). The results for probabilities of failure obtained from the RSM analysis were identical to results obtained from SFEA using direct coupling of FEA and reliability codes for probabilities of failure within 10^{-10} and 10^{-1}. As far as efficiency is concerned, Pendola et al. (2000) show that the response surface approach allows dividing by 10 the number of finite element runs for the specific example. When the response surfaces are carefully generated and checked at each step, convergence to the design point is always obtained in these comparisons.

In summary, the response surface method appears to give accurate results for most problems applied, and it may be faster than the direct coupling when a small number of random variables is considered, and when it is not possible to implement the direct differentiation method (for instance, when a commercial finite element code is used). Otherwise, direct coupling will probably require less or equal amount of computation. Finally, RSM is applicable to the most general problems and does not require the implementation of gradients in the finite element code. Whether one method is more efficient than the other depends fundamentally on the number of random variables included in the analysis and the way gradients are computed.

Appendix D – Review of SFEA Software

D.1 Commercial Software

At this time, a general commercial-off-the-shelf (COTS) SFEA software system is not available in the marketplace. SFEA, in general, requires coupling of one or more separate reliability and FE codes. These are discussed in the following paragraphs.

1. **NESSUS** (Numerical Evaluation of Stochastic Structures under Stress), was developed by the Southwest Research Institute ((Cruse 1988), (SRI 1991)) under the sponsorship of the NASA Lewis Research Center. The software was initially developed for NASA to perform probabilistic analysis of space shuttle main engine components. NESSUS combines probabilistic analysis tools with a general purpose finite element/boundary element code. The probabilistic analysis component features most well established reliability analysis methods, including FORM, SORM, Monte Carlo simulation, and various optimal sampling techniques. The program also includes techniques such as fast convolution and curvature-based adaptive importance sampling. A schematic of the NESSUS system is illustrated in Figure D-1.

   The finite element code which is part of the NESSUS software is **limited to the analysis of linear elastic problems** and thus not suitable for modeling of concrete/RC. However, NESSUS was designed to interface with major commercial finite element packages, such as Abaqus, ANSYS, NASTRAN, LS-DYNA, and many others, thereby extending its capability to non-linear analysis. Since some of these general FE packages have built-in concrete material models and/or allow the user to develop and integrate their own material models, NESSUS could potentially be used for SFEA of RC structures. The annual licensing costs for NESSUS are several thousand per license. The cost of the

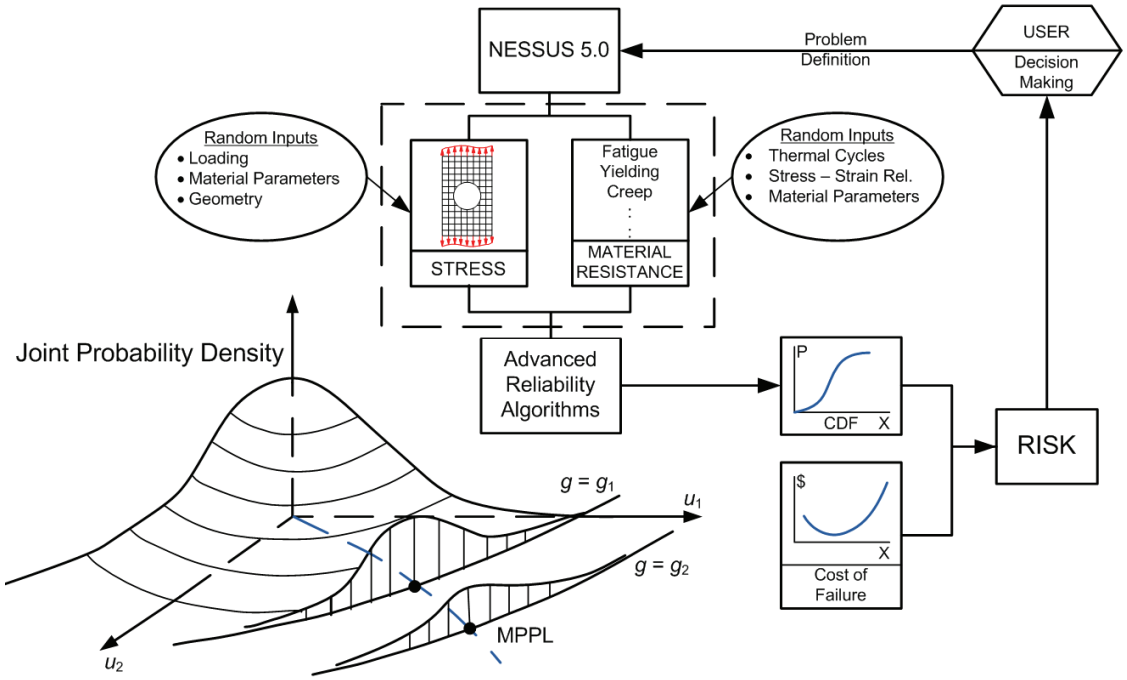

Figure D-1: Schematic of the NESSUS System (adapted from Orisamolu et al. (1993))

essential third party finite element package would of course be additional, although such programs (Abaqus, etc.) are available for academic research at reduced licensing pricing. To date, there is no evidence in the literature that NESSUS coupled with general FE package had been used for SFEA of RC structures.

Since the late 1980's the University of California at Berkeley continues to be one of the principal academic institutions involved in developing structural reliability and SFEA methodologies. As part of this work, several computer programs have been developed at Berkeley, both commercial and open source, the latter being addressed separately in the next sub-section. On the commercial side, two programs, namely CalREL (Cal-RELiability) and FEAP (Finite Element Analysis Program) have been successfully coupled by Der Kiureghian and his colleagues (1991) as CalREL-FEAP.

2. **CalREL-FEAP** (Liu, Lin et al. 1989) is a general-purpose structural reliability analysis program designed to compute probability integrals in the form given by Eq. (A.7). It is designed to work on its own or to operate as a shell program in conjunction with other structural analysis programs. Structural failure criteria are defined in terms of one or

more limit-state functions specified by the user in user-defined subroutines. CalREL is capable of computing the reliability of structural components as well as structural systems. It incorporates four general techniques for computing the probability of failure: FORM, SORM, directional simulation with exact or approximate surfaces, and Monte Carlo simulation. It has a library of probability distributions of independent and dependent random variables. Additional distributions can be included through a user-defined subroutine. FEAP developed by Taylor (2010) is a general finite element code for linear and nonlinear analysis. Although the integrated CalREL-FEAP is not available, the user can purchase CalREL and FEAP and link the programs with CalREL being the master program. FEAP does not provide concrete material models or bond elements, therefore such would have to be developed and linked with the program source code.

3. **COSSAN** ("COmputational Stochastic Structural ANalysis"), developed at the Institute of Engineering Mechanics, University of Innsbruck, Austria, is a general purpose software package for structural analysis taking into account the statistical uncertainties of various geometric, material, and loading parameters (IfM 2010). The main capabilities of COSSAN are simulation-based reliability analysis, stochastic finite elements analysis, and reliability-based optimization (RBO). The software has been under development since about 1990, and past versions of COSSAN were an attempt at full integration between FEA and reliability analysis methods. The program was limited to linear structural systems only. The researchers involved realized that replicating the functionality of general non-linear FE packages was an enormous undertaking and thus, present efforts aim at capitalizing on highly developed third-party FE codes in the computational stochastic structural analysis, by constructing interfaces and tools capable of interacting with these third-party codes (IfM 2010). For proper interface with deterministic software, a graphical user interface is essential, a communication interface that must be flexible enough to cope with different application programming interfaces and data formats, and the reduction of problem sizes before undertaking reliability analysis. This is an ongoing project and the product is still under development.

4. **STRUREL** (RCP 2010) is a set of programs for the reliability analysis of structural, operational, and other systems, developed and marketed by RCP GmbH, in Germany, an independent consultancy specialising in reliability and risk analysis of technical systems. RCP is closely linked to research and development efforts in these areas at the Technical University of Munich. The programs have been applied in structural engineering and code development, in the nuclear power plant, offshore, ship and aerospace industries, in hydrology, operations research, financial planning, and in statistics. The programs which comprise the complete system (some of which are optional) include programs for component and system reliability, statistical and design of experiments, and a comprehensive general finite element code. Initially the company used its own FE code which was restricted to linear analysis. The current generation of STRUREL integrates the general commercial FE software PERMAS (INTES 2010) available from INTES in Stuttgart, Germany. PERMAS is a well established general nonlinear finite element program and a major competitor to similar systems, such as ANSYS and Abaqus. Each individual component of this system costs several thousand dollars, making this option somewhat prohibitive in an academic research setting even with reduced pricing. However, in engineering practice/consulting such costs are of the same order as licensing of well known commercial FE packages, which do not offer reliability analysis capability.

   A unique feature in STRUREL is that the individual programs have been merged at source-code level, which makes this solution far more efficient than other approaches, such as coupling of programs as "black boxes" communicating through programming interfaces. This makes SRUREL the closest to a truly integrated SFEA software package. This is very promising software for SFEA of RC structures provided that accurate concrete constitutive models can be implemented in PERMAS.

D.2 Open Source Software (OSS)

Open-source software is computer software that is available in source code form, for which the source code and certain other rights normally reserved for copyright holders are provided

under a software license that permits users to study, change, and improve the software. Open source licenses often meet the requirements of the Open Source Definition. Some open source software is available within the public domain. The principal benefit of OSS is the rapid development by a large number of distributed developers in a collaborative manner.

1. **OpenSees** (Open System for Earthquake Engineering Simulation) is a general-purpose deterministic finite element framework developed by a multi university team under the sponsorship of the Pacific Earthquake Engineering Research (PEER) Center (McKenna, Fenves et al. 2002). OpenSees is a collection of software components rather than packaged code. It uses an object-oriented software architecture (Haukaas 2003). The OpenSees libraries of elements (discrete and continuum) and material models are quite rich. As the name implies, the software has mainly been used for dynamic analysis of structural and geotechnical problems, such as the response of building frames, bridge structures, and soils subjected to earthquake time histories.

   More recently, Haukaas and Der Kiureghian (2004) extended OpenSees with objects to perform reliability analysis in conjunction with the finite element analysis. The authors claimed that the program is capable of performing sensitivity analysis by the direct differentiation method (DDM), uncertainty propagation analysis by the first-order second-moment (FOSM) method, and reliability analysis by the first-order reliability method (FORM), importance sampling, and Monte Carlo simulation. Several variable importance measures were also provided as part of the standard output. Linear and nonlinear static and dynamic problems can be analyzed.

   In theory, the latter OpenSees appears to be an ideal platform for the development of fully integrated and custom SFEA software, particularly in a research setting. It apparently provides a fully functional FE and reliability code allowing the analyst to focus on solving problems rather than writing source code. One can download fully functional precompiled example problems involving stochastic frame structures. However, it is emphasized that in the current version of OpenSees (as of late 2011) the reliability-based finite element analysis is no longer functional. The reliability extension

to OpenSees was developed by Terje Haukaas (2003) as part of his doctoral work at the University of California, Berkeley. Dr. Haukaas, who is currently an Associate Professor of Civil Engineering at the University of British Columbia (UBC), no longer maintains the reliability code in OpenSees, and thus the finite element reliability functionality in OpenSees has been lost.

2. **Rt** (Reliability tools) is a new reliability software currently being developed at UBC under the supervision of Professor Haukaas (UBC 2010). Although not open source, Rt is a free object-oriented and fully parameterized computer program for reliability. Several features distinguish Rt from the reliability analysis functionality formerly available in OpenSees. First, it focuses on the probabilistic models that enter the reliability analysis. Although the option of algebraic limit state expressions is readily available, modern reliability analysis entails more complex models. Comprehensive hazard models, finite element infrastructure models, and wide-ranging consequence models are included (UBC 2010). Secondly, Rt features a graphical user interface to create and manage data, control analysis tools, visualize inputs and results, and a link with Google Maps visualizes regional results. According to the website, the user can alter analysis parameters in real time during execution (UBC 2010). Third, the user creates individual objects for parameters (random variables, decision variables, constants, and model responses), as well as for the models. Finally, other engineering software can be employed as a model. Interfaces with programs such as Matlab and SAP2000 are underway. It is planned to link Rt with the finite element capabilities of OpenSees. Rt appears to be a very promising tool for SFEA and with time it is possible that it could be adapted for SFEA of RC structures. However, this capability is not yet available.

Appendix E – Implementation of SFEAP

Consider a rigid steel portal frame shown in Figure E-1, from Haldar and Mahadevan (2000). All three members of the frame are made of the same grade of steel and have identical cross-sections (AISC W10 × 15). The frame is subjected to uniformly distributed loads W, D, and L as shown. These loads correspond to wind load, dead load, and live load, respectively. Eight variables are considered to be stochastic: W, the lateral load; D, the vertical (dead) load; L, the vertical (live) load; E, the Young's Modulus; F_y, the yield stress; A, the area of cross section; I, the moment of inertia; and Z, the plastic section modulus. The first three variables refer to the loads, the next two to the material properties, and the last three to the sectional properties. Table E-1 provides the statistical description of the random variables, with means, coefficients of variation, and types of distribution.

The reliability of member 3 (at node 3), under combined axial compression and bending, is here determined through the application of the SFEAP program developed as part of the research.

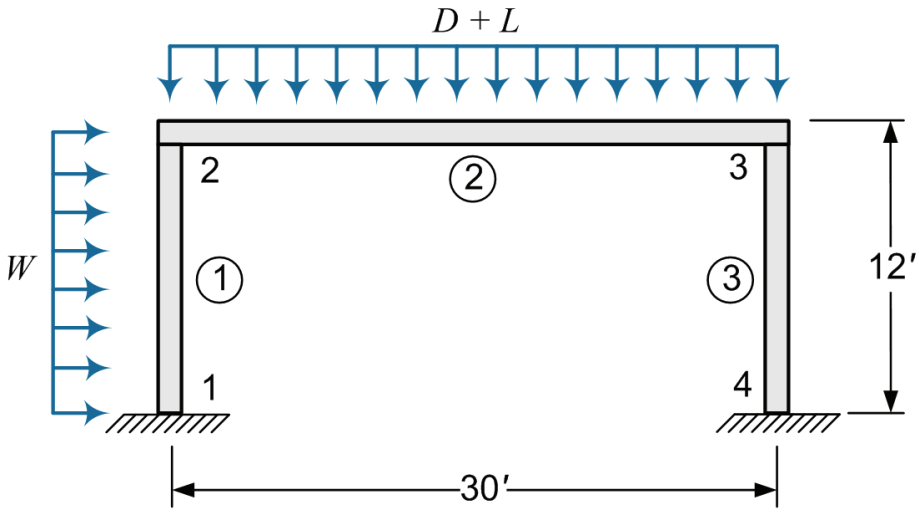

Figure E-1: Rigid steel portal frame from Haldar and Mahadevan (2000)

Table E-1: Rigid Steel Frame: description of the random variables

Variable	Units	Mean	COV	Type of Distribution
D	kip/ft	0.44	0.10	Normal
L	kip/ft	0.05	0.25	Type I
W	kip	0.41	0.37	Type I
A	in^2	4.41	0.05	Normal
I	in^4	68.90	0.05	Normal
Z	in^3	16.00	0.05	Normal
E	ksi	29,000	0.06	Normal
F_y	ksi	39.60	0.11	Normal

The input data file for the above problem is shown below, while the output file follows on the next page.

Input File SFEA_Frame_1.dat:

```
"SFEA Frame"
"PFrame"
"Joints",4
0,0
0,144
360,144
360,0
"Supports",2
1,1,1,1
4,1,1,1
"Materials",1
29000,39.6
.06,"Normal",.11,"Normal"
"Cross-Sections",1
4.41,68.9,16
.05,"Normal",.05,"Normal",.05,"Normal"
"Members",3
1,2,1,1
2,3,1,1
4,3,1,1
"Member Loads",3
1,3,.002847222,0,0,0
.37,"TypeI"
2,3,.03666667,0,0,0
.10,"Normal"
2,3,.004166667,0,0,0
.25,"TypeI"
```

Results File SFEA_Frame_1.out:

```
                ****************************
                Echo of Structural Input Data
                ****************************


File Name: SFEA Frame
Number of Joints: 4
Number of Members: 3
Number of Material Property Sets (E): 1
Number of Cross-Sectional Property Sets: 1


==================
Joint Coordinates
==================

Joint No.   X Coordinate   Y Coordinate
---------   ------------   ------------
    1        0.0000E+00     0.0000E+00
    2        0.0000E+00     1.4400E+02
    3        3.6000E+02     1.4400E+02
    4        3.6000E+02     0.0000E+00


========
Supports
========

Joint No.  X Restraint  Y Restraint  Rot. Restraint
---------  -----------  -----------  --------------
    1          Yes          Yes          Yes
    4          Yes          Yes          Yes


====================================
Material Properties (Mean; CoV; PDF)
====================================

Material No.    Modulus of Elasticity (E)    Yield Stress (Fy)
------------    -------------------------    -----------------
     1                 2.9000E+04                  39.600
     1                       0.06                    0.11
     1                     Normal                  Normal


============================================
Cross-Sectional Properties (Mean; CoV; PDF)
============================================

Property No.   Area (A)   Moment of Inertia (I)  Plast. Section Modulus (Z)
------------  ----------  ---------------------  --------------------------
     1        4.4100E+00       6.8900E+01          16.000
     1             0.05             0.05            0.05
     1           Normal           Normal          Normal
```

```
===========
Member Data
===========

Member  Beginning   End    Material  Cross-Sectional
  No.     Joint    Joint      No.      Property No.
------  ---------  -----  ---------  ---------------
   1        1        2        1             1
   2        2        3        1             1
   3        4        3        1             1


==============================
Member Loads (Mean; CoV; PDF)
==============================

Member    Load      Intensity    Intensity  Distance  Distance
  No.     Type    (w, w1, or P)     (w2)        a         b
------  --------  -------------  ---------  --------  --------
   1     Uniform     2.847E-3       ---      0.00E+0   0.00E+0
   2     Uniform     3.667E-2       ---      0.00E+0   0.00E+0
   2     Uniform     4.167E-3       ---      0.00E+0   0.00E+0
Load      Load
COV       PDF
--------  ---------
 0.37     2.847E-3
 0.10     3.667E-2
 0.25     4.167E-3


************************ End of Input Data **************************


            ************************************************
            Results of Deterministic Finite Element Analysis
            ************************************************


===================
Joint Displacements
===================

Joint No.   X Translation   Y Translation   Rotation (Rad)
---------   -------------   -------------   --------------
    1         0.0000E+00      0.0000E+00      0.0000E+00
    2         2.5759E-02     -8.2541E-03     -6.7363E-03
    3         1.4801E-02     -8.2976E-03      6.5275E-03
    4         0.0000E+00      0.0000E+00      0.0000E+00

======================================
Member End Forces in Local Coordinates
======================================

Member      Joint      Axial Force      Shear Force        Moment
------      -----      -----------      -----------      -----------
   1          1         7.3307E+00      -3.4828E+00      -1.6713E+02
              2        -7.3307E+00       3.8928E+00      -3.6391E+02

   2          2         3.8928E+00       7.3307E+00       3.6391E+02
              3        -3.8928E+00       7.3693E+00      -3.7085E+02
```

3	4	7.3693E+00	3.8928E+00	1.8971E+02
	3	-7.3693E+00	-3.8928E+00	3.7085E+02

==========
Support Reactions
==========

Joint No.	X Force	Y Force	Moment
1	3.4828E+00	7.3307E+00	-1.6713E+02
4	-3.8928E+00	7.3693E+00	1.8971E+02

********** End of Finite Element Analysis **********

****
Results of Stochastic Finite Element Analysis
****

==========
Performance Function
==========

g( ) = 1.0 - {(Pu / 2Pn) + (Mu / Mn)}

=====
sults
=====

K	lc	lc2	Fcr	Pn	Mn	Pu	Mu	aL	uL	aW	uW
2.1	0.9	0.81	28.216	124.432	633.6	7.369	370.85	102.604	0.0444	8.4545	0.3417
2.1	0.783	0.614	21.642	95.173	421.453	8.885	446.49	110.986	0.0494	9.1376	0.3339
2.1	0.777	0.604	21.754	95.763	428.461	8.353	419.79	98.6342	0.0537	11.9207	0.3297
2.1	0.784	0.614	22.109	97.334	438.611	8.395	421.75	105.9083	0.0562	13.117	0.3198
2.1	0.786	0.618	22.225	97.844	441.718	8.418	422.82	114.4725	0.0583	14.1957	0.3101
2.1	0.787	0.62	22.262	98.006	442.696	8.435	423.61	123.7266	0.0600	15.347	0.3008
2.1	0.787	0.62	22.262	98.004	442.668	8.435	423.58	128.255	0.0601	15.4524	0.2981

w*	a*	i*	z*	e*	fy*	g( )
0.41	4.41	68.9	16	29000	39.6	0.385

sigN_L	muN_W	sigN_W	muN_A	sigN_A	muN_I	sigN_I	muN_Z	sigN_Z	muN_E	sigN_E	muN_Fy	sigN_Fy
0.0116	0.385	0.14	4.41	0.221	68.9	3.445	16	0.8	29000	1740	39.6	4.356

a'*	i'*	z'*	e'*	fy'*
0	0	0	0	0

*	(dg/dW)*	(dg/dA)*	(dg/dI)*	(dg/dZ)*	(dg/dE)*	(dg/dFy)*
	-0.0151	0.0064	0.01	0.0366	0	0.0153

)*	(dg/dW')*	(dg/dA')*	(dg/dI')*	(dg/dZ')*	(dg/dE')*	(dg/dFy')*
	-0.0021	0.0014	0.0344	0.0293	0.0006	0.0665

	New w'*	New a'*	New i'*	New z'*	New e'*	New fy'*
	0.0852	-0.0566	-1.3808	-1.1731	-0.0241	-2.6671

New a*	New i*	New z*	New e*	New fy*	New g( )
4.3975	64.127	15.058	28957.86	27.9431	-0.1078

```
==============
Iteration No.2
==============

muN_D  sigN_D muN_L  sigN_L muN_W  sigN_W muN_A  sigN_A muN_I  sigN_I muN_Z  sigN_Z muN_E  sigN_E muN_Fy sigN_Fy
0.44   0.044  0.0546 0.013  0.374  0.108  4.41   0.221  68.9   3.445  16     0.8    29000  1740   39.6   4.356

d'*    l'*    w'*    a'*          i'*          z'*          e'*          fy'*
2.194  0.1773 0.1773 -0.0566      -1.3808      -1.1731      -0.0241      -2.6671

(dg/dD)*      (dg/dL)*      (dg/dW)*      (dg/dA)*      (dg/dI)*      (dg/dZ)*      (dg/dE)*      (dg/dFy)*
-1.8584       -1.8584       -0.0227       0.0103        0.0196         0.0703       0             0.0391

(dg/dD')*     (dg/dL')*     (dg/dW')*     (dg/dA')*     (dg/dI')*     (dg/dZ')*     (dg/dE')*     (dg/dFy')*
-0.0818       -0.0235       -0.0031       0.0023        0.0674        0.0563        0.0007        0.1703

New d'*       New l'*       New w'*       New a'*       New i'*       New z'*       New e'*       New fy'*
1.286         0.3691        0.0487        -0.0357       -1.0597       -0.885        -0.0113       -2.6787

New b  Db
3.281  -0.674

New d* New l* New w* New a* New i* New z*        New e*        New fy*       New g( )
0.4962 0.0595 0.3781 4.4022 65.272 15.2964       28980.44      27.9906       -0.0241

==============
Iteration No.3
==============

muN_D  sigN_D muN_L  sigN_L muN_W  sigN_W muN_A  sigN_A muN_I  sigN_I muN_Z  sigN_Z muN_E  sigN_E muN_Fy sigN_Fy
0.44   0.044  0.0574 0.0121 0.36   0.098  4.41   0.221  68.9   3.445  16     0.8    29000  1740   39.6   4.356

d'*    l'*    w'*    a'*          i'*          z'*    e'*          fy'*
1.286  0.1774 0.1773 -0.0357      -1.0597      -0.885 -0.0113      -2.6787

(dg/dD)*      (dg/dL)*      (dg/dW)*      (dg/dA)*      (dg/dI)*      (dg/dZ)*      (dg/dE)*      (dg/dFy)*
-1.8344       -1.8344       -0.0224       0.0096        0.0177        0.064         0             0.0362

(dg/dD')*     (dg/dL')*     (dg/dW')*     (dg/dA')*     (dg/dI')*     (dg/dZ')*     (dg/dE')*     (dg/dFy')*
-0.0807       -0.0242       -0.0029       0.0021        0.0611        0.0512        0.0007        0.1578

New d'*       New l'*       New w'*       New a'*       New i'*       New z'*       New e'*       New fy'*
1.3016        0.3903        0.047         -0.0341       -0.9853       -0.8261       -0.0106       -2.5445

New b  Db
3.135  -0.146
```

```
New d* New l* New w* New a* New i* New z* New e*        New fy*       New g( )
0.4968 0.0617 0.3638 4.4025 65.521 15.342 28981.53      28.5848       -0.0048

==============
Iteration No.4
==============

muN_D  sigN_D muN_L  sigN_L muN_W  sigN_W muN_A  sigN_A muN_I  sigN_I muN_Z  sigN_Z muN_E  sigN_E muN_Fy sigN_Fy
0.44   0.044  0.0597 0.0112 0.348  0.09   4.41   0.221  68.9   3.445  16     0.8    29000  1740   39.6   4.356

d'*    l'*    w'*    a'*           i'*           z'*           e'*           fy'*
1.3016 0.0028 0.1774 -0.0341       -0.9853       -0.8261       -0.0106       -2.5445

(dg/dD)*       (dg/dL)*       (dg/dW)*       (dg/dA)*       (dg/dI)*       (dg/dZ)*       (dg/dE)*       (dg/dFy)*
-1.7918        -1.7918        -0.0219        0.0095         0.0173         0.0627         0              0.0349

(dg/dD')*      (dg/dL')*      (dg/dW')*      (dg/dA')*      (dg/dI')*      (dg/dZ')*      (dg/dE')*      (dg/dFy')*
-0.0788        -0.0248        -0.0027        0.0021         0.0597         0.0502         0.0007         0.1518

New d'*        New l'*        New w'*        New a'*        New i'*        New z'*        New e'*        New fy'*
1.2819         0.4038         0.0441         -0.034         -0.9714        -0.8156        -0.0108        -2.4684

New b  Db
3.092  -0.043

New d* New l* New w* New a* New i* New z*        New e*        New fy*       New g( )
0.4967 0.0634 0.3507 4.4024 65.529 15.3426       28981.03      28.7907       -0.0002

==============
Iteration No.5
==============

muN_D  sigN_D muN_L  sigN_L muN_W  sigN_W muN_A  sigN_A muN_I  sigN_I muN_Z  sigN_Z muN_E  sigN_E muN_Fy sigN_Fy
0.44   0.044  0.0615 0.0104 0.336  0.084  0.44   0.044  0.44   0.044  0.44   0.044  0.44   0.044  0.44   0.044

d'*    l'*    w'*    a'*    i'*           z'*           e'*           fy'*
1.2819 0.1774 0.1774 -0.034 -0.9714       -0.8156       -0.0108       -2.4684

(dg/dD)*       (dg/dL)*       (dg/dW)*       (dg/dA)*       (dg/dI)*       (dg/dZ)*       (dg/dE)*       (dg/dFy)*
-1.7705        -1.7705        -0.0216        0.0095         0.0173         0.0624         0              0.0343

(dg/dD')*      (dg/dL')*      (dg/dW')*      (dg/dA')*      (dg/dI')*      (dg/dZ')*      (dg/dE')*      (dg/dFy')*
-0.0779        -0.0268        -0.0026        0.0021         0.0594         0.0499         0.0007         0.1494

New d'*        New l'*        New w'*        New a'*        New i'*        New z'*        New e'*        New fy'*
```

```
1.2666        0.4359        0.0416 -      0.034         -0.9666       -0.8117       -0.0109       -2.4298

New b  Db
3.077  -0.015

New d* New l* New w* New a* New i* New z*        New e*        New fy*       New g( )

0.4966 0.0647 0.3384 4.4024 65.525 15.3419       28980.83      28.856        0.0001

==============
Iteration No.6
==============

muN_D  sigN_D muN_L  sigN_L muN_W  sigN_W muN_A  sigN_A muN_I  sigN_I muN_Z  sigN_Z muN_E  sigN_E muN_Fy sigN_Fy
0.44   0.044  0.0617 0.01   0.333  0.083  0.44   0.044  0.44   0.044  0.44   0.044  0.44   0.044  0.44   0.044

d'*    l'*    w'*    a'*           i'*           z'*           e'*           fy'*
1.2869 0.2973 0.065  -0.0344       -0.9797       -0.8226       -0.011        -2.4665

(dg/dD)*      (dg/dL)*      (dg/dW)*      (dg/dA)*      (dg/dI)*      (dg/dZ)*      (dg/dE)*      (dg/dFy)*
-1.7707       -1.7707       -0.0216       0.0095        0.0172        0.0624        0             0.0343

(dg/dD')*     (dg/dL')*     (dg/dW')*     (dg/dA')*     (dg/dI')*     (dg/dZ')*     (dg/dE')*     (dg/dFy')*
-0.0779       -0.0177       -0.0018       0.0021        0.0594        0.0499        0.0007        0.1493


New d'*       New l'*       New w'*       New a'*       New i'*       New z'*       New e'*       New fy'*

1.2874        0.2926        0.0297        -0.0345       -0.9819       -0.8245       -0.0111       -2.4664

New b  Db
3.078  0

New d* New l* New w* New a* New i* New z*        New e*        New fy*       New g( )
0.4966 0.0646 0.3355 4.4024 65.517 15.3404       28980.73      28.8565       0.0001


********** End of Analysis **********
```

Results from the SFEAP output file are shown in the table below in a more readable manner.

Table E-2: SFEA for Combined Axial Compression and Bending of Member 3 at Node 3

1.		$g(\ ) = 1.0 - \{(P_u / 2P_n) + (M_u / M_n)\}$								
2. Initial Values:		d*	l*	w*	a*	i*	z*	e*	f_y*	$g(\ )$
		0.44	**0.05**	**0.41**	**4.41**	**68.90**	**16.0**	**29000**	**39.60**	**0.385**
3.	μ_D^N	0.440	0.440	0.440	0.440	0.440	0.440			
	σ_D^N	0.044	0.044	0.044	0.044	0.044	0.044			
	μ_L^N	0.0480	0.0546	0.0574	0.0597	0.0615	0.0617			
	σ_L^N	0.0116	0.0130	0.0121	0.0112	0.0104	0.0100			
	μ_W^N	0.385	0.374	0.360	0.348	0.336	0.333			
	σ_W^N	0.140	0.108	0.098	0.090	0.084	0.083			
	μ_A^N	4.410	4.410	4.410	4.410	0.440	0.440			
	σ_A^N	0.221	0.221	0.221	0.221	0.044	0.044			
	μ_I^N	68.900	68.900	68.900	68.900	0.440	0.440			
	σ_I^N	3.445	3.445	3.445	3.445	0.044	0.044			
	μ_Z^N	16.00	16.00	16.00	16.00	0.440	0.440			
	σ_Z^N	0.80	0.80	0.80	0.80	0.044	0.044			
	μ_E^N	29000.0	29000.0	29000.0	29000.0	0.440	0.440			
	σ_E^N	1740.0	1740.0	1740.0	1740.0	0.044	0.044			
	$\mu_{F_y}^N$	39.600	39.600	39.600	39.600	0.440	0.440			
	$\sigma_{F_y}^N$	4.356	4.356	4.356	4.356	0.044	0.044			
	d'*	0.0000	2.1940	1.2860	1.3016	1.2819	1.2869			
	l'*	0.1774	0.1773	0.1774	0.0028	0.1774	0.2973			
	w'*	0.1774	0.1773	0.1773	0.1774	0.1774	0.0650			
	a'*	0.0000	-0.0566	-0.0357	-0.0341	-0.0340	-0.0344			
	i'*	0.0000	-1.3808	-1.0597	-0.9853	-0.9714	-0.9797			
	z'*	0.0000	-1.1731	-0.8850	-0.8261	-0.8156	-0.8226			
	e'*	0.0000	-0.0241	-0.0113	-0.0106	-0.0108	-0.0110			
	f_y'*	0.0000	-2.6671	-2.6787	-2.5445	-2.4684	-2.4665			

4.	$(\partial g/\partial D)$*	-1.2440	-1.8584	-1.8344	-1.7918	-1.7705	-1.7707
	$(\partial g/\partial L)$*	-1.2440	-1.8584	-1.8344	-1.7918	-1.7705	-1.7707
	$(\partial g/\partial W)$*	-0.0151	-0.0227	-0.0224	-0.0219	-0.0216	-0.0216
	$(\partial g/\partial A)$*	0.0064	0.0103	0.0096	0.0095	0.0095	0.0095
	$(\partial g/\partial I)$*	0.0100	0.0196	0.0177	0.0173	0.0173	0.0172
	$(\partial g/\partial Z)$*	0.0366	0.0703	0.0640	0.0627	0.0624	0.0624
	$(\partial g/\partial E)$*	0.0000	0.0000	0.0000	0.0000	0.0000	0.0000
	$(\partial g/\partial F_y)$*	0.0153	0.0391	0.0362	0.0349	0.0343	0.0343
5.	$(\partial g/\partial D')$*	-0.0547	-0.0818	-0.0807	-0.0788	-0.0779	-0.0779
	$(\partial g/\partial L')$*	-0.0144	-0.0235	-0.0242	-0.0248	-0.0268	-0.0177
	$(\partial g/\partial W')$*	-0.0021	-0.0031	-0.0029	-0.0027	-0.0026	-0.0018
	$(\partial g/\partial A')$*	0.0014	0.0023	0.0021	0.0021	0.0021	0.0021
	$(\partial g/\partial I')$*	0.0344	0.0674	0.0611	0.0597	0.0594	0.0594
	$(\partial g/\partial Z')$*	0.0293	0.0563	0.0512	0.0502	0.0499	0.0499
	$(\partial g/\partial E')$*	0.0006	0.0007	0.0007	0.0007	0.0007	0.0007
	$(\partial g/\partial F_y')$*	0.0665	0.1703	0.1578	0.1518	0.1494	0.1493
6.	New d'*	2.1940	1.2860	1.3016	1.2819	1.2666	1.2874
	New l'*	0.5762	0.3691	0.3903	0.4038	0.4359	0.2926
	New w'*	0.0852	0.0487	0.0470	0.0441	0.0416	0.0297
	New a'*	-0.0566	-0.0357	-0.0341	-0.0340	-0.0340	-0.0345
	New i'*	-1.3808	-1.0597	-0.9853	-0.9714	-0.9666	-0.9819
	New z'*	-1.1731	-0.8850	-0.8261	-0.8156	-0.8117	-0.8245
	New e'*	-0.0241	-0.0113	-0.0106	-0.0108	-0.0109	-0.0111
	New f_y'*	-2.6671	-2.6787	-2.5445	-2.4684	-2.4298	-2.4664
7.	New β	3.955	3.281	3.135	3.092	3.077	**3.078**
	$\Delta\beta$		-0.674	-0.146	-0.043	-0.015	0.000
8.	New d*	0.5367	0.4962	0.4968	0.4967	0.4966	**0.4966**
	New l*	0.0546	0.0595	0.0617	0.0634	0.0647	**0.0646**
	New w*	0.3971	0.3781	0.3638	0.3507	0.3384	**0.3355**
	New a*	4.3975	4.4022	4.4025	4.4024	4.4024	**4.4024**

New i*	64.127	65.272	65.521	65.529	65.525	**65.517**
New z*	15.0584	15.2964	15.3420	15.3426	15.3419	**15.3404**
New e*	28957.86	28980.44	28981.53	28981.03	28980.83	**28980.73**
New f_y*	27.9431	27.9906	28.5848	28.7907	28.8560	**28.8565**
New g( )	-0.1078	-0.0241	-0.0048	-0.0002	0.0001	0.0001

After five iterations of the FORM algorithm in SFEAP the solution converges to a value of the reliability index of $\boldsymbol{\beta = 3.078}$, corresponding to a failure probability of $\boldsymbol{p_f = 0.001}$.

Results of analysis for the same problem, as summarized in Haldar and Mahadevan (2000), show a performance index of **3.088**. This small difference can be explained by the fact that the authors did not indicate the value of the effective length coefficient for the column element used in their analysis, which method was used for the transformation of the means and standard deviations of the type I random variables (L and W) to their equivalent normal values, and which variation of FORM was applied.

Appendix F – RSM: Simple Example

To illustrate the application of RSM in reliability analysis, consider the following simple problem. Assume a cantilever beam using a standard W130×24 steel section, as illustrated in Figure F-1. The deterministic parameters for the problem are: beam length l = 5m, modulus of elasticity E = 200,000 MPa, moment of inertia $I = 8.87\times10^{6}\text{mm}^4$, and a static tip load P = 700 N. The objective is to calculate the reliability of the beam for the serviceability limit state: maximum allowable free end deflection of $l/200$. Thus, the maximum allowable deflection corresponds to δ_{max} = 25 mm.

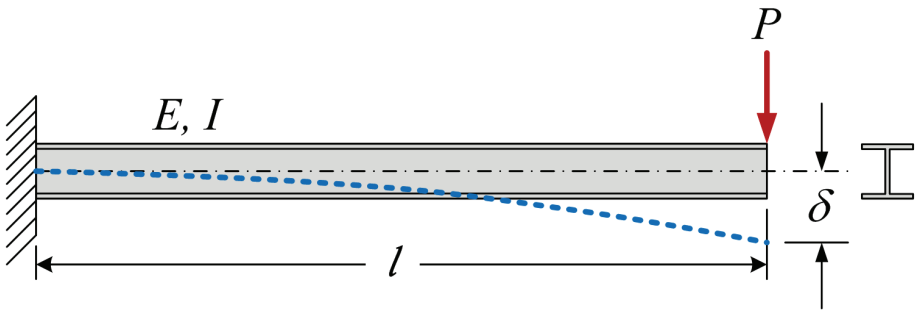

Figure F-1: Deflection of a cantilever beam

Assuming linear elastic behaviour, the tip deflection of an Euler-Bernoulli beam is given by the well-known formula: $\delta = Pl^3/3EI$. For the given deterministic parameters the tip deflection of in the above cantilever beam is 16.4 mm. The reliability for this problem can be easily obtained using any of the techniques in Appendix A.4, which is useful for comparison with results of RSM based approach.

The results of the RSM based reliability analysis are compared to those obtained from direct Monte Carlo simulation (MCS). The beam length is assumed to be deterministic while the tip load, modulus of elasticity, and the moment of inertia are assumed to be single the random variables (spatially invariable) as given in Table F-1. To ensure that the reliability is kept relatively low, and hence keeping the minimum required number of MCS runs to a minimum, a load of 700 N was chosen because it is fairly close to the load required to reach δ_{max} (i.e.

1064 N). This load also keeps the flexural stresses generated in the beam well within the assumed elastic range.

The closed-form serviceability limit state function for the problem at hand is simply:

$$g(\boldsymbol{X}) = \delta_{\max} - \delta(\boldsymbol{X}) = 25 \text{ mm} - \frac{Pl^3}{3EI} \tag{F.1}$$

where $\boldsymbol{X} = \{P, E, I\}^T$ is the vector random variables considered in the analysis and δ represents the load effects; here, the tip deflection.

Table F-1: Random variables for cantilever beam example

Random Variable	Units	Mean μ	COV	Std. Dev. σ	PDF
$\boldsymbol{P}$	N	700	0.257	180	Normal
$\boldsymbol{E}$	MPa	200,000	0.025	5,000	Normal
$\boldsymbol{I}$	mm^4	8.87×10^6	0.020	1.77×10^5	Normal

The direct Monte Carlo simulation approach, summarized in Appendix C.1, uses randomly generated samples of the input variables to perform deterministic analysis of the system response. The response can be evaluated explicitly if a closed-form solution is available or implicitly when a complex numerical model is used. The results can then be used to quantify the response statistics and the reliability of the system. In essence, the application of MCS in reliability analysis boils down to counting the number of instances that the performance function $g(\boldsymbol{X})$, given by Eq. (F.1), is less than zero, and dividing this number by the total number of simulations.

The analysis was implemented in Microsoft Excel. For each input random variable (P,E, and I) 10,000 uniformly distributed numbers ranging [0,1] were generated. These numbers were then transformed to their normally distributed counterparts using the following transformation:

$$CDF(\text{uniform}) \rightarrow CDF(\text{normal}) \rightarrow PDF(\text{normal}) \tag{F.2}$$

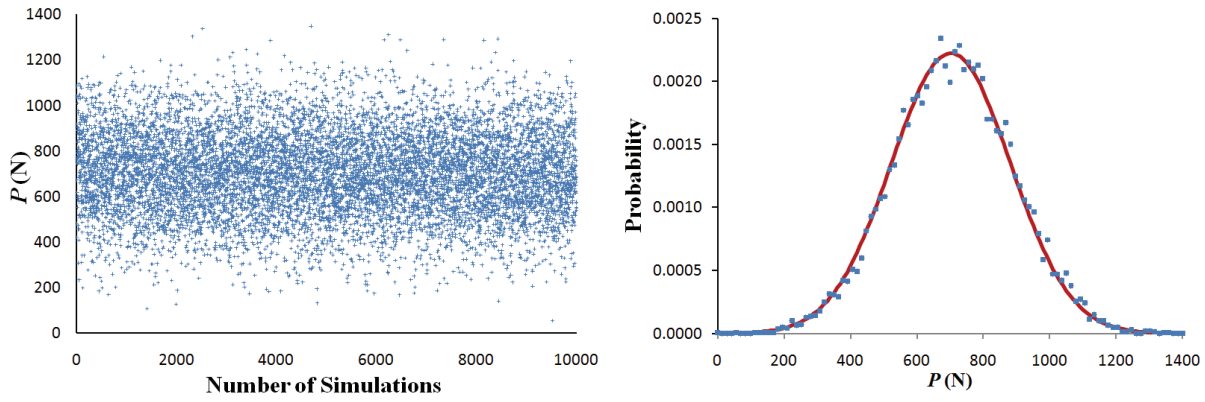

Figure F-2: Generation of random variables for load P

For instance, Figure F-2 shows the results of procedure (F.2) in generating 10,000 values of the random variable for the load $\boldsymbol{P}$, following a normal distribution. Random variables following any other statistical distribution can be obtained in a similar fashion.

Using the generated random variables with the limit state function given by Eq. (F.1) and counting the number of instances that $g(\boldsymbol{X}) < 0$ leads to the probability of failure (i.e. exceedence of the maximum allowable deflection). For the given example, in 10,000 simulations the limit state function was negative 227 times. The probability of failure is therefore $p_f = 0.0227$ corresponding to a performance index of $\beta = 2.001$. The results also include the statistics of the response: $\mu = 16.47$ mm, $\sigma = 4.27$ mm, and normal PDF, as expected. Had the input variables followed other distribution the response would also reflect that.

The performance function for the assumed basic random variables can be reasonably assumed to be linear. Therefore, the surrogate response surface can be effectively defined using a polynomial with linear terms only. Applying Eq. (6.4) gives:

$$\begin{aligned}\hat{g}(\mathbf{X}) &= a_0 + \sum_{i=1}^{k} a_i X_i + \sum_{i=1}^{k} a_{ii} X_i^2 + \sum_{i=1}^{k} \sum_{j=1, j\neq i}^{k} a_{ij} X_i X_j \\ &= a_0 + a_1 X_1 + a_2 X_2 + a_3 X_3 \\ &= a_0 + a_1 P + a_2 E + a_3 I\end{aligned} \tag{F.3}$$

Because the number of variables is very small a full factorial approach is easily implemented. However, since the CCD method is used with the FE model, it will also be used here.

It is reasonable in this case to begin the analysis at the mean values of each random variable with a span of two standard deviations, hence $\mu \pm \sigma$. For the 3 random variables in this problem CCD requires 15 points ($k^2 + 2k + 1$). If the centre point is replicated once the design will have 16 points to describe the limit state function. The CCD experimental design in original basic random variables is presented in Table F-2, columns 1 through 4. Performing linear regression (least squares method) as outlined in Chapter 6, section 6.2.2, results in the solution of the response surface coefficients. Equation (F.3) can now be rewritten as:

$$\hat{g}(\mathbf{X}) = -7.91403 - 0.0235 \cdot P + 8.228 \times 10^{-05} \cdot E + 1.855 \times 10^{-06} \cdot I \qquad \text{(F.4)}$$

Table F-2: Response Surface Generation

	Random Variables				Actual Limit State $g = R - S$		Response Surface $\hat{g} = R - S'$		Error
Trial	P	E	I	R	S	g	$\hat{S}$	$\hat{g}$	%
1	520	195000	8692600	25	12.782	12.218	12.924	12.076	-1.1600
2	520	195000	9047400	25	12.281	12.719	12.340	12.660	-0.4638
3	520	200000	8870000	25	12.213	12.787	12.220	12.780	-0.0550
4	520	205000	8692600	25	12.159	12.841	12.101	12.899	0.4497
5	520	205000	9047400	25	11.682	13.318	11.517	13.483	1.2385
6	700	195000	8870000	25	16.863	8.137	16.863	8.137	-0.0053
7	700	200000	8692600	25	16.777	8.223	16.744	8.256	0.4017
8	700	200000	8870000	25	16.441	8.559	16.452	8.548	-0.1227
9	700	200000	8870000	25	16.441	8.559	16.452	8.548	-0.1227
10	700	200000	9047400	25	16.119	8.881	16.160	8.840	-0.4603
11	700	205000	8870000	25	16.040	8.960	16.040	8.960	-0.0001
12	880	195000	8692600	25	21.632	3.368	21.386	3.614	7.2774
13	880	195000	9047400	25	20.783	4.217	20.802	4.198	-0.4543
14	880	200000	8870000	25	20.669	4.331	20.683	4.317	-0.3225
15	880	205000	8692600	25	20.576	4.424	20.563	4.437	0.2925
16	880	205000	9047400	25	19.769	5.231	19.979	5.021	-4.0144

The performance function given by Equation (F.4) can now be used with any of the reliability methods presented in Appendix A.4 to determine the performance index, probability of failure, and response statistics.

Using COMPASS with this performance function and the FORM algorithm results in a performance index $\beta = 2.005$ ($p_f = 0.0225$) in only three iterations, comparing closely with the results obtained from MCS on the closed-form performance function: $\beta = 2.001$ ($p_f = 0.0227$), even though only a first order RSM was used. Clearly, 15 evaluations of the response and 3 iterations of FORM are vastly more efficient than 10,000 iterations of direct MCS. However, the real advantage of RSM is when the limit state function is unknown.

Appendix G – RSM: Case Study

This appendix presents the detailed statistical analysis of the response surfaces generated in section 6.4.3 for the RC girder G2. The results of the statistical tests presented here apply only to the ultimate limit state of the girder at t = 25 years and 37 years. However, the same analysis was used for both limit states considered and for each annual increment of time.

G.1 Detailed Statistical Analysis of RC Girder G2 at t = 25 years.

Polynomial Order	Sequential *p*-value	Lack of Fit *p*-value	Adjusted R^2	Predicted R^2	
Linear	< 0.0001	Not Calc.	0.9983088	0.9967144	Suggested
2 cross-terms	0.0782	Not Calc.	0.9986937	0.9955658	
Quadratic	0.0659	Not Calc.	0.9992279	0.9954166	
Cubic	< 0.0001	Not Calc.	0.9999982	0.9999113	Aliased

The Predicted R^2 of 0.9967 is in close agreement with the Adjusted R^2 of 0.9983, indicating nearly perfect fit between the design space points and the generated surface.

Model Summary Statistics Table:

Polynomial Order	Standard Deviation	R^2	Adjusted R^2	Predicted R^2	PRESS	
Linear	4175197.89	0.9985906	0.9983088	0.9967144	4.0639E+14	Suggested
2 cross-terms	3669372.86	0.9990203	0.9986937	0.9955658	5.4846E+14	
Quadratic	2821128.96	0.9995496	0.9992279	0.9954166	5.6691E+14	
Cubic	137414.55	0.9999992	0.9999982	0.9999113	1.0971E+13	Aliased

The linear model is perfectly adequate for description of the response surface model of the girder. However, the quadratic model was selected to demonstrate the ANOVA results for the quadratic model.

ANOVA for the Response Surface Quadratic Model

Analysis of Variance Table (partial sum of squares – Type III)

	Sum of Squares	*df*	Mean Square	*F*-value	*p*-value Prob > F	
Model	1.2363E+17	5	2.47266E+16	3106.83638	< 0.0001	significant
i_{corr}	3.6467E+15	1	3.64672E+15	458.20167	< 0.0001	significant
f_y	1.1987E+17	1	1.19868E+17	15061.07700	< 0.0001	significant
$i_{corr} \cdot f_y$	5.3144E+13	1	5.31441E+13	6.67743	0.0363	
i^2_{corr}	3.9853E+13	1	3.9853E+13	5.00743	0.0603	
f^2_y	5.1734E+12	1	5.17339E+12	0.65002	0.4466	
Residual	5.5711E+13	7	7.95877E+12			
Lack of Fit	5.5711E+13	3	1.85705E+13			not significant
Pure Error	0	4	0			
Cor Total	1.6772E+18	12				

The Model *F*-value of 306.84 implies the model is significant and that there is only a 0.01% chance that a Model *F*-Value this large could occur due to noise. In general, *p*-values less than 0.05 indicate model terms are significant, while *p*-values greater than 0.1000 indicate the model terms are not significant.

Signal to Noise Ratio

Std. Dev.	2821128.96	R^2	0.9995496
Mean	1477136154	Adj. R^2	0.9992279
C.V. %	0.19098639	Pred. R^2	0.9954166
PRESS	5.6691E+14	Adeq. Precision	173.2217708

Adequate Precision measures the signal to noise ratio; a ratio greater than 4 is desirable. The ratio of 173.222 indicates an adequate signal which implies that the model can be used to navigate the design space.

G.2 Detailed Statistical Analysis of RC Girder G2 at t = 37 years.

Polynomial Order	Sequential *p*-value	Lack of Fit *p*-value	Adjusted R^2	Predicted R^2	
Linear	0.0035	0.0019	0.6124130	0.3884799	
2 cross-terms	0.8089	0.0014	0.5722966	-0.0686721	
Quadratic	< 0.0001	0.2785	0.9760869	0.90907664	Best
Cubic	0.1157	0.8682	0.9858706	0.98616444	Aliased

The above results underscore the complete inadequacy of the linear and linear-with-cross-terms polynomial surface in fitting the design space. This can be clearly seen in the graphical representation of the ULS response surface at t = 37 years, shown in Figure 6-4. The Predicted R^2 of 0.9091 is in reasonable agreement with the Adjusted R^2 of 0.9761 for the quadratic model.

Lack of Fit Tests Table:

Polynomial Order	Sum of Squares	*df*	Mean Square	*F*-value Value	*p*-value Prob > F	
Linear	5.3191E+17	6	8.8652E+16	36.1931	0.0019	
2 cross-terms	5.2820E+17	5	1.0564E+17	43.1288	0.0014	
Quadratic	1.3598E+16	3	4.5326E+15	1.8505	0.2785	Suggested
Cubic	7.6586E+13	1	7.6586E+13	0.0313	0.8682	
Pure Error	9.7977E+15	4	2.4494E+15			

Model Summary Statistics Table:

Polynomial Order	Standard Deviation	R^2	Adjusted R^2	Predicted R^2	PRESS	
Linear	232746318	0.6770111	0.6124133	0.3884799	1.0256E+18	
2 cross-terms	244494870	0.6792224	0.5722970	-0.0686721	1.7923E+18	
Quadratic	57811829.5	0.9860507	0.9760869	0.9090766	1.5249E+17	Suggested
Cubic	44439269.8	0.9941126	0.9858702	0.9861644	2.3205E+16	

The lack of fit *F*-value of 1.85, and the model statistics summarized above support the selection of the quadratic response surface model.

ANOVA for the Response Surface Quadratic Model

Analysis of Variance Table (partial sum of squares – Type III)

	Sum of Squares	*df*	Mean Square	*F*-value	*p*-value Prob > F	
Model	1.6538E+18	5	3.3076E+17	**98.9632**	< 0.0001	significant
i_{corr}	1.1252E+18	1	1.1252E+18	336.6670	< 0.0001	significant
f_y	1.0254E+16	1	1.0254E+16	3.0680	0.1233	
$i_{corr} \cdot f_y$	3.7088E+15	1	3.7088E+15	1.1097	0.3271	
i^2_{corr}	4.9617E+17	1	4.9617E+17	148.4571	< 0.0001	significant
f^2_y	2.0398E+16	1	2.0398E+16	6.1032	0.0428	significant
Residual	2.3395E+16	7	3.3422E+15			
Lack of Fit	1.3598E+16	3	4.5326E+15	**1.8505**	0.2785	not significant
Pure Error	9.7977E+15	4	2.4494E+15			
Cor Total	1.6772E+18	12				

The Model *F*-value of 98.96 implies the model is significant and that there is only a 0.01% chance that a Model *F*-Value this large could occur due to noise. In general, *p*-values less than 0.05 indicate model terms are significant, while *p*-values greater than 0.10 indicate the model terms are not significant. The Lack of Fit *F*-value of 1.85 implies the Lack of Fit is not significant relative to the pure error; there is a 27.85% chance that the Lack of Fit *F*-value this large could occur due noise.

Signal to Noise Ratio

Std. Dev.	57811829.5	R^2	0.9860507
Mean	1264805385	Adj. R^2	0.9760869
C.V. %	4.5708083	Pred. R^2	0.9090766
PRESS	1.5249E+17	Adeq. Precision	26.0681207

Adequate Precision measures the signal to noise ratio; a ratio greater than 4 is desirable. The ratio of 26.068 indicates an adequate signal which implies that the model can be used to navigate the design space.

Appendix H – COMPASS Script

```
C***********************************************************************
      SUBROUTINE USRLIM(GG,X,NR,I,IDP,IDPMAX,CH)
C***********************************************************************
C
C     THIS IS THE ROUTINE FOR LIMIT STATE FUNCTIONS
C
C (INPUT)
C     NR      --- THE NUMBER OF BASIC VARIABLES INVOLVED STRUCTURAL RESPONSE
C                 PLUS ONE VARIABLE FOR CAPACITY. THE CAPACITY VARIABLE IS
C                 ALWAYS TAKEN AS NUMBER 2
C                 FUNCTION (INPUT IF I.NE.1; OUTPUT IF I.EQ.1)
C     IDP     --- IDETIFICATION NUMBER OF LIMIT STATE FUNCTION (INPUT)
C     I       --- CONTROL CODE (INPUT)
C             = 1 RETURNS NR, LNR AND CH
C             = 2 RETURNS GG
C     X       --- VALUES OF BASIC VARIABLES
C (OUTPUT)
C     GG      --- VALUE OF RESPONSE (OUTPUT IF I.EQ.2)
C     LNR     --- LINEAR LIMIT STATE FUNCTION CODE (OUTPUT)
C             = 1 LINEAR LIMIT STATE FUNCTION
C             = 0 NONLINEAR LIMIT STATE FUNCTION
C     IDPMAX --- TOTAL NUMBER OF STRUCTURAL RESPONSE FUNCTIONS IN THIS C
LIBRARY
C     CH      --- NAME OF LIMIT STATE FUNCTION
C
      IMPLICIT REAL*8 (A-H,O-Z)
C
      DIMENSION  X(NR)
      CHARACTER  CH*40
C
       PI=3.141592653589793D0
       IDPMAX =5

       IF(I.NE.1)GO TO 100

       IF(IDP.EQ.1)THEN
                                        !ULTIMATE LIMIT STATE - FLEXURE
              NR =13
              LNR =0
              CH='MOMENT CAPACITY'
!             write a file
              NIN=7000
              OPEN  (UNIT=NIN,FILE="moment.out",FORM='FORMATTED',
      &           STATUS='UNKNOWN') !INPUT FILE AS DEFINED THROUGH GUI

              RETURN
       ENDIF

       IF(IDP.EQ.2)THEN
                                        !ULTIMATE LIMIT STATE - SHEAR
              NR =14
              LNR =0
```

```
      CH='SHEAR CAPACITY'

      RETURN
ENDIF


IF(IDP.EQ.3)THEN
                                  !R-S
      NR =2
      LNR =1
      CH='R-S'

      RETURN
ENDIF


IF(IDP.EQ.4)THEN
                  !ULS - Maximum flexural strength
                  !RS represented by 2nd-Order Polynomial for 5 random
                  !variables of the form: a0 + a1X1 + a2X2 + a3X3 +
                  !a4X4 + a5X5 + a6X1^2 + a7X2^2 + a8X3^2 + a9X4^2 + !a10X5^2
                  !where a0, a1, ..., a10 are constant coefficients
                  !and X1, X2, ..., X5 are the random variables
      NR = 25
      LNR = 0
      CH = 'ULS-Moment, up to 5 random variables'

      RETURN
ENDIF


IF(IDP.EQ.5)THEN
                  !SLS - Maximum allowable deflection exceeded
                  !RS represented by 2nd-Order Polynomial for 5 random
                  !variables of the form: a0 + a1X1 + a2X2 + a3X3 +
                  !a4X4 + a5X5 + a6X1^2 + a7X2^2 + a8X3^2 + a9X4^2 + !a10X5^2
                  !where a0, a1, ..., a10 are constant coefficients
                  !and X1, X2, ..., X5 are the random variables
      NR = 13
      LNR = 0
      CH='SLS-Deflection, up to 5 random variables'

      RETURN
ENDIF


100  CONTINUE

 !Closed form flexural failure mode analysis of RC-Beam
IF(IDP.EQ.1)THEN
      RI = X(1)          !corrosion rate - icorr
      T  = X(2)          !time in years - t
      DB = X(3)          !individual bar diameter - db (mm^2)
      RN = X(4)          !number or tension rebar - nb
      AY = X(5)          !ductility reduction constant - alpha y
      FY = X(6)          !yield strength of steel - fy (MPa)
      BL = X(7)          !beam span length (mm)
      FC = X(8)          !cylinder strength of concrete (MPa)
      B = X(9)           !width of beam cross section (mm)
      D = X(10)          !depth of reinforcement (mm)
      WL = X(12)         !uniformly distributed live load (N/mm)
      WD = X(11)         !uniformly distributed dead load (N/mm)
```

```
        CL = X(13)          !concentrated load (N)

        !Total area of reinforcing steel at time=0
        AS = ((RN*PI)/4.D0)*(DB**2)
        !Total area of reinforcing steel at time t due to loss of section
        !due to corrosion
        AST = ((RN*PI)/4.D0)*((DB-0.0232*RI*T)**2)

        !Yield strength with time due to loss of ductility
        FYT = (1.D0-100*AY*((AS-AST)/AS))*FY

        AL1 = 0.85D0-0.0015D0*FC
        IF(AL1.LT.0.67)THEN
              AL1 = 0.67
        END IF

        !Nominal moment capacity Mn from the CSA A23.3 2004 Concrete
        !Design Standard representing the available flexural strength
        !Supply R
        R = AST*FYT*(D-(AST*FYT)/(2.D0*AL1*FC*B))
        !Unfactored moment flexural response of the RC beam due to loads
        !representing the moments due to concentrated and UD loads
        !Demand S
        S = ((WD+WL)/(8.D0))*BL**2 +(CL*BL)/(4.D0)

        !Limit state g() = R - S = 0
        GG = (R/S)-1.D0

        RETURN
 ENDIF


 !Closed form shear failure mode analysis of an RC-Beam
IF(IDP.EQ.2)THEN
        RI = X(1)
        T  = X(2)
        DV = X(3)
        RN = X(4)
        AY = X(5)
        FY = X(6)
        BL = X(7)
        FC = X(8)
        B = X(9)
        D = X(10)
        WD = X(11)
        WL = X(12)
        CL = X(13)
        S = X(14)
        AVT = ((RN*PI)/4.D0)*((DV-0.0232*RI*T)**2)
        AV = ((RN*PI)/4.D0)*(DV**2)
        FYT = (1.D0-AY*100*((AV-AVT)/AV))*FY

        R = 0.2*DSQRT(FC)*B*D+(AVT*FYT*D)/(S)
        S = (WD+WL)*BL/(2.D0)+CL/2.D0

        GG = (R/S)-1.D0

        RETURN
 ENDIF


 !Reliability analysis as a function of the basic random variables R,S
```

```
IF(IDP.EQ.3)THEN
       R = X(1)
       S = X(2)

       GG = (R/S)-1.D0

       RETURN
 ENDIF


 !RS - FE based reliability analysis formulation for the
 !analysis of RC-Beams in the flexural failure mode (moments)
 IF(IDP.EQ.4)THEN
       RI = X(1)           !corrosion rate - icorr
       T  = X(2)           !time in years - t
       DB = X(3)           !individual rebar diameter - db (mm^2)
       RN = X(4)           !number or tension rebar - nb
       AY = X(5)           !ductility reduction constant - alpha y
       FY = X(6)           !yield strength of steel - fy (MPa)
       BL = X(7)           !beam span length (mm)
       FC = X(8)           !cylinder strength of concrete (MPa)
       B = X(9)            !width of beam cross section at top fibre (mm)
       D = X(10)           !depth to reinforcement (mm)
       WD = X(11)          !uniformly distributed dead load (N/mm)
       WL = X(12)          !uniformly distributed live load (N/mm)
       CL = X(13)          !concentrated load (N)
       MFE = X(14)         !Moment obtained fron FE analysis (S)
       A0 = X(15)          !Regression constant a0 - intercept
       A1 = X(16)          !Regression constant a1
       X1 = RI             !Random variable 1 (icorr)
       A2 = X(17)          !Regression constant a2
       X2 = WD             !Random variable 2 (wd)
       A3 = X(18)          !Regression constant a3
       X3 = WL             !Random variable 3 (wl)
       A4 = X(19)          !Regression constant a4
       X4 = FY             !Random variable 4 (fy)
       A5 = X(20)          !Regression constant a5
       X5 = FC             !Random variable 5 (fc)
       A6 = X(21)          !Regression constant a6
       A7 = X(22)          !Regression constant a7
       A8 = X(23)          !Regression constant a8
       A9 = X(24)          !Regression constant a9
       A10 = X(25)         !Regression constant a10

       !Total area of reinforcing steel at time = 0
       AS = ((RN*PI)/4.D0)*(DB**2)
       !Total area of reinforcing steel at time t due to loss of section
       !due to corrosion
       AST = ((RN*PI)/4.D0)*((DB-0.0232*RI*T)**2)

       !Yield strength with time due to loss of ductility
       FYT = (1.D0-100*AY*((AS-AST)/AS))*FY

       !Concrete rectangular compressive stress block factor
       AL1 = 0.85D0-0.0015D0*FC
       IF(AL1.LT.0.67)THEN
             AL1 = 0.67
       END IF

       !Nominal moment capacity Mn based on the CSA A23.3 2004 Concrete
       !Design Standard representing the available flexural strength
       !Supply R
```

```
            R = AST*FYT*(D-(AST*FYT)/(2.D0*AL1*FC*B))
            S = MFE - A0 - A1*X1 - A2*X2 - A3*X3 - A4*X4 - A5*X5 &
                         - A6*X1**2 - A7*X2**2 - A8*X3**2 - A9*X4**2 &
                         - A10*X5**2

            GG =(R/S)-1.D0

            RETURN

      ENDIF


      !RS - FE based reliability analysis formulation for RC-Beams
      !in the deflection Limt State; deflection failure mode
      IF(IDP.EQ.5)THEN
            BL = X(1)           !Beam span length (mm)
            DF = X(2)           !Deflection factor obtained from design
                                !standard/code
            DFE = X(3)          !Deflection obtained from FE analysis (S)
            A0 = X(4)           !Regression constant a0 - intercept
            A1 = X(5)           !Regression constant a1
            X1 = X(6)           !Random variable 1
            A2 = X(7)           !Regression constant a2
            X2 = X(8)           !Random variable 2
            A3 = X(9)           !Regression constant a3
            X3 = X(10)          !Random variable 3
            A4 = X(11)          !Regression constant a4
            X4 = X(12)          !Random variable 4
            A5 = X(13)          !Regression constant a5
            X5 = X(14)          !Random variable 5
            A6 = X(9)           !Regression constant a6
            A7 = X(10)          !Regression constant a7
            A8 = X(11)          !Regression constant a8
            A9 = X(12)          !Regression constant a9
            A10 = X(13)         !Regression constant a10

            R = BL/DF           !Maximum allowable deflection as per NBCC
            S = DFE + A0 + A1*X1 + A2*X2 + A3*X3 + A4*X4 + A5*X5 &
                        + A6*X1**2 + A7*X2**2 + A8*X3**2 + A9*X4**2 &
                        + A10*X5**2

            GG =(R/S)-1.D0

            RETURN

      ENDIF

      RETURN

      END


C*********************************************************************
      SUBROUTINE USRLIM(GG,X,NR,I,IDP,IDPMAX,CH)
C*********************************************************************
C
C     THIS IS THE ROUTINE FOR LIMIT STATE FUNCTIONS
C
C (INPUT)
C     NR     --- THE NUMBER OF BASIC VARIABLES INVOLVED STRUCTURAL
C                 RESPONSE
C                PLUS ONE VARIABLE FOR CAPACITY. THE CAPACITY VARIABLE IS
```

```
C                ALWAYS TAKEN AS NUMBER 2
C                FUNCTION (INPUT IF I.NE.1; OUTPUT IF I.EQ.1)
C     IDP    --- IDETIFICATION NUMBER OF LIMIT STATE FUNCTION (INPUT)
C     I      --- CONTROL CODE (INPUT)
C            = 1 RETURNS NR, LNR AND CH
C            = 2 RETURNS GG
C     X      --- VALUES OF BASIC VARIABLES
C (OUTPUT)
C     GG     --- VALUE OF RESPONSE (OUTPUT IF I.EQ.2)
C     LNR    --- LINEAR LIMIT STATE FUNCTION CODE (OUTPUT)
C            = 1 LINEAR LIMIT STATE FUNCTION
C            = 0 NONLINEAR LIMIT STATE FUNCTION
C     IDPMAX --- TOTAL NUMBER OF STRUCTURAL RESPONSE FUNCTIONS IN THIS
C                 LIBRARY
C     CH     --- NAME OF LIMIT STATE FUNCTION
C
      IMPLICIT REAL*8 (A-H,O-Z)
C
      DIMENSION  X(NR)
      CHARACTER  CH*40
C
       PI=3.141592653589793D0
       IDPMAX =7

       IF(I.NE.1)GO TO 100

       IF(IDP.EQ.1)THEN
                                        !ULTIMATE LIMIT STATE - FLEXURE
              NR =13
              LNR =0
              CH='MOMENT CAPACITY'
       !      write a file
              NIN=7000
              OPEN  (UNIT=NIN,FILE="moment.out",FORM='FORMATTED',
     &          STATUS='UNKNOWN') !INPUT FILE AS DEFINED THROUGH GUI

              RETURN
       ENDIF


       IF(IDP.EQ.2)THEN
                                        !ULTIMATE LIMIT STATE - SHEAR
              NR =14
              LNR =0
              CH='SHEAR CAPACITY'

              RETURN
       ENDIF


       IF(IDP.EQ.3)THEN
                                        !R-S
              NR =2
              LNR =1
              CH='R-S'

              RETURN
       ENDIF


       IF(IDP.EQ.4)THEN
                                !ULS - Maximum flexural strength
```

```
                                !RS represented by 2nd-Order Polynomial for !5
                                random variables of the form:
                                !a0 + a1X1 + a2X2 + a3X3 + a4X4 + a5X5
                                !   + a6X1^2 + a7X2^2 + a8X3^2 + a9X4^2
                                !   +a10X5^2
                                !where a0, a1, ..., a10 are constant
                                !coefficients and X1, X2, ..., X5 are the
                                !random variables
              NR = 25
              LNR = 0
              CH = 'ULS-Moment, up to 5 random variables'

              RETURN
       ENDIF
       IF(IDP.EQ.5)THEN
                                !SLS - Maximum allowable deflection exceeded
                                !RS represented by 2nd-Order Polynomial for 5
random
                                !variables of the form: a0 + a1X1 + a2X2 + a3X3 +
a4X4 + a5X5
                                !               + a6X1^2 + a7X2^2 + a8X3^2 +
a9X4^2 + a10X5^2
                                !where a0, a1, ..., a10 are constant coefficients
                                !and X1, X2, ..., X5 are the random variables
              NR = 19
              LNR = 0
              CH='SLS-Deflection, up to 5 random variables'

              RETURN
       ENDIF


       IF(IDP.EQ.6)THEN !Unyimes version
                                !ULS - Maximum flexural strength
                                !RS represented by 2nd-Order Polynomial for 5
random
                                !variables of the form: a0 + a1X1 + a2X2 + a3X3 +
a4X4 + a5X5
                                !               + a6X1^2 + a7X2^2 + a8X3^2 +
a9X4^2 + a10X5^2
                                !where a0, a1, ..., a10 are constant coefficients
                                !and X1, X2, ..., X5 are the random variables
              NR = 40
              LNR = 0
              CH = 'ULS-Moment, up to 5 random variables'

              RETURN
       ENDIF



       IF(IDP.EQ.7)THEN !Unyimes version
                                !SLS - Maximum allowable deflection exceeded
                                !RS represented by 2nd-Order Polynomial for 5
random
                                !variables of the form: a0 + a1X1 + a2X2 + a3X3 +
a4X4 + a5X5
                                !               + a6X1^2 + a7X2^2 + a8X3^2 +
a9X4^2 + a10X5^2
                                !where a0, a1, ..., a10 are constant coefficients
                                !and X1, X2, ..., X5 are the random variables
              NR = 33
```

```
      LNR = 0
      CH='SLS-Deflection, up to 5 random variables'

      RETURN
 ENDIF



100  CONTINUE

 !Closed form flexural failure mode analysis of RC-Beam
 IF(IDP.EQ.1)THEN
      RI = X(1)          !corrosion rate - icorr
      T  = X(2)          !time in years - t
      DB = X(3)          !individual bar diameter - db (mm^2)
      RN = X(4)          !number or tension rebar - nb
      AY = X(5)          !ductility reduction constant - alpha y
      FY = X(6)          !yield strength of steel - fy (MPa)
      BL = X(7)          !beam span length (mm)
      FC = X(8)          !cylinder strength of concrete (MPa)
      B = X(9)           !width of beam cross section (mm)
      D = X(10)          !depth of reinforcement (mm)
      WL = X(12)         !uniformly distributed live load (N/mm)
      WD = X(11)         !uniformly distributed dead load (N/mm)
      CL = X(13)         !concentrated load (N)

      !Total area of reinforcing steel at time=0
      AS = ((RN*PI)/4.D0)*(DB**2)
      !Total area of reinforcing steel at time t due to loss of section
      !due to corrosion
      AST = ((RN*PI)/4.D0)*((DB-0.0232*RI*T)**2)

      !Yield strength with time due to loss of ductility
      FYT = (1.D0-100*AY*((AS-AST)/AS))*FY  !UOA CORRECTED
!DB    FYT = (1.D0-100*AY*((AS-AST)/AS)*FY

      AL1 = 0.85D0-0.0015D0*FC
      IF(AL1.LT.0.67)THEN
            AL1 = 0.67
      END IF

      !Nominal moment capacity Mn from the CSA A23.3 2004 Concrete
      !Design Standard representing the available flexural strength
      !Supply R
      R = AST*FYT*(D-(AST*FYT)/(2.D0*AL1*FC*B))
      !Unfactored moment flexural response of the RC beam due to loads
      !representing the moments due to concentrated and UD loads
      !Demand S
      S = ((WD+WL)/(8.D0))*BL**2 +(CL*BL)/(4.D0)

      !Limit state g() = R - S = 0
      GG = (R/S)-1.D0

      RETURN
 ENDIF


 !Closed form shear failure mode analysis of an RC-Beam
 IF(IDP.EQ.2)THEN
      RI = X(1)
      T  = X(2)
```

```
              DV = X(3)
              RN = X(4)
              AY = X(5)
              FY = X(6)
              BL = X(7)
              FC = X(8)
              B = X(9)
              D = X(10)
              WD = X(11)
              WL = X(12)
              CL = X(13)
              S = X(14)
              AVT = ((RN*PI)/4.D0)*((DV-0.0232*RI*T)**2)
              AV = ((RN*PI)/4.D0)*(DV**2)
              FYT = (1.D0-AY*100*((AV-AVT)/AV))*FY   !UOA CORRECTED
!DB           FYT = (1.D0-AY*100*((AV-AVT)/AV)*FY

              R = 0.2*DSQRT(FC)*B*D+(AVT*FYT*D)/(S)
              S = (WD+WL)*BL/(2.D0)+CL/2.D0

              GG = (R/S)-1.D0

              RETURN
       ENDIF


       !Reliability analysis as a function of the basic random variables R,S
      IF(IDP.EQ.3)THEN
              R = X(1)
              S = X(2)

              GG = (R/S)-1.D0

              RETURN
       ENDIF


       !RS - FE based reliability analysis formulation for the
       !analysis of RC-Beams in the flexural failure mode (moments)
       IF(IDP.EQ.4)THEN
              RI = X(1)           !corrosion rate - icorr
              T  = X(2)           !time in years - t
              DB = X(3)           !individual rebar diameter - db (mm^2)
              RN = X(4)           !number or tension rebar - nb
              AY = X(5)           !ductility reduction constant - alpha y
              FY = X(6)           !yield strength of steel - fy (MPa)
              BL = X(7)           !beam span length (mm)
              FC = X(8)           !cylinder strength of concrete (MPa)
              B = X(9)            !width of beam cross section at top fibre (mm)
              D = X(10)           !depth to reinforcement (mm)
              WD = X(11)          !uniformly distributed dead load (N/mm)
              WL = X(12)          !uniformly distributed live load (N/mm)
              CL = X(13)          !concentrated load (N)
              MFE = X(14)         !Moment obtained fron FE analysis (S)
              A0 = X(15)          !Regression constant a0 - intercept
              A1 = X(16)          !Regression constant a1
              X1 = RI                    !Random variable 1 (icorr)
              A2 = X(17)          !Regression constant a2
              X2 = WD                    !Random variable 2 (wd)
              A3 = X(18)          !Regression constant a3
              X3 = WL                    !Random variable 3 (wl)
              A4 = X(19)          !Regression constant a4
```

```
            X4 = FY                    !Random variable 4 (fy)
            A5 = X(20)          !Regression constant a5
            X5 = FC                    !Random variable 5 (fc)
            A6 = X(21)          !Regression constant a6
            A7 = X(22)          !Regression constant a7
            A8 = X(23)          !Regression constant a8
            A9 = X(24)          !Regression constant a9
            A10 = X(25)         !Regression constant a10

            !Total area of reinforcing steel at time = 0
            AS = ((RN*PI)/4.D0)*(DB**2)
            !Total area of reinforcing steel at time t due to loss of section
            !due to corrosion
            AST = ((RN*PI)/4.D0)*((DB-0.0232*RI*T)**2)

            !Yield strength with time due to loss of ductility
            FYT = (1.D0-100*AY*((AS-AST)/AS))*FY  !UOA CORRECTED

            !Concrete rectangular compressive stress block factor
            AL1 = 0.85D0-0.0015D0*FC
            IF(AL1.LT.0.67)THEN
                  AL1 = 0.67
            END IF

            !Nominal moment capacity Mn based on the CSA A23.3 2004 Concrete
            !Design Standard representing the available flexural strength
            !Supply R
            R = AST*FYT*(D-(AST*FYT)/(2.D0*AL1*FC*B))
            S = MFE - A0 - A1*X1 - A2*X2 - A3*X3 - A4*X4 - A5*X5
     &      - A6*X1**2 - A7*X2**2 - A8*X3**2 - A9*X4**2 - A10*X5**2

            GG =(R/S)-1.D0

            RETURN

      ENDIF


      !RS - FE based reliability analysis formulation for RC-Beams
      !in the deflection Limt State; deflection failure mode
      IF(IDP.EQ.5)THEN
            BL = X(1)           !Beam span length (mm)
            DF = X(2)           !Deflection factor obtained from design
standard/code
            DFE = X(3)          !Deflection obtained from FE analysis (S)
            A0 = X(4)           !Regression constant a0 - intercept
            A1 = X(5)           !Regression constant a1
            X1 = X(6)           !Random variable 1
            A2 = X(7)           !Regression constant a2
            X2 = X(8)           !Random variable 2
            A3 = X(9)           !Regression constant a3
            X3 = X(10)          !Random variable 3
            A4 = X(11)          !Regression constant a4
            X4 = X(12)          !Random variable 4
            A5 = X(13)          !Regression constant a5
            X5 = X(14)          !Random variable 5
            A6 = X(15)          !Regression constant a6
            A7 = X(16)          !Regression constant a7
            A8 = X(17)          !Regression constant a8
            A9 = X(18)          !Regression constant a9
            A10 = X(19)         !Regression constant a10
```

```
            R = BL/DF           !Maximum allowable deflection as per NBCC
            S = DFE + A0 + A1*X1 + A2*X2 + A3*X3 + A4*X4 + A5*X5
     &      + A6*X1**2 + A7*X2**2 + A8*X3**2 + A9*X4**2 + A10*X5**2

            GG =(R/S)-1.D0

            RETURN

       ENDIF


!*****************************************************************************
!         BEGIN  UNYIMES RS LIMIT STATES

       !RS - FE based reliability analysis formulation for the
       !analysis of RC-Beams in the flexural failure mode (moments)
       IF(IDP.EQ.6)THEN
             RI = X(1)           !corrosion rate - icorr
             T  = X(2)           !time in years - t
             DB = X(3)           !individual rebar diameter - db (mm^2)
             RN = X(4)           !number or tension rebar - nb
             AY = X(5)           !ductility reduction constant - alpha y
             FY = X(6)           !yield strength of steel - fy (MPa)
             BL = X(7)           !beam span length (mm)
             FC = X(8)           !cylinder strength of concrete (MPa)
             B = X(9)            !width of beam cross section at top fibre (mm)
             D = X(10)           !depth to reinforcement (mm)
             WD = X(11)          !uniformly distributed dead load (N/mm)
             WL = X(12)          !uniformly distributed live load (N/mm)
             CL = X(13)          !concentrated load (N)
             MFE = X(14)         !Moment obtained fron FE analysis (S)
             A0 = X(15)          !Regression constant a0 - intercept


!                          LINEAR TERMS
             A1 = X(16)          !Regression constant a1
             X1 = RI                   !Random variable 1 (icorr)
             X1_mean = X(17)           !Random variable 2
             A2 = X(18)          !Regression constant a2
             X2 = WD                   !Random variable 2 (wd)
             X2_mean = X(19)           !Random variable 2
             A3 = X(20)          !Regression constant a3
             X3 = WL                   !Random variable 3 (wl)
             X3_mean = X(21)           !Random variable 2
             A4 = X(22)          !Regression constant a4
             X4 = FY                   !Random variable 4 (fy)
             X4_mean = X(23)           !Random variable 2
             A5 = X(24)          !Regression constant a5
             X5 = FC                   !Random variable 5 (fc)
             X5_mean = X(25)           !Random variable 2

!                          QUADRATIC
             A6 = X(26)          !Regression constant a6
             A7 = X(27)          !Regression constant a7
             A8 = X(28)          !Regression constant a8
             A9 = X(29)          !Regression constant a9
             A10 = X(30)         !Regression constant a10

!                       MIXED QUADRATIC

             A_12 = X(31)        !Regression constant
```

```
              A_13 = X(32)        !Regression constant
              A_14 = X(33)        !Regression constant
              A_15 = X(34)        !Regression constant
              A_23 = X(35)        !Regression constant
              A_24 = X(36)        !Regression constant
              A_25 = X(37)        !Regression constant
              A_34 = X(38)        !Regression constant
              A_35 = X(39)        !Regression constant
              A_45 = X(40)        !Regression constant

              !Total area of reinforcing steel at time = 0
              AS = ((RN*PI)/4.D0)*(DB**2)
              !Total area of reinforcing steel at time t due to loss of section
              !due to corrosion
              AST = ((RN*PI)/4.D0)*((DB-0.0232*RI*T)**2)

              !Yield strength with time due to loss of ductility
              FYT = (1.D0-100*AY*((AS-AST)/AS))*FY  !UOA CORRECTED

              !Concrete rectangular compressive stress block factor
              AL1 = 0.85D0-0.0015D0*FC
              IF(AL1.LT.0.67)THEN
                     AL1 = 0.67
              END IF

              !Nominal moment capacity Mn based on the CSA A23.3 2004 Concrete
              !Design Standard representing the available flexural strength
              !Supply R
              R = AST*FYT*(D-(AST*FYT)/(2.D0*AL1*FC*B))
              S = A0 + A1*(X1-X1_mean) + A2*(X2-X2_mean)
     &           + A3*(X3-X3_mean) + A4*(X4-X4_mean) + A5*(X5-X5_mean)
     &        + A6*(X1-X1_mean)**2 + A7*(X2-X2_mean)**2
     &         + A8*(X3-X3_mean)**2 + A9*(X4-X4_mean)**2
     &         + A10*(X5-X5_mean)**2
     &         +A_12*(X1-X1_mean)*(X2-X2_mean)
     &         +A_13*(X1-X1_mean)*(X3-X3_mean)
     &         +A_14*(X1-X1_mean)*(X4-X4_mean)
     &         +A_15*(X1-X1_mean)*(X5-X5_mean)
     &         +A_23*(X2-X2_mean)*(X3-X3_mean)
     &         +A_24*(X2-X2_mean)*(X4-X4_mean)
     &         +A_25*(X2-X2_mean)*(X5-X5_mean)
     &         +A_34*(X3-X3_mean)*(X4-X4_mean)
     &         +A_35*(X3-X3_mean)*(X5-X5_mean)
     &         +A_45*(X4-X4_mean)*(X5-X5_mean)

              GG =(R/S)-1.D0

              RETURN

       ENDIF


       !RS - FE based reliability analysis formulation for RC-Beams
       !in the deflection Limt State; deflection failure mode
       IF(IDP.EQ.7)THEN
              BL = X(1)           !Beam span length (mm)
              DF = X(2)           !Deflection factor obtained from design
standard/code
              A0 = X(3)           !Regression constant a0 - intercept

!                          LINEAR
              A1 = X(4)           !Regression constant a1
```

```
              X1 = X(5)           !Random variable 1
              X1_mean = X(6)            !Random variable 2
              A2 = X(7)           !Regression constant a2
              X2 = X(8)           !Random variable 3
              X2_mean = X(9)            !Random variable 4
              A3 = X(10)          !Regression constant a3
              X3 = X(11)          !Random variable 5
              X3_mean = X(12)           !Random variable 6
              A4 = X(13)          !Regression constant a4
              X4 = X(14)          !Random variable 7
              X4_mean = X(15)           !Random variable 8
              A5 = X(16)          !Regression constant a5
              X5 = X(17)          !Random variable 11
              X5_mean = X(18)           !Random variable 12

!                       QUADRATIC COMPONENTS
              A6 = X(19)          !Regression constant a6
              A7 = X(20)          !Regression constant a7
              A8 = X(21)          !Regression constant a8
              A9 = X(22)          !Regression constant a9
              A10 = X(23)         !Regression constant a10

!                       MIXED QUADRATIC
              A_12 = X(24)        !Regression constant
              A_13 = X(25)        !Regression constant
              A_14 = X(26)        !Regression constant
              A_15 = X(27)        !Regression constant
              A_23 = X(28)        !Regression constant
              A_24 = X(29)        !Regression constant
              A_25 = X(30)        !Regression constant
              A_34 = X(31)        !Regression constant
              A_35 = X(32)        !Regression constant
              A_45 = X(33)        !Regression constant

              R = BL/DF           !Maximum allowable deflection as per NBCC
              S = A0 + A1*(X1-X1_mean) + A2*(X2-X2_mean)
     &           + A3*(X3-X3_mean) + A4*(X4-X4_mean) + A5*(X5-X5_mean)
     &        + A6*(X1-X1_mean)**2 + A7*(X2-X2_mean)**2
     &         + A8*(X3-X3_mean)**2 + A9*(X4-X4_mean)**2
     &         + A10*(X5-X5_mean)**2
     &         +A_12*(X1-X1_mean)*(X2-X2_mean)
     &         +A_13*(X1-X1_mean)*(X3-X3_mean)
     &         +A_14*(X1-X1_mean)*(X4-X4_mean)
     &         +A_15*(X1-X1_mean)*(X5-X5_mean)
     &         +A_23*(X2-X2_mean)*(X3-X3_mean)
     &         +A_24*(X2-X2_mean)*(X4-X4_mean)
     &         +A_25*(X2-X2_mean)*(X5-X5_mean)
     &         +A_34*(X3-X3_mean)*(X4-X4_mean)
     &         +A_35*(X3-X3_mean)*(X5-X5_mean)
     &         +A_45*(X4-X4_mean)*(X5-X5_mean)

              GG =(R/S)-1.D0

              RETURN

       ENDIF


       RETURN

       END
```